CELL DEATH IN HYPOXIC INJURY – SIGNALING MECHANISMS AND DYNAMICS IN THE DECISION MAKING PROCESS

by

Benjamin Loos

Dissertation presented for the Degree of

DOCTOR OF PHILOSOPHY

(Physiological Sciences)

In the

Department of Physiological Sciences

at

Stellenbosch University

STELLENBOSCH

Promotor: Dr Anna-Mart Engelbrecht

September 2009

DECLARATION

I, the undersigned, hereby declare that the work contained in this dissertation is my own original work and that I have not previously in its entirety or in part submitted it at any university for a degree.

Signature: **……**

Date: **……**

ABSTRACT

Three main morphologies of cell death have been described in the diseased myocardium, type I, better known as apoptotic cell death, which is characterized by cell shrinkage and chromatin condensation, type II, or cell death with autophagy, presents a morphology with intracellular accumulation of autophagic vacuoles and type III, better known as necrosis, is characterized by cellular swelling and rapid loss in cellular membrane integrity. However, recent literature strongly argues against rigid classifications in the context of cell death mechanisms but rather suggests to adopt a view of cell death as a dynamic and integrative cellular response. Furthermore, the contribution of autophagy in cell death or cell survival is still poorly understood. Therefore the aims of this study were twofold: (i) to characterize the contribution of each cell death type in context of the severity and duration of an ischaemic insult and (ii) to determine whether manipulation of the autophagic pathway affects the contribution of cell death and translates into protection of the heart.

Rodent derived cardiac myoblast cells were grown in Dulbecco's Modified Eagle's Medium (DMEM) supplemented with 10% fetal bovine serum (FBS), and incubated under 5% CO_2 conditions. Cells were submitted to protocols of 2, 4 and 8 hrs of simulated ischaemia (SI) under hypoxic conditions in a humidified environment containing 0.1% O_2, 5% CO_2 and the balance N_2, followed by 1 hr of reperfusion respectively. We employed a modified ischaemic buffer containing either 2-deoxy-D-glucose, sodium dithionate or both, with the aim to create an ischaemic insult of mild (mild SI), moderate (moderate SI) and severe (severe SI) character respectively.

We evaluated the contribution of each cell death mode using a combination of viability- and ATP assays. Molecular markers for each cell death process such as LC3, PARP and HMGB1 were evaluated using 3-dimensional fluorescence techniques as well as western blot analysis and flow cytometry. Next, autophagy

was induced or inhibited prior to the ischaemic insult, using rapamycin and 3MA respectively, and similar parameters were evaluated after 2 hours of mild or moderate SI. Propidium Iodide exclusion and Fluorescence Resonance Energy Transfer (FRET) in combination with mitochondrial inner membrane depolarization were employed to assess the onset of cell death dynamically. Flow cytometry was employed to evaluate the degree of protection. In addition, the ATP levels and reactive oxygen species (ROS) were evaluated.

Our results strongly indicate a differential induction of cell death, which is dependent on the severity and duration of the ischaemic insult. Mild SI led to the induction of autophagy and apoptosis, whilst moderate or severe SI induced both apoptotic and necrotic cell death without an indication of autophagy. Only mild SI, but not moderate and severe SI, resulted in an ATP surge.

Moreover, our data provide direct evidence that increased autophagy delays the loss of cellular membrane integrity and delays caspase-3 activation as well as mitochondrial depolarization in ischaemic cardiomyocytes. Our results show a profound effect of increased autophagy on the onset of apoptosis as well as necrosis under simulated ischaemic conditions, providing cellular protection. This ATP surge observed during mild SI was abolished with increased autophagy. Furthermore, our results indicate a profound effect of autophagy on ROS generation. Under normoxic conditions, increased autophagy induced a significant decrease in ROS while the inhibition of autophagy significantly increased ROS generation. However, when increasing or decreasing autophagy prior to the ischaemic insult, ROS increased significantly in both scenarios.

The results suggest that the severity of ischaemia determines the mode of cell death differentially. An increase in autophagic responsiveness and flux, as induced through rapamycin treatment, provides a selective advantage for tissue against injury, possibly by maintaining intracellular ATP levels through the provision of metabolic substrates. Autophagy is described as an inherent cellular mechanism

which affects the onset of cell death and exhibits protective effects in the ischaemic myocardium when upregulated prior to the ischaemic insult.

The protective effect of increased autophagy was mirrored in the isolated perfused rat heart model, reflected by improved functional recovery during ischaemia/reperfusion.

OPSOMMING

Die drie belangrikste morfologiese beskrywings van seldood in die hart sluit die volgende in: tipe I, beter bekend as apoptose wat gekenmerk word deur selkrimping en chromatienkondensering, tipe II, of seldood deur middel van autofagie wat gekenmerk word deur die intrasellulêre versameling van autofagiese vakuole en tipe III, beter bekend as nekrose wat gekenmerk word deur sel swelling en ‘n vinnige verlies aan membraanintegriteit. Onlangse literatuur waarsku egter teen die onbuigsame klassifikasie van seldoodmeganismes en stel voor dat seldood as ‘n dinamiese proses met integrerende sellulêre meganismes beskou moet word. Die bydrae van autofagie in seldoodmeganismes word ook nog nie goed verstaan nie. Die doel van hierdie studie is dus tweevoudig: (i) om die bydrae van elke tipe seldood te bepaal in konteks van die felheid en tydperk van die iskemiese ingryping en (ii) om te bepaal of the manupilering van autofagie ‘n betekenisvolle bydrae lewer in seldoodmeganismes en sodoende tot beskerming van die hart kan lei.

Kardiale mioblaste wat van rotweefsel afkomstig is, is in Dulbecco se gemodifiseerde Eagle medium (DMEM), waarby daar 10% fetale kalfserum gevoeg is en wat onderhewig was aan 5% CO_2 toestande, onderhou. Selle was onderhewig aan protokolle van 2, 4 en 8 ure gesimuleerde iskemie (SI) onder hipoksiese toestande in ‘n humiditeitsomgewing wat 0.1% O_2, 5% CO_2 en die balans N_2 bevat. Daarna was die selle onderhewig aan 1 uur reperfusie. ‘n Gemodifiseerde iskemiese buffer wat óf 2-deoksie-D-glukose óf natriumdithionaat, of beide bevat, is gebruik om lig, matig en strawwe iskemiese toestande na te boots.

Die bydrae van elke tipe seldood is geëvalueer tydens bogenoemde toestande deur gebruik te maak van ‘n kombinasie van sellewensvatbaarheid- en ATP tegnieke. Molekulêre merkers, wat LC3, PARP en HMGB1 insluit, is gebruik om deur middel van 3-dimensionele fluoresensie tegnieke, westelike kladtegnieke en

vloeisitometrie die verskillende vorme van seldood te ondersoek. Autofagie is ook geïnduseer en geïnhibeer voor die iskemiese ingryping, deur middel van rapamycin en 3MA, respektiewelik om die rol van autofagie tydens seldood te bepaal. Propidium iodite uitluiting en fluoresensie resonansie energie oordrag (FRET) in kombinasie met ‘n merker vir mitochondriale binneste membraan depolarisasie is gebruik om die aanvang van seldood dinamies te ondersoek. Vloeisitometrie is gebruik om die graad van beskerming aan te dui, terwyl intrasellulêre ATP vlakke en reaktiewe suurstof spesies (ROS) ook gemeet is.

Ons resultate het getoon dat daar ‘n differensiële indusering van seldood plaasvind wat afhanklik is van die felheid en tydsduur van die iskemiese ingryping. ‘n Ligte graad van iskemie lei tot die indusering van autofagie en apoptose, terwyl matige en strawwe iskemie beide apoptose en nekrose induseer sonder autofagie. Verder het slegs ‘n ligte graad van iskemie ‘n skerp styging in ATP tweeggebring, terwyl dit nie die geval was tydens matige en strawwe iskemie nie.

Ons data verskaf ook direkte bewyse dat ‘n toename in autofagie die verlies van sellulêre membraanintegriteit vertraag. Dit het ook ‘n vermindering in caspase-3 aktivering en mitochondriale depolarisasie in iskemiese kardiomiosiete teweegebring. Die data dui aan dat ‘n toename in autofagie ‘n beduidende effek op apoptose en nekrose tydens gesimuleerde iskemiese toestande het om sodoende selbeskerming te verskaf. Die skerp styging in ATP wat tydens die ligte graad van iskemie teweeggebring is, is opgehef met ‘n toename in autofagie. Ons resultate dui ook daarop dat autofagie ‘n beduidende rol in ROS generering speel. Onder normoksiese omstandighede veroorsaak ‘n toename in autofagie ‘n insiggewende afname in ROS generering, terwyl die inhibisie van autofagie ROS generering insiggewend laat toeneem. Wanneer autofagie egter voor die iskemiese ingryping verhoog of verlaag word, vermeerder ROS generering in beide gevalle.

Hierdie resultate bewys dat die graad van iskemie ‘n invloed het op die tipe seldood wat geïnduseer word. ‘n Toename in autofagie reaksietyd en vloei, soos

bewerkstellig deur rapamycin, verskaf ‘n selektiewe voordeel vir weefsel teen beskadiging, heel waarskynlik deur die handhawing van intrasellulêre ATP-vlakke deur die verskaffing van metaboliese substrate. Autofagie word beskryf as ‘n inherente sellulêre meganisme wat seldood beïnvloed en die iskemiese miokardium beskerm wanneer dit opgereguleer word voor die iskemiese ingryping. Hierdie beskermende rol van autofagie wat in die weefselkultuur waargeneem is, is ook in die geïsoleerde geperfuseerde rot hart model waargeneem, waar funksionele herstel verbeter is tydens iskemie/reperfusie.

Zusammenfassung

Die drei morphologischen Erscheinungen des Zelltodes im Herzen sind Typ I Apoptose, gekennzeichnet durch Zellschrumpfung und Chromatinverdichtung, Typ II Autophagie, charakterisiert durch die Bildung von Autophagosomen und Typ III, Nekrose, gekennzeichnet durch den Verlust der Zellmembranintegrität. Die gegenwärtige Literatur postuliert jedoch gegen eine rigide Klassifizierung der Zelltodmechanismen und schlägt vor, Zelltod als einen dynamischen und integrativen Prozess zu betrachten. Weiterhin wird die eigentliche Beteiligung von Autophagie in der Entwicklung des Zelltodes oder an dem Versuch des Zellüberlebens kaum verstanden. Der Zweck der vorliegenden Studie ist daher zweifach: (i) die Beteiligung eines jeden Zelltodtypes im Verhältnis zur Stärke und Dauer eines ischämischen Zustandes zu charakterisieren und (ii) festzustellen, ob eine Manipulation des Signalweges der Autophagie diese Beteiligung beeinflusst und zu einem Schutz des Herzgewebes beiträgt.

Herzmyoblastzellen wurden in Dulbecco's Modified Eagle's Medium (DMEM) und 10% fötalem bovinem Serum (FBS) kultiviert und unter 5% CO_2 inkubiert. Zellen wurden einem Protokoll von 2,4 und acht Stunden simulierter Ischämie (SI) unter sauerstoffarmen Bedingungen (0.1% O_2, 5% CO_2 und Stickstoffbalance) ausgesetzt, gefolgt von einer Stunde einer Reperfusion. Ein ischämischer Puffer versetzt mit entweder 2-deoxy-D-glucose oder Sodiumdithionat oder beidem wurde jeweils genutzt, um eine Ischämie von mildem (mild SI), moderatem (moderate SI) oder starkem (severe SI) Charakter herbeizuführen.

Die Beteiligung eines jeden der verschiedenen Zelltode wurde durch die Nutzung einer Kombination von ATP und Viabilitätstechniken evaluiert. Molekulare Marker für jeden Zelltodprozess, wie LC3, PARP und HMGB1 wurden unter der Nutzung von drei- dimensionaler Fluoreszenztechnik, Western Blot und Durchflusszytometrie evaluiert. Als nächstes wurden Autophagie durch Rapamycin und 3MA vor dem ischämischen Zustand induziert oder gehemmt und gleiche

Parameter nach zwei Stunden milder und moderater SI evaluiert. Techniken wie Propidium Iodide Ausschlussverfahren und Fluorescence Resonsance Energy Transfer (FRET) in Kombination mit mitochondrialer Membrandepolarisation wurden eingesetzt, um den Beginn oder den Ausbruch des Zelltodes dynamisch zu messen. Durchflusszytometrie wurde genutzt, um das Ausmaß des Zellschutzes zu evaluieren. Zusätzlich wurden ATP und reaktive Sauerstoffspezies (ROS) evaluiert.

Unsere Ergebnisse zeigen deutlich eine differenzierte Zelltodinduktion auf, die in Abhängigkeit von der Stärke und Dauer der Ischämie steht. Milde SI führte zu Autophagie und Apoptose, während moderate und starke SI Apoptose und Nekrose herbeiführte, ohne Anzeichen für Autophagie. Nur milde SI, nicht jedoch moderate und starke SI, führte zu einem Anstieg in ATP.

Weitherhin liefern unsere Ergebnisse direkten Beweis dafür, dass induzierte Autophagie den Verlust der Zellmembranintegrität und die Aktivierung von Caspase-3, sowohl auch mitochondriale Depolarisation in ischämischen Myozyten verzögert. Unsere Ergebnisse verdeutlichen einen tiefgreifenden Effekt von induzierter Autophagie auf den Ansatz von Apoptose- und Nekrosebeginn während simulierter Ischämie, was zum Zellschutz führt. Der während der milden SI beobachtete ATP- Anstieg konnte aufgehoben werden, wenn Autophagie induziert wurde. Weitherhin zeigen unsere Ergebnisse einen tiefgreifenden Effekt von Autophagie auf die Herstellung von reaktiven Sauerstoffspezies. Unter normalen Sauerstoffbedingungen führt induzierte Autophagie zu einer Abnahme in ROS, während die Hemmung von Autophagie die ROS- Herstellung signifikant erhöht. Wenn jedoch Autophagie vor der Ischämie induziert oder gehemmt wird, steigt ROS in beiden Fällen an.

Die Ergebnisse weisen darauf hin, dass die Stärke einer Ischämie den Typus Zelltod differenziert bestimmt. Ein Anstieg in der Reaktionsfähigkeit und- kapazität für den Autophagieprozess, herbeigeführt durch die Vorbehandlung mit

Rapamycin, führt einen selektiven Vorteil herbei, der sich schützend auf das Gewebe auswirkt. Dies ist möglicherweise durch die Erhaltung des intrazellulärem ATP- Gehaltes und durch eine Bereitstellung von metabolischen Substraten bewirkt. Autophagie wird hier als ein zellulär innewohnender Mechanismus beschrieben, der, wenn induziert, den Ausbruch des Zelltodes zeitlich beiinflusst und sich schützend auf das ischämische Herzmuskelgewebe auswirkt.

Die schützende Wirkung von induzierter Autophagie wurde auch im isolierten perfusionierten Herzmodell widergespiegelt, in dem sich funktionelle Wiederherstellung nach Ischämie/Reperfusion verbesserte.

ACKNOWLEDGEMENTS

I wish to express my sincere appreciation to a number of people, who have guided, inspired and supported me throughout this study.

I would like to thank my supervisor, Dr Anna-Mart Engelbrecht, for this highly enjoyable and beautiful journey. I thank her for academic inspiration in the field of cell death and autophagy, for advice and suggestions, and also for anticipation in the excitement of the work. I also thank her for allowing me the freedom to explore unknown avenues, for patience with my long “german” sentence structures and for friendship.

I would like to thank Prof Kathy Myburgh, for the opportunity to study in her Department, and for teaching an “integrative” approach in Physiology.

I am grateful to Prof Amanda Lochner, for advise, expertise and support regarding the perfusion work, and for the willingness to critically asses the review on autophagy in the heart. It was highly inspirational.

I would like to thank Prof Jacques van Rooyen, for exposing me to the field of ischaemic heart disease, way back in 2004.

I would like to thank Prof Johan Koeslag, for teaching me the “good for what?” approach of thinking in the critical assessment studies.

I thank Prof Faadiel Essop for teaching the importance of being guided by a hypothesis.

I would like to express my warmest thank you to Beverly Ellis and Sonja Genade for the fantastic technical assistance.

I also would like to thank the many students and colleges in the department, for creating a great and “full of humour” working atmosphere, especially Mark, Naomi, Gustav, Bali, Phillippo, Theo, Maritza and the DSG team. I thank Martine for keeping the tissue culture lab nice and sterile. I thank Katriena for the friendly chats and clean lab coats and Johnifer for help with the nitrogen tanks and rats.

I thank Prof Gary Stevens and the CAF team for the support in handling both, the Cell Imaging Unit and the studies. Special thanks to Madelaine Frazenburg for the scanning electron images. On the technical side, I thank “Olli” my Olympus microscope and “Howard”, my FACS Aria, for the good company and hard work.

I also thank the PSSA members for the opportunity provided to attend the IUPS 2009 in Japan.

I would like to acknowledge and thank the University of Stellenbosch, the National Research Foundation and the Harry Crossley Foundation for financial support.

I thank my friends and family members, my parents and sisters and my pastor for support and love. I also have to thank my dog Jordan for being my patient audience, when preparing for a talk or poster.

Most importantly, I would like to thank my wife, Unathi. Without you my world would not make sense. Thank you for the encouragement and patience and all the support during the time of study. This thesis is dedicated to you.

LIST OF CONFERENCE CONTRIBUTIONS AND PUBLICATIONS

International:

- Loos B & Engelbrecht A-M. *Cell death in ischaemic injury – a dynamic response concept*. Presented at the 36th International Congress of Physiological Sciences, IUPS 2009, Function of Life: Elements and Integration; Kyoto, Japan; 27th July-1st August 2009.

- Loos B & Engelbrecht A-M. *Cell death in ischaemic injury - a dynamic response concept.* EMBO Conference on: Autophagy, Cell Biology, Physiology and Pathology. 18th-21st October 2009. Ascona, Switzerland. Abstract accepted for poster presentation.

National:

- Loos B & Engelbrecht A-M. *Cell death in ischaemic injury – a dynamic response concept.* 36th meeting of the Physiology Society of Southern Africa, PSSA. 16th-19th September 2008. University of Pretoria, South Africa. Wyndham Student Presentation Prize.

- Loos B, Thomas M and Engelbrecht A-M. *Take autophagic flux control and consider what the cell demands.* 37th meeting of the Physiology Society of Southern Africa, PSSA. 7th-9th September 2009. University of Stellenbosch, South Africa. Abstract accepted for poster presentation.

- Loos B & Engelbrecht A-M. *Cell death in ischaemic injury - a dynamic response concept.* 10th Annual Congress of the South African Heart Association. 22nd- 25th October 2009. Sun City, South Africa. Abstract accepted.

Publications:

- Loos B, Engelbrecht AM. Cell death: a dynamic response concept. Autophagy 2009; 5:5:1-14.

- Loos B & Engelbrecht A-M. *Cell death in ischaemic injury – a dynamic response concept*. Proceedings of the XXXVI International Congress of Physiological Sciences (IUPS2009). The Journal of Physiological Sciences. 2009; 59: 319.

- Loos B, Lochner A and Engelbrecht A-M. Autophagy in Cardiovascular Disease - Survival through improved Metabolic Management - A hypothesis. Journal of Molecular and Cellular Cardiology. Manuscript submitted in July 2009, revised manuscript submitted in September 2009.

- Loos B & Engelbrecht A-M. At the core of cell survival: Autophagy delays onset of both apoptotic and necrotic cell death in ischaemic injury. Article in preparation, to be submitted shortly to Cell Death and Differentiation.

- Loos B & Engelbrecht A-M. Severity of ischaemic insult results in differential cell death induction. Article in preparation, to be submitted shortly to the Journal of Molecular and Cellular Cardiology.

INDEX

LIST OF FIGURES

LIST OF TABLES

LIST OF ABBREVIATIONS

Chapter 1 INTRODUCTION

1.1. Motivation for study 1

Chapter 2 LITERATURE DISCUSSION

2.1. Introduction 4

2.2. Autophagy 6
2.2.1. Definition and role 6
2.2.2. The induction of autophagy 8
2.2.3. Regulation and control of autophagy 11
2.2.4. Autophagy in the myocardium 17
2.2.5. Detection methods for autophagy 19

2.3. Apoptosis 21

2.3.1. Definition and role 21
2.3.2. Pathway of apoptosis 23
2.3.3. Modulating molecules of the apoptotic pathway 26
2.3.4. Apoptosis in the myocardium 28
2.3.5. Detection methods for apoptosis 29

2.4. Necrosis 31
2.4.1. Definition and role 31
2.4.2. Pathway of necrosis 32
2.4.3. Regulation and control of necrosis 33
2.4.3.1. Inducing and key molecules 34
2.4.3.2. Modulating molecules 36
2.4.4. Detection methods for necrosis 38

2.5. Dynamics within modes of cell death 39
2.5.1. Defining the point-of-no-return 39
2.5.2. Conceptualizing the point-of-no-return 40
2.5.3. Assessing the point-of-no-return 41

2.6. Dynamics between modes of cell death 45
2.6.1. Greyzones autophagy/apoptosis 48
2.6.2. Greyzones apoptosis/necrosis 49
2.6.3. Greyzones autophagy/necrosis 51

2.7. Cell death with autophagy – a rare exception? 53

2.8. Conclusion and future outlook 53
2.9. Hypothesis 54

Chapter 3 MATERIAL AND METHODS

3.1. Antibodies and chemicals 56
3.2. Experimental animals 59
3.3. Cell culture preparation 59
3.3.1. Cells 59
3.3.3. Passaging protocol 60

3.4. Simulated ischaemia (SI) and reperfusion 60
3.5. Treatment of cells with rapamycin and 3MA 61
3.6. Determination of myocyte viability 62
3.6.1. PI exclusion 62
3.6.2. Nuclear condensation 63
3.6.3. MTT assay 64
3.7. ATP analysis 65

3.8. Western blot analysis 65
3.8.1. Protein extraction 65
3.8.2. Bradford protein quantitation 66
3.8.3. Sodium-dodecyl-sulfate-polyacrylamide gel electrophoresis (SDS-PAGE) 67
3.8.4. Western blot analysis 67

3.9. Immunofluorescence 68
3.10. Fluorescence microscopy 69
3.11. Transfections with GFP-LC3 and CFP-DEVD-YFP 70
3.12. Live Cell Imaging 70
3.12.1. Fluorescence Resonance Energy Transfer (FRET) and mitochondrial depolarization dynamics 70
3.12.2. Propidium Iodide uptake dynamics 71
3.12.3. LC3 imaging 71
3.13. Scanning Electron Microscopy 72

3.14. Flow Cytometry 72
3.14.1. PI exclusion 72
3.14.2. Tetramethylrhodamine Ethyl Ester (TMRE) intensity analysis 73
3.14.3. ROS assessment 73
3.14.4. Acridine Orange staining 74

3.15. Perfusion technique of isolated perfused rat heart 74
3.16. Perfusion Buffer 75
3.17. Determination of function 75
3.18. Perfusion sequence 76

3.19. Histology 77
3.19.1. Fixation and sectioning 77
3.19.2 Haematoxylin Eosin (H&E) staining 78
3.19.3. Immunofluorescence staining 78
3.20. Statistical analysis 79

CHAPTER 4 RESULTS: TIME POINTS

4.1. *In vitro* model: Three time points and three severities of simulated Ischaemia 80

4.2 Experimental measurements after 2 hrs SI 82
4.2.1. $_{2hrs\ SI/R}$ PI exclusion and Nuclear condensation 82
4.2.2. $_{2hrs\ SI/R}$ MTT assay and ATP analysis 84
4.2.3. $_{2hrs\ SI/R}$ Western blot analysis 87
4.2.4. $_{2hrs\ SI/R}$ Immunofluorescence- and Scanning Electron Microscopy 90
4.2.4. $_{2hrs\ SI/R}$ Quantification of cells with numerous LC3 punctae 93
4.2.4. $_{2hrs\ SI/R}$ Fluorescence Microscopy 94
4.2.4. $_{2hrs\ SI/R}$ Scanning Electron Microscopy (SEM) 97

4.3. Experimental measurements after 4 hrs SI 98
4.3.1. $_{4hrs\ SI/R}$ PI exclusion and Nuclear condensation 98
4.3.2. $_{4hrs\ SI/R}$ MTT assay and ATP analysis 100
4.3.3. $_{4hrs\ SI/R}$ Western blot analysis 102
4.3.4. $_{4hrs\ SI/R}$ Immunofluorescence- and Scanning Electron Microscopy 105
4.3.4. $_{4hrs\ SI/R}$ Quantification of cells with numerous LC3 punctae 106
4.3.4. $_{4hrs\ SI/R}$ Fluorescence Microscopy 107
4.3.4. $_{4hrs\ SI/R}$ Scanning Electron Microscopy (SEM) 110

4.4. Experimental measurements after 8 hrs SI 111
4.4.1. $_{8hrs\ SI/R}$ PI exclusion and Nuclear condensation 111

4.4.2. $_{8hrs\ SI/R}$ MTT assay and ATP analysis 112
4.4.3. $_{8hrs\ SI/R}$ Western blot analysis 115
4.4.4. $_{8hrs\ SI/R}$ Immunofluorescence- and Scanning Electron Microscopy 118
4.4.4. $_{8hrs\ SI/R}$ Quantification of cells with numerous LC3 punctae 119
4.4.4. $_{4hrs\ SI/R}$ Fluorescence Microscopy 120
4.4.4. $_{8hrs\ SI/R}$ Scanning Electron Microscopy (SEM) 122

CHAPTER 5 DISCUSSION: TIME POINTS

5.1. Autophagy, apoptosis and necrosis evaluated concomitantly and dynamically 124

5.2. The effect of mild, moderate and severe simulated ischaemia on apoptosis and necrosis 125

5.3. The effect of mild, moderate and severe simulated ischaemia on cellular ATP and mitochondrial reductive capacity 126

5.4. The effect of mild, moderate and severe simulated ischaemia: metabolic sensing, autophagy and apoptosis 129

5.5. The effect of mild, moderate and severe simulated ischaemia: Fluorescence and scanning electron microscopy 131

5.6. Summary 133

CHAPTER 6 RESULTS: ONSET DYNAMICS

6.1. Protocol - onset dynamics *in vitro* 136
6.2. Live Cell Imaging 137
6.2.1. LC3 imaging 138
6.2.2. Propidium Iodide uptake dynamics 139
6.2.3. Fluorescence Resonance Energy Transfer (FRET) and mitochondrial depolarization dynamics 144

6.3. Flow Cytometry 150
6.3.1. PI exclusion 151
6.3.2. Tetramethylrhodamine Ethyl Ester (TMRE) intensity analysis 152
6.3.3. Reactive oxygen species (ROS) assessment 154
6.4. ATP 158

CHAPTER 7 DISCUSSION: ONSET DYNAMICS

7.1. *In vitro* onset dynamics of apoptosis and necrosis 161
7.2. *In vitro* onset dynamics – ROS assessed by flow cytometry 162
7.3. *In vitro* onset dynamics – ATP availability 164
7.4. Summary 166
7.5. *In vitro* model: shortcomings 167

CHAPTER 8 RESULTS: FUNCTIONAL RECOVERY

8.1. Functional recovery: three durations of ischaemia 171

8.2. Functional recovery: Rapamycin and 3MA treatment 174

CHAPTER 9 DISCUSSION: FUNCTIONAL RECOVERY

9.1. *Ex vivo* model: functional recovery 176
9.2. Summary 177

CHAPTER 10 SUMMARY AND CONCLUSIONS

10.1. Is autophagy beneficial or detrimental? A model is proposed 181
10.2. Final Conclusions 183
10.3. Future Prospects 184

ACKNOWLEDGEMENTS
ADDENDUM
REFERENCES

LIST OF FIGURES

Chapter 2

Figure 2.1 Cell with extensive accumulation of autophagic vacuoles, indicating type II cell death with autophagy.

Figure 2.2 Type II, apoptotic cell death

Figure 2.3 Type III, necrotic cell death

Figure 2.4 Model of typical appearance of different types of cell death

Figure 2.5 The pathways of cell death with autophagy, apoptosis and necrosis molecularly overlap

Figure 2.6 The overlap of autophagy, apoptosis and necrosis pathways, their onset and the PONR position translates time- dependently into the observed morphology and cellular survival rate

Figure 2.7 ATP- dependent relationship between autophagy, apoptosis and necrosis

Chapter 3

Figure 3.1 *In vitro* experimental protocol for three time points of SI

Figure 3.2 *In vitro* experimental protocol of SI for study of onset dynamics

Figure 3.3 Fluorescence micrograph showing PI-negative and PI-positive cells

Figure 3.4 Fluorescence micrograph showing normal and pyknotic nuclei

Figure 3.5 *Ex vivo* experimental protocol for global ischaemia

Figure 3.6 *Ex vivo* experimental protocol for global ischaemia with induced and inhibited autophagic activity

Chapter 4

Figure 4.1 *In vitro* experimental protocol

Figure 4.2 2 hrs SI. PI exclusion and nuclear condensation

Figure 4.3 2 hrs SI/R. PI exclusion and nuclear condensation
Figure 4.4 2 hrs SI. MTT assay and ATP analysis
Figure 4.5 2 hrs SI/R. MTT assay and ATP analysis
Figure 4.6 2 hrs SI and SI/R. pAMPKα activation
Figure 4.7 2 hrs SI and SI/R. pmTOR activation
Figure 4.8 2 hrs SI and SI/R. Beclin-1 activation
Figure 4.9 2 hrs SI and SI/R. Caspase-3 activation
Figure 4.10 2 hrs SI and SI/R. PARP cleavage
Figure 4.11 Fluorescence micrograph showing LC3 punctae
Figure 4.12 2 hrs SI. Cell count with numerous LC3 punctae
Figure 4.13 2 hrs SI/R. Cell count with numerous LC3 punctae
Figure 4.14 2 hrs SI. H9c-2 cells labelled with LC3/FITC, Actin/TexRed
Figure 4.15 2 hrs SI/R. H9c-2 cells labelled with LC3/FITC, Actin/TexRed
Figure 4.16 2 hrs SI. H9c-2 cells labelled with Cyt-c/FITC, Beclin-1/TexRed
Figure 4.17 2 hrs SI/R. H9c-2 cells labelled with Cyt-c/FITC, Beclin- 1/TexRed
Figure 4.18 2 hrs SI. H9c-2 cells labelled with HMGB1/FITC
Figure 4.19 2 hrs SI/R. H9c-2 myoblasts labelled with HMGB1/FITC
Figure 4.20 2 hrs SI. SEM micrographs of H9c-2 cells
Figure 4.21 4 hrs SI. PI exclusion and nuclear condensation
Figure 4.22 4 hrs SI/R. PI exclusion and nuclear condensation
Figure 4.23 4 hrs SI. MTT assay and ATP analysis
Figure 4.24 4 hrs SI/R. MTT assay and ATP analysis
Figure 4.25 4 hrs SI and SI/R. pAMPKα activation
Figure 4.26 4 hrs SI and SI/R. pmTOR activation
Figure 4.27 4 hrs SI and SI/R. Beclin-1 activation
Figure 4.28 4 hrs SI and SI/R. Caspase-3 activation
Figure 4.29 4 hrs SI and SI/R. PARP cleavage
Figure 4.30 4 hrs SI. Cell count with numerous LC3 punctae
Figure 4.31 4 hrs SI/R. Cell count with numerous LC3 punctae
Figure 4.32 4 hrs SI. H9c-2 cells labelled with LC3/FITC, Actin/TexRed
Figure 4.33 4 hrs SI/R. H9c-2 cells labelled with LC3/FITC, Actin/TexRed

Figure 4.34 4 hrs SI. H9c-2 cells labelled with Cyt-c/FITC, Beclin-1/TexRed
Figure 4.35 4 hrs SI/R. H9c-2 cells labelled with Cyt-c/FITC, Beclin-1/TexRed
Figure 4.36 4 hrs SI. H9c-2 cells labelled with HMGB1/FITC
Figure 4.37 4 hrs SI/R. H9c-2 myoblasts labelled with HMGB1/FITC
Figure 4.38 4 hrs SI. SEM micrographs of H9c-2 cells
Figure 4.39 8 hrs SI. PI exclusion and nuclear condensation
Figure 4.40 8 hrs SI/R. PI exclusion and nuclear condensation
Figure 4.41 8 hrs SI. MTT assay and ATP analysis
Figure 4.42 8 hrs SI/R. MTT assay and ATP analysis
Figure 4.43 8 hrs SI and SI/R. pAMPKα activation
Figure 4.44 8 hrs SI and SI/R. pmTOR activation
Figure 4.45 8 hrs SI and SI/R. Beclin-1 activation
Figure 4.46 8 hrs SI and SI/R. Caspase-3 activation
Figure 4.47 8 hrs SI and SI/R. PARP cleavage
Figure 4.48 8 hrs SI. Cell count with numerous LC3 punctae
Figure 4.49 8 hrs SI/R. Cell count with numerous LC3 punctae
Figure 4.50 8 hrs SI. H9c-2 cells labelled with LC3/FITC, Actin/TexRed
Figure 4.51 8 hrs SI/R. H9c-2 cells labelled with LC3/FITC, Actin/TexRed
Figure 4.52 8 hrs SI. H9c-2 cells labelled with Cyt-c/FITC, Beclin-1/TexRed
Figure 4.53 8 hrs SI/R. H9c-2 cells labelled with Cyt-c/FITC, Beclin-1/TexRed
Figure 4.54 8 hrs SI. H9c-2 cells labelled with HMGB1/FITC
Figure 4.55 8 hrs SI/R. H9c-2 myoblasts labelled with HMGB1/FITC
Figure 4.56 8 hrs SI. SEM micrographs of H9c-2 cells

Chapter 5

Figure 5.1 Model of the cell's capacity to respond to a defined insult, indicating the typical morphological features of different types of cell death

Chapter 6

Figure 6.1: *In vitro* experimental protocol for study of onset dynamics.

Figure 6.2: H9c-2 myoblasts transfected with LC3-GFP and counterstained with Lyostracker Red or Tetramethylrhodamine Ethyl Ester
Figure 6.3: Fluorescent micrographs showing LC3 autophagosomes in cells exposed to mild SI or moderate SI
Figure 6.4: Dynamic characteristics of PI uptake
Figure 6.5: Intensity distribution over time, indicating the onset of PI uptake
Figure 6.6: EC50 data showing moderate SI, moderate SI + Rapamycin treatment and moderate SI + 3MA treatment
Figure 6.7: Dynamic characteristics of caspase-3 activity and loss of mitochondrial membrane potential
Figure 6.8: CFP/YFP emission ratio and the TMRE fluorescence intensity, measured simultaneously during mild SI
Figure 6.9: CFP/YFP emission ratio and the TMRE fluorescence intensity, measured simultaneously under normoxic conditions
Figure 6.10: Intensity distribution over time, indicating the onset of caspase-3 cleavage and loss in mitochondrial membrane depolarization
Figure 6.11: EC50 data showing mild SI, mild SI + Rapamycin treatment and mild SI + 3MA treatment
Figure 6.12: 3-dimensional forward and side scatter of cells exposed to mild and moderate SI
Figure 6.13: PI positive cells assessed by flow cytometry
Figure 6.14: TMRE mean intensity assessed by flow cytometry
Figure 6.15: TMRE intensity histogram
Figure 6.16: H9c-2 myoblasts following incubation with DCF and Hoechst 33432
Figure 6.17: DCF mean intensity assessed by flow cytometry following 24 hrs rapamycin and 3MA treatment, under control conditions
Figure 6.18: DCF mean intensity assessed by flow cytometry following 24 hrs rapamycin and 3MA treatment and 2 hrs mild SI
Figure 6.19: DCF intensity histogram mild SI
Figure 6.20: DCF mean intensity assessed by flow cytometry following 24 hrs rapamycin and 3MA treatment and 2 hrs moderate SI

Figure 6.21: DCF intensity histogram: moderate SI
Figure 6.22: ATP levels of control cells following 24 hrs rapamycin and 3MA treatment
Figure 6.23: ATP levels following 24 hrs rapamycin and 3MA treatment and 2 hrs mild SI
Figure 6.24: ATP levels following 24 hrs rapamycin and 3MA treatment and 2 hrs moderate SI

Chapter 7

Figure 7.1: Relationship between the severity of the insult and the induction/ execution of cell death
Figure 7.2: Relationship between autophagic flux, autophagic response time and the induction/execution of cell death

Chapter 8

Figure 8.1: In vivo experimental protocol
Figure 8.2: Cardiac output (CO) in ml/min [CO=Coronary (Qe) + aortic (Qa) flow rates]
Figure 8.3: Stroke volume in ml (SV=CO/heart rate)
Figure 8.4: Mean external power produced by the left ventricle
Figure 8.5: *Ex vivo* experimental protocol of global ischaemia with induced and inhibited autophagic activity.
Figure 8.6: Cardiac output CO in ml/min (CO=Coronary (Qe) + aortic (Qa)
Figure 8.7: Mean external power produced by the left ventricle

Chapter 9

Figure 9.1: Relationship between increased autophagy and amino acid generation.

Chapter 10

Figure 10.1: Conceptual model defining the functional role of autophagy in cardiomyocytes: Protection vs bioenergetic failure and autophagic cell death

LIST OF TABLES

Chapter 2

Table 2.1. Suggestions of kinetic parameters to be acquired to complement detection methods for the assessment of autophagy and cell death dynamics.

LIST OF ABBREVIATIONS

2DG	2-deoxy-D-glucose
3MA	3-methyladenine
AIF	Apoptosis inducing factor
AMPK	AMP-activated protein kinase
ATG	Autophagy-related-genes
ATP	Adenosine triphosphate
BH-3	Bcl-2-homology-3
CARD	Caspase activation and recruitment domain
CFP	Cyan fluorescent protein
CMA	Chaperone-mediated autophagy
DAP	Death associated proteins
DCF	6-carboxy-2'7'-dichlorodihydrofluorescin diacetate di(acetoxymethyl) ester
DD	Death domain
DED	Death effector domain
DMEM	Dulbecco's Modified Eagle's Medium (DMEM)
DNA	Deoxyribonucleic acid
ER	Endoplasmic reticulum
ERK	Extracellular signal-regulated kinase
FADD	Fas-associated death domain
FAO	Fatty acid oxidation
FasL	Fas ligand
FBS	Fetal bovine serum
FITC	Fluorescein isothiocyanate
FRET	Fluorescence Resonance Energy Transfer
GFP	Green fluorescent protein
HMGB1	High mobility group box I
JNK	c-Jun N-terminal kinase/stress-activated protein kinase
LAMP1	Lysosome-associated membrane protein-1

MAC	Membrane attack complex
MAP1-LC3	Microtubule Associated Protein 1-Light Chain 3
MAPK	Mitogen-activated protein kinase
MMP	Mitochondrial membrane permeabilization
MOMP	Mitochondrial outer membrane permeability
mTOR kinase	mammalian target of rapamycin kinase
MTT	3-[4,5-dimethylthiazol-2-yl]-2,5-diphenyl tetrazolium bromide
n	number of experiments
NO	Nitric oxide
PARP	Poly (ADP-ribose) polymerase
PBS	Phosphate-buffered saline
PE	phosphatidylethanolamine
PI	Propidium iodide
PI3K	Phosphatidylinositol 3-kinase
PIP_3	Phosphatidylinositol 3-phosphate
PKB	Protein kinase B
PONR	Point-of-no-return
PTEN	Phosphatase and tensin homolog
RIP	Receptor-interacting protein
ROI	region of interest
ROS	Reactive oxygen species
SDT	Sodium Dithionite
SI	Simulated ischaemia
SI/R	Simulated ischaemia/reperfusion
TCA	Tricarboxylic acid
Tex-red	Texas red
TNF-α	Tumour necrosis factor alpha
TRME	Tetramethylrhodamine Ethyl Ester
TUNEL	dUTP nick-end labeling
YFP	Yellow fluorescent protein

Units of measurement

A	ampere
%	percentage
ºC	degrees Celsius
µl	microlitre
µg	microgram
µm	micrometer
µM	micromolar
g	gram
hr	hour
hrs	hours
kDa	kilodalton
l/L	litre
M	molar
mg	milligram
min	minutes
ml	milliliters
mM	millimolar
nm	nanometer
V	volt
U	units

CHAPTER 1 INTRODUCTION

1.1. MOTIVATION FOR STUDY

The myocardium relies on a highly efficient system of energy conversion as sufficient ATP availability is crucial to maintain its contractile function. The ATP demand in the heart is extremely high. If this demand cannot be met due to an ischaemic event, cardiac myocytes die rapidly with deleterious effects on the myocardial tissue. This tissue damage impairs organ function both acutely and chronically to an extent that can threaten the patient's life. The morbidity and mortality from myocardial infarction and heart failure remain significant and unacceptably high (Kloner & Rezkalla, 2004, Ashrafian *et al*., 2007).

Two challenges arise when addressing the diseased myocardium, which include the dynamics of cell death and the role of autophagy. Cardiac myocytes may die through three differential cell death pathways, namely autophagy, apoptosis and necrosis. These have previously been described as distinct static processes that induce and execute cell death. The accurate distinction between the modes of cell death is crucial, because of their association with cell loss in human pathologies (Lemasters, 1999, Degterev *et al*., 2005, Golstein & Kroemer, 2006). However, recent advances in reporting real-time data of dying cells suggest that cell death is a much more dynamic and molecularly overlapping event than previously described. Hence, there is a strong argument against a rigid classification of cell death mechanisms (Maiuri *et al*., 2007, Leist & Nicotera, 1997) which is supported by recent recommendations to exercise cautious use of cell death terminologies (Kroemer *et al*., 2009, Kroemer *et al*., 2005). Moreover, the existence of "grey zones" between cell death modes and the existence of the "point of no return" (PONR) within these have been revealed. This revelation challenges for the integration of new concepts in describing the cellular death process. It motivates the current challenge of re-defining and re-describing cell death modes and may necessitate a different more dynamic contextualization of known cell death

parameters. This may include the need for distinguishing between cells that are in the process of dying and dead cells to better locate and control the onset of cell death.

Secondly, although autophagy has been described as a mode of cell death, this degradation process of redundant or faulty cell components is constitutive in all cell types containing a lysosomal compartment. Autophagy occurs as part of the cell's daily activities and as a response to metabolic stress or starvation. However, extremely little is known about the role of autophagy in the heart and whether it is beneficial for the myocardial energy profile. Limited knowledge is available on the effects of autophagy and autophagic flux on the dynamics of apoptosis and necrosis onset in context of the intracellular metabolic environment, as well as the role of autophagically generated adenosine triphosphate (ATP) in this regard. Therefore, when adopting a view of cell death as a dynamic and integrative cellular response, the impact of autophagy on the cell's metabolic capacity and ATP availability has also to be assessed integratively.

Using H9c-2 myoblasts as model, the aims of this study are:

(i)

- to determine the contribution of each death mode in dependency of the duration and severity of simulated ischaemia
- to determine metabolic parameters
- to determine molecular parameters
- to relate results to *ex vivo* model

and (ii)

- to induce/inhibit autophagy and investigate the onset of cell death
- to determine necrotic cell death dynamically
- to determine apoptotic cell death dynamically
- to determine metabolic parameters

- to determine molecular parameters
- to relate results to *ex vivo* model

HYPOTHESIS

Firstly, it is hypothesized, that the relative contribution of each mode of cell death is dependent on the duration and severity of the ischaemic insult which is governed by the cell's underlying metabolic capacity at a given point in time. Secondly, it is hypothesized that the onset of apoptosis and necrosis depends on the cell's autophagic activity prior to the ischaemic event due its impact on the cells metabolic capacity.

If the above hypothesis is verified, then autophagy in the metabolically perturbed heart has to be re-evaluated as an underestimated contributor to energy-producing metabolism, and hence, a novel avenue for metabolic-based treatment.

An in-depth knowledge of the process and mechanism of autophagy, apoptosis and necrosis is required, in order to conduct this study. The following literature discussion addresses the current understanding of the cell death pathways, their molecular aspects in general as well as in the diseased myocardium.

Before that, however, and in line with this discussion and study, I would like to draw the attention to an important question: Are cells dying for the sake of dying or is cell death a response to ensure the highest likelihood of self preservation?
Therefore, the biochemical parameters and the morphology which indicate cell death might actually be a failed self preservation response.

CHAPTER 2 LITERATURE DISCUSSION

2.1. Introduction

The concept of damage control in the myocardium was for the first time introduced by Braunwald in 1974: "…just because myocardial tissue lies within the distribution of a recently occluded artery does not mean that it is necessarily condemned to death" (Braunwald, 1974). It has since been the aspiration to therapeutically reduce the amount of cell death which may be associated with a better clinical outcome. However, despite the development of various interventions to provide cardiac protection and to reduce the morbidity and mortality from myocardial infarction and heart failure, the residual death rate remains significant (Ashrafian *et al*., 2007). A constant effort is being made to identify therapeutic strategies with a growing focus on the improvement of cardiac energetics. Nevertheless, cardiac illness ranks as the most frequent cause of mortality, and has reached epidemic proportions (Cohen *et al*., 2000). It has been estimated that, in 10 years time, it will be the major cause of death in the world (Murray & Lopez, 1997).

The accurate distinction between the modes of cell death is crucial, because of their association with cell loss in human pathologies (Golstein & Kroemer, 2006). The recent advances in reporting real-time data of dying cells suggest that cell death is a much more dynamic and molecularly overlapping event than previously described (Degterev *et al*., 2005). Currently there is a strong argument against a rigid classification of cell death mechanisms (Maiuri *et al*., 2007, Leist & Nicotera, 1997) which is supported by recent recommendations to exercise cautious use of cell death terminologies (Kroemer & Galluzzi, 2009, Kroemer *et al*., 2005). This motivates the current challenge of re-defining and re-describing cell death modes and their underlying mechanism, and may necessitate a different more dynamic contextualization of known cell death parameters (Lemasters, 1999). Moreover, limited knowledge is available on the effects of autophagy and autophagic flux on

the dynamics of apoptosis and necrosis onset within the intracellular metabolic environment, as well as the role of autophagically generated adenosine triphosphate (ATP) in this regard.

The recognition of extensive cross talk between different cell death pathways begins to provide insights into the complexity of the cell death decision making process. It becomes clear that cell death with autophagy, apoptosis and necrosis molecularly interdigitates on various levels, and thus constructs a dynamic response. Its outcome may depend on a cell- specific net result of signals, which are governed by the type of insult, its duration, and the intracellular metabolic capacity to maintain a favourable cellular environment (Degterev *et al*., 2005, Izyumov *et al*., 2004, Bonfoco *et al*., 1995). This suggests the need for consideration of stress-, time- and response kinetics and demands precise use of multiple detection methods (Klionsky *et al*., 2008) as well as a clear terminology when reporting measured parameters (Kroemer *et al*., 2009, Kroemer *et al*., 2005).

In this literature discussion, cell death is viewed as a dynamic and integrative cellular response to ensure the highest likelihood of self preservation. Suggestions are offered for conceptualizing cell death modes and their morphological features, both individually and in relation to one another. It addresses the need for distinguishing between dying cells and dead cells so as to better locate and control the onset of cell death in the myocardium. Most importantly, the fundamental role of autophagy and the effects of the intracellular metabolic environment on the kinetics of the cell death modes are stressed.

This discussion will firstly introduce the different types of cell death, discussing their current definition and cell morphology. The signalling pathways forming the molecular basis for the morphological changes will then be addressed, as well as their key- and modulating molecules. The occurrence of each mode of cell death in the diseased myocardium will be addressed, as well as detection methodologies used to asses cell death. The molecular overlap of cell death pathways will be

examined, substantiating the view of a dynamic and integrative response concept. Importantly, the context of the energetic condition of the cell will be stressed, with the aim of dissecting out the relationship between energy availability, severity and duration of cellular stress and mode of cell death. Understanding the dynamic nature of the cell death process and autophagy's central role, new insights for therapeutic intervention in preventing cell death might be revealed.

Three main morphologies of cell death are described. Type I: apoptotic cell death, (Kerr, 1971) which is characterized by cell shrinkage and chromatin condensation. Type II: cell death with autophagy, (De Duve & Wattiaux, 1966, Schweichel & Merker, 1973) which presents a morphology with intracellular accumulation of autophagic vacuoles. Type III: necrosis, characterized by cellular swelling and rapid loss of cellular membrane integrity (Festjens *et al*., 2006). A cell may show morphological or molecular features characteristic of autophagy, apoptosis or necrosis without having *completely* lost membrane integrity, having undergone *complete* nuclear fragmentation or having been engulfed by a neighbouring cell (Kroemer *et al*., 2005). In other words, the cell is in the process of dying but still alive, as the membrane disintegration or nuclear fragmentation or engulfment is not yet complete. This bears the crucial possibility of cells being salvageable after the onset of dying. This view necessitates the recognition that cell death is induced as opposed to executed.

2.2. Autophagy

2.2.1. Definition and Role

Cells make use of two major systems for protein degradation, the ubiquitin-proteasome system for short-lived proteins and the vacuolar degradative pathway, also termed the lysosomal system, for long-lived proteins (Yorimitsu & Klionsky, 2005). The lysosomal system sources its material from intra- or extracellular loci. Degradation of exogenous materials and plasma membrane proteins is mediated

via endo- and phagocytosis, whilst degradation of cytoplasmic proteins and organelles is achieved by autophagy (Yorimitsu & Klionsky, 2005). This non-selective vacuolar degradation process is a highly conserved pathway within eukaryotes. Autophagy, from the Greek *self-eating*, was first described in 1965 (De Duve & Wattiaux, 1966); however, the extent of its physiological importance in maintaining cellular homeostasis only recently became clear.

Three types of autophagy are known: (i) chaperone-mediated autophagy (CMA), (ii) microautophagy and (iii) macroautophagy (Mizushima, 2005). CMA involves selective motif tagged protein translocation directly through the lysosomal membrane, (Dice, 2007) microautophagy involves the trapping and engulfing of cytosolic regions by lysosomes, and macroautophagy is characterized by the formation and accumulation of double membrane intermediate vesicles (Baba *et al*., 1994). Most importantly, macroautophagy is the primary mechanism for cytoplasm-to-lysosome delivery and is commonly termed autophagy. The possible degree of collaboration between these proteolytic systems (Mizushima, 2007) is influenced by growth conditions (Fuertes *et al*., 2003).

Macroautophagy is the primary mechanism for cytoplasm-to-lysosome delivery, and is commonly termed autophagy. Autophagy is the degradation of redundant or faulty cell components. This occurs as part of the cell's daily activities as a response to metabolic stress or starvation, which determines the flux through the autophagic pathway (Fig 2.1). Autophagy is mediated by a unique organelle, the autophagosome, and is constitutive in all cell types containing a lysosomal compartment. However, the cellular autophagic capacity varies between tissue type and tissue condition and determines a number of pathophysiological outcomes. It needs to be stressed that autophagy is a mechanism used by all mammalian cells to control and maintain protein homeostasis.

Autophagy not only governs the baseline turnover of intracellular proteins and organelles, but also drives the generation of amino acids under nutrient poor

conditions. These generated amino acids are recycled and provide an additional energy source for intermediary metabolism, ATP generation and biosynthetic pathways. On the one hand, in order to preserve normal cellular function, a fast and responsive degradation system for irreversibly damaged proteins is essential (the reader is directed to reviews Levine & Yuan, 2005, Codogno & Meijer, 2005, Klionsky, 2005, Hamacher-Brady *et al*., 2006). The dimension of time is crucial in a cell's response scheme. If this autophagic degradation system is not in place, proteins will rapidly undergo molecular interactions, leading to their accumulation and storage with adverse effects on the intracellular environment (Cuervo, 2004). Therefore, this "preventative" mechanism of protein replacement at a baseline level, when the cell is still functional, provides rapid adaptation to a changing environment and to changing cellular demands.

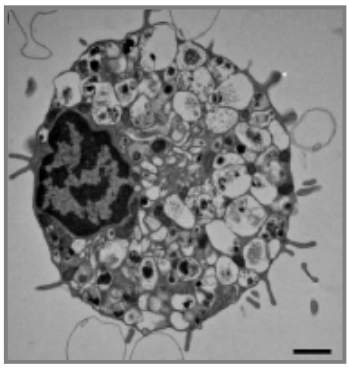

Figure 2.1: Representative cell with extensive accumulation of autophagic vaculoles, indicating type II cell death with autophagy. Increased autophagy is seen after 40 min of myocardial ischaemia (Edinger & Thompson, 2004).

2.2.2. The induction of Autophagy

Since the autophagic degradation mechanism is nonspecific and does not need a consensus protein motif, it allows for high capacity bulk degradation. In view of pathway flux through a system, this is advantageous, as it brings about a high degree of adaptability and efficiency. The identification of the genes underlying this process, which are termed autophagy-related-genes (ATG), greatly contributed to

the understanding of the molecular pathway and has led to the introduction of an ATG nomenclature to describe the molecular control of autophagosome formation. Autophagy related genes are designated as ATG and their proteins as Atg. The majority of ATG genes are conserved from yeast to human and even in plants (Cuervo, 2004). Three basic steps can describe the autophagic pathway:

(1). Formation of isolation membrane and preautophagosome
(2). Formation of Autophagosome
(3). Formation of autolysosome

(1). Formation of isolation membrane and preautophagosome

Inactivation of mammalian target of rapamycin kinase (mTOR kinase), induce the formation of a membrane sac, the isolation membrane, which elongates and encloses a fraction of the cytoplasm (Mizushima, 2005). The origin of the isolation membrane has not yet been identified; either it could be formed *de novo* or the endoplasmic reticulum (ER) could be the membrane provider (Cuervo, 2004). The assembly of what is called a preautophagosome now commences. Two coordinated conjugation events (Cuervo, 2004) drive this assembly and elongation of participating proteins in the formation of the isolation membrane.

In brief, in the first conjugation system, Atg proteins 5, 7, 10 and 12 undergo multimerization with Atg16. This leads to the formation of an Atg16 homotetramer which assembles with four Atg12-Atg5 conjugates. This complex exists in the cytosol, and only a small fraction of the complex localizes to the autophagic isolation membrane throughout the elongation process (Yorimitsu & Klionsky, 2005). Importantly, the Atg12-Atg5 conjugation is a constitutive process, since the complex is formed immediately after Atg12 and Atg5 synthesis, independent of starvation induced autophagy.

In the second conjugation system, the protein Atg8 is conjugated with phosphatidylethanolamine (PE). This process is dependent on Atg7 and Atg3. For the process to occur, Atg4, a cysteine protease, c-terminally cleaves Atg8 at a specific recognition site (Fass *et al*., 2007). This provides access to a glycine residue, needed for the conjugation of Atg8 with PE, a process mediated by Atg3. The first conjugation product is now needed to stabilize the Atg8/PE conjugation product. Atg8/PE or its mammalian homologue, microtubule associated protein 1-light chain 3 (MAP1-LC3) is required as a structural component of the autophagosome and is therefore recruited to the autophagosome membrane. The two conjugation systems are strongly interdependent. If the first complex is defective, the second one cannot be functional (Ferraro & Cecconi, 2007).

(2). Formation of Autophagosome

Two kinase complexes, PI3 kinase and Atg1, participate in the late stages of autophagosome formation, inducing tubulation of the autophagosome. Atg6 (and the mammalian orthologue, beclin-1) belong to the PI3 kinase (PI3-K) class III complex. Phosphatidylinositol 3-phosphate (PIP_3), the reaction product of the mammalian homologue PI3-K class III, Vps34, is also directed to the preautophagosomal membrane. Together with class III PI3-K, it possibly provides a scaffold on the post-Golgi membrane for supplying membrane components (Kihara *et al*., 2001). This complex therefore plays a key role in increasing the size of the pre-autophagosomal membrane. When Atg1 interacts with Atg13, progression towards a complete autophagosome takes place, where complete closure of the membrane leads to the sequestration of cytoplasm into a double-membrane cytosolic vesicle (Yorimitsu & Klionsky, 2005). At this stage the autophagosome maturation process has generated large structures of 300-900 nm. The Atg16-Atg12-Atg5 complex now dissociates, as the autophagosome formation is completed (Yorimitsu & Klionsky, 2005).

(3). Formation of autolysosome

The Atg9 membrane protein plays a role prior to the autophagosome closure. Fusion of the autophagosome sides to one another is followed by another fusion event between the autophagosome and lysosome, generating an autolysosome. The former autophagosomal and phagocytosed content now becomes accessible to hydrolases, and degradation and recycling can now take place (Cuervo, 2004). The degradation process takes place rapidly (5-10 min) due to the enormous accumulation of cathepsin proteases. The low pH and a thiolreductase ensure substrate denaturation.

2.2.3. Regulation and control of Autophagy

Nutrient deprivation, leading to a shift in the cytosolic AMP/ATP ratio is the usual stimulus for autophagy. However, regulation of autophagy induced by nutrient starvation seems to be an organ dependent process as it occurs in varying degrees in different organs (Yorimitsu & Klionsky, 2005). Autophagy is regulated mainly at the sequestration and maturation steps. One may differentiate between:

(1). Regulatory molecules upstream of the autophagic pathway,
(2). Key regulatory molecules of the autophagic pathway, and
(3). Modulating molecules, proximal to the autophagic machinery.

(1). Regulatory molecules upstream of the autophagic pathway

It is now generally accepted that mTOR kinase**,** as a nutrient sensor kinase, negatively regulates autophagy. This enzyme, which receives negative input from AMPK, may be interpreted as the ‘thalamic gateway to autophagic conscience’. mTOR itself is regulated through the class I phosphoinositol 3-kinase (PI3-K), that allows membrane binding and activation of Akt/PKB. Class I PI3-K phosphorylates phosphatidylinositol-phosphate (PIP) and phosphatidylinositol-4,5-bisphosphate (PIP_2) to generate phosphatidylinositol-3,4-bisphosphate and phosphatidylinositol-

3,4,5-trisphosphate (PIP_3), which bind via Pleckstrin Homology (PH) domains to protein kinase B (PKB/AKT) and its activator phosphoinositide dependent kinase 1 (PDK-1). Activation of this pathway has an inhibitory effect on autophagy.

mTOR is a sensor for amino acids and ATP and can integrate hormone stimuli via the class I PI3-kinase/PKB pathway. The phosphoinosite phosphatase, PTEN, positively regulates autophagy by inhibiting the actions of PI3-K (Klionsky, 2005). mTOR is controlled by specific amino acids, such as leucine and histidine (Nixon, 2006). The inhibitory effect of amino acids on autophagy can be relieved by rapamycin. Only a few amino acids are required for regulation, the number and kind varying among different tissues (Kadowaki *et al*., 2006).

mTOR acts in two ways:

Firstly, it directly or indirectly causes hyperphosphorylation of the autophagy protein Atg13. This protein modulates Atg1, a serine/threonine-specific kinase and appears to act as a convergence point for signals that regulate autophagy (Neufeld, 2007). When mTOR is not stimulated by nutrients, for example during starvation, or when it is inhibited by rapamycin, autophagosome formation is favoured and kinase activity of Atg1 increases. On the other hand, when mTOR is stimulated by nutrients, Atg13 becomes hyperphosphorylated which reduces its affinity to- and association with Atg1. This blocking of the association between Atg1 and Atg13 results in autophagy not being favoured. There is evidence that Atg1 might be sufficient to override nutrient signals to induce autophagy, since its over expression leads to rapid induction of autophagy (Neufeld, 2007). Furthermore, Atg1 overexpression strongly decreases mTOR activity, suggesting an mTOR Atg1 mutually antagonistic feedback loop possibly amplifying nutrient signals (Neufeld, 2007). However, the mammalian homologue of Atg1 has not yet been identified (Mavrakis *et al*., 2007). Furthermore, although Atg1 is a key regulator of autophagy, Atg substrates in that context have not yet been found (Deminoff & Herman, 2007).

Secondly, mTOR interacts with a signalling cascade that controls phosphorylation of effectors that regulate transcription and translation of specific proteins, some of which are required for autophagy (Klionsky, 2005). The protein kinase p70S6K is regulated by mTOR and plays a role in protein translation and autophagy activation (Klionsky *et al*., 2005). The inhibition of mTOR is also required to enhance the expression of specific autophagic genes, such as Atg8 and Atg14. Autophagy sequestration, fusion and degradation are ATP dependent processes. It is noteworthy to mention the association of mTOR with the outer mitochondrial membrane, where it is ideally situated to sense changes in the ATP/AMP ratio. Furthermore it also localizes with LC3-positive membranes, suggesting an involvement in the autophagosome maturation step (Mavrakis *et al*., 2007).

Amino acids play a central role in the regulation of mTOR, and therefore of autophagy. The autophagic machinery receives negative regulatory input from amino acids through different entry points on the cell. Leucine for example may be sensed at the plasma membrane, and can act on mTOR, on Class III PI3-K and the ERK signalling pathway, thereby inhibiting autophagy via those three avenues (Kadowaki *et al*., 2006). Other amino acids, such as glutamine, may act via the axis of integrins-p38 MAPK pathway, causing cell swelling and inhibition of autophagy (Kadowaki *et al*., 2006).

Metabolically, amino acid availability, which is modulated through autophagy, affects proteolysis and ATP generation. Amino acids may be the product of autophagic protein degeneration and a substrate for the citric acid cycle and ATP synthesis.

Recent data suggest that AMPK is required for autophagy in yeast as well as in mammalian cells. However, to what extent AMPK induces and mediates autophagy, is not known. AMPK negatively modulates protein synthesis, and

therefore switches off ATP dependent processes (Dyck & Lopaschuk, 2006). AMP binds to AMPK, inducing phosphorylation and activation of AMPK through LKB1 (Høyer-Hansen & Jäättelä, 2007). Autophagy itself is an ATP dependent mechanism and requires a certain degree of ATP input (Meijer & Codogno, 2007). Moreover, the cell can then survive for some time by utilizing autophagically generated amino acids feeding into the tricarboxylic acid cycle and to synthesize new proteins needed to adapt to the altered condition. In many cases, where AMPK is known to be activated, autophagic flux is increased. An example is the hypoxic environment, where AMPK activation is involved in maintaining energy homeostasis.

Autophagy induced by glucose deprivation in cardiac myocytes has been shown to inactivate mTOR and to activate AMPK. When AMPK is inhibited, the induced autophagic response is inhibited, suggesting a specific role of AMPK for autophagy in ischaemic events. Moreover, AMPK may be required for autophagy of mitochondria, since inhibition of mitochondrial ATP synthesis promotes massive autophagy of mitochondria (Meijer & Codogno, 2007).

(2). Key regulatory molecules of the autophagic pathway

Atg6/Beclin-1 is an evolutionary conserved protein family that functions in autophagy in yeast and mammals, as part of a complex with Class III PI3K/Vps34. This interaction is formed via a highly conserved beclin-1 domain, which is needed for autophagy to take place (Furuya *et al*., 2005). It was first described as a protein that interacts with bcl-2 in mouse brain, where its overexpression has been shown to reduce viral infection and neural cell apoptosis in sindbis virus encephalitis (Liang *et al*., 1998). Due to its properties of interacting with bcl-2 and its structure, it has been named beclin. Beclin-1 promotes autophagy as cells with reduced beclin-1 expression show reduced autophagy (Erlich *et al*., 2007, Yu *et al*., 2004). Traumatic brain injury has shown to dramatically elevate beclin-1 levels near the injury site (Erlich *et al*., 2006). Furthermore, heterozygous disruption of beclin-1

induces spontaneous tumours (Qu *et al*., 2003, Erlich *et al*., 2006). The beclin-1 gene is monoallelically deleted in 40-75% of cases of human sporadic breast, ovarian and prostate cancer (Qu *et al*., 2003). Furthermore, the disruption of beclin-1 increases the frequency of spontaneous malignancies and accelerates the formation of pre-malignant lesions (Qu *et al*., 2003). These findings indicate that beclin-1 functions as a haplo-insufficient tumour suppressor gene. Furthermore, endogenous beclin-1 is frequently expressed at low levels in human breast carcinoma epithelial tissue, but is highly and ubiquitously expressed in normal breast epithelia (Liang *et al*., 1999). The protein, beclin-1, is able to shuttle from the cytoplasm into the nucleus, where it loses its function in the control of autophagy and tumourigenicity.

Most interesting is the finding that beclin-1 binds to bcl-2, an important negative regulator of apoptosis. Beclin-1 has recently been identified as a novel Bcl-2-homology-3 (BH-3) only protein, carrying a BH3 domain. It interacts with Bcl-2 and its homologue Bcl-XL (Maiuri *et al*., 2007). Importantly, BH3 domains of other proteins, such as Bad, competitively disrupt this bcl-2/beclin-1 interaction, which causes autophagy of mitochondria (mitophagy). However, only ER targeted Bcl-2 can inhibit autophagy induced by beclin-1, suggesting a spatial organization of autophagy and apoptosis control (Maiuri *et al*., 2007). Bcl-2 inhibits autophagy through its direct interaction with beclin1. Bcl-2 downregulation increases autophagy. This might possibly function as a homeostat, maintaining autophagy for cellular survival (Levine & Yuan, 2005). Beclin-1 physically interacts with several Bcl-2 antiapoptotic proteins, an interaction which may be disrupted by proapoptotic proteins (Erlich *et al*., 2007). It has been hypothesized that this interaction may sensitize cells to apoptosis, due to neutralizing the antiapoptotic effect and additionally inhibiting autophagy (Erlich *et al*., 2007).

Recent literature points out that the PI3-K signalling pathway also controls autophagy, despite its known antiapototic effects (Levine *et al*., 2008, Sarbassov *et al*., 2005, Petiot *et al*., 2000). PI3-K belongs to a family of enzymes that

phosphorylates the 3'-hydroxyl group on the inositol ring of phosphoinositides. It is involved in signal transduction pathways which control, for example, differentiation and apoptosis (Petiot *et al*., 2000, McIlroy *et al*., 1997). Due to their control of proliferation and survival, they are attractive drug targets (Stephens *et al*., 2005). The PI3-K/Akt signalling pathway encompasses enzymes with known anti-apoptotic functions (Walls *et al*., 2007). Distinct classes of PI3-K control autophagy in opposite directions. The product of class III PI3-K is required for autophagy, whilst the products of class I PI3-K have inhibitory effects (Codogno & Meijer, 2005).

Interestingly, glucose deprived H9c-2 cells, derived from rat cardiomyocytes, have been shown to undergo cell death with autophagy, which could be reduced with 3-methyladenine (3MA), an inhibitor of the autophagic pathway (Aki *et al*., 2003, Seglen & Gordon, 1982). However, when the dominant negative PI3-K class I was overexpressed, this mode of cell death was accelerated (Aki *et al*., 2003). In human colon cancer, HT-29 cells, it has been shown that an increase in class I PI3-K products reduced autophagy. In contrast, an increase in class III PI3-K products stimulates autophagy, which is inhibited when silencing class III PI3-K (Petiot *et al*., 2000). The distinct functional roles of the two families of kinases also become clear when considering their product localization. Phosphatidylinositol 3-phosphate, PI(3)P, has been shown to accumulate to a great extent, but transiently, on the phagosomal membrane; however, it is only detectable after the phagosome has sealed (Vieira *et al*., 2001). Class III PI3-K, which is responsible for PI(3)P synthesis, is essential for phagolysosome formation, whilst class I PI3-K is required for optimal phagocytosis, but not phagosomal maturation (Vieira *et al*., 2001). Class III PI3-K is anchored to cytoplasmic membranes via the p150 adaptor protein, which is the homologue to the yeast Vps 15 protein. In mammalian cells, this adaptor/enzyme complex is associated with the protein, beclin-1. Furthermore, distinct roles of the two classes have been described regarding control and regulation of the actin cytoskeleton, vesicular trafficking and insulin-stimulated DNA synthesis (Siddhanta *et al*., 1998).

(3). Modulating molecules, proximal to the autophagic machinery

A role for MAPKs in the control of the maturation step has been proposed. Evidence is provided that especially the MAPK, ERK, is involved in the regulation of the autophagosome maturation process. Furthermore, inhibition of p38 has been shown to promote autophagosome accumulation (Corcelle *et al*., 2007). In a colorectal cancer cell line, a p38 inhibitor or genetic ablation of p38α kinase induced cell cycle arrest and autophagy (Simone, 2007). Furthermore, p38 is activated in the regulation of autophagy associated with cell swelling. This process is sensitized by integrins, which in turn activates Src to activate p38 and leads finally to suppression of autophagy (Codogno & Meijer, 2005).

2.2.4. Autophagy in the myocardium

Already 30 years ago, autophagy has been described in cardiomyocytes and has been emphasized as an important repair mechanism during sublethal injury. Especially because of the terminally differentiated nature of cardiomyocytes, a functional degradative system like autophagy is essential for cellular function. It was observed that a fetal mouse heart, kept for 1 h in organ culture, undergoes autophagy, which was accelerated by oxygen and glucose deprivation. However, its function could be restored following resupply of oxygen and glucose. It was also observed that when the period of injury lasted for three to four hours, many cells became necrotic (Sybers *et al*., 1978). Two years later, Decker and co-workers observed the initiation of lysosomal autophagy during and after hypoxia in perfused rabbit hearts, and highlighted the role of this phenomenon as a repair effort employed by cardiac cells (Decker & Wildenthal, 1980).

Thirty years later, autophagy and its role in cell survival and death is a growing focus of attention in cardiovascular research; however, only a limited number of studies have determined the role of autophagy in the myocardium. For unknown

reasons, cell death with autophagy has not previously been considered as a significant role player in ischaemia.

Recent studies have demonstrated that autophagy occurs in the hypertrophied, failing and hybernating myocardium (Kunapuli *et al*., 2006). In an anoxia/reoxygenation study of isolated cardiomyocytes, the inhibition of autophagy caused an inrease in the number of necrotic cells, which was dramatically increased when apoptosis was inhibited simultaneously (Dosenko *et al*., 2006). Autophagy is induced by ischaemia and reperfusion (Takagi *et al*., 2007). However, the activation mechanisms seem to differ. Firstly, glucose deprivation but not serum starvation strongly induces myocyte autophagy (Matsui *et al*., 2007). Amino acid deprivation also induces autophagy, however not as strongly as the former. These results indicate the role of a differential autophagic response, depending on the intracellular metabolic microenvironment.

In failing human hearts it has been shown that the three cell death modes act in parallel to varying degrees, as assessed by terminal deoxytransferase-mediated dUTP nick-end labeling (TUNEL), complement 9- and ubiquitin labelling (Kostin *et al*., 2003). The tissue was sampled from the left ventricular free wall of hearts from patients with end stage heart failure due to idiopathic dilated cardiomyopathy. However, the exact state of tissue in terms of cell composition, bioenergetics and vascularization has unfortunately not been investigated. The incidence of autophagic cardiomyocytes in failing hearts has been shown to be greater than the incidence of apoptotic cells (Takemura & Fujiwara, 2006).

Autophagy has also been described in the ischaemic myocardium after six episodes of ischaemia. An increase in cathepsin D, beclin-1 and other autophagic indicators were observed. Most interestingly, apoptosis was activated after the first episode, attenuated after three episodes, and then decreased drastically after 6 cycles. Apoptosis was present primarily in patchy areas of necrosis. These results indicate the stress dependent response of the myocardium with all three response

schemes, autophagy, apooptosis and necrosis (Yan *et al*., 2005). It has been suggested that autophagy participates in the phase leading from cardiac hypertrophy to cardiac failure, and that load-induced activation of autophagy is maladaptive, as it amplifies pathological remodelling of the heart (Rothermel & Hill, 2007). These findings underline the fine line between autophagy as adaptive response, and autophagy which becomes maladaptive when, although metabolically viable, the cell cannot functionally perform.

2.2.5. Detection Methods for Autophagy

The detection methodology determines the extent of pathway characterization. A number of aspects of the molecular machinery can be monitored. However, only a limited number of specific molecular marker proteins are available to monitor the autophagic process due to lack of differential gene expression. This is the case especially for higher eukaryotes. A combination of analytical techniques seems to be necessary to gain best insight into the dynamic nature of the autophagic pathway (Klionsky *et al*., 2007).

Transmission electron microscopy (TEM) remains the standard method for monitoring autophagy in tissue; however, it is labour intensive and gives no indication of the progress within or flux through the autophagic pathway. A growing body of evidence suggests that mammalian microtubule-associated protein 1 light chain 3, LC3, which functions as a structural component during autophagosome maturation, is a reliable biomarker for autophagy (Martinet *et al*., 2006). The major challenge is that the level of autophagosomes, as measured through LC3 visualization, is not equivalent to the flux through the autophagic system (Brady *et al*., 2006). The punctate and ring-shaped structures of GFP-LC3, which can be visualized through fluorescence microscopy, have been proposed as a good molecular marker for isolation membranes and autophagosomes (Yorimitsu & Klionsky, 2005). Autolysosomes, on the other hand, are only weakly stained (Mizushima, 2004). Therefore, this pattern does not indicate the autophagy

process per se (Klionsky, 2005). Furthermore, not only can LC3 be present under normal nutrient conditions, but is also rapidly degraded during autophagy (Martinet *et al*., 2006). Changes in the steady state concentrations of pathway intermediates do not give any conclusive information about the flux through the pathway. Low levels of LC3 may in fact be indicative of very active autophagy, and high LC3 levels may indicate the opposite.

Monitoring lysosomal LC3 turnover in the absence and presence of inhibitors would circumvent this problem and has been proposed as a new methodology standard (Klionsky, 2005). Inhibition of lysosome activity by protease inhibitors, for example, would represent the cumulative autophagic activity at a given time point (Mizushima, 2004). Overexpression of GFP-linked LC3, using lysosomal protease inhibitors, in combination with TEM, fluorescence microscopy and immunoblotting analysis seems to be an elegant and thorough solution for monitoring autophagy. Via immunoblotting, the ratio of unlipidated cytosolic LC3-I to autophagosome-associated phosphatidylethanolamine-modified LC3-II, can be semi-quantified electrophoretically (Kabeya et al., 2000). The 16 kD to 18 kD ratio correlates with the extent of change in LC3 conversion (Mizushima, 2004). The amount of LC3-II clearly correlates with the number of autophagosomes (Mizushima & Yoshimori, 2007). However, LC3-II itself is degraded by autophagy, making interpretation of results problematic. Furthermore, the increase in LC3-II is often much larger than the decrease in LC3-I, due to their different immunoreactivity (Mizushima & Yoshimori, 2007). A comparison of LC3-II between samples in the presence or absence of lysosomal protease inhibitors is again advised, rather than summation of LC3-I and LC3-II (Mizushima & Yoshimori, 2007). An increase in the LC3-II signal despite the presence of a lysosomal protease inhibitor would indicate increase in autophagic flux (Mizushima & Yoshimori, 2007).

A combination with real-time observation in living cells is a feasible approach to trace organelle autophagy (Mizushima, 2004) using mitotracker and lysotracker dyes. The use of fluorescent LC3 and a counter-fluorescent lysosmal- or

mitochondrial marker allows the entire autophagic process to be followed (Bampton *et al*., 2005). Another challenge, however, lies in the fact that the extent of LC3 accumulation is cell line dependent (Klionsky, 2005). In some pathologies, additional immunohistochemical detection of granular cytoplasmic ubiquitin inclusions may be used as an additional indicator for autophagic cell degeneration (Martinet *et al*., 2006).

For immunocytochemistry analysis, care should be taken with the use of detergents in the fixation and pemeabilisation protocol, as for example, saponin, Triton X-100, CAPS or digitonin have been shown to induce fluorescence puncta regardless of autophagy induction (Ciechomska and Tolkovsky, 2007). Also, especially in cells transiently overexpressing LC3, aggregates and punctate dots containing LC3 have been described, calling for careful interpretation in these cases (Kuma *et al*., 2007). Furthermore, recently a tandem fluorescent reporter protein has been suggested to avoid the degradation of GFP-LC3 due to lysosomal and acidic conditions. Here a construct using a mRFP-GFP tandem fluorescent-tagged LC3 has been shown to give useful information about the maturation process, as the monomeric red fluorescent protein is stable in an acidic environment (Kimura *et al*., 2007).

2.3. Apoptosis

2.3.1. Definition and Role

In the 1960s it was observed that ischaemic liver tissue showed scattered hepatocytes in surviving parenchyma, with small masses of cytoplasm and specks of condensed nuclear chromatin. The name shrinkage necrosis was suggested (Kerr, 1971). Early in the 70s Currie, Wyllie and Kerr detected shrinkage necrosis in a set of other experiments, and it became clear that this distinctive form of cell death with defined ultrastructural features was an inherent programmed

phenomenon with homeostatic function on cell population size (Kerr *et al*., 1972). It was decided to name it apoptosis, a morphological term from the Greek “falling off”, as autumn leaves fall off trees in an inherently seasonal manner. This homeostatic role of selected apoptosis is manifest, not only in the embryological process, but also ongoing in the adult organism, such as in the control of the formation and maintenance of glandular architecture (Debnath *et al*., 2002).

Cell shrinkage is combined with pyknosis (chromatin condensation) and karyorrhexis (nuclear fragmentation) (Fig 2.2). At an early stage, condensed chromatin tends to marginate in crescents around the nuclear envelope. The plasma membrane of the cell begins to bleb, which will lead to apoptotic bodies, if phagocytes are not present (Denecker *et al*., 2001). Apoptosis may be separated into phases of initiation or induction, integration or determination and execution. It might be of importance to integrate these phases into apoptosis as process, represented by the induction- and integration phase versus apoptosis as endpoint, represented by the execution phase. These phases would be separated by the point of no return, where induction changes to execution. Induction involves the introduction of apoptotic stimuli or signals (Takemura & Fujiwara, 2006). During determination, the signal is transferred to the nucleus, where it controls expression of proapoptotic or prosurvival mediators. In biochemical terms, the execution is a well preserved phase of the death machinery.

The term apoptosis was originally used to describe a defined morphology, however, criticism has been raised, that the same terminology is now being used to describe a concept (Sloviter, 2002). The exact description of molecular and morphological events has therefore been urged (Kroemer *et al.*, 2009).

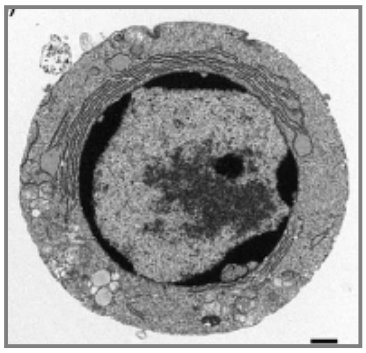

Figure 2.2: Type II, apoptotic cell death. This type of cell death is morphologically characterized by cell shrinkage and pyknosis, and occurs after 2-4 hrs of coronary artery occlusion (Edinger & Thompson, 2004).

2.3.2. Pathway of Apoptosis

The signal for apoptosis can either arise from the extracellular or intracellular environment, giving rise to an intrinsic and extrinsic apoptotic pathway (Galluzzi *et al*., 2007). The intrinsic pathway of apoptosis relies on mitochondria to integrate and release a number of regulatory components that subsequently activate caspase proteases, which in turn cleave death- inducing substrates. Central to the intrinsic pathway are mitochondria, which in this context, are literally a matter of life and death in the cell. For life, due to their crucial role as ATP provider through the process of oxidative phosphorylation, for death, due to their role in sequestering pro-apoptotic signals and in releasing cytochrome c, required for cytosolic caspase-9 activation. Moreover, mitochondrial Ca^{2+} uptake has been shown to be critical in initiating depolarization of mitochondria and propagating an apoptotic signal by mitochondrial waves (Pacher & Hajnóczky, 2001). In contrast, the extrinsic pathway relies on extracellular death ligands, which transmit the signal via caspases within the cytoplasm, which ultimately activate the same executioner caspases as employed by the intrinsic pathway.

Caspases have been subdivided into subfamilies, based on their substrate preference and extent of sequence identity. Functionally, caspases can be classified into three groups. Firstly there are initiator caspases, containing a death effector domain (DED), such as caspase-8 and caspase-10, or a caspase activation and recruitment domain (CARD), such as caspase-2 and -9. Both domains interact with complementary domains from adaptor proteins in order to cluster initiator caspases and subsequently to induce autoproteolysis. Secondly, there are effector or executioner caspases, such as caspase-3, -6 and -7, which contain short prodomains. Lastly, there are also caspases involved in immune control. Importantly, activated initiator caspases induce a proteolytic cascade with all benefits of signal amplification, by activating downstream effector caspases (Kunapuli *et al*., 2006). Caspases are synthesized as zymogens, which can be activated by either proteolytic cleavage, by self activation or through interaction with a regulatory subunit (Hengartner, 2000). The caspases cleave a restricted set of target proteins at a position after an aspartate residue. Close to 100 caspase substrates have been suggested, indicating the complexity of this molecular death programme.

A number of models have been developed for the mitochondrial release of apoptogenic factors, however, none of them has been proved. They involve either pore/channel formation in- or rupture of the outer mitochondrial membrane. In this pathway, the mitochondrial outer membrane permeability (MOMP) is activated and triggers the release of apoptogenic factors such as cytochrome c, apoptosis inducing factor (AIF), SMAC (Second mitochondria-derived activator of caspase)/DIABLO (Direct IAP-Binding Protein with low pI) and the serine protease, Omi/HtrA2. The mitochondrial membrane permeabilization (MMP) has been considered as point-of-no-return in the process of apoptosis. Cytochrome c contributes to caspase-9 activation via the formation of a cytosolic apoptosome complex with subsequent caspase-3 activation.

The integrity of the mitochondrial membrane is largely under the control of the Bcl-2 family (Denecker *et al*., 2001). At least 20 members of the Bcl-2 family have been identified, all sharing at least one Bcl-2 homology (BH) domain. MOMP is regulated by members of the Bcl-2 family. Members of this family can homodimerize, but can also form pro/anti-apoptotic heterodimers (Hengartner, 2000). This capability gives rise to a large number of dimer combinations within a cell, providing a large information network pool, which can sensitize or desensitize the cell to commit to a death pathway, including the neutralization of signals (Hengartner, 2000). The bcl-2 family of proteins can be divided into three groups, based on their conserved bcl-2 homology domains. The prosurvival members are Bcl-2, Bcl-XL, Bcl-w and A1, which all contain BH1-4 domains. Bcl-2 is anchored to the outer mitochondrial and endoplasmic reticulum membrane and blocks the release of mitochondrial cytochrome c into the cytoplasm (Grandgirard *et al*., 1998). The proapoptotic members, on the one hand, can be further divided into those containing only one BH3 domain, the so called BH3-only proteins. These include Bad, Bid, Bik, Bmf, Bim, Hrk, Noxa and Puma and act as apoptosis sensors. On the other hand there are members such as Bak, Bax and Box, which contain multi-BH3 domains and serve as executioners of apoptosis (Shroff *et al*., 2007). Importantly, cell death during anoxia occurs via the bcl-2 regulated intrinsic apoptotic pathway (Shroff *et al*., 2007). Whilst anti-apoptotic Bcl-2 and Bcl-xl block MOMP, the pro-apoptotic BH3-only proteins, Bim and Bid promote MOMP via activation of the multi-domain proteins Bax and Bak (O'Connell & Stenson-Cox, 2007).

The extrinisic pathway relies on extracellular death ligands to recruit and integrate adapter proteins that recruit the initiator caspases-8 and 10. In brief, extracellular death signals, such as TNF-α or Fas-L, bind to their receptor, inducing it to form a trimeric complex, which then recruits a number of intracellular adaptor proteins, forming a complex known as death-inducing signalling complex or DISC. DISC formation leads to the recruitment and activation of the initiator caspases (Kunapuli *et al*., 2006), which starts the proteolytic cascade. Caspase-8, once activated, cleaves and activates procaspase-3 as well as Bid. In that way Bid connects the

extrinsic and intrinsic pathway, as truncated Bid triggers the activation of Bax and Bak with subsequent cytochrome c release.

Both extrinsic and intrinsic pathways merge on the level of execution with caspase-3, which is activated and whose proteolytic activity results in cell death. Caspase mediated cleavage of the nuclear lamins is required for nuclear condensation and fragmentation (Hengartner, 2000). However, a network model of this simplistic dichytome pathway view has been suggested, taking into account that different components of the death machinery differ in their impact on system performance (Kimchi, 2007). In this context, high throughput genome screening of cells exposed to death signals identified a large number of death promoting genes, encoding so called death associated proteins (DAP) confirming this model (Kimchi, 2007). One of the most extensively studied proteins is DAP-kinase, a Ca^{2+} regulated Ser/Thr kinase, whose substrates are involved in membrane blebbing and cell death with autophagy (Kimchi, 2007). It has therefore been suggested that this kinase acts as a molecular switch, driving the cell's phenotypic outcome in different directions.

2.3.3. Modulating molecules of the apoptotic pathway

A large number of molecules inducing apoptosis have been described. However, the signalling mechanism within the network of pro-apoptotic triggers is less well understood. In particular, the molecular overlap of the signalling pathway inducing apoptosis in context with the cell's metabolic profile remains to be elucidated.

Biological oxidants, peroxynitrite, free radicals, and superoxides have been shown to be triggers of apoptosis (Levrand *et al*., 2006). Mitogen activated protein kinases (MAPKs) play a distinct role in modulating apoptosis and therefore, the fate of the cell (Wang *et al*., 1998). Induction of apoptosis in HeLa cells using H_2O_2 caused a sustained activation of all three MAPK subfamilies, namely extracellular signal-regulated protein kinase (ERK), c-Jun N-terminal kinase/stress-activated protein kinase (JNK) and p38 (Wang *et al*., 1998). Apoptosis was enhanced when ERK

activation was inhibited (Wang *et al*., 1998). In this model, however, p38 inhibition had no effect on apoptosis. Furthermore, it has been shown that c-Jun N-terminal kinase/stress-activated protein kinase (JNK) inhibitory mutants almost double their rate of apoptosis, induced by oxidative stress and reperfusion injury (Dougherty *et al*., 2002). Interestingly, ERK has been shown to induce α-enolase, a rate limiting enzyme in the glycolytic pathway (Mizukami *et al*., 2004). Therefore, a direct ERK modulated molecular link might exist between ATP availability and induction of apoptosis (Mizukami *et al*., 2004).

Local metabolic conditions and the intensity of the initial insult determine the prevalence of either apoptosis or necrosis (Nicotera *et al*., 1999). There is evidence that this decision is controlled on both the mitochondrial and caspase activation levels (Stridh *et al*., 1999). In both *in vitro* and *in vivo* studies where ATP was depleted by phosphate-trapping carbohydrates such as fructose, TNF-induced apoptosis was completely blocked (Latta *et al*., 2000). In glucose deprived rat neonatal cardiac myocytes exposed to hypoxia, a significant positive correlation between myocyte ATP concentration and percentage apoptotic cells has been described. In particular, ATP generation through glycolysis is a determinant of the form of cell death, independent of cellular acidification (Tatsumi *et al*., 2003). This indicates that a possibly preferred apoptotic mode of cell death with caspase activation can be replaced by an ATP independent pathway, such as necrosis. On the other hand, several caspases may possibly have vital functions that are not death related, indicating that their activation may not always indicate cell death (Nicotera *et al*., 1999). Interestingly, loss of mitochondrial transmembrane potential and cytochrome c release has been observed in both apoptotic and necrotic cells (Shiraishi *et al*., 2001, Tatsumi *et al*., 2003).

Interestingly, proteolytic mediators involved in necrotic cell death, such as cathepsins, have also been described as role players in apoptosis (Leist & Jäättelä, 2001). This view is supported by the notion that the caspase inhibitor zVAD-fmk efficiently blocks cathepsin B (Leist & Jäättelä, 2001). Moreover,

interactions between cathepsins and caspases, such as cathepsin B mediated caspase-3 activation, might synergistically control the induction of either apoptosis or necrosis (Yamashima, 2000, Yamashima, 2004). Other physiological factors, such as hormonal feedback mechanisms also appear to have an impact on apoptosis induction (Zhu *et al*., 2006).

2.3.4. Apoptosis in the myocardium

Over the last 10 years, increasing evidence has suggested an important role for apoptosis in myocyte death (Takemura & Fujiwara, 2006). Myocardial apoptosis has been detected in a number of cardiovascular pathologies such as ischaemia/reperfusion injury, myocardial infarction, hypertrophy, heart failure and hypoxia. In experimental models for myocardial infarction it has been shown that particularly in the first 2-4 hours of coronary artery occlusion, most cell death manifests with apoptotic morphology (Kajstura *et al*., 1996). Importantly, research indicates that apoptosis is deeply involved in the pathology of almost all types of heart disease. Due to the central position of apoptosis, which occurs most likely time wise between cell death with autophagy and necrosis, this is of particular importance. TUNEL positive cells are especially increased at the borders of subacute and old infarcts, indicating apoptotic cell death which might be dependent on the metabolic environment across the injury. Moreover, bcl-2 has been shown to be overexpressed in the surviving cardiomyocytes around the acute infarcted region (Takemura & Fujiwara, 2006).

There is substantial evidence that the MAPKs ERK, p38 and JNK are activated in cardiac myocytes in response to stress. For example, in rat neonatal cardiac myocytes exposed to ischaemia, a rapid activation of these MAPKs is observed. Reoxygenation further activates the MAPKs, which lead to morphological characteristics of apoptosis in 18% of cells (Yue *et al*., 2000). However, when pretreated with an ERK inhibitor, the number of cells showing apoptotic morphology increased to 33%, indicating a protective role of ERK. On the other

hand, p38 and JNK have been shown to mediate apoptosis in cardiomyocytes subjected to ischaemia/reperfusion (Yue *et al*., 2000). Other models have shown an increase in JNK activation only upon reperfusion, but not by ischaemia alone (Engelbrecht *et al*., 2004). Antisense oligonucleotide treatment targeting JNK isoforms revealed that the JNK1 isoform plays a preferential role in apoptosis induced by ischaemia/reperfusion (Hreniuk *et al*., 2001).

2.3.5. Detection Methods for Apoptosis

Usually a combination of techniques is employed to report morphological features and to assess the process of apoptosis (Krysko *et al*., 2008). Various methodologies are available to describe and quantify the characteristic morphological and molecular changes associated with apoptosis. Electron microscopy is the gold standard for diagnosing apoptosis, providing most convincing evidence for the presence of an apoptotic morphology and ultrastructure (Takemura & Fujiwara, 2006). A number of biochemical markers have been used to identify the onset of apoptosis. DNA fragmentation into 180-200 base pairs, manifesting in a DNA ladder, can be assessed through gel electrophoresis - the DNA ladder is opposed to the DNA smear found in necrosis.

Furthermore, the TUNEL assay has been used widely for apoptosis detection, where the dUMP is attached to the 3' end of DNA, which is then visualized using fluorescence microscopy. However, false positive TUNEL results have demanded additional techniques. Another hallmark for apoptosis is the loss in membrane polarization, leading to translocation of phosphatidyl serine from the inner to its outer leaflet. Phospholipid binding proteins, such as Annexin-V, interact in a Ca^{2+} dependent fashion with phosphatidyl serine, which can be visualized through immunocytochemical techniques, using flow cytometry or microscopy.

An efficient clearance mechanism of dying cells is crucial for tissue homeostasis, not only for modulation of immune responses, but also for a functional living

organism in general. *In vivo*, under pathological conditions, apoptosis and necrosis may often co-exist (Nicotera *et al*., 1999). In this regard it has been demonstrated that necrotic cells can also externalize phosphatidylserine, a hallmark for early apoptosis, indicating - at least in part - a controlled mechanism of necrotic cell death (Krysko *et al*., 2006). Another emerging technique to detect apoptosis is time-lapse imaging. Time-lapse imaging allows morphological changes to be followed, and gives insight into the dynamics of apoptosis as process. A combination of epifluorescence- and differential interference contrast- microscopy allows molecular- and general cell morphology to be monitored (Krysko *et al*., 2008). Furthermore, changes in the nucleus through pyknosis or karyorrhexis lead to specific patterns of cellular granularity or internal complexity, which can be examined through fluorescence microscopy or flow cytometry.

Flow fluorocytometry is effectively employed to identify morphological changes, simply through the characterization of the forward and side scatter pattern of a given cell population. Cell permeable fluorochromes, such as propidium iodide, and surface markers such as Annexin V, can be used to distinguish early and late stage apoptotic cells from necrotic cells (Krysko *et al*., 2008). Immunoblot detection techniques or multi-colour fluorescence microscopy are widely used techniques to determine subcellular protein redistribution of cytochrome c or AIF, and are often used in combination with colocalization studies using mitochondrial markers. As caspase-3 cleavage and downstream poly (ADP-ribose) polymerase (PARP) cleavage are crucial components within the apoptotic pathway, their activation and cleavage in living cells can be used to determine the onset of apoptosis dynamically. Using fluorescence-resonance energy transfer (FRET) with a suitable FRET pair, possessing the caspase-3 cleavage sequence, the cellular commitment to apoptosis can be visualized and temporal and spatial interrelationships described (Tyas *et al*., 2000).

2.4. Necrosis

2.4.1. Definition and Role

Necrosis, from the Greek “death, causing to die”, is a degenerative process in which cellular integrity is completely lost, causing the cell to die (Hamacher-Brady *et al*., 2006). The term has been used for about 2 000 years to define drastic changes in tissue, visible to the naked eye (Kunapuli *et al*., 2006). Necrosis is characterized by cytoplasmic swelling, irreversible plasma membrane damage and irreversible changes in the nucleus such as pyknosis, karyorrhexis and karyolysis as well as organelle swelling and breakdown (Fig 2.3) (Festjens *et al*., 2006). Necrosis has historically been described not as a controlled mode of cell death, but rather as a passive and accidental process that is a consequence of physical and chemical stress. However, recent literature shows that necrosis is a result of a well-orchestrated interplay of signalling cascades, with an extensive crosstalk between biochemical and molecular events on various cellular levels. Furthermore, some signalling molecules, which play a role in autophagy and apoptosis, are also found to take part in this “programmed necrosis” (Edinger & Thompson, 2004). Physiological settings where necrosis occurs, include immune defence mechanisms, chondrocytes in the mammalian growth plate, ovulation and colon epithelial cell turnover (Festjens *et al*., 2006). Programmed necrosis has been described in actively proliferating cells in response to DNA damage, where it was initiated through hyperphosphorylation of the DNA repair protein, PARP (Edinger & Thompson, 2004). Moreover, necrosis has been implicated in a number of pathological settings, such as neurodegenerative diseases, stroke and ischaemia. It has also been described as a role player in tumour promotion and growth (Han *et al*., 2008).

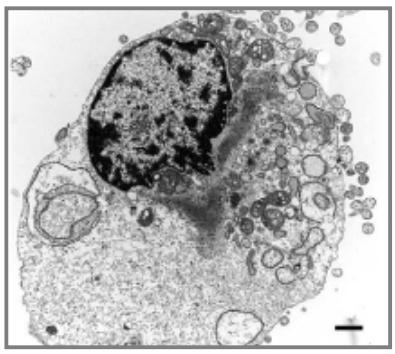

Figure 2.3: Type III, necrotic cell death. This morphology is seen in the central zone of myocardial infarction (Edinger & Thompson, 2004).

2.4.2. Pathway of Necrosis

Different experimental systems representing various cell types and death inducers have demonstrated a common sequence or programmed course of intracellular events specific to necrotic cell death. This sequence includes mitochondrial dysfunction and swelling, ROS production and perinuclear clustering, ATP depletion, loss of Ca^{2+} homeostasis as well as the activation of calpains and cathepsins with subsequent lysosomal- and plasma membrane rupture (Golstein & Kroemer, 2006). It has been suggested that necrosis serves as the cell's default pathway, as inhibition of apoptosis and autophagy can induce necrosis (Golstein & Kroemer, 2006). This is the case when the mitochondrial membrane permeabilization (MMP) is suppressed and at the same time pro-apoptotic proteins and beclin-1 are knocked out. In other models the deletion of functional caspases is sufficient to induce necrotic cell death. Both cases show that apoptotic signalling directs the pathway flux and the apoptotic capacity determines at what time point this new pathway is entered. Sufficient ATP is needed for caspase activation as well as for the rearrangements of the cytoskeleton for trafficking and clustering.

ATP generation, either via glycolysis or mitochondrial oxidative phosphorylation, is needed to execute nuclear pyknosis, DNA fragmentation and phosphatidylserine exposure (Denecker *et al*., 2001). Most interestingly, due to the PARP induced rapid cytoplasmic NAD depletion, glycolysis is inhibited, inducing an ATP dependent necrotic cell death (Edinger & Thompson, 2004). This would indicate that PARP activation runs a metabolic test on the cell, which results in a decision between necrosis or cell survival and DNA repair. Inactivation of PARP through caspase mediated cleavage would preserve the intracellular ATP pool and would allow apoptosis to proceed and to be completed (Denecker *et al*., 2001). How much PARP induced DNA repair a cell can metabolically afford, before entering necrosis, remains to be elucidated.

Necrotic cells are found in the central zone of the infarct, indicating a relationship between the mode of cell death and the metabolic microenvironment of the tissue. In the setting of acute myocardial infarction, there is a need for therapy that reduces the amount of necrosis, leading to a better clinical outcome (Kloner & Rezkalla, 2004). Necrotic cell death of cardiomyocytes is a major contributor to heart failure associated with cardiac pathologies such as ischaemia/reperfusion injury (Tavernarakis, 2007). It is therefore crucial to understand the underlying molecular mechanisms generating the cellular morphology so characteristic for necrosis. PI3-kinase is known to activate glucose metabolism. In myoblasts dying from hypoxia- induced necrosis, PI3-K accelerates this mode of cell death, due to its acidosis inducing effects (Aki *et al*., 2001). This highlights the role of glucose metabolism and anaerobic glycolysis in hypoxia and its effect on the mode and extent of cell death (Aki *et al*., 2001).

2.4.3. Regulation and control of Necrosis

The current state of knowledge cannot yet provide clear distinctions between induction, propagation and execution of necrosis. Death receptors, belonging to the TNF-receptor super family, play a crucial role in transmitting extracellular stimuli

and to induce a stress response. The pleiotropic cytokine and ligand TNF-α mediated receptor-induced necrosis has been well described in L929 cells (Denecker *et al*., 2001, Denecker *et al*., 2001), which can be inhibited with antioxidants or a respiratory chain complex I inhibitor, indicating the profound role of ROS generation. In contrast to apoptotic cells, cells undergoing necrosis are still able to synthesize proteins (Saelens *et al*., 2005), which supports the fact that necrosis may also be programmed. Synthesis of proteins is sustained and the rate remains constant until the cell loses its membrane integrity. It has been suggested that this extended time window for protein translation might result in newly synthesized products that alert other cells, or can provide “danger” signals for immune competent cells.

2.4.3.1. Inducing and key molecules

Death receptors can elicit non-apoptotic, caspase independent cell death, that appears necrotic, through the receptor-interacting protein (RIP). When RIP expression is reduced, a decrease in autophagic cell death can be observed (Yu *et al*., 2006). It has been suggested that the kinase, RIP1, acts as a main initiator and propagator of necrosis. It has been demonstrated that TNF-induced programmed necrosis can be inhibited by caspase-8 cleavage of RIP or by RIP deficiency (Chan *et al*., 2003). Furthermore, this caspase independent death, induced by the Fas ligand, is absent in cells deficient of the Fas-associated death domain (FADD) (Holler *et al*., 2000). FADD is an important adaptor molecule which is situated upstream from RIP1. RIP1 knockout models have shown protection against necrosis in L929 cells. When caspase-8 is suppressed, a RIP1 dependent non-apoptotic cell death has been described in macrophages treated with LPS. Furthermore, the reduction of caspase-8 expression also shows features of autophagy, indicating that caspase-8 can regulate both apoptotic and non-apoptotic cell death (Holler *et al*., 2000).

It has also been shown that DR signalling in the presence of caspase inhibition triggers an alternative non-apoptotic cell death pathway that showed morphologies of both necrosis and autophagy. It has therefore been termed necroptosis (Degterev *et al*., 2005). The same group identified a small molecule out of a large chemical library screen, termed necrostatin-1, which inhibits this morphological picture (Degterev *et al*., 2005). Most interestingly, necrostatin has been shown to potently inhibit all examples of DR induced necrosis, such as in TNF-α treated L929 cells, or necrosis induced through RIP kinase activity. These results suggest the existence of a common DR mediated pathway (Degterev *et al*., 2005). The pan-caspase inhibitor z-VAD-fmk has been shown to induce autophagy and necrotic cell death in macrophages, but not in muscle cells such as vascular smooth muscle cells or C2C12 myoblasts (Martinet *et al*., 2006). This observed sensitivity has been attributed to a differential expression level of RIP1, suggesting that caspase inhibition causes RIP activation and subsequent autophagy. These data indicate that Fas, TRAIL and TNF-receptors can initiate cell death via two signalling mechanisms, the caspase-8 and RIP dependent pathway. Moreover, RIP has shown to be a substrate of caspase-8, which enhances TNF-induced apoptosis. Caspase-8 might therefore play a role as a molecular crossover point between extrinsic apoptotic and necrotic cell death (Lin *et al*., 2007). Furthermore, overexpression of bcl-2 can delay the onset of TNF-α induced necrosis. Most interestingly, this does not manifest in early cytochrome c release. It is plausible that the binding of bcl-2 to beclin-1 creates a molecular link between autophagy and necrosis. Furthermore, the second messenger, ceramide, which is generated through sphingomyelin hydrolysis accumulates before the onset of caspase-independent cell death. RIP1 knockdown protected cells against TNF-α induced ceramide generation and cell death, indicating sharing of the same pathway between ceramide and RIP1.

Necrotic cells are phagocytosed only after loss of membrane integrity, which provides them with a time window to activate and release pro-inflammatory molecules. One such pro-inflammatory molecule, which is passively released in

necrotic cells, is the protein high mobility group box I (HMGB1). In the nucleus it acts as an architectural component, binding to chromatin. Outside the cell it functions as an inflammatory mediator. The high mobility group proteins are small DNA-binding proteins that play an important role in the control of transcription. Some members of this group have also been shown to exert extracellular functions. They are also termed alarmins, denoting host proteins that are rapidly released during infection or tissue damage, and that have mobilizing and activating effects for host defence and tissue repair (Apetoh *et al*., 2007). HMGB1 is released by activated macrophages as well as necrotic cells, and in turn activates more macrophages to secrete angiogenetic factors (Schlueter *et al*., 2005).

Most interestingly, HMGB1 rapidly leaks out of necrotic cells, but not from apoptotic cells. It has been observed that in activated monocytes, HMGB1 redistributes from the nucleus to endolysosomes, indicating a non-classical, vesicle mediated secretion pathway (Gardella *et al*., 2001). Whether necrotic cells show a similar HMGB1 release pattern, is not clear (Gardella *et al*., 2001).

2.4.3.2. Modulating molecules

Calcium homeostasis is crucial for cellular signalling. Ca^{2+} is to a large extent stored in the ER, and its release is tightly regulated. It is also a positive effector of mitochondrial function. Ca^{2+} overload leads to excessive stimulation of the TCA cycle, with an overproduction of ROS. It has therefore been suggested that Ca^{2+} acts as an amplifier of necrosis. Furthermore, tissue acidosis, which is a result of excessive anaerobic glycolysis, increases Ca^{2+} influx and contributes to Ca^{2+} overload. The interplay of phospholipases (particularly the Ca^{2+} dependent $cPLA_2$, which cleaves arachidonic acid (AA) out of phopholipid bilayers) with ROS to generate lipid peroxides, may contribute to the disruption of organelle- and plasma membranes. Contribution of $cPLA_2$ to necrotic cell death has previously been indicated (Sapirstein & Bonventre, 2000). In a model of ischaemic injury, we have recently shown a p38 driven $cPLA_2$ translocation pattern, with a possible role for

$cPLA_2$ in deciding cell fate (Loos *et al*., 2008). Translocation processes, however, are dependent on a functional cytoskeleton to provide a framework for molecular trafficking. The cytoskeletal actin filament is important, not only to maintain architectural integrity of the cell, but also plays a role in regulating cell survival and death. Actin has been shown to be involved in the re-distribution process of mitochondria during TNF-α induced necrosis. Furthermore, it has been demonstrated that the inhibition of F-actin reorganization with cytochalasin in an ischaemic model with cardiomyocytes, prevents the onset of apoptosis (Okada *et al*., 2005). Furthermore, F-actin reorganization has also been shown to play a role in protection against necrosis induced by osmotic stress, during reoxygenation (Okada *et al*., 2005).

ATP availability plays a crucial role in determining the onset of necrosis, and has been described as a switch from apoptosis to necrosis (Leist *et al*., 1997). A growing body of knowledge suggests that ATP availability determines the mode of cellular death. A highly interesting study has been performed in human T cells, which showed an ATP dependent switch in the decision making between apoptotic and necrotic cell death. When ATP depletion was achieved through pyruvate, to allow only mitochondrial ATP production, apoptosis was induced. However, when treated with a blocker of mitochondrial synthesis, cells died necrotically. Furthermore, an ATP depletion of >50% was needed to change the mode of cell death from apoptotic to necrotic (Leist *et al*., 1997). Restoration of glycolytic ATP generation was sufficient to allow apoptosis to take place. Nitric oxide (NO) has also been shown to drive the decision making process between apoptosis and necrosis through NO-dependent failure of mitochondrial ATP synthesis. In this model, cells undergoing apoptosis converted to necrosis, a process which could be reversed by replenishing the cells by glucose supplementation (Leist *et al*., 1999). Moreover, a protective role for bcl-2 in this context has been described, where ATP depleted and bcl-2 transfected cells were treated with the apoptosis inducer, staurosporine (Single *et al*., 2001). In the ischaemic myocardium, it has been shown that ATP levels at reperfusion were replenished faster and necrosis was

reduced, when using an ATP-hydrolase inhibitor (Grover *et al*., 2004). These results provide evidence for an ATP dependent onset of necrosis. On the other hand, the observation that translation persists during necrosis of Jurkat and L292 cells speaks against a massive loss in intracellular ATP (Festjens *et al*., 2006).

2.4.4. Detection Methods for Necrosis

The evaluation of cell morphology and cellular membrane integrity is a hallmark for detecting necrotic cell death. Cellular swelling and membrane damage can be evaluated with light, fluorescent or electron microscopy methods. The most commonly used techniques often address cellular membrane integrity with fluorescent dyes, such as propidium iodide (Saelens *et al*., 2005), or the nonspecific DNA degradation process resulting in the characteristic DNA smear compared to the 200bp fragments occurring in apoptosis. Membrane integrity can also be assessed through monitoring the release of enzymes, for example lactate dehydrogenase, which is measured indirectly spectrophotometrically through NADH. However, recently immunohistochemical analyses of key role players such as HMGB1 have also been employed, where its release into the cytoplasm was indicative of necrotic processes. Moreover, the onset of lysosomal membrane integrity loss and the subsequent cathepsin B release resulting in a diffuse cytoplasmic signal pattern, is also employed (Carloni *et al*., 2007). In the myocardium, immunohistochemical detection of the ninth component of complement (C9), part of the membrane attack complex (MAC) has been shown to be a useful marker for necrosis, especially in tissue undergoing autolysis or when inflammatory infiltration is less obvious (Lazda *et al*., 2000). Moreover, immunohistological C9 staining has shown to be a simple, reliable and sensitive method, especially for the detection of early necrosis (Doran *et al*., 2007). Another advantage in this method is the usability of paraffin wax embedded material. Even within necrotic myocardial tissue, different states of cell death depending on cellular function have been described, such as coagulation necrosis, coagulative myocytolysis and colliquative myocytolysis (Baroldi, 1974).

The mitochondrial permeability transition (MPT) has been described as a causative event in necrotic cell death induced by oxidative stress or ischaemia/reperfusion injury. Using confocal microscopy, its onset can be visualized by the redistribution of the cytosolic fluorophore, calcein, into depolarized mitochondria (Lemasters *et al*., 1998). Cyclosporin A, which blocks the MPT, prevents necrotic cell death in response to a number of injury types. Moreover, as the onset of MPT occurs in increasing numbers of mitochondria, it has been proposed that the cellular response proceeds in the order of autophagy, apoptosis and finally necrosis. The progression to the next death mode is at least in part dependent on cellular ATP levels (Lemasters, 1999). The release of creatine kinase as a measure of membrane integrity and nuclear staining with ethidium homodimer-1 are also widely used techniques to assess necrosis (Shiraishi *et al*., 2001).

2.5. Dynamics within modes of cell death

2.5.1. Defining the PONR

Although the existence of the point-of-no-return (PONR) is still controversial, unravelling the identity of a restriction point for cell death could be highly significant, as it could lead to a better understanding of the time point when a cell is still salvageable. The PONR enables the distinction of cell death induction from cell death execution; of cell death as a process from cell death as endpoint and thus the distinction between a living and an already dead cell. A better understanding of locating and characterizing the PONR may introduce novel interventions to modulate its position, so as to increase the chance of reversibility for the benefit of cell survival. Similar to the need for cautious use of nomenclature for cell death, a clear report on parameters and a combination of techniques are needed to indicate the position of the PONR. Mitochondrial membrane permeabilization has been considered as the PONR in many models of programmed cell death (Galluzzi *et al*., 2008, Leber *et al*., 2007, Galluzzi *et al*., 2007) Other parameters have also

been indicated such as: caspase activation (Youle & Strasser, 2008, Golbs *et al*., 2007) governed by Bcl-2 family proteins, a point beyond which interference with caspase cannot salvage the cell (Rami *et al*., 2008) and the dissipation of mitochondrial transmembrane potential $\Delta\Psi m$ (Galluzzi *et al*., 2007) or cytochrome c interactions (Kagan et al., 2009).

However, only a dynamic perspective on the position of the PONR can reveal its significance. The PONR indicates that the cellular stress response is highly dynamic and characterized by organellar population kinetics, (Pacher & Hajnóczky, 2001) permeability kinetics, release kinetics, diffusion and transport kinetics. These in turn will determine accumulation kinetics, thresholds, degradation capacity and turnover kinetics. This suggests that not only apoptosis, but necrosis and cell death with autophagy may also be delineated by the cell's PONR. As the cell death process is not static, but rather a net result of regulatory networks, the PONR is unlikely to be restricted in position. A common theme of these regulatory networks is a perturbation in ATP and mitochondrial function, linking stress signal transduction pathways to regulators which control characteristic (Ferraro *et al*., 2008) and often progressively developing (Lemasters *et al*., 1999) morphological changes. Control of the PONR position through the cell's metabolic efforts would ensure the highest likelihood of cellular preservation.

2.5.2. Conceptualizing the PONR

A conceptual model which considers kinetics, for understanding the dynamic interrelationship between autophagy, apoptosis and necrosis is therefore proposed. According to this model, characteristic morphological features for each cell death mode are layered in the z-dimension, where the z-distance between them indicates the process and endpoint of dying, separated by the PONR. The features (Fig 2.4) are titled: 1 - "autophagy baseline", which indicates a viable cell with basal autophagic flux, 2 - "autophagy induced" indicating increased autophagic flux beyond basal levels, 3 - "cell death with autophagy", indicating

excessive autophagy, 4 - “apoptosis induced”, indicating the onset of the apoptotic cascade, 5 - “apoptosis executed” indicating the endpoint of apoptotic cell death, 6 - “necrosis induced”, indicating the onset of a leaky membrane, and 7 - ”necrosis executed”, indicating complete loss of membrane integrity. In experimentally controlled conditions, a “pure” morphology and type of cell death may often be described. As a basal level of autophagic flux is inherent to all eukaryotic cells with a lysosomal system, (Codongo & Meijer, 2005) feature 1 is indicated in any given stress response and mode of cell death. Cell death with autophagy is thus represented by features 1, 2, and 3, apoptotic cell death by features 1, 4, and 5 and necrotic cell death by features 1, 6, and 7 (Golstein & Kroemer, 2006, Degterev *et al*., 2005, Maiuri *et al*., 2007).

2.5.3. Assessing the PONR

When endogenous regulators that control the intracellular metabolic environment and cell death, (Klionsky *et al.*, 2008, Golstein & Kroemer, 2006, Kroemer *et al*., 2009, Festjens *et al*., 2006) are examined according to this model, their role in the time process of cell death may be indicated more clearly. Any control condition can thus be described as stage 1 with a cell- and tissue specific basal autophagic flux, and the sum of all kinetic parameters can indicate the cell’s or tissue’s position (stages 2-7) within this dynamic model. Moreover, the effect of specific endogenous modulators or signalling events such as the release and translocation of key molecules may be dissected out in their relation to the PONR and the stages of this model. However, in order to asses the PONR, a combination of recommended detection methods (Klionsky *et al.*, 2008, Golstein & Kroemer, 2006, Kroemer *et al*., 2009, Festjens *et al*., 2006) is suggested. Further it is suggested that kinetic parameters for autophagy, apoptosis and necrosis as well as cell specific parameters, intra- and extracellular metabolic parameters and insult parameters be carefully considered (Table 2.1). For example, a combination of data on basal autophagic flux, (Hamacher-Brady *et al*., 2006, Klionsky *et al.*, 2008, Klionsky, 2008) the time needed to reach its maximal attainable activity, as well as

vital dye uptake dynamics (Clausen & Gissel, 2005, Miyata *et al*., 2006, Ramadass & Bereiter-Hahn, 2008) and onset of dissipation of mitochondrial transmembrane potential $\Delta\Psi_m$ (Galluzzi *et al.*, 2007) should be placed into context with the cell's metabolic substrate preference and ATP household over time (Ferraro *et al*., 2008) in order to describe the PONR. It is crucial that multiple parameters be acquired at multiple points in time, and examined in context with one another, to capture the dynamic character of temporal signalling during cellular response. This approach may be aided by: (i) increased utilization of live cell imaging techniques which report the dynamics of dye exclusion between the onset of a leaky membrane up to the loss of its integrity during necrosis or (ii) assessment of the time scale of caspase activation through fluorescence resonance energy transfer (FRET) microscopy (Li *et al*., 2009, Tyas *et al*., 2000). To allow increased understanding of such dynamic events on a cell population level, this approach may be strengthened by data generated from living cells with fluorescence- activated cell sorting, particularly when tandem dyes are available (Shvets *et al*., 2008).

TABLE I

Suggestions of kinetic parameters to be acquired for the assessment of autophagy and cell death dynamics.

Parameter	Observation- assessment	Ref.
Autophagic kinetic parameters:	Basal autophagic flux, autophagic capacity, time required to respond with increased autophagy, time required to achieve maximal attainable autophagic activity, degradative capacity, ATP levels and kinetic measure of ATP synthesis	Hamacher-Brady *et al.*, 2006, Cumming *et al.*, 2008, Klionsky, 2007, Manfredi *et al.*, 2002
Apoptotic kinetic parameters:	Time required to: display Annexin V, start dissipating MMP, release of Cytochrome c, cleaved caspase-3 and to show onset of pyknosis/karyorhexis, p53 localization, ATP levels and kinetic measure of ATP synthesis	Galluzzi *et al.*, 2007, Golstein *et al.*, 2005, Li *et al.*, 2009, Tyas *et al.*, 2000, Manfredi *et al.*, 2002
Necrotic kinetic parameters:	Time required to: display membrane leakage, show lysosomal leakage, start high mobility group box-1 (HMG-1) release, dye uptake dynamics until complete loss of membrane integrity achieved, ATP levels and kinetic measure of ATP synthesis	Yang *et al.*, 1998, Schilling *et al.*, 2006, Manfredi *et al.*, 2002
Cell specific parameters:	Cell type: index for proliferation, senescence, differentiation, cell function: sub-cellular characteristics, mitochondrial load, activity of Golgi apparatus and Endoplasmic Reticulum, inherent combination of Bcl-2 family proteins	Medeiros, 2008
Intracellular metabolic parameters:	Basal ATP level, % glycolyitic flux and oxidative phosphorylation, estimated basal metabolic flux, oxygen consumption, ATP demand, substrate preference	Zhdanov *et al.*, 2008, Will *et al.*, 2006, Marin *et al.*, 2004, Manfredi *et al.*, 2002
Extracellular metabolic parameters:	Microenvironment, % substrate distribution in growth media, diffusion gradients for growth factors, substrates and O_2/CO_2	Srinivas *et al.*, 2009
Insult parameters:	Type of insult/stress, duration, severity, mode of action	

Table 2.1: Suggestions of kinetic parameters to be acquired to complement detection methods for the assessment of autophagy and cell death dynamics. It is advised to report acquired data as measured (e.g. FRET efficiency, intensity profile in arbitrary units), avoiding terminology like '%autophagy', '%apoptosis', '%necrosis', '% viability', and to contextualize the listed parameters in relation to one another.

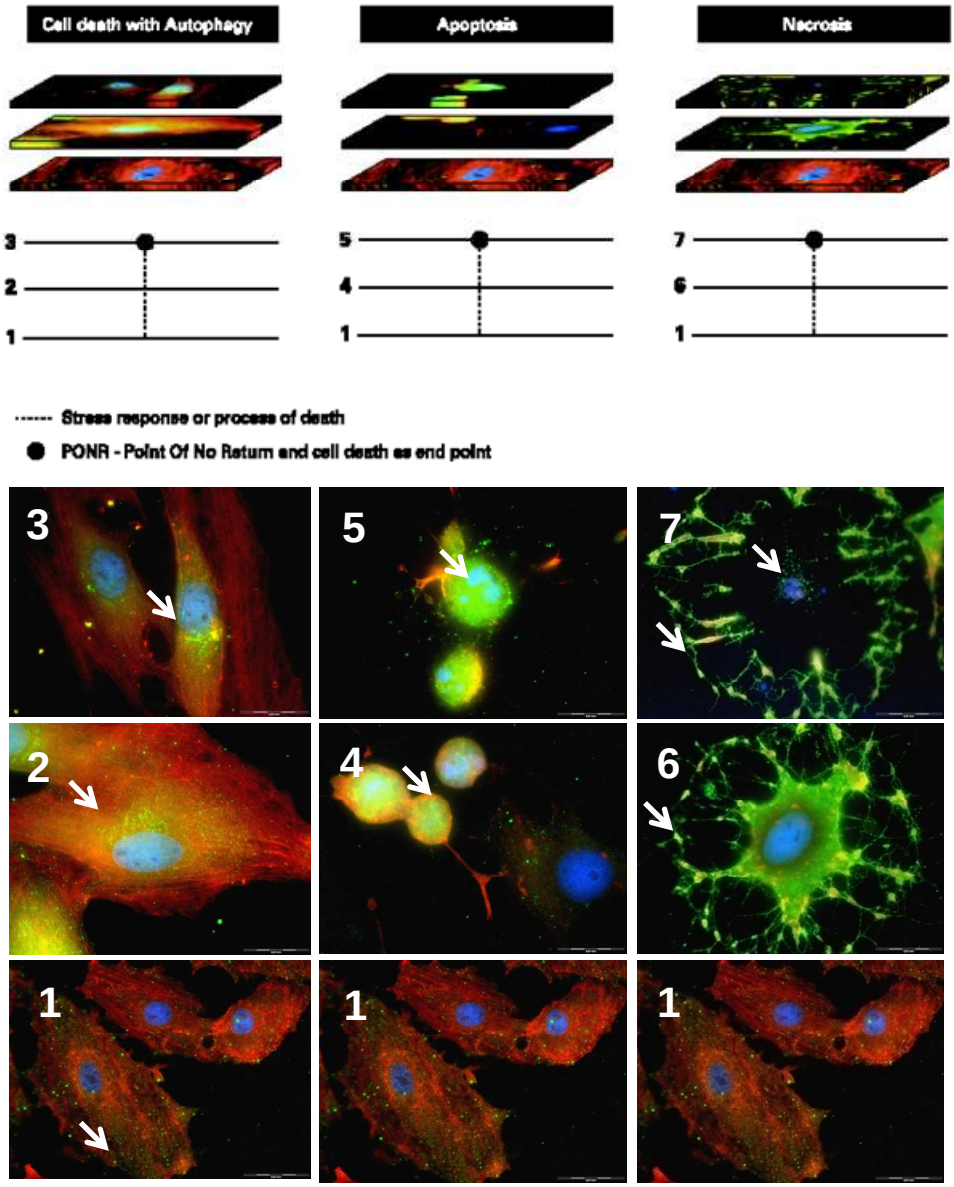

Figure 2.4: Model of typical appearance of different types of cell death. Cells are counterstained for LC3 (green), actin (red) and nuclei (blue). Fluorescence micrographs indicate morphological features for cell death with autophagy (micrograph 1, 2 and 3), apoptosis (micrograph 1, 4 and 5) and necrosis (micrograph 1, 6 and 7). Cell death with autophagy is indicated with increasing accumulation of autophagic vacuoles (micrograph 2 and 3), apoptosis shows cell shrinkage, nuclear pyknosis and karyorrhexis (micrograph 4 and 5) and necrosis shows cell swelling, membrane impairment and karyolysis (micrograph 6 and 7). The z-distance between the micrographs may indicate the process and endpoint of dying, separated by the point-of-no-return, PONR.

2.6. Dynamics between modes of cell death

A growing body of knowledge disputes the view that the cell death process is merely one static “suicide” pathway a cell commits to, but rather argues that it is the net result of a dynamic integrative signalling network, which permits molecular overlap and grey zones. Recognition of the extensive cross talk between different cell death pathways begins to provide insight into the complexity of the cell death decision-making process. Although in many conditions a distinct morphology of one of the above types of cell death may be encountered, multiple pathological conditions present themselves with morphological overlap (Degterev *et al*., 2005, Lockshin & Zakeri, 2004). As the position of the PONR is likely to be dynamic, so is the onset of cell death modes. This contributes to the shared morphological features. Furthermore, the order of the appearance of morphological characteristics for cell death with autophagy, apoptosis and necrosis over time may not necessarily suggest a preferred cellular way of dying, but may rather result from the metabolic condition that governs the cell’s stress response at that point in time. Importantly, autophagy appears to be a central and upstream role player when cells respond to metabolic perturbations (Karantza-Wadsworth *et al*., 2007). Autophagy helps cells avoid a metabolic crisis and thus affects the downstream cell death pathways. The cell protects itself from dying, therefore autophagic activity has an impact on the onset of other death modes through intricating the cell’s metabolic balance sheet. Cell death may therefore be viewed from the perspective of a dynamic response that provides cellular adaptability to a given stressful condition which can, context specific, extend into the process and endpoint of death (Kroemer *et al*., 2009). If there is a genetically encoded cellular intention, then it is likely to foster a will for survival as opposed to death. The overlap of autophagy, apoptosis and necrosis pathways, their onset and the PONR position translates time dependently into the observed morphology and cellular survival rate. It is therefore important to understand these dynamics, because only then can the opportunities presented, by delaying an onset of cell death, as opposed to inhibiting a pathway, be utilized.

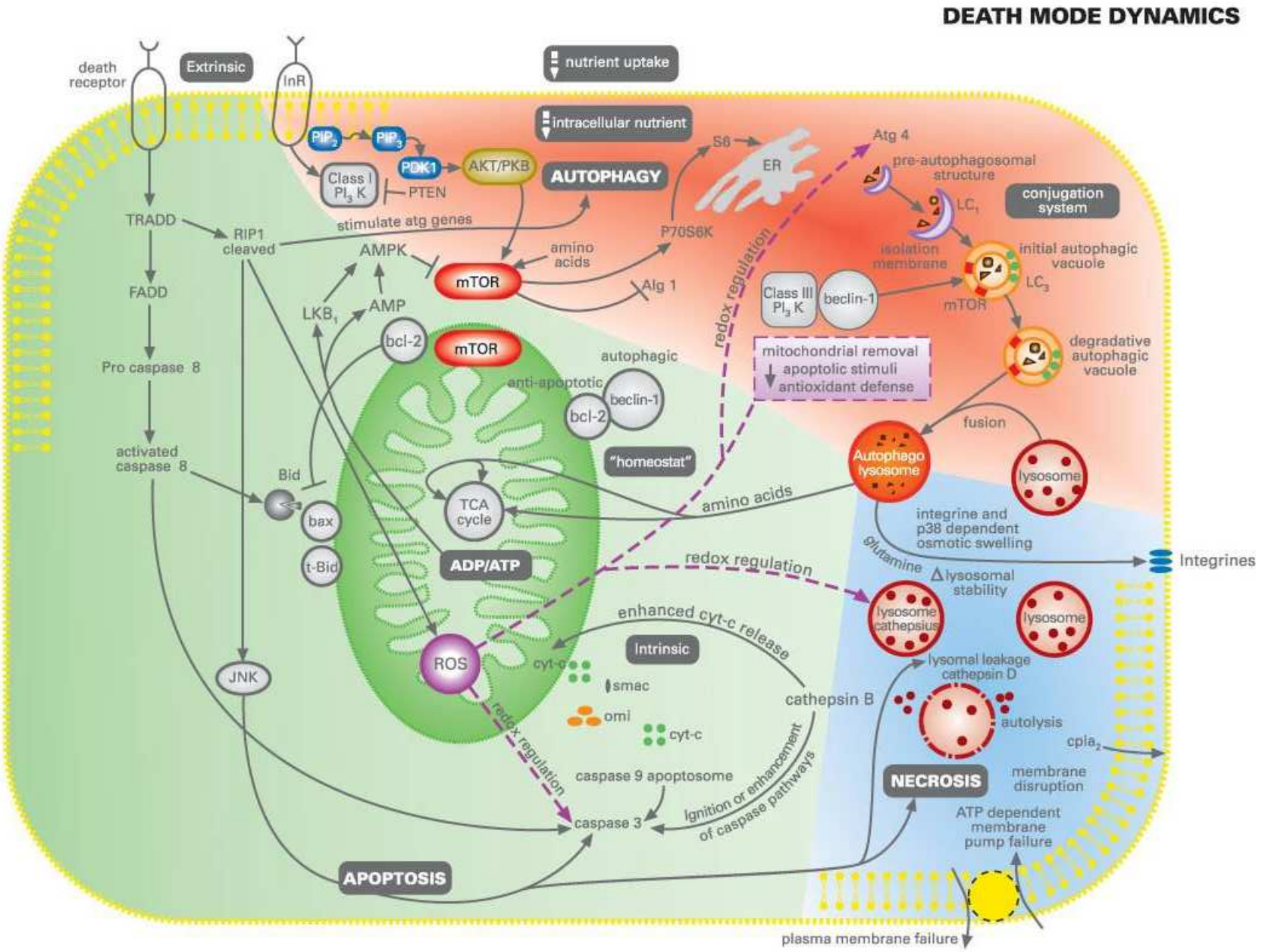

Figure 2.5: The pathways of cell death with autophagy, apoptosis and necrosis molecularly overlap and form an integral cellular response to the ischaemic insult, to increase the cell's likelihood for survival.

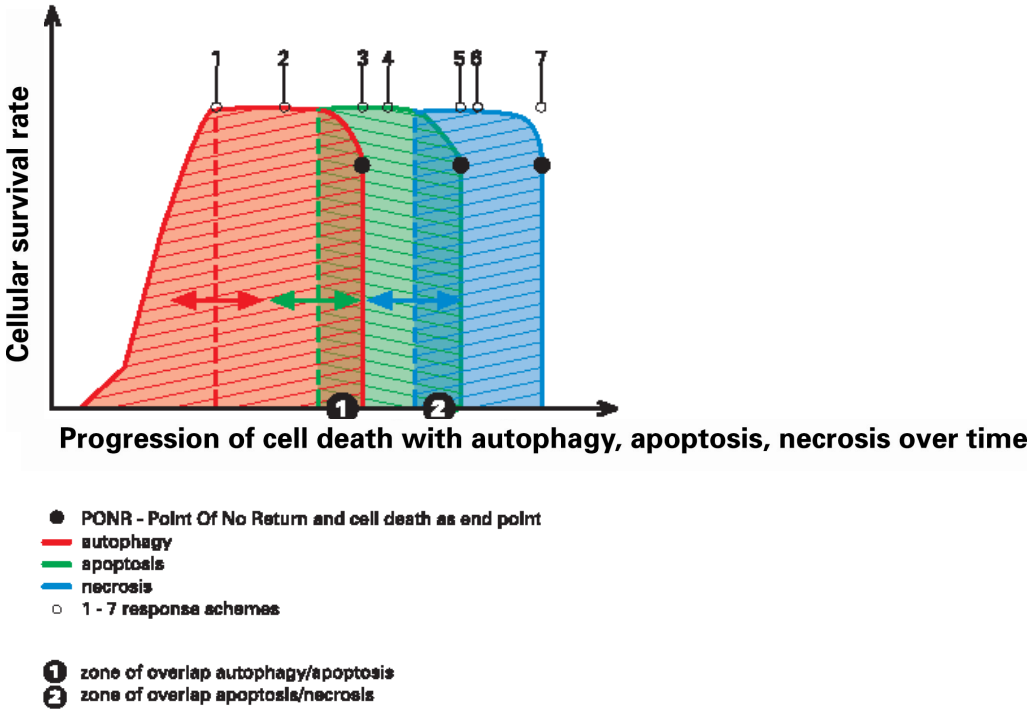

Figure 2.6: The overlap of autophagy, apoptosis and necrosis pathways, their onset and the PONR position translates time- dependently into the observed morphology and cellular survival rate. The cell's response to an insult is highly dynamic and morphological features between the death modes can overlap. The control of the PONR position through the cells metabolic efforts would maintain a high survival rate, ensuring highest likelihood of cellular preservation.

2.6.1. Greyzones Autophagy/Apoptosis

The dynamic relationship between autophagy and apoptosis is most clear before the activation of caspases is triggered (Debnath *et al*., 2005). Similar stimuli can either induce autophagy, apoptosis or both because several signals are shared between them. Autophagy may end with apoptosis and apoptosis may begin with autophagy. Caspases and autophagy can be simultaneously activated within a dying cell (Yu *et al*., 2004). Cells with substantial amounts of autophagic vacuoles mostly do not die (Lockshin & Zakeri, 2004). Cells with high levels of autophagy induced by Atg1 over-expression present themselves with a hybrid cell death-showing cell death with autophagy and apoptotic characteristics (Neufeld, 2007). When using caspase inhibitors, their survival is enhanced (Neufeld, 2007).

There is an indication that autophagy occurs or is de-inhibited, when apoptosis is not functional. In cells that are unable to undergo Bax/Bak mediated apoptosis (Bax/Bak-/-), irradiation massively upregulates autophagy, which suggests that autophagy may be the first line of defence against a cellular insult. Fibroblasts from double knockout Bax-/- Bak-/- respond with substantial autophagy followed by delayed cell death, when treated with DNA-damaging agents (Maiuri *et al*., 2007). In addition, autophagy not only limits metabolic stress but also minimizes genomic instability (Lockshin & Zakeri, 2004). These findings support the dynamic response concept of autophagy mediating a direct onset delay of apoptosis. Apoptosis-deficient cells with functional autophagy machinery induce additional autophagy under stress which increases the likelihood of recovery. In support of the concept of cell death being dynamic is the recent investigation of caspase regulatory network dynamics, where the use of live cell reporters revealed a partial state of cell death, which can persist for hours (Albeck *et al*., 2008).

The inverse relationship between autophagy and the onset of apoptosis is likely to manifest when decreasing or inhibiting autophagy. If the autophagic energy control mechanism is inhibited, apoptosis competent cells become sensitized and undergo

apoptosis earlier. The use of inhibitors of autophagy leads to cell death through apoptosis which can be reduced with caspase inhibitors (Boya *et al*., 2005). Cells which are deprived of the cytoprotective functions of autophagy might be more vulnerable and sensitized to insult. This view is supported by the notion that RNAi against beclin-1 and atg5 enhances starvation- induced apoptotic cell death (Levine & Yuan, 2005). A decrease in autophagic responsiveness and flux may induce tissue injury earlier, due increased accumulation of damaged protein aggregates and large dysfunctional mitochondria, leading to increased ROS, defective ATP generation, less efficient metabolic pathways and a decrease in lysosomal stability. Loss of lysosomal integrity leads to a release of lysosomal hydrolases into the cytosol (Wattiaux & Wattiaux-De Coninck, 1984) which brings about an inhibition in autophagic maturation, contributing to the accumulation of dysfunctional mitochondria. This process sensitizes cells to pro-apoptotic signals (Kiselyov *et al*., 2007). The inactivation of lysosome-associated membrane protein-1 (LAMP1), through RNA interference, inhibits the fusion of autophagosomes and lysosomes in HeLa cells, which adopt characteristics of both autophagy and apoptosis (Gonzalez-Polo *et al*., 2005).

2.6.2. Greyzones Apoptosis/Necrosis

Despite a possible direct onset delay of necrotic cell death we, however, propose that the profound effect of autophagy on necrosis is brought about indirectly. The indirect onset delay of necrosis is due to autophagy's role in causing onset delay of apoptotic cell death. This necessitates a closer look at the cell's metabolic performance in the light of the dynamic relationship between apoptotic and necrotic cell death. Common denominators for both apoptotic and necrotic cell death are triggers such as hypoxia, heat shock, viruses or oxidative stress, and second messengers such as Ca^{2+}, capase-8 or stress-dependent transcription factors (Leist & Nicotera, 1997). It is suggested that necrosis serves as the cell's default pathway, as it can be induced by the inhibition of apoptosis and autophagy (Golstein & Kroemer, 2006). It is important to note that ATP availability plays a

crucial role in determining the onset of necrosis. When ATP depletion is achieved in the cell through culture in glucose-free medium with pyruvate, allowing only mitochondrial ATP production, apoptosis is induced. However, when cells are treated with a blocker of mitochondrial ATP synthesis, necrosis is induced. ATP depletion of >50% is needed to change the mode of cell death from apoptotic to necrotic (Leist *et al*., 1997). Also, restoration of glycolytic ATP generation is sufficient to allow apoptosis to take place. We propose that autophagically generated amino acids and substrate intermediates may be involved in maintaining ATP at sufficient levels for longer, thus delaying the switch from apoptosis to necrosis. Conversely, when autophagy is dysfunctional or an additional autophagic response is not occurring timely, one may speak of an indirect premature onset of necrosis.

Despite the above described ATP- dependent effect on apoptosis and necrosis, nitric oxide (NO) has also been shown to drive the decision-making process between apoptosis and necrosis through NO-dependent failure of mitochondrial ATP synthesis. In this model, cells undergoing staurosporine induced apoptosis converted to necrosis, where the cell's ability to activate caspases and undergoing apoptosis could be recovered when replenished with glucose supplementation (Leist *et al*., 1999).

In the ischaemic myocardium it is demonstrated that ATP levels at reperfusion are replenished faster and necrosis is reduced when using an ATP-hydrolase inhibitor (Grover *et al*., 2004). In glucose- deprived rat neonatal cardiac myocytes exposed to hypoxia, a positive correlation between myocyte ATP concentration and the percentage of apoptotic cells is described. By increasing the glucose concentration, apoptosis progressively replaces necrotic cells, (Tatsumi *et al*., 2003) underlining the importance of substrate availability in the cell death decision-making process. ATP generation, through either glycolysis or mitochondrial oxidative phosphorylation, is needed to execute nuclear pyknosis, DNA fragmentation and phosphatidylserine exposure (Denecker *et al*., 2001). It may be speculated that the duration and severity of the insult determines whether

autophagy can be induced timely, in order to have an effect on the cell's ATP household. It also becomes clear that the cell's inherent ATP supply and demand behaviour influences the prevalence of either apoptosis or necrosis (Nicotera *et al*., 1999).

2.6.3. Greyzones Autophagy/Necrosis

Recent studies also show a molecular link between autophagy and necrosis. It is suggested that necrosis manifests as a result of an unsuccessful autophagic stress response (Maruyama *et al*., 2008), which supports our view that autophagy is induced as a stress response to increase likelihood of survival. When autophagy and apoptosis are inhibited in mouse- derived photo-receptor cells, necrotic cell death is induced (Kunchithapautham & Rohrer, 2007). It was also observed that a foetal mouse heart kept for 1 hr in organ culture undergoes autophagy followed by progressive necrosis (Artal-Sanz & Tavernarakis, 2005, Sybers *et al*., 1976). This confirms that autophagy acts as the first line of defence during a stress response.

The heart's capacity for sensing ROS and reacting to it through increased degradation of oxidatively damaged proteins to maintain intracellular ATP may lead to a direct onset delay of necrosis. This scenario may be the case during death receptor-induced necrosis, where ROS is generated from either mitochondrial or non-mitochondrial sources (Morgan *et al.*, 2008). On the one hand, the autophagic removal of oxidatively damaged mitochondria may preserve the cell for a specific time which may depend on the intensity and duration of the initial insult (Bonfoco *et al*., 1995). On the other hand, mutation studies demonstrated that autophagosomes and lysosomes synergize as proteolytic systems to facilitate necrosis (Samara *et al*., 2008). This suggests that autophagy may be using proteases that also mediate necrosis or that parts of the machinery for apoptosis and necrosis are recruited to complete execution initiated by autophagy. Despite the close relationship of proteolytic systems in autophagy and necrosis, another level of pathway interaction becomes clear, as autophagically generated amino

acids such as glutamine may act through the integrin-p38 mitogen-activated protein kinase (MAPK)- pathway, causing cell swelling and inhibition of autophagy (Ravikumar et al., 2003). This interaction suggests that necrosis can be induced when autophagic capacity is insufficient to maintain a favourable environment. In C. elegans, autophagy is induced early during necrotic cell death (Samara *et al*., 2008).

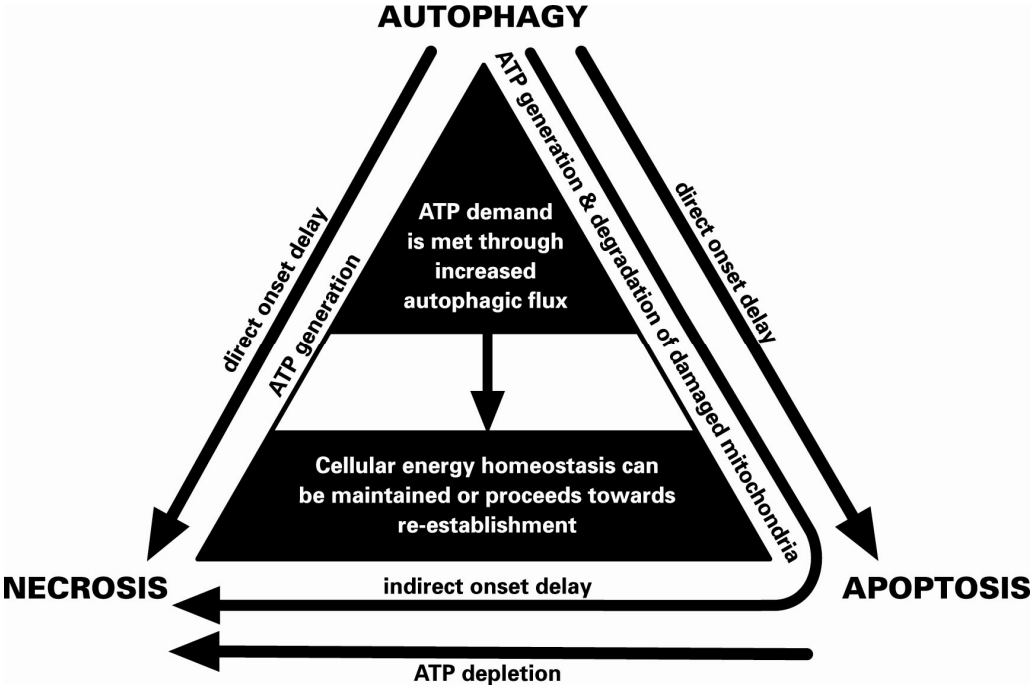

Figure 2.7: ATP- dependent relationship between autophagy, apoptosis and necrosis. Autophagy induces direct and indirect onset delay of apoptosis and necrosis through ATP generation and removal of damaged mitochondria and apoptotic stimuli. Energy homeostasis is more likely to be maintained.

2.7. Cell death with autophagy – a rare exception?

The exact contribution of cell death with autophagy and its role in pathophysiological conditions remains to be elucidated. Only a few conditions are known where cell death with autophagy functions as a physiological mechanism. In cells of salivary glands of *Drosophila* larvae, autophagy is not a failed survival attempt, but rather a physiologically controlled cell death mechanism (Bergmann, 2007). Moreover, cell death with autophagy also seems to play a role in cardiovascular diseases such as degenerative aortic valve disease (Mistiaen *et al*., 2005). In these rare cases, autophagy may be a “complete” cell suicide mode (Nixon, 2006). The other point of view is that excessive levels of autophagy can induce cell death with autophagy without the activation of caspases, leading to a degradation of organelles with a preservation of the cytoskeleton until late stages (Levine & Yuan, 2005). Cells that lack critical apoptosis regulators appear to die with massive amounts of autophagic vacuoles, (Debnath *et al*., 2005) possibly compensating for the defects in apoptosis. Thus it can be argued that there is some indication that cell death with autophagy, when excessively induced, is due to bioenergetic failure (Ferraro & Cecconi, 2007). Such cases deserve more study in highlighting the central role of the cell’s metabolic capacity.

2.8. Conclusion and future outlook

This review emphasizes the importance of understanding cell death as a dynamic response concept by discussing the dynamics within and between cell death modes. By proposing a conceptual model for understanding the dynamic interrelationship between autophagy, apoptosis and necrosis it is hoped that this can contribute towards clarifying cell death definitions and processes in order to accelerate communication. It is also hoped that it can shed light onto the centrality of autophagy within the cell death machinery in context of cellular energy homeostasis and its effect on the onset of apoptosis and necrosis. It becomes apparent that kinetic parameters such as autophagic capacity, its response time

and the cell's metabolic capacity may affect the PONR and offer opportunities for cell survival. The importance of locating and characterizing the PONR has been stressed, as this may introduce novel interventions to modulate the PONR position, interventions which may be applied to increase the chance of reversibility for the benefit of cell survival.

The high degree of plasticity in the induction and execution of cell death will require the use of more sophisticated and inclusive assays. The use of advanced real-time observation techniques in combination with simulated network models (Huber, et al., 2007) will offer clues to unravel the dynamic behaviour of cellular commitment to survival and may offer the platform for analyzing the position of each PONR between the individual death modes. Moreover, it is hoped to have shown that autophagic response parameters provide additional time to the process of dying, and thus ultimately increase the window of opportunity for novel therapeutic interventions.

This review highlights that new treatment strategies may focus on delaying the onset of each death mode, rather than inhibiting it. Such strategies may be based on a combined therapy, targeting autophagic as well as apoptotic pathways (McMullen *et al*., 2004). Most crucially, the role of autophagy in delaying the onset of cell death by the modification of cellular metabolic performance deserves more study.

2.9. Hypothesis

In this study it is hypothesized, that the relative contribution of each mode of cell death is dependent on the duration and severity of the ischaemic insult, and is governed by the cells underlying metabolic capacity at a given point in time. Secondly, it is hypothesized that the onset of apoptosis and necrosis depends on

the cell’s autophagic activity prior to the ischaemic event due to an impact of autophagy on the cells metabolic capacity.

CHAPTER 3 MATERIALS AND METHODS

3.1. Antibodies and chemicals

The following antibodies were obtained from Cell Signaling Technology (MA, USA): cleaved caspase-3 antibody (Asp 175) and PARP antibody, pAMPK, mTOR. The antibody specific to HMGB1 was purchased from Santa Cruz Biotechnology (California, USA). LC3 antibody was obtained from Nano Tools (Germany) and beclin-1 was obtained from Assay Designs (MI, USA). Tissue culture tubes, 50 ml and 15 ml were used from Greiner Bio-One (Germany). Sterile serological pipettes (25 ml and 10 ml) were obtained from LP Italiana SPA and Sterilin Ltd. Pipette tips were purchased from Greiner Bio-One. Culture medium, Dulbecco's modified Eagle's medium (DMEM) was obtained from Highveld (South Africa), trypsin and phosphate buffered saline (PBS) from SIGMA-ALDRICH (South Africa) and tissue culture flasks and -dishes, cell scraper and microcentrifuge tubes were purchased from Greiner Bio-One (Germany). Chambered coverglass slides were used from Nunc Lab-Tek (Lab-Tek, 155411, USA). Syringe millipore filter, trypan blue reagent, albumine bovine serum (BSA) and Bradford reagent were obtained from SIGMA-ALDRICH (South Africa). For the gel electrophoresis a Mini-Protean BIO RAD system was used. Ammonium persulfate was purchased from SIGMA-ALDRICH (South Africa), Acrylamide/bis-Acrylamide from Promega (South Africa) and N,N,N,N'-Tetramethylethylendiamin from MERCK (Germany).

Antibodies and Markers

Primary antibody for western blot				
Antibody	*Company/Catnr*	*Host*	*Size (kDa)*	*Dilution*
LC3	Nano Tools 0231-100/LC3-5F10	Mouse Monoclonal	LC3-I: 18kDa LC3-II:16kDa	30µl:5000 µl
Beclin-1	Assay Designs 905-721-100	Rabbit polyclonal	~ 57kDa	4µl:5000 µl
Caspase-3 (corresponding to amino acids 28-44)	Cell Signaling #9665	Rabbit monoclonal	17,19,35 kDa	5µl:5000 µl
Cleaved PARP (Asp 214)	Cell Signaling #9541	Rabbit monoclonal	89 kDa	6µl:5000 µl
pmTOR (Ser 2448)	Cell Signaling #2971	Rabbit monoclonal	289 kDa	5µl:5000 µl
pAMPKα (Thr 172)	Cell Signaling #2535	Rabbit monoclonal	62 kDa	5µl:5000 µl
Secondary antibody for western blot				
Antibody	*Company/Catnr*	*Dilution*		
Anti-Rabbit IgG Horseradish Peroxidase linked	ECL™ NA934V	1.25µl:5000 µl		

Polyclonal Rabbit anti mouse	Dako Cytomation	1.25µl:5000 µl		
Primary antibody for immuno fluorescence				
Antibody	*Company/Catnr*	*Host*	*Size (kDa)*	*Dilution*
LC3	Nano Tools 0231-100/LC3-5F10	Mouse Monoclonal	LC3-I: 18kDa LC3-II:16kDa	1:50
Actin	Santa Cruz Sc-1616	Rabbit polyclonal	~ 42kDa	1:50
Cytochrome-c	Santa Cruz Sc-13560	Mouse monoclonal	~ 12kDa	1:50
Beclin-1	Assay Designs 905-721-100	Rabbit polyclonal	~ 57kDa	1:50
HMGB1	Santa Cruz sc-26351	Goat polyclonal	~ 25kDa	1:50
Secondary antibody for immuno fluorescence				
Antibody	*Description*	*Company/Catnr*	*Dilution*	
Donkey anti-rabbit FITC	F(ab')2 Fragment	AEC-Amersham 711-096-152	1:200	

Donkey anti-goat FITC	F(ab')2 Fragment	AEC-Amersham 705-096-147	1:200	
Donkey anti-mouse FITC	F(ab')2 Fragment	AEC-Amersham 715-096-151	1:200	
Donkey anti-rabbit Texas Red	F(ab')2 Fragment	AEC-Amersham 711-076-152	1:200	
Donkey anti-rabbit FITC	F(ab')2 Fragment	AEC-Amersham 711-096-152	1:200	

3.2. Experimental animals

Male Wistar rats weighing 220-240 grams were used. Institutional and international ethical guidelines were applied with respect to the handling of experimental animals. Before experimentation, rats were allowed free access to food and water. Animals were anaesthetized with pentobarbital (50 mg/kg) administered intraperitoneally before experimentation. Animals were weighed before excision of the heart.

3.3. Cell culture preparation

3.3.1. Cells

H9c-2 rat heart myoblasts (European Collection of Cell Cultures – ECACC, Kimes & Brandt, 1976), were seeded at 12 000/cm^2, and cultured in Dulbecco's modified Eagle's medium supplemented with 10% fetal calf serum, 4% glutamine and 1%

penicillin/streptomycin in a humidified atmosphere, 37℃, in the presence of 5% CO_2. In detail, cells were washed with 0.01 M sterile phosphate-buffered saline, (PBS), trypsinized (0.25% Trypsin – EDTA), centrifuged for 3 min at 6000 x g and seeded as follows: $3x10^5$ myoblasts per 25 cm² tissue culture flask, $1x10^5$ myoblasts per culture dish in six-well plates and $2x10^4$ myoblasts per 8 chamber slide. Growth medium was changed every 48 hrs.

3.3.3. Passaging protocol

Cells were passaged when reaching 70-80% confluence. Growth medium was discarded and cells rinsed with warm (37℃), steril e PBS. Warm (37℃) 0.25% trypsin-EDTA (3 ml) was added and cells were incubated until cells detached from the surface (3-4 min). Culture medium (double the volume of trypsin used; 6 ml) was added to the cell suspension, which was then transferred to a 15 ml falcon tube, centrifuged for 3 min at 6000 x g. Medium was decanted and cells re-suspended in fresh medium, aliquots for new flasks were made as required according to the seeding density.

3.4. Simulated ischaemia (SI) and reperfusion

Control cells were kept under normoxic conditions and 5% CO_2. The simulated ischaemia lasted for 2, 4 and 8 hrs. Cells were washed with sterile PBS and incubated with a filtered sterilized modified ischaemic buffer (Esumi *et al.*, 1991), pH 6.4, containing (in mM): 137 NaCl, 12 KCl, 0.5 $MgCl_2$, 0.9 $CaCl_2$, 20 Hepes, 20 2-deoxy-D-glucose (2DG, Sigma, D-8375), or 0.5 sodium dithionite (SDT, Fluka, BioChemika, 71699), or 2DG and SDT under hypoxic conditions in a humidified environment containing 0.1% O_2, 5% CO_2 and the balance N_2, followed by a 60 min washout time under normoxic conditions with growth medium. We employed the modified ischaemic buffer (Esumi *et al.,* 1991) with either 2-deoxy-D-glucose (Fuglesteg *et al.,* 2008), sodium dithionate (Seyedi *et al.,* 2002), or both (Cumming *et al.*, 1996), with the aim to create an ischaemic insult of mild (mild SI), moderate

(moderate SI) and severe (severe SI) character respectively. Temperature was maintained at 37℃.

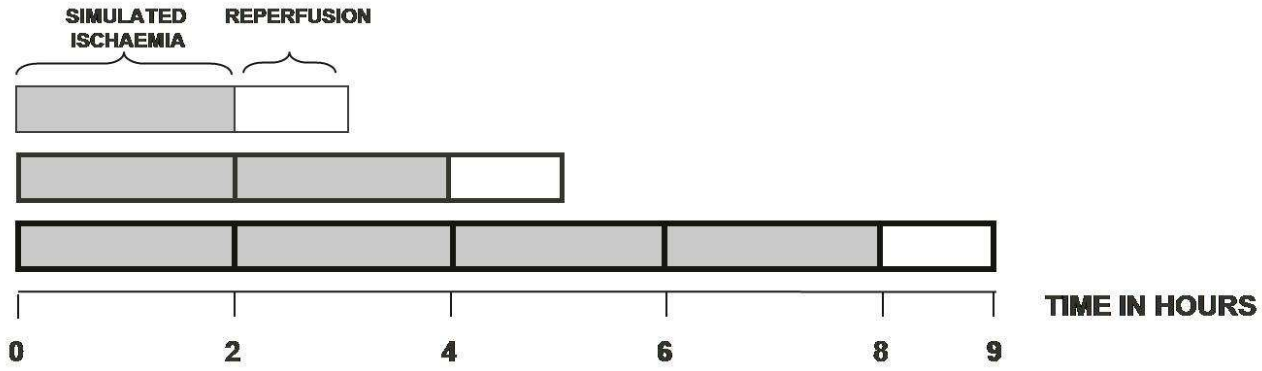

Figure 3.1: ***In vitro*** **experimental protocol for three time points of SI.**

3.5. Treatment of cells with rapamycin and 3MA

To establish a dynamic approach of monitoring the onset of apoptosis and necrosis over time during the ischaemic insult, in dependency of autophagic activity, cells were treated with 5 mM 3MA (Sigma, M9281) or 50 µM rapamycin (Sigma, K4060) for 24 hrs. Cells were then washed with PBS and submitted to 2 hrs SI. Live cell imaging was performed (see below).

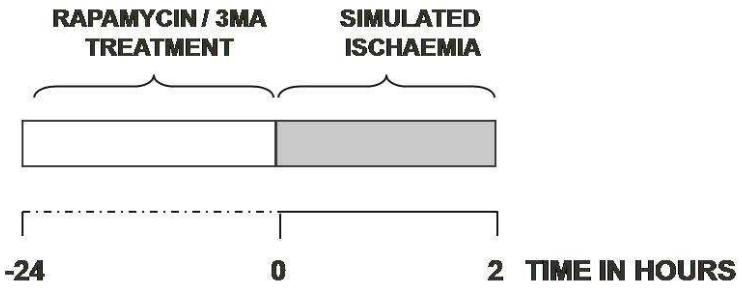

Figure 3.2: *In vitro* experimental protocol of SI for study of onset dynamics with induced and inhibited autophagic activity.

3.6. Determination of myocyte viability

3.6.1. PI exclusion

The loss of membrane integrity has been described as an indicator for necrotic cell death (Festiens *et al*., 2006). The DNA intercalating dye Propidium Iodide (PI) is not able to diffuse through the membrane of viable cells, it is therefore excluded from binding to the cells' nucleus. However, as soon as the cells' membrane integrity is lost, PI diffuses into the cell and intercalates with the DNA. This dye has a specificity for double-stranded nucleic acids, absorbing in blue-green (493 nm), fluorescing red (630 nm). In combination with Hoechst which diffuses through an intact cellular membrane, the PI exclusion technique allows to clearly distinguish between viable cells (PI-negative), and cells which have lost their membrane integrity (PI-positive). After submission to the experimental protocol, Hoechst (Hoechst 33342, Sigma) and PI (Sigma, P4170), in a 1:200 dilution in PBS, were directly added onto the cells, using a final concentration of 50 µg/ml and 1 µg/ml respectively. Incubation took 10 min and images were acquired immediately thereafter. Using the automatic stage setting (Olympus Cell^^{R} Soft Imaging Systems), random fields of view were acquired. Using a Xenon-Arc burner

(Olympus Biosystems GMBH) as light source, images were excited with the 360 nm and 572 nm excitation filter; emission was collected using a UBG triple-bandpass emission filter cube (Chroma). Necrotic cells showed bright red nuclei. For each experimental condition, four random fields of view were acquired. The % PI-positive cells was calculated as number of PI-positive cells/total cells x 100.

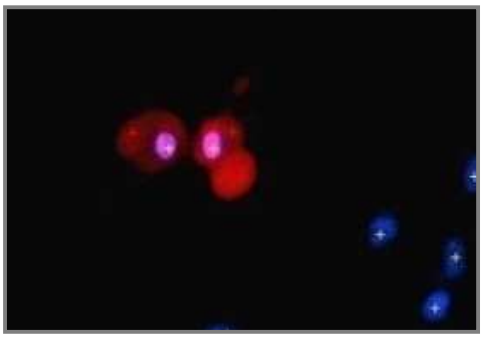

Figure 3.3: Fluorescence micrograph showing PI-negative (right) and PI-positive (left) H9c-2 cells.

3.6.2. Nuclear condensation

Nuclear condensation (pyknosis) and fragmentation (karyorrhexis) have been described as morphological hallmarks for apoptosis (Kajustra *et al*., 1996). Using the DNA intercalating dye, Hoechst, one is able to clearly distinguish between normal nuclear morphology and apoptotic morphology. After submission to the experimental protocol, Hoechst 33342 (in a 1:200 dilution in PBS) was directly added onto the cells, using a final concentration of 50 µg/ml, and incubated for 10 min. Images were acquired immediately thereafter. Using the automatic stage setting (Olympus Cell^^{R} Soft Imaging Systems), random fields of view were acquired. Cells were graded according to their nuclear signal: 1. normal nuclei with

blue chromatin, showing an organized structure with a distribution of hetero- and euchromatin, 2. Apoptotic cells, showing bright and highly condensed or fragmented nuclei. For each experimental condition, four random fields of view were acquired. The apoptotic index was calculated as number of apoptotic cells/total cells x 100.

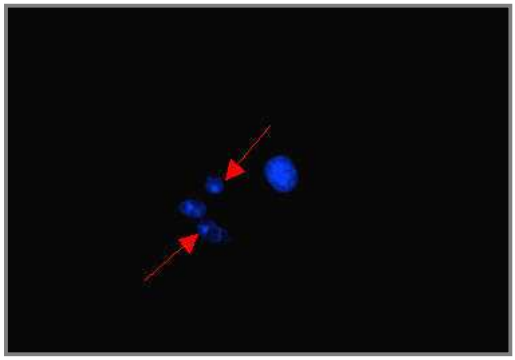

Figure 3.4: Fluorescence micrograph showing normal nucleus (right) and pyknotic (arrows) nuclei of H9c-2 cells.

3.6.3. MTT assay

For the assessment of mitochondrial reductive activity, a modification of the 3-[4,5-dimethylthiazol-2-yl]-2,5-diphenyl tetrazolium bromide (MTT) assay was used (Goodwin *et al*., 1995, Gomez *et al*., 1997). The assay is based on the cells capacity to reduce MTT into blue formazan pigments mainly through mitochondrial enzymes of viable cells. Following the submission of cells to SI, cells were washed twice with PBS. MTT (0.01 g/ml) was dissolved in PBS, and 500 µl was added per culture dish. Cells were incubated for 2 hrs at 37°C and 5% CO_2. Cells were then washed with PBS and 1000 µl of HCl-isopropanol-Triton (1% HCl in isopropanol; 0.1% Triton X-100; 50:1) was added to the cells, followed by an agitation period of 5 min. During this process, cell membranes would lyse and release the formazan

pigments. The suspension was centrifuged at 14 000 rpm for 2 min, and the optical density (OD) was determined spectrophometrically (Cary Varian) using a wavelength of 540 nm. Values were expressed as percentages of control values.

3.7. ATP analysis

ATP levels were determined using the ATP Bioluminescence detection kit (ENLITEN®, Promega). This assay uses recombinant luciferase to catalize the following reaction:

ATP + D-Luciferin + O_2 → Oxyluciferin + AMP + PPi + CO_2 + Light (560 nm)

Since ATP is the limiting component in the above reaction, the emitted light is proportional to the concentration of ATP. Following trypsinization, cells were centrifuged at 4℃ and washed in PBS. The pellet was then resuspended in 50 µl ice-cold lysis buffer (100 mM Tris-HCl and 4 mM EDTA, pH 7.75), which was followed by the addition of 150 µl of boiling lysis buffer (Essmann *et al*., 2003). Samples were then incubated for 2 min at 99℃. Lysates were centrifuged at 10 000 rpm at 4℃ for 1 min (ALC, PK121R, multispeed refrigerated centrifuge). Supernatants were collected for ATP detection; 50 µl of supernatant and 50 µl luciferase reagent were used and chemiluminescence was acquired in a luminometer (Glomax-96 luminometer, Promega).

3.8. Western blot analysis

3.8.1. Protein extraction

After completion of the experimental protocol, cells were rapidly placed on ice, Esumi buffer was removed and cells were carefully washed with cold PBS. Total myoblast protein was extracted with a lysis buffer [modified radioimmunoprecipitation (RIPA) buffer], pH 7.4, containing (in mM): Tris/HCl 2.5, EDTA 1, NaF 50, NaPPi 50, DTT 1, Phenylmethylsulfonyl fluoride (PMSF) 0.1,

benzamidine 1, 4 µg/ml SBTI, 10 µg/ml leupeptin, 1% NP40, 0.1% SDS, 0.5% Na-Deoxycholate. A volume of 260 µl lysis buffer was added to the culture flask and cells were removed from the plastic surface using a cell scraper. Cell lysates were stored short termed at -20℃ in microcentrifuge tub es.

3.8.2. Bradford protein quantitation

The rapid and sensitive Bradford method for the quantitation of microgram quantities of protein utilizing the principle of protein-dye binding was employed (Bradford, 1976). It involves the binding of Coomassie Brilliant Blue G-250 to protein which causes a shift in the absorption maximum of the dye from 465 nm to 595 nm. The increase in absorption at 595 nm is monitored spectrophotometrically (Cary Varian).

Cell lysates were defrosted, kept on ice and sonicated for 5 seconds at power level 3 (Vir Sonic 300, Virtis Gardiner) followed by centrifugation for 10 min at 4℃ at 5000 x g (ALC-PK121R) in order to pellet cell debris and to expose the whole cellular protein fraction. For the establishment of a standard curve, a protein dilution series was set up, pipetting 2 µg, 4 µg, 8 µg, 12 µg, 16 µg and 20 µg albumine bovine serum dissolved in PBS (BSA, 200 µg/ml) and 900 µl Bradford reagent into test tubes, adjusted to 1000 µl with deionized water. Sample protein concentrations were determined through pipetting 5 µl of the sample supernatant with 900 µl Bradford reagent and adjusted to 1000 µl with 95 µl deionized water.

Test tube content was mixed by vortexing, incubated for 5 min at room temperature and the absorbance was measured at a wavelength of 595 nm against a reagent blank prepared from 900 µl Bradford reagent and 100 µl deionized water, using semi-micro cuvettes. The weight of protein in µg/ml was plotted against the absorbance and protein concentration was determined.

3.8.3. Sodium-dodecyl-sulfate-polyacrylamide gel electrophoresis (SDS-PAGE)

Laemmli sample buffer was prepared, using (in M): TRIS 0.5, pH 6.8, 10% SDS, 2.5 ml glycerol, 0.2 ml 0.5% bromophenol blue in deionized water. A volume of 150 µl mercaptoethanol was then added to 850 µl sample buffer. Cell lysates were boiled for 5 min and shortly spun in a microcentrifuge to assure complete sample acquisition. Total protein (20 µg) was separated by 10% sodium-dodecyl-sulfate-polyacrylamide-gel-electrophoresis (SDS-PAGE) and a 4% stacking gel.

3.8.4. Western blot analysis

After completion of the protein separation, proteins were transferred to a PVDF membrane (ImmobilonTM P, Millipore) using a semi dry blotting system (BIO RAD trans-blot SD). Three blotting buffers were prepared using for anode buffer I (in M): Tris-base 0.3, pH 10.4, 20% methanol; for the anode buffer II (in mM): Tris-base 25, pH 10.4, 20% methanol and for the cathode buffer (in mM): Tris-base 25, ε-aminohexanoic acid 40, pH 9.4, 20% methanol. The PVDF membrane was soaked in methanol for 15 sec, allowed to dry and then soaked in anode buffer II. On the anode plate four blotting papers were placed, after being soaked in anode buffer I. Two blotting papers, soaked in anode buffer II were added, followed by the PVDF membrane and the gel without the stacking gel. Six blotting papers, soaked in the cathode buffer were added. To avoid air bubbles, the blotting sandwich was rolled with a clean wet glass tube. The systems' cathode lid was tightly closed and the transfer proceeded with 0.5 A, 15 V for 60 min.

Following protein transfer, non-specific binding sites on the membranes were blocked for 120 min at room temperature with 5% fat free milk in Tris-buffered saline-0.1% Tween 20 (Polyoxyethylenesorbitan monolaurate, Tween 20) (TBST). Followed by a washing step with TBST, the membranes were incubated overnight

at 4℃ with the specific primary antibodies. The primary antibody dilution was in each case diluted in TBST as stated above.

Membranes were subsequently washed with large volumes of TBST (3x5 min) and the immobilized antibody conjugated with a 2.5:10 000 diluted horseradish peroxidase-labelled secondary antibody (Amersham Life Sciences), incubated for 50-60 min at room temperature. After thorough washing with TBST, membranes were incubated at room temperature for 1 min with ECL™ detection reagents (Amersham Life Sciences) and quickly exposed to an autoradiography film (HyperfilmTM) to detect light emission through a non-radioactive method (AXIM fixer/developer).

3.9. Immunofluorescence

All solvents and buffers for the labeling were freshly made up and filter sterilized to ensure that they are free of particles.

Cells were grown on autoclaved cover glasses which were placed into the culture dish. After completion of the experimental protocol, cells were gently washed with 0.1 M PBS and fixed using 1000 µl fixative per culture dish, made up as methanol/acetone in a 1:1 ratio. Culture dishes were incubated for 10 min on ice at 4˚C and then left to air-dry for 20 min at room temperature. Dried cover glasses were then gently rinsed with 1ml PBS and transferred to microscope slides.

For the rest of the labeling procedure, slides were kept in light protected humidified staining chambers. The slides were then incubated at room temperature for 20 min with 5% donkey serum in PBS, 100 µl per cover glass, to block non specific binding sites. Serum was then drained and specific primary antibodies were added in a 1:50 PBS dilution (50 µl volume) and incubated for 90 min at room temperature. In some cases, an overnight incubation step was employed to yield better results. For the controls, 50 µl PBS was used instead of primary antibody. The slides were then

carefully washed with 1 ml PBS per slide and secondary antibody FITC or Texas Red (Jackson, donkey anti rabbit/donkey anti goat) was added in a 1:200 dilution (50 µl volume) to all slides, including the PBS controls. To avoid crystals, the secondary antibody was briefly centrifuged and the supernatant was used for the labeling. Following 30 min incubation at room temperature, the nuclear stain Hoechst was added additionally in a 1:200 dilution and incubated for another 10 min at room temperature. Cover glasses were then carefully washed 3 times with 1000 µl PBS and transferred to glass microscope slides, mounted with fluorescent mounting medium (Dako Cytomation) and finally sealed with commercially available nail polish. Slides were then analysed and stored in silver foil at -20˚C.

3.10. Fluorescence Microscopy

Image acquisition was performed on an Olympus Cell^^{R} system attached to an IX 81 Inverted fluorescence microscope equipped with a F-view-II cooled CCD camera (Soft Imaging Systems). Using a Xenon-Arc burner (Olympus Biosystems GMBH) as light source, images were acquired using the 360 nm, 472 nm or 572 nm excitation filter. Emission was collected using a UBG triple-bandpass emission filter cube (Chroma). Images were acquired through z-stacks, using an Olympus Plan Apo N60x/1.4 Oil objective. The top and bottom focus position parameter were selected, indicating the upper and lower dimensions of the sample to be acquired, with a step width of 0.26 µm between the image frames. Images were processed and background-subtracted using the Cell^^{R} software, and presented in a maximum intensity projection.

Through setting up a defined experiment in the *Experiment Manager* feature of the Cell^^{R} software, image acquisition parameters such as exposure time, illumination settings and emission filter cube selection were kept constant for all groups and ensured appropriate selection of parameters. The DAPI 360 nm excitation wave length was used for setting the focal plane, avoiding unnecessary photo-bleaching.

3.11. Transfections with GFP-LC3 and CFP-DEVD-YFP

H9c-2 cells were transfected using GenJuice® Transfection Reagent (Novagen®), according to the manufacturers protocol. In brief, cells were seeded in 8-chamber dishes with a density of $2x10^4$ cells. Per sample, 3 µl of transfection reagent was added to 100 µl of serum-free medium, vortexed, and incubated for 10 min at room temperature. Thereafter 800 ng of DNA was added, then mixed through gentle pipetting and incubated for 15 min at room temperature. DNA/reagent mix was added in a drop-wise manner to the cells, which were kept in complete growth medium. The DNA/reagent mix was added over the entire surface of the culture dish, which was then gently rocked. Cells were incubated for 24 hours, which was followed by a change of growth medium. An estimated transfection efficiency of 10% was achieved. Cells were then incubated for another 24 hrs and visualized.

3.12. Live Cell Imaging

To establish a dynamic approach of monitoring the onset of apoptosis and necrosis over time during the ischaemic insult, live cell imaging was performed.
For that purpose, H9c-2 cells were maintained at 37 ℃ in growth medium, seeded in 8-chamber dishes with a density of $2x10^4$ cells.

3.12.1. Fluorescence Resonance Energy Transfer (FRET) and mitochondrial depolarization dynamics

Caspase-3 activity and loss of mitochondrial membrane potential are associated with apoptosis, and have been considered as a PONR for apoptosis. To visualize this process over time, cells were transfected with 800 ng of CFP-DEVD-YFP plasmid DNA construct (Tyas *et al*., 2000). Cells expressing the CFP-DEVD-YFP fusion protein were imaged after pretreatment with 20 nM Tetramethylrhodamine Ethyl Ester (TRME, Molecular Probes, T669) for 30 min at 37℃. The cells were then treated with modified ischaemic buffer (Esumi *et al*., 1991, Seyedi *et al.,*

2002), which was vigorously gassed with nitrogen to ensure that the buffer was largely free of oxygen and then layered with mineral oil (Meldrum *et al*., 2001, Covington *et al*., 2005, Patel *et al*., 2006) and placed in a heated chamber (37℃) encasing the IX-81 stage. FRET was determined using an IX-81 Olympus microscope, coupled to an MT-20 (Soft Imaging Systems) xenon arc lamp, by excitation using FRET excitation filters (S430/25x and S500/200, Chroma). Fluorescence emission was monitored at 1 frame per 180 seconds by collection windows for CFP emission and YFP emission (S470/30m and S535/30m, Chroma). CFP/YFP ratios were calculated using the Olympus Cell^^{R} package. Mitochondrial membrane potential was monitored simultaneously through exciting TMRE by using a 572 nm excitation filter with emission being collected in a third channel using a UBG triple bandpass emission filter. Automatic stage settings were employed to acquire data from the various conditions concomitantly.

3.12.2. Propidium Iodide uptake dynamics

Propidium Iodide (PI) is a membrane-impermeable dye which intercalates with the DNA. Its uptake is therefore an indication for the loss of membrane integrity, a hallmark of necrotic cell death. The cells were treated with pre-gassed modified ischaemic buffer (containing SDT) containing PI, layered with mineral oil (Meldrum *et al*., 2001, Patel *et al*., 2006,) and placed in a heated chamber (37℃) surrounding the stage. PI uptake was determined using an IX-81 Olympus microscope, coupled to a MT-20 (Soft Imaging Systems) xenon arc lamp by excitation using 572 nm excitation filters. Fluorescence emission was monitored at 1 frame per 180 seconds by collection windows for TexRed emission using a UBG triple bandpass emission filter. Automatic stage settings were employed to acquire data from the various conditions concomitantly.

3.12.3. LC3 imaging

Autophagy is a highly dynamic process. Autophagosomes fuse with lysosomes, to form autophagolysosomes, which are responsible for the rapid enzymatic degradation of lysosomal content. (Mizushima, 2005). It has also been shown, that damaged mitochondria may be part of this cargo, a process called mitophagy (Lemasters, 2005). To visualize these processes in our model, H9c-2 cells were transfected with 800 ng of LC3-GFP plasmid DNA construct (Yoshimori, 2000). Cells expressing the LC3-GFP fusion protein were incubated with 50 nM rapamycin for 24 hrs and imaged following pretreatment with 20 nM Tetramethylrhodamine Ethyl Ester (TMRE, Molecular Probes, T669) for 30 min at 37℃ or with 10 nM Lysotracker (Lysotracker® Red DN D-99, Molecular Probes, L7528). Fluorescence emission was monitored at 1 image frame per four seconds, by collection windows for GFP emission and TexRed emission.

3.13. Scanning Electron Microscopy

Cells were seeded onto coverslips, contained in petri dishes with a density of $1x10^5$ cells and submitted to simulated ischaemia. Imaging of the samples was accomplished using a Leo® 1430VP Scanning Electron Microscope. Prior to imaging, the coverslips were mounted on a stub with double sided carbon tape. The sample was then coated with a thin layer of gold in order to make the sample surface electrically conducting. The Scanning electron (SE) images show the surface structure of the cells. Beam conditions during surface analysis were 7 KV and approximately 1.5 nA, with a working distance of 13 mm and a spot size of 150.

3.14. Flow Cytometry

3.14.1. PI exclusion

Following submission to the SI protocol, cells were trypsinized using warm (37℃) 0.25% trypsin-EDTA, incubated until cells detached from the surface (3-4 min),

centrifuged for 3 min at 6000 x g and re-suspended in cold PBS. PI was directly added onto the unfixed cells, using a final concentration of 1 µg/ml, incubated for 10 min, and analyzed on the flow cytometer (BD FACSAria I) immediately thereafter. A minimum of 5000 events were collected using the 488 nm laser and 610LP, 616/23BP emission filters.

3.14.2. Tetramethylrhodamine Ethyl Ester (TMRE) intensity

The membrane potential-dependent dye tetramethylrhodamine ethyl ester selectively stains for mitochondria with an intact membrane, as described previously (Hanley *et al*., 2002). Following submission to the SI protocol, cells were trypsinized using warm (37℃) 0.25% trypsin-EDTA, incubated until cells detached from the surface (3-4 min), centrifuged for 3 min at 6000 x g and re-suspended in cold PBS. Unfixed cells were incubated with 1 µmol/l TMRE in PBS for 30 min at 37℃, then washed in PBS and immediately analyzed at room temperature. A concentration of 5 µmol/l Carbonyl cyanide m-chlorophenylhydrazone (CCCP, Sigma, C2759) was used as a positive control. Samples were analyzed on the flow cytometer (BD FACSAria I) and a minimum of 5000 events were collected, using the 488 nm laser and 610LP, 616/23BP emission filters. Fluorescence intensity signal was measured using the geometric mean on the intensity histogram.

3.14.3. ROS assessment

Relative ROS generation was evaluated with the aid of 6-carboxy-2'7'-dichlorodihydrofluorescein diacetate, di(acetoxymethyl ester (DCF, Molecular Probes, D399). Following submission to the SI protocol, cells were trypsinized using warm (37℃) 0.25% trypsin-EDTA, incubated until cells detached from the surface (3-4 min), centrifuged for 3 min at 6000 x g and re-suspended in cold PBS. Unfixed cells were incubated with 50 µmol/l DCF in PBS for 20 min at 37℃, and then washed in PBS and immediately analyzed at room temperature. A concentration of 100 µmol/l H_2O_2 was used as a positive control. Samples were

analyzed on the flow cytometer (BD FACSAria I) and a minimum of 5 000 events were collected. The 488 nm laser and 502LP, 530/30BP emission filters were employed. Fluorescence intensity signal was measured using the geometric mean on the intensity histogram.

3.14.4. Acridine Orange staining

Acridine Orange (AO) is a ratiometric dye, which binds to DNA but also accumulates in acidic compartments such as lysosomes. (emission particulars). It is therefore being used for DNA related studies as well as an indicator for an increase in acidic compartments (Harhaji-Trajkovic *et al*., 2008). As autophagy is characterized by the development of acidic vesicular organelles (AVO's), AO can has been employed to detect and quantify AVO's (Azad *et al*., 2008). Following submission to the SI protocol, cells were trypsinized using warm (37℃) 0.25% trypsin-EDTA, incubated until cells detached from the surface (3-4 min), centrifuged for 3 min at 6000 x g and re-suspended in cold PBS. Acridine Orange (Sigma, 212536) was added to the unfixed cells, using a final concentration of 5 mM, and incubated for 15 min at room temperature. Samples were analyzed on the flow cytometer (BD FACSAria I) immediately thereafter and a minimum of 5000 events were collected. The 488 nm laser and 610LP, 616/23BP and 502LP, 530/30BP emission filters were employed. Fluorescence intensity signal was measured using the geometric mean on the intensity histogram and expressed as ratio.

3.15. Perfusion technique of isolated perfused rat heart

Hearts were rapidly excised, arrested in ice-cold (4℃) normal saline solution and mounted onto the aortic cannula. Hearts were perfused retrogradely in a non-recirculating manner at 100 cm H_2O for 15 min. During this time, the left atrium was cannulated to allow atrial perfusion (atrial pressure 15 cm H_2O) according to the working heart model of Neely as modified by Opie and co-workers (1971). The left

ventricle ejected against a hydrostatic pressure of 100 cm H_2O. Perfusate temperature was 37 ℃ and thermostatically controlled as well as continuously monitored by inserting a temperature probe into the pulmonary artery.

3.16. Perfusion Buffer

A modified Krebs-Henseleit bicarbonate buffer was used containing (in mM) NaCl 119, $NaHCO_3$ 25, KCl 4.7, KH_2PO_4 1.2, $MgSO_4.7H_2O$ 0.59, Na_2SO_4 0.59, $CaClH_2O$ 1.25 and glucose 10. Oxygenation was achieved by gassing the perfusate with 95%O_2/5%CO_2.

3.17. Determination of function

Coronary (Qe) and aortic (Qa) flow rates in ml/minute were measured manually. Aortic pressure was obtained through a side-arm of the aortic cannula which was connected to a Viggo-Spectramed pressure transducer and was recorded in mm Hg. The peak systolic pressure (PSP) and heart rate (HR) were obtained from the recordings made. The following parameters were calculated:

Cardiac output (CO) (ml/min) = (Qa+Qe)

Stroke volume (SV) (ml/min) = (CO/HR)

Mean external power produced by the left ventricle (TW) in mWatts according to Kannengieser and coworkers (1979):
$0.002222(P_{AO}-11.25)(CO)$ where P_{AO} = aortic pressure, CO = cardiac output

3.18. Perfusion sequence

Hearts were perfused for a control period, followed by 3 different periods of sustained ischaemia and one defined period of reperfusion. The exact perfusion protocol will be described in the relevant sections.

Hearts were subjected to sustained ischaemia (normothermic total global ischaemia) by simultaneous clamping of both aorta and left atrial supply tubes. During the ischaemic period, hearts were enchambered by a small stoppered water jacketed chamber for maintenance of the temperature at 36.5 ℃. The duration of sustained ischaemia will be indicated in the relevant sections. The hearts were subsequently reperfused, first retrogradely for 10 min, and then as working hearts for 20 min.

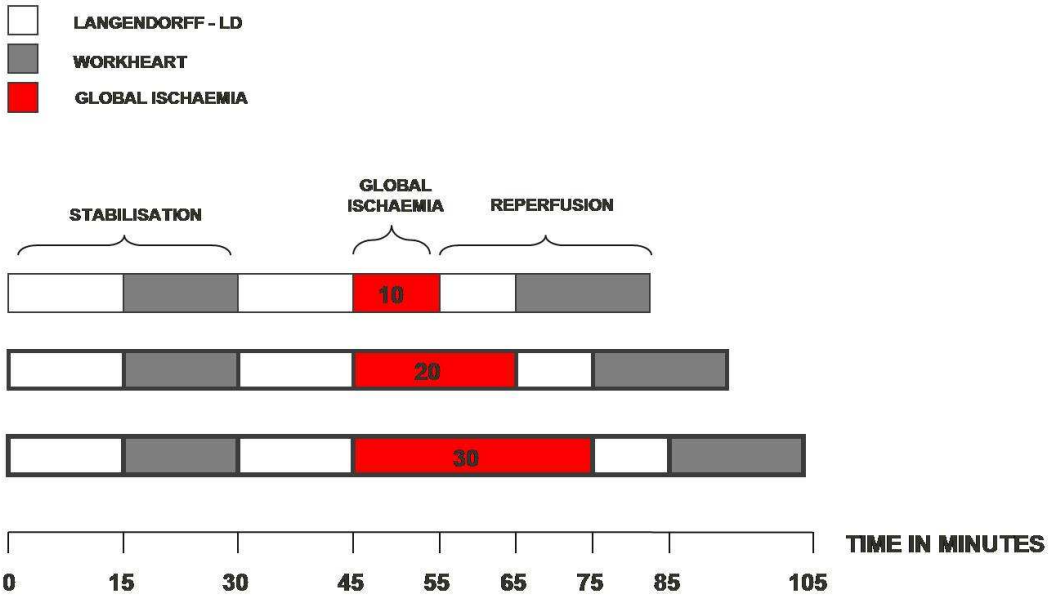

Figure 3.5: *Ex vivo* experimental protocol for 3 time points of global ischaemia.

In an additional series of perfusions, hearts were stabilized and then perfused with either 1 nM Rapamycin or 1 mM 3MA for 10 min in working heart mode, followed by 40 min retrograde perfusion in the Langendorff mode. Hearts were then

subjected to 20 min sustained ischaemia (normothermic total global ischaemia) by simultaneous clamping of both aorta and left atrial supply tubes. During the ischaemic period, hearts were enchambered by a small stoppered water jacketed chamber for maintenance of the temperature at 36.5 ℃. The hearts were subsequently reperfused, first retrogradely for 10 min, and then as working hearts for 20 min.

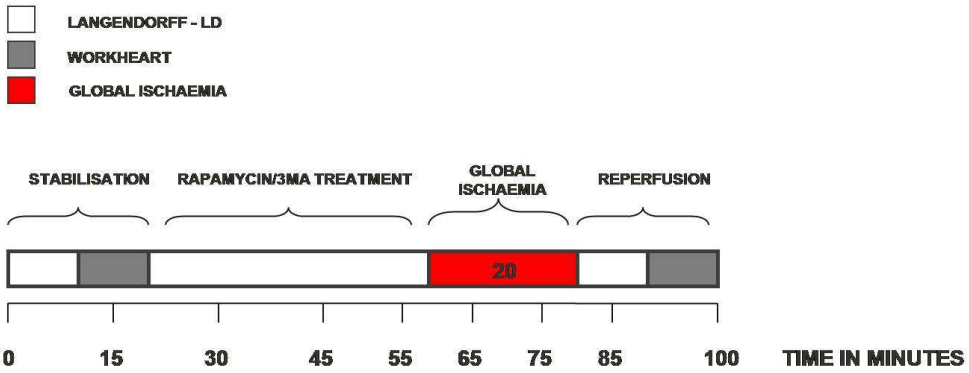

Figure 3.6: *Ex vivo* experimental protocol of global ischaemia with induced and inhibited autophagic activity.

3.19. Histology

3.19.1. Fixation and sectioning

Heart tissue was fixed in 10% paraformaldehyde at 4℃ to allow slow preservative penetration of the fixative into the myocardial tissue (Histologische Technik, Burck, 1988). The samples were then processed, utilizing automated tissue processing (Tissue Tek II). In brief, samples were dehydrated using 70%, 90%, 95% and 100% ethanol and cleared by using xylol which was followed by paraffin wax impregnation (Histosec paraffin wax). Total processing time was 20 hrs.

Paraffin embedded sectioning was performed on a R Jung microtome (Heidelberg, Germany), generating 5 µm sections which were collected on poly-L-lysine (P8920, Sigma) coated slides. Samples were then processed and rehydrated using a xylol and an ethanol dilution range. In brief, sections were incubated in xylol, 100%, 95%, 80% and 50% ethanol, followed by a rinsing step in distilled water.

3.19.2 Haematoxylin Eosin (H&E) staining

Sections were stained using Harris haematoxylin (Merck, solution to Meyer's, 161207) (5g Harris haematoxylin, 100g Ammonium Alum, 50 ml 100% ethanol, 2.5g mercuric acid and 1 l distilled water), 10% acid alcohol (10 ml 1% HCl dissolved in 70% ethanol), Scott's tap water (3.5g $NaHCO_3$, 20g $MgSO_4$, 10 ml 37% formalin and 1 l tap water) and Eosin (Riedel De-Haën, 32617). H&E staining results in deep blue nuclei and pink cytoplasm. Samples were submitted to a staining procedure by using a sequence of: xylol, absolute, 95% and 70% ethanol, distilled water, Harris haematoxylin, distilled water, acid alcohol, distilled water, Scott's tap water, distilled water, eosin, distilled water, 70%, 95% and absolute ethanol followed by xylol. Slides were mounted using mounting media (Jung, tissue freezing medium, 020108926).

3.19.3. Immunofluorescence staining

After completion of sectioning and rehydration, slides were incubated for 15 min in pre-warmed (37℃) 0.1% trypsin in PBS, followed by a rinsing step with distilled water. This "unmasking" or antigen retrieval facilitates the immunological reaction of antibodies with antigens. Samples were then immunostained for LC3, cleaved PARP and HMGB1 (as described in section 3.9) where after slides were mounted using fluorescence mounting media.

3.20. Statistical analysis

The results are expressed as mean values ± SEM and were analyzed by one-way Analysis of Variance (ANOVA) with the Bonferroni correction. The α-level was 0.05. The statistics software, Graph Pad Prism 2.01, was employed to perform statistical tests. Data were considered to be statistically significant with a p value <0.05. For the time lapse experiments as part of the dynamic onset study, sigmoid curves were fitted with Prism according to: LSD test; variable EC50 (Rep=1 Model: V4=bottom+(top-bottom)/(1+10^((V3-EC50)*slope)) and probabilities for Post Hoc tests with the effect of treatment, were determined.

CHAPTER 4 RESULTS: TIME POINTS

4.1. *In vitro* model: Three time points and three severities of simulated ischaemia

The term *ischaemia* is derived from the Greek “ischein”, to restrict and “haima”, meaning blood. In plain terms, it means too little blood (Opie, 1991). This condition of ischaemia can be mimicked in an experimental setup and is termed simulated or experimental ischaemia.

In order to assess the role of an ischaemic insult in the induction and execution of cell death, H9c-2 cells were submitted to a protocol of simulated ischaemia lasting for 2, 4 and 8 hrs followed by a 1 hr reperfusion phase (Fig. 4.1). Rat ventricular cardiomyoblast cells, H9c-2, have been widely used as an *in vitro* model of acute myocardial infarct (Krijnen *et al.,* 2005, Agnetti *et al*., 2005, Bonavita *et al*., 2003). We have therefore chosen this cell line to study the contribution of autophagy, apoptosis and necrosis in differential simulated ischaemic settings.

Components characteristic of an ischaemic event include substrate omission, lactate formation, acidosis, high potassium levels and hypoxia (Coetzee & Opie, 1987). Although ischaemia leads, due to the reduction in coronary flow, to foci of tissue hypoxia and anoxia, the metabolic aspects of ischaemia and anoxia in the myocardial tissue differ in regard to tissue acidosis, glucose uptake and residual oxidative capacity (Opie, 1991). This model of simulated ischaemia we employed, has widely been used in the field of cardiovascular research (Krijnen *et al.,* 2005, Agnetti *et al*., 2005, Bonavita *et al*., 2003). We have chosen a combination of originally independent models, as it is our aim to create differential severities of simulated ischaemia. A combination of hyperkalemia, acidosis, hypoxia, the absence of glucose and metabolic inhibition was chosen to simulate an ischaemic event. A modified ischaemic buffer (Esumi *et al.,* 1991) with either 2-deoxy-D-glucose (Fuglesteg *et al.,* 2008), sodium dithionate (Seyedi *et al.,* 2002), or both

(Cumming *et al.*, 1996) was employed with the aim to create an ischaemic insult of mild, moderate and severe character respectively. In the myocardium these severities may represent the scenarios described as mild, severe and lethal ischaemia, found between the infarct zone and the area at risk (Hearse *et al*., 1981, Opie, 1991). Sodium dithionite was chosen, as it allows a reversible reperfusion phase, unlike metabolic inhibitors such as KCN (Al-Dadah *et al*., 2007).

Reperfusion was mimicked by incubating the cells subsequent to the simulated ischaemic event in normal culture medium under a 5% CO_2 atmosphere at 37℃.

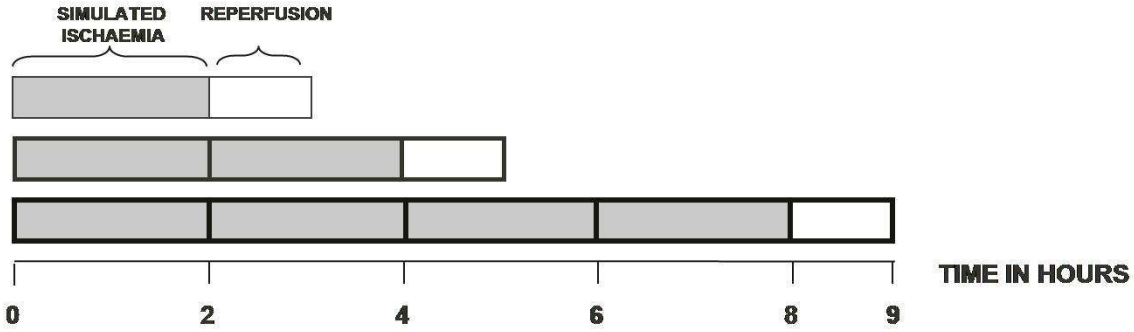

Figure 4.1: *In vitro* experimental protocol. Cells were exposed to 2, 4 and 8 hrs mild, moderate or severe SI, followed by 1 hr reperfusion respectively.

4.2. Experimental measurements after 2 hrs SI

4.2.1. PI exclusion and nuclear condensation

The loss of membrane integrity as well as nuclear condensation (pyknosis) and fragmentation (karyorhexis) have been described as morphological hallmarks for necrosis and apoptosis respectively (Kajstura *et al*., 1996). Propidium iodide exclusion and Hoechst imaging techniques (Asoh *et al*., 2005) were used to assess the contribution of necrosis and apoptosis in this experimental model of simulated ischaemia.

As shown in Fig 4.2., control cells (Con) kept under normoxic conditions, are highly viable (0.3±0.2% PI positive cells and 4.8±0.8% pyknotic cells), whilst exposure to mild SI increased the number of pyknotic cells significantly [14.1±0.9% ($p<0.05$)]. A significant increase in both PI positive cells and pyknotic cells compared to Con cells was observed in cells exposed to moderate SI [10.3±2.3% PI positive cells ($p<0.05$), 9.8 ±1.4% pyknotic cells ($p<0.05$)] and severe SI [12.1±2.0% PI positive cells ($p<0.05$), 10.9±1.5% pyknotic cells ($p<0.05$)] respectively. Following a 1 hr reperfusion phase (Fig. 4.3.), the number of pyknotic cells further increased in mild SI (17.2±1.7%). However, PI positive cells remained at control levels (2.2±1.2%). Cell death further increased in cells submitted to moderate SI (18.3±5.3% PI positive cells, 18.3±1.5% pyknosis) and severe SI (20.8±4.9% PI positive cells, 21.3±1.8% pyknotic cells).

The buffer alone did not have any significant effect on cell death (1.6±0.4% PI positive cells, 1.3±0.7% pyknosis) compared to control cells (addendum).

4.2.1. $_{2hrs\ SI/R}$ PI exclusion and nuclear condensation

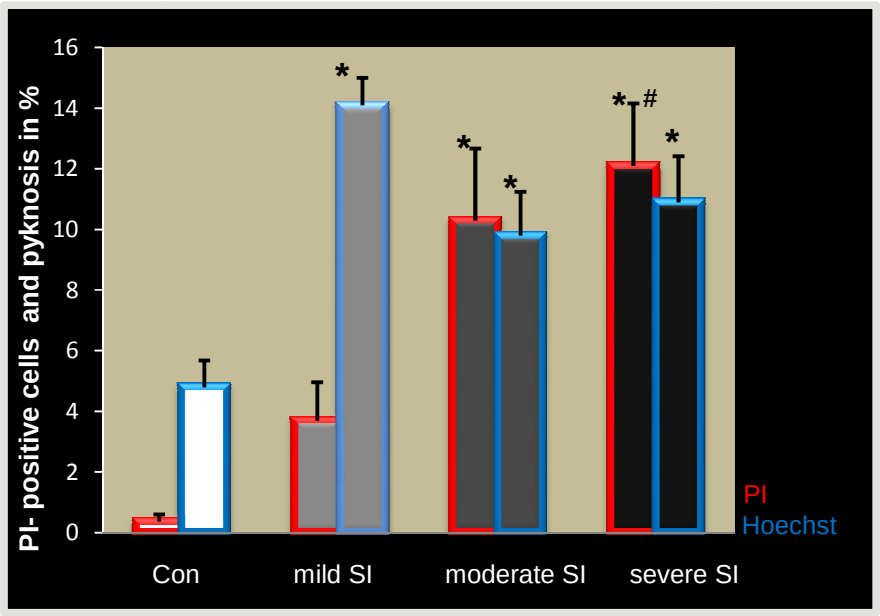

Figure 4.2: 2 hrs SI. Data expressed as mean ± SEM, statistical analysis: ANOVA & Bonferroni correction, * p<0.05 vs Con, # p<0.05 vs mild SI, n=9, >150 cells counted.

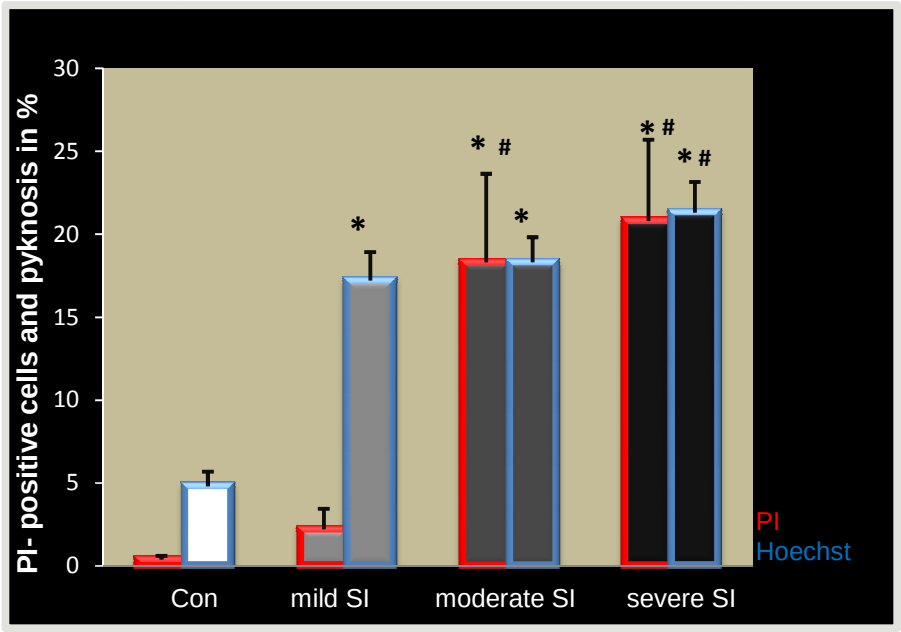

Figure 4.3 2 hrs SI/R. Data expressed as mean ± SEM, statistical analysis: ANOVA & Bonferroni correction,* p<0.05 vs Con, # p<0.05 vs mild SI, n=9, >150 cells counted.

4.2.2. MTT assay and ATP analysis

About two percent of the total myocyte ATP is consumed per systole-diastole cycle, indicating that the total ATP amount in the cell is consumed in less than one minute (Jafri *et al*., 2001). As the heart beats about three billion times in its life time (Hamacher-Brady *et al.*, 2006), it becomes clear that an extremely efficient system of energy conversion needs to be in place to maintain myocardial ATP homeostasis.

In order to assess the cell's metabolic state during the ischaemic event, an MTT assay (Gomez *et al*., 1997, Goodwin *et al*., 1995) and ATP analysis (Essman *et al*., 2003) were performed and results normalized. The MTT assay is based on the cell's capacity to reduce MTT into formazan pigments by (primarily) mitochondrial enzymes, indicating the cell's reductive capacity, which in turn serves as an indication for the relative survival rate of the cell. The ATP assay measures total ATP availability at the time of injury. A reduction in oxygen availability will attenuate oxidative phosphorylation, leading to increased ADP and creatine and decreased ATP and creatine phosphate. ATP levels decrease rapidly during ischaemia but also recover rapidly after reperfusion (Takagi *et al*., 2007). The dynamics of ATP depletion becomes highly relevant when considering the molecular overlap between autophagy, apoptosis and necrosis (Klionsky *et al*., 2008, Ziporen *et al.*, 2009, Karantza-Wadsworth *et al*., 2007). A progressive replacement of necrosis with apoptosis has been described when intracellular ATP becomes available (Han *et al*., 2007).

As shown in Fig 4.4, the relative viability based on MTT decreased significantly after 2 hrs mild SI (31.5±2.6%), moderate SI (36.6±4.4%) and severe SI (30.3±2.7%) compared to control cells. However, compared to control ATP levels, ATP significantly increased in mild SI (264±62.1%) but not so in moderate SI (99.5±39%) or severe SI (91±28.9%). Following 1 hr reperfusion (Fig. 4.5), mitochondrial viability recovered but remained significantly lower compared to control viability [mild SI: 81.1±2.9%; moderate SI: 79.7±1.1%; severe SI: 78.7±1.0% ($p<0.05$)]. ATP levels returned to control levels in mild SI (85.5±8.8%),

whilst ATP levels significantly decreased in moderate SI [68.3±14.4% ($p<0.05$)] and in severe SI [47.3±5.8% ($p<0.05$)].

4.2.2. $_{2hrs\ SI/R}$ MTT assay and ATP analysis

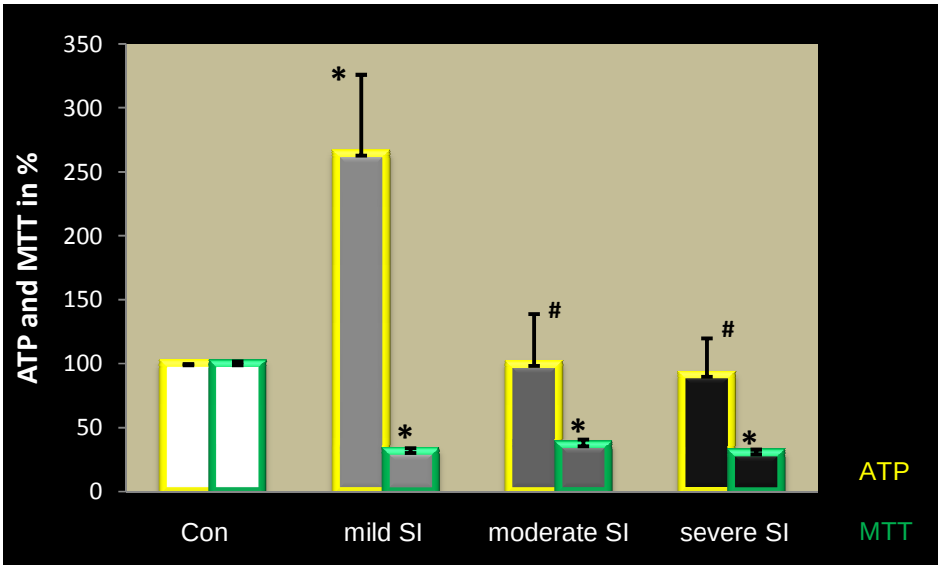

Figure 4.4 2 hrs SI. Normalised data expressed as mean ± SEM, statistical analysis: ANOVA & Bonferroni correction, * p<0.05 vs Con, # p<0.05 vs mild SI, n=9-14.

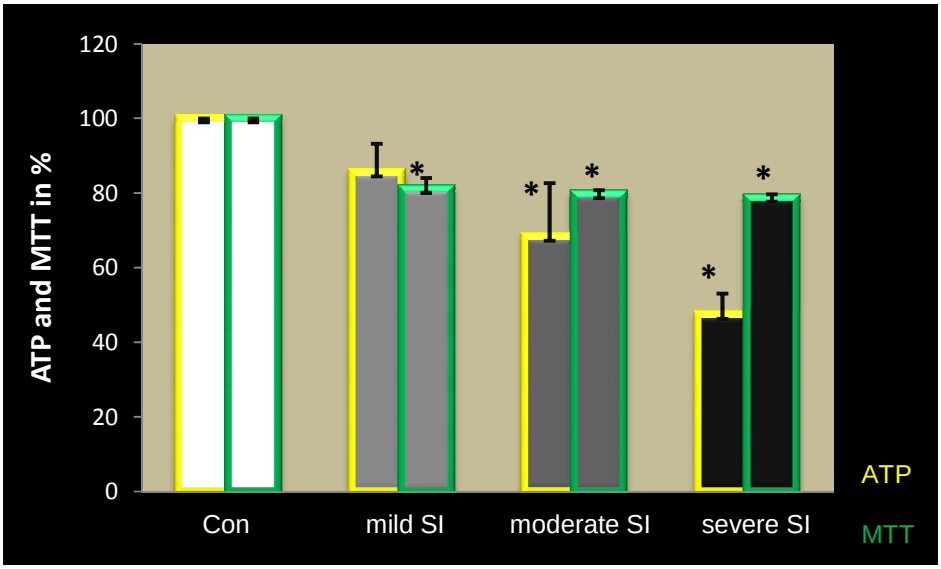

Figure 4.5 2 hrs SI/R. Normalised data expressed as mean ± SEM, statistical analysis: ANOVA & Bonferroni correction, * p<0.05 vs Con, # p<0.05 vs mild SI, n=9-10.

4.2.3. Western blot analysis

Western blot analysis reveals a differential and gradual induction of phosphorylated AMPK following 2 hrs of the ischaemic event (Fig. 4.6). No phosphorylation is apparent in control cells but a gradual increase in the band signal is visible from mild SI to moderate SI with the strongest signal in severe SI. This phosphorylation pattern is lost at reperfusion (Fig. 4.6). Caspase-3 (Fig. 4.9) and cleaved PARP (Fig. 4.10) analysis revealed an increased cleavage of caspase-3 and PARP primarily in mild SI. A faint band of cleaved PARP also seems to be present during moderate and severe SI. No changes in beclin-1 (Fig. 4.8) and the phosphorylation state of mTOR (Fig. 4.7) are visible at this early time of ischaemia.

4.2.3. $_{2hrs\ SI/R}$ Western blot analysis

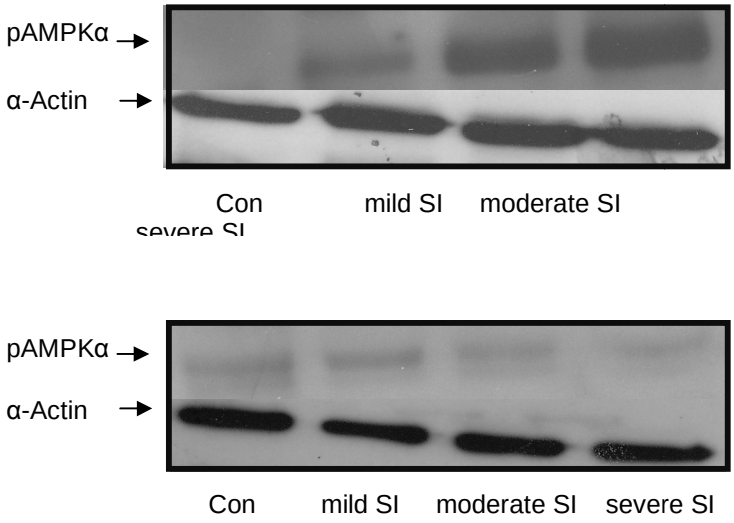

Figure 4.6: pAMPKα activation indicated through the 62 kDa band following 2 hrs SI (top) and SI/R (below). A representative blot is shown.

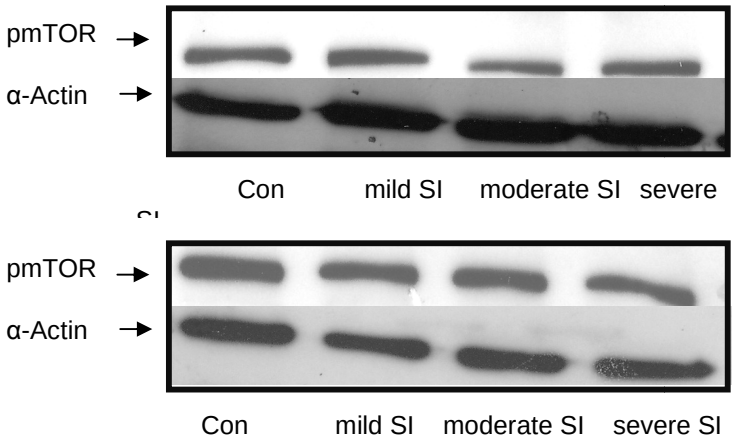

Figure 4.7: pmTOR activation indicated through the 289 kDa band following 2 hrs SI (top) and SI/R (below). A representative blot is shown.

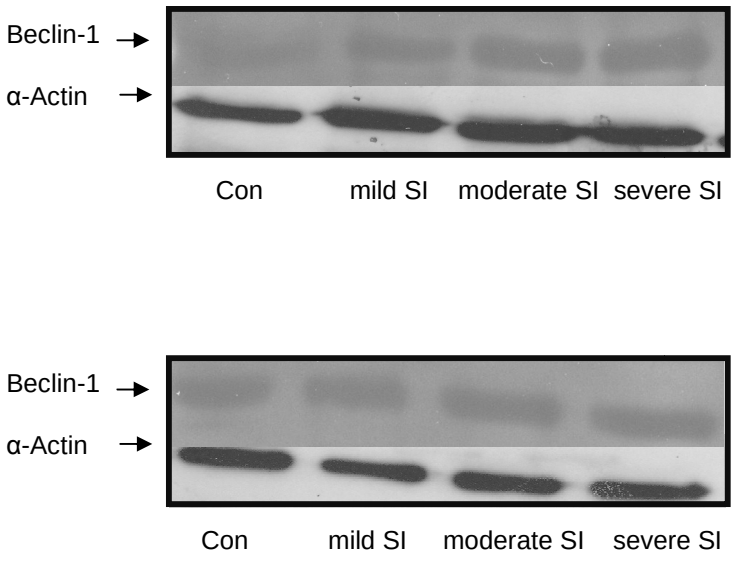

Figure 4.8: Beclin-1 activation indicated through the 57 kDa band following 2 hrs SI (top) and SI/R (below). A representative blot is shown.

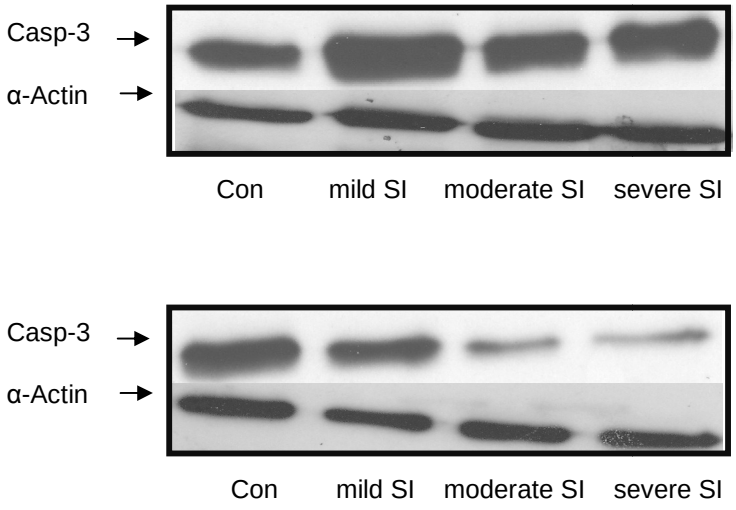

Figure 4.9: Uncleaved caspase-3 indicated through the 35 kDa band following 2 hrs SI (top) and SI/R (below). A representative blot is shown.

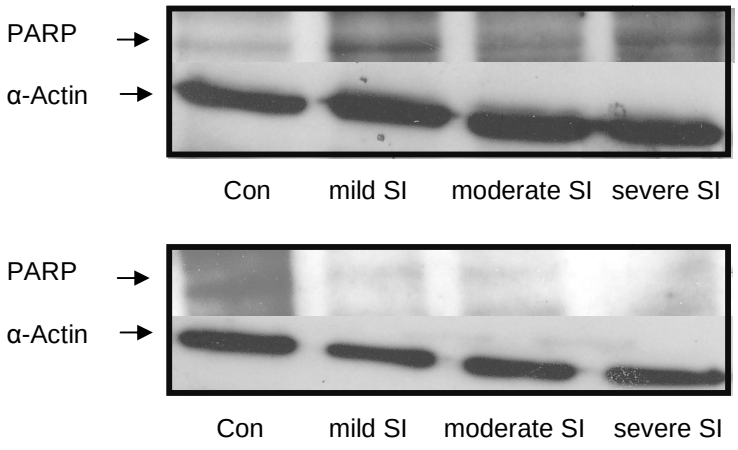

Figure 4.10: PARP cleavage indicated through the 89 kDA band following 2 hrs SI (top) and SI/R (below). A representative blot is shown.

4.2.4. Immunofluorescence and Scanning Electron Microscopy

Although transmission electron microscopy (TEM) remains the standard method for monitoring autophagy in tissue, it is, however, extremely labour intensive and gives no indication of the progress within or flux through the autophagic pathway. A growing body of evidence suggests that mammalian microtubule-associated protein 1 light chain 3 (LC3), which functions as a structural component during autophagosome maturation, is also a reliable biomarker for autophagy. In order to assess cellular autophagic activity, cells with numerous LC3 autophagosomes were counted (Fig 4.11). Our results indicate that following 2 hrs ischaemia, mild SI leads to a significant increase in cells with numerous LC3 punctae [27.8±4.4% ($p<0.05$)] compared to control cells (0.9±0.4%), with no significant increase in moderate (6.1±1.4%) and severe SI (3.6±1.1%) (Fig. 4.12). During reperfusion this increase in LC3-positive cells in mild SI is lost (Fig. 4.13).

The fluorescence LC3 images (Fig. 4.14) reveal a perinuclear LC3 accumulation in mild SI but not in moderate and severe SI. The morphological structure of the cells, based on the actin cytoskeleton, indicates loss of membrane integrity in cells exposed to moderate and severe SI (Fig. 4.14, 4.15). Immunofluorescence staining for beclin-1 (Fig. 4.16, 4.17) reveals a fine tubulin-like pattern in control cells as well as in cells exposed to SI. Moreover, cytochrome-c appears to be released in mild, moderate and severe SI compared to control cells (Fig 4.16, 4.17).

The chromatin component, High Mobility Group Box chromosomal protein 1 (HMGB1) has been shown to be released by necrotic cells, triggering inflammation (Bonaldi *et al*., 2003). Our results show a clear relocation of HMGB1 from the nucleus to the cytosol during all three ischaemic conditions (Fig. 4.18).

The scanning electron (SE) images (Fig. 4.20) show distinct surface morphology between the ischaemic groups. Mild SI shows primarily shrunk and membrane-blebbed cells, which is typical of a morphology associated with apoptosis (Kerr *et al*., 1972). Moderate SI and severe SI on the other hand, show cells which appear flat adherent to the surface of the slide and swollen in their morphology, indicating loss of membrane integrity and an increase in cell volume. These results are in agreement with the morphology of necrosis (Festjens *et al.,* 2006).

4.2.4. $_{2hrs\ SI/R}$ Immunofluorescence- and Scanning Electron Microscopy

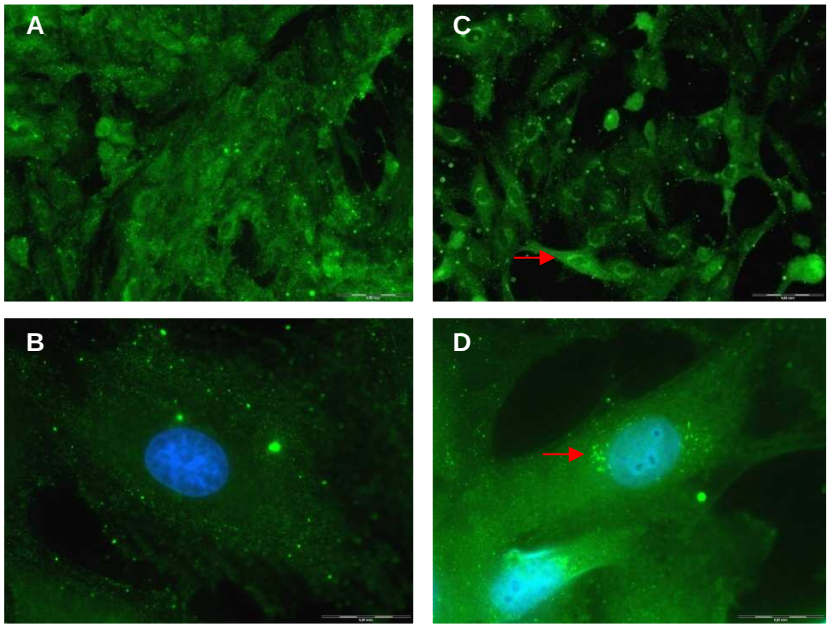

Figure 4.11: Fluorescence micrographs showing cells with numerous LC3 punctae (right) compared to control conditions (left). Scale bar: 0.05 mm (A and C) and 0.02 mm (B and D).

4.2.4. $_{2hrs\ SI/R}$ Quantification of cells with numerous LC3 punctae

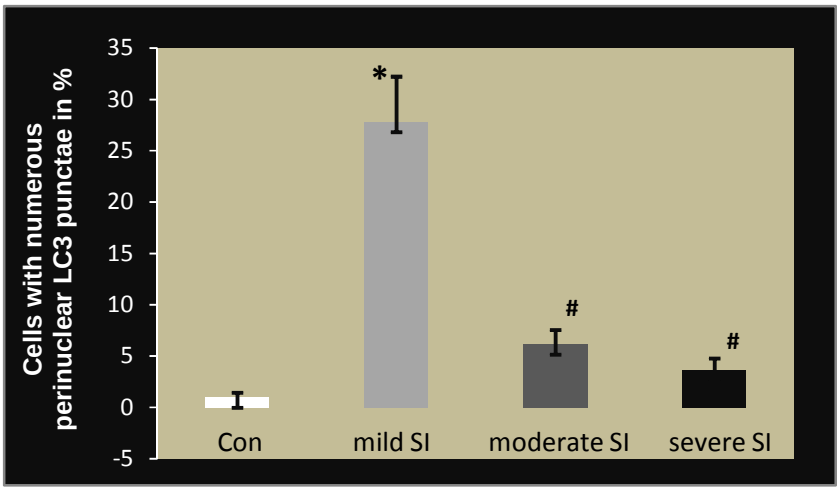

Figure 4.12: 2 hrs SI. Data expressed as mean ± SEM, statistical analysis: ANOVA & Bonferroni correction, * p<0.05 vs Con, # p<0.05 vs mild SI n=9, >150 cells counted.

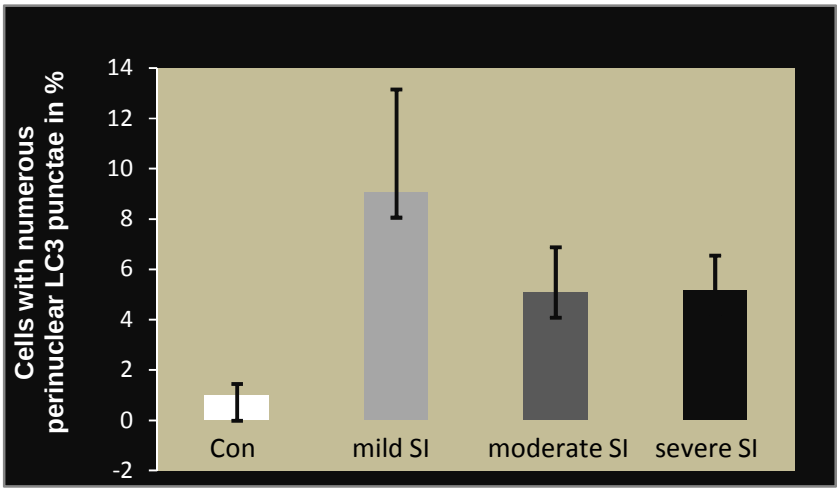

Figure 4.13: 2 hrs SI/R. Data expressed as mean ± SEM, statistical analysis: ANOVA & Bonferroni correction, * p<0.05 vs Con, # p<0.05 vs mild SI n=9, >150 cells counted.

4.2.4. $_{2hrs\ SI/R}$ Fluorescence Microscopy

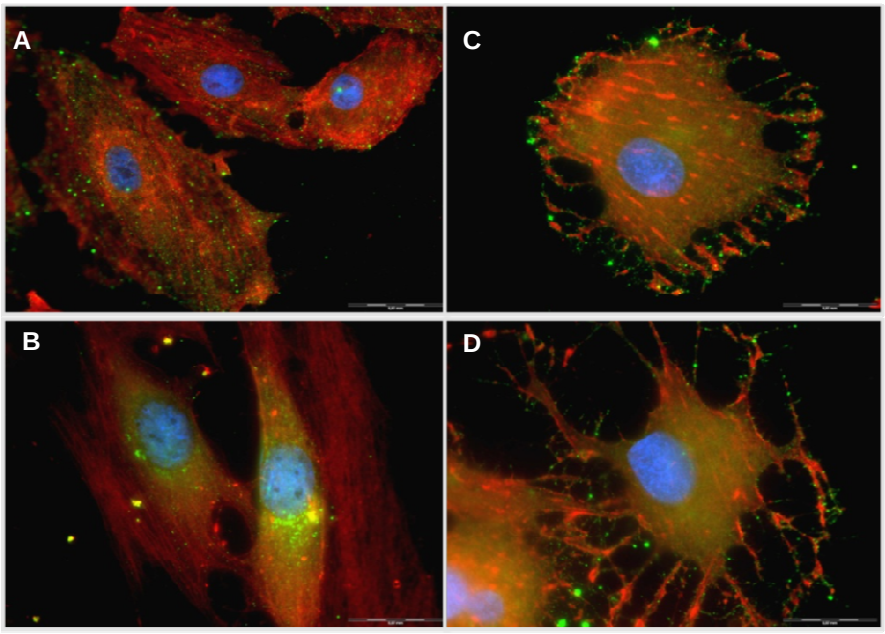

Figure 4.14: 2 hrs SI. H9c-2 myoblasts labelled with LC3/FITC, Actin/TexRed & Hoechst 33342. A: Con, B: mild SI, C: moderate SI, D: severe SI.

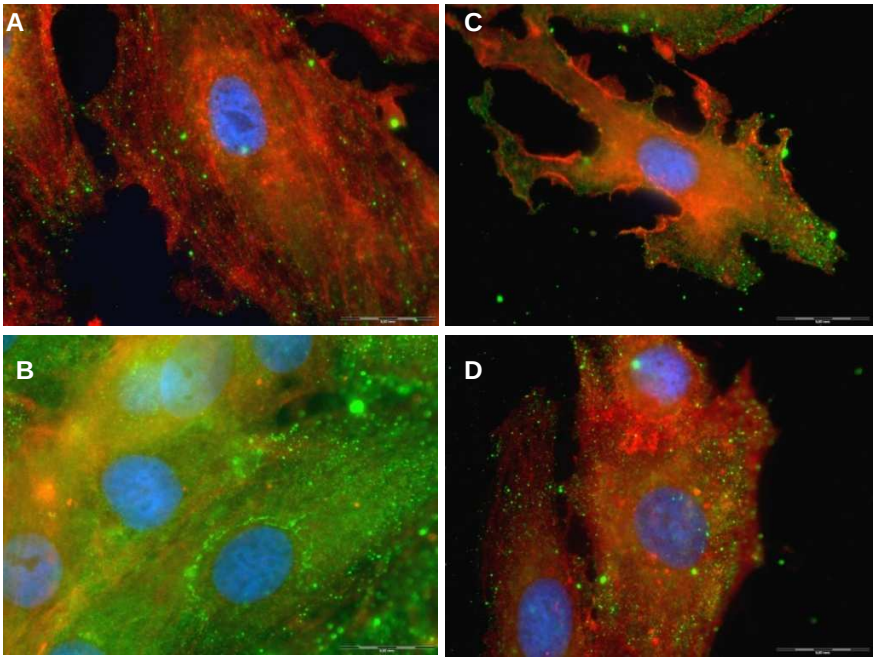

Figure 4.15: 2 hrs SI/R H9c-2 myoblasts labelled with LC3/FITC, Actin/TexRed & Hoechst 33342. A: Con, B: mild SI, C: moderate SI, D: severe SI.

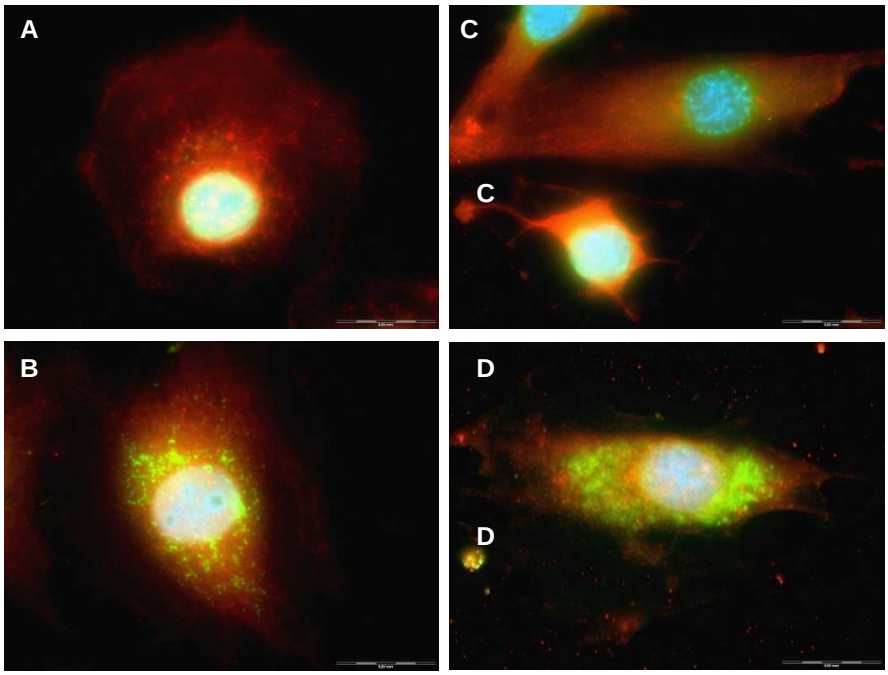

Figure 4.16: 2 hrs SI. H9c-2 myoblasts labelled with Cyt-c/FITC, Beclin-1/TexRed & Hoechst 33342. A: Con, B: mild SI, C: moderate SI, D: severe SI.

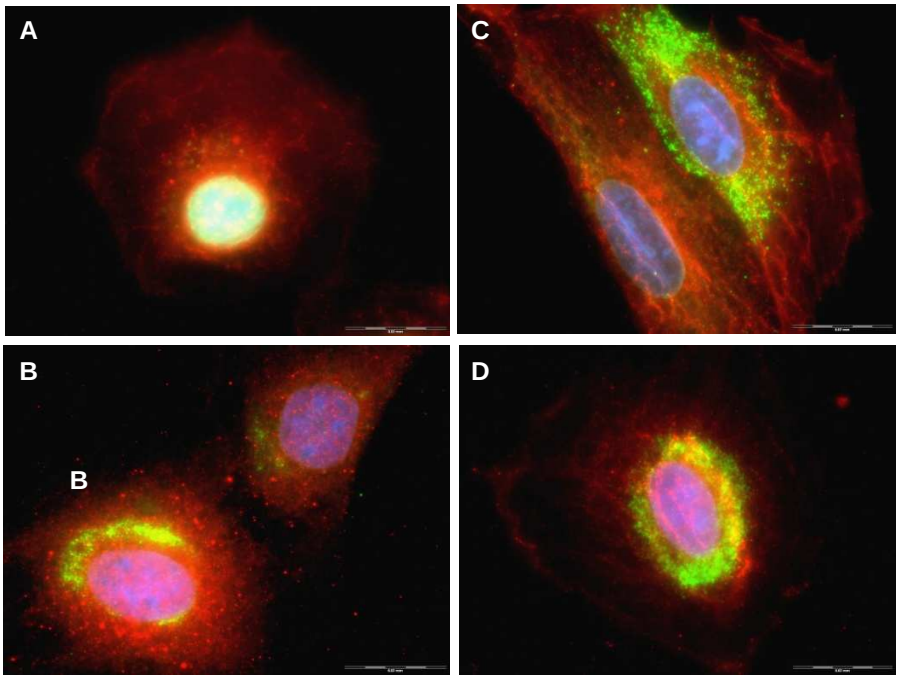

Figure 4.17: 2 hrs SI/R. H9c-2 myoblasts labelled with Cyt-c/FITC, Beclin-1/TexRed & Hoechst 33342. A: Con, B: mild SI, C: moderate SI, D: severe SI.

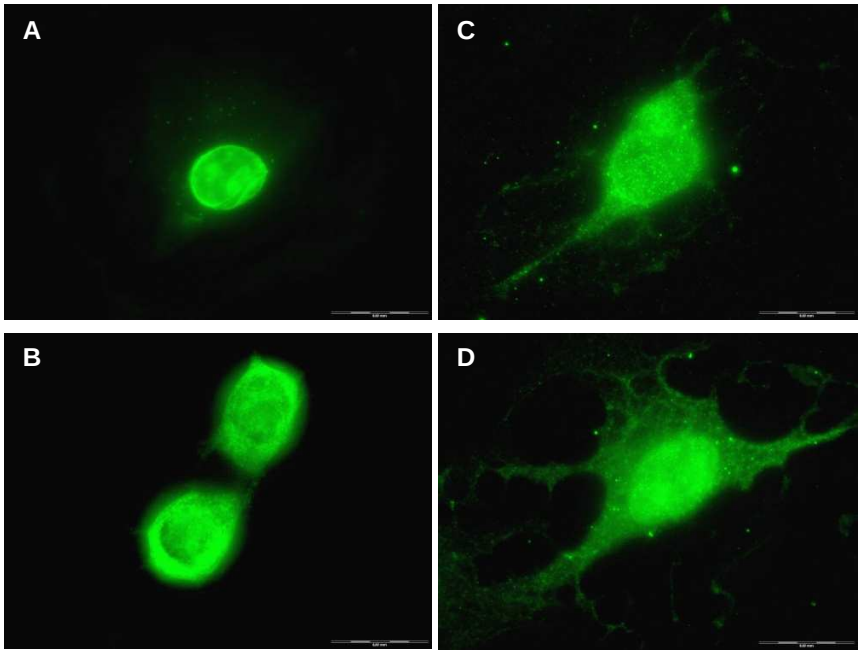

Figure 4.18: 2 hrs SI. H9c-2 myoblasts labelled with HMGB1/FITC. A: Con, B: mild SI, C: moderate SI, D: severe SI.

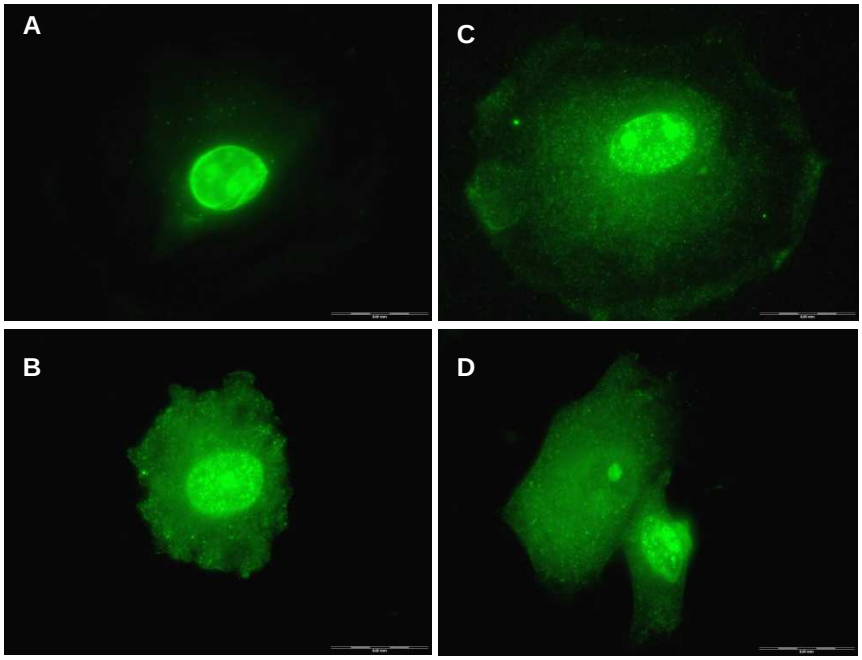

Figure 4.19: 2 hrs SI/R. H9c-2 myoblasts labelled with HMGB1/FITC. A: Con, B: mild SI, C: moderate SI, D: severe SI.

4.2.4. $_{2hrs\ SI/R}$ Scanning Electron Microscopy (SEM)

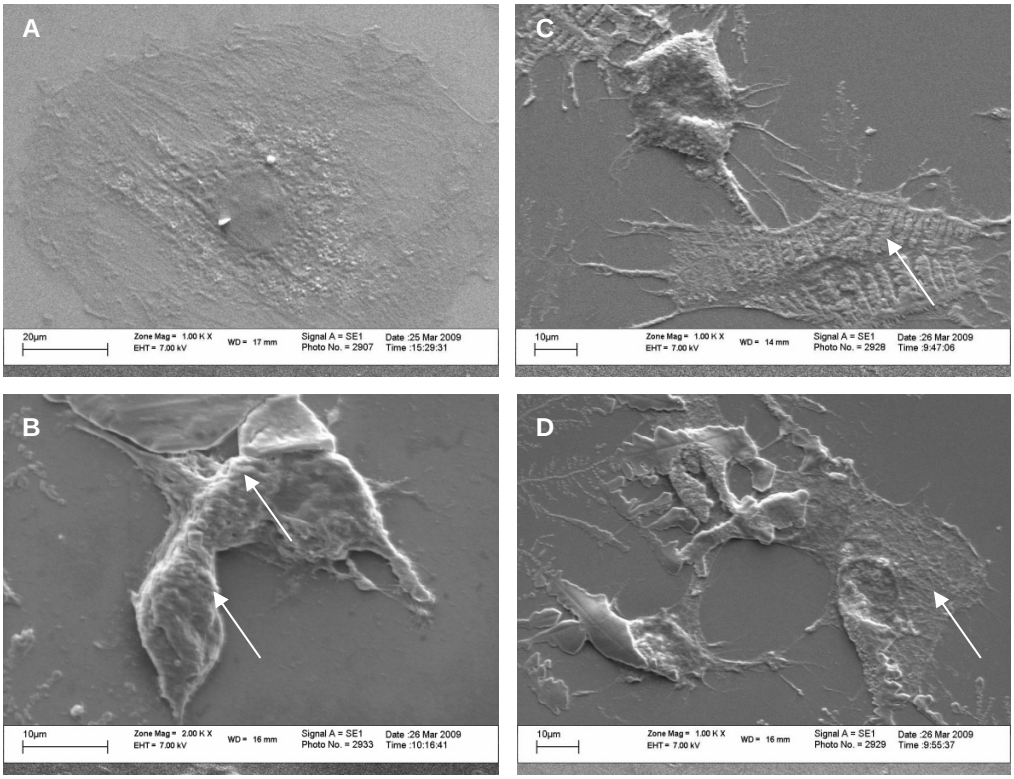

Figure 4.20: 2 hrs SI. SEM micrographs of H9c-2 myoblasts. A: Con, B: mild SI, C: moderate SI, D: severe SI. Apoptotic cells show characteristic shrinkage and membrane blebbing (B). Necrotic cells appear attached and swollen (C and D).

4.3. Experimental measurements after 4 hrs SI

Due to the highly dynamic character of cell death modes within and between one another during the progression of an ischaemic insult, it is important to also adopt a dynamic approach that includes the investigation of multiple time points during ischaemic injury.

4.3.1. PI exclusion and nuclear condensation

Following 4 hrs SI the results for PI-positive and pyknotic cells indicate an exacerbation of the results described at 2 hrs SI. In mild SI no significant increase in PI-positive cells was observed (4.5±1.5%) compared to control cells (0.9±0.4%) (Fig. 4.21). Pyknotic cells, however, increased significantly [33±3.3% ($p<0.05$)] compared to control cells (10.1±1.0%). In moderate [14.6±3.0% ($p<0.05$)] and severe SI [24.4±2.7% ($p<0.05$)] a significant increase in PI-positive cells was observed. Pyknotic cells increased significantly in moderate SI [16.9±2.6% ($p<0.05$)] and severe SI [17.3±2.2% ($p<0.05$)] respectively compared to control cells (Fig. 4.21).

With reperfusion no increase in PI-positive cells was observed in mild SI (1.7±0.8%). However, a significant increase was apparent in moderate SI [40.3±6.7% ($p<0.05$)] and severe SI [92.4±1.8% ($p<0.05$)] respectively, compared to control cells (Fig. 4.22). An increase in pyknotic cells was observed in mild SI [34.6±3.9% ($p<0.05$)], moderate SI [33.4±5.5% ($p<0.05$)] and severe SI [31.2±4.5% ($p<0.05$)].

4.3.1. 4hrs SI/R PI exclusion and nuclear condensation

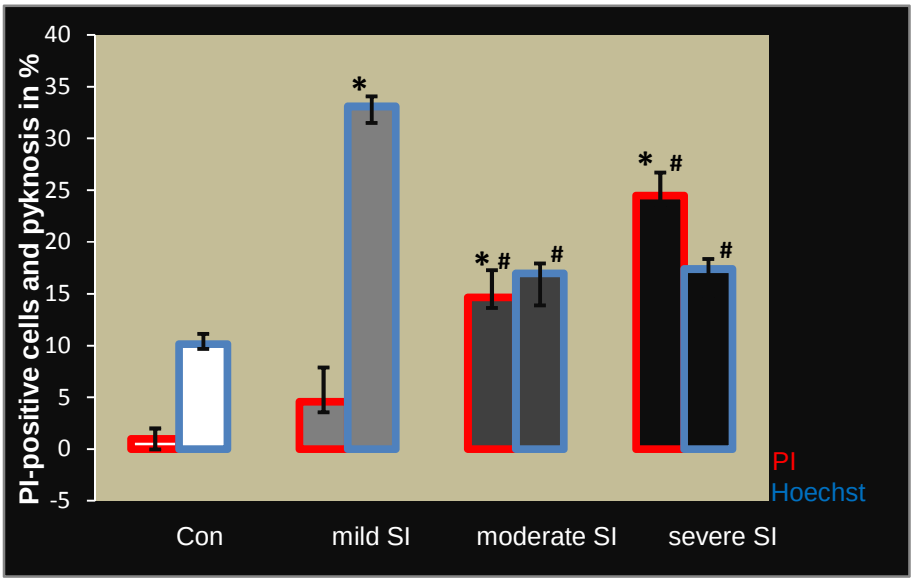

Figure 4.21: 4 hrs SI. Data expressed as mean ± SEM, statistical analysis: ANOVA & Bonferroni correction, * p<0.05 vs Con, # p<0.05 vs mild SI, n=9, >150 cells counted

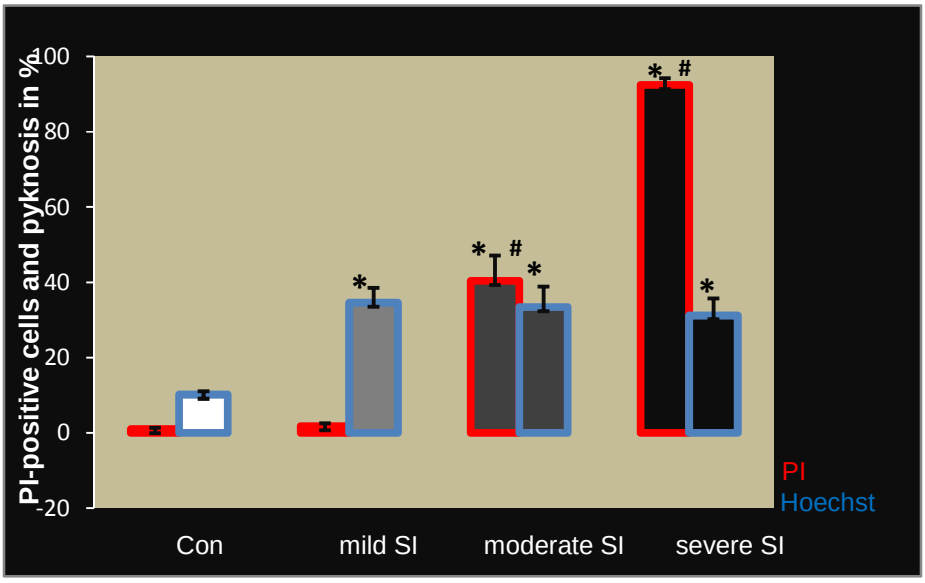

Figure 4.22: 4 hrs SI/R. Data expressed as mean ± SEM, statistical analysis: ANOVA & Bonferroni correction, * p<0.05 vs Con, # p<0.05 vs mild SI, n=9, >150 cells counted.

4.3.2. MTT assay and ATP analysis

As shown in Fig. 4.22, the relative viability based on MTT decreased significantly after 4 hrs mild SI (42.3±1.9%), moderate SI (34.5±1.4%) and severe SI (33.0±1.7%) compared to control cells. Compared to control ATP levels, ATP significantly increased in mild SI (966.3±85.1%), but not in moderate SI (160.0±40.2%); or severe SI (101.7±13.6%). Following a 1 hr reperfusion (Fig. 4.23), relative mitochondrial viability recovered but remained significantly decreased compared to control viability [mild SI: 73.7±2.1%; moderate SI: 84±3.3%; severe SI: 81.3±3.0% ($p<0.05$)]. The relative recovery of cells between mild and moderate SI is significant. ATP returned to control levels in mild SI [84.3±6.4%], moderate SI [87.5±12.9%] and in severe SI [117.2±20.2%].

4.3.2. $_{4hrs\ SI/R}$ MTT assay and ATP analysis

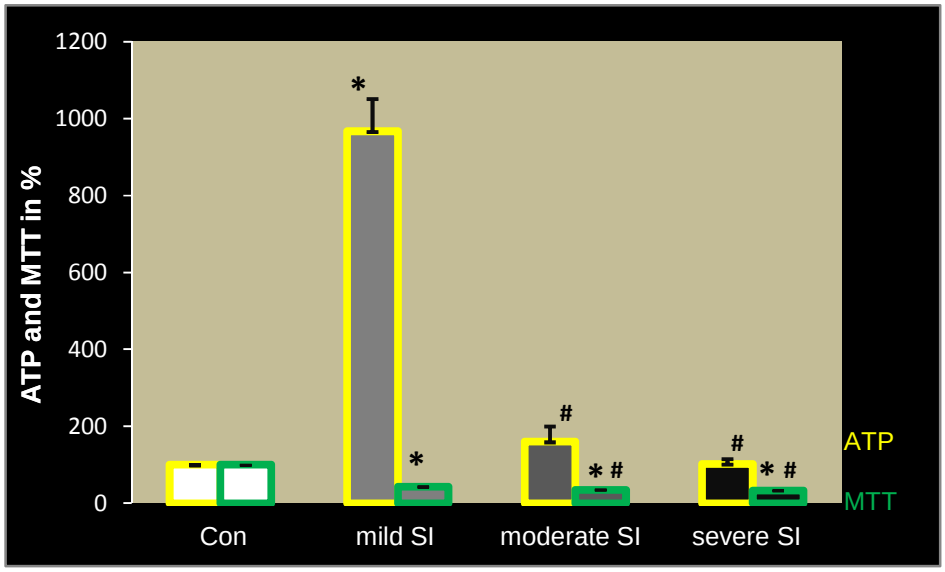

Figure 4.23: 4 hrs SI. Normalised data expressed as mean ± SEM, statistical analysis: ANOVA & Bonferroni correction, * p<0.05 vs Con, # p<0.05 vs mild SI, n=6-9.

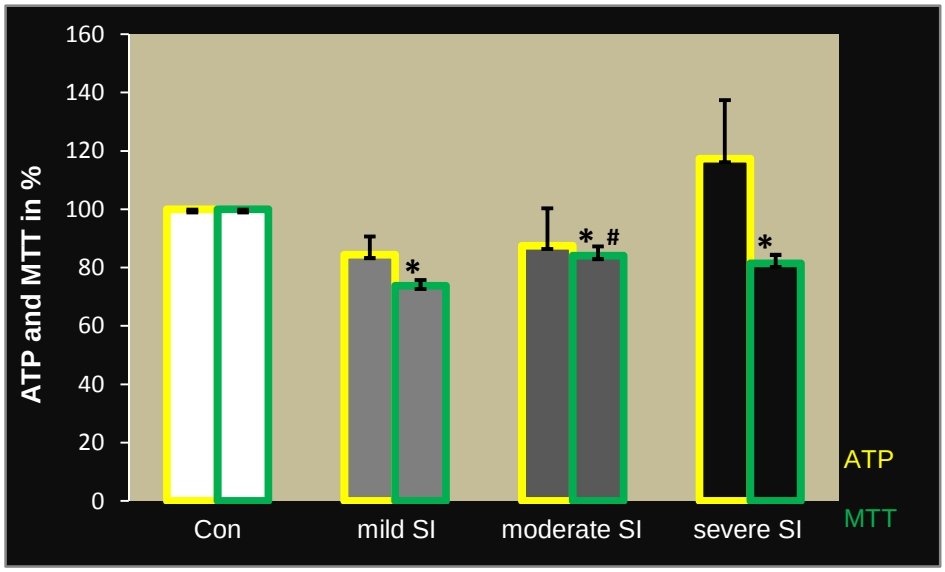

Figure 4.24: 4 hrs SI/R. Normalised data expressed as mean ± SEM, statistical analysis: ANOVA & Bonferroni correction, * p<0.05 vs Con, # p<0.05 vs mild SI, n=6-9.

4.3.3. Western blot analysis

Western blot analysis following 4 hrs ischaemia reveals a strong signal of phosphorylated AMPK (Fig. 4.25). The gradual trend seen at 2 hrs (Fig. 4.6) is now lost, showing an evenly strong signal in mild, moderate and severe SI. This phosphorylation pattern is lost with reperfusion. Caspase-3 (Fig. 4.28) and cleaved PARP (Fig. 4.29) analyses reveal a strong signal, with the strongest signal in cleaved PARP during mild SI. Beclin-1 shows a gradual decrease in signal, with almost no signal in severe SI (Fig. 4.27). This gradual decrease is lost with reperfusion, manifesting in an even beclin-1 signal. A decrease in mTOR phosphorylation in mild and moderate SI but not in severe SI, was observed (Fig. 4.26).

4.3.3. $_{4hrs\ SI/R}$ Western blot analysis

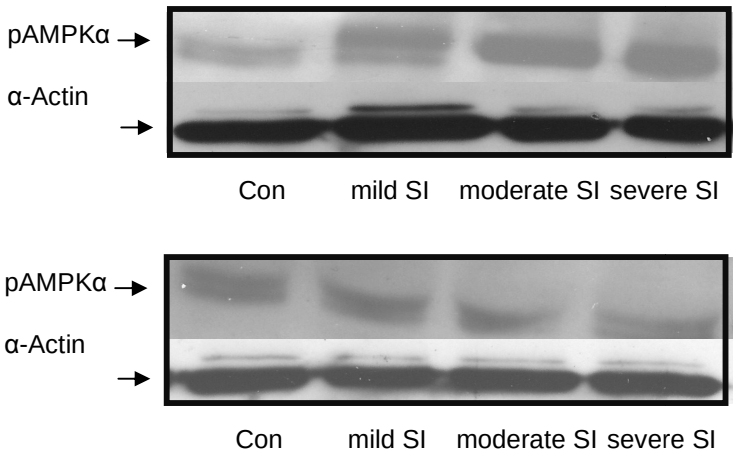

Figure 4.25: pAMPKα activation indicated through the 62 kDa band following 4 hrs SI (top) and SI/R (below). A representative blot is shown.

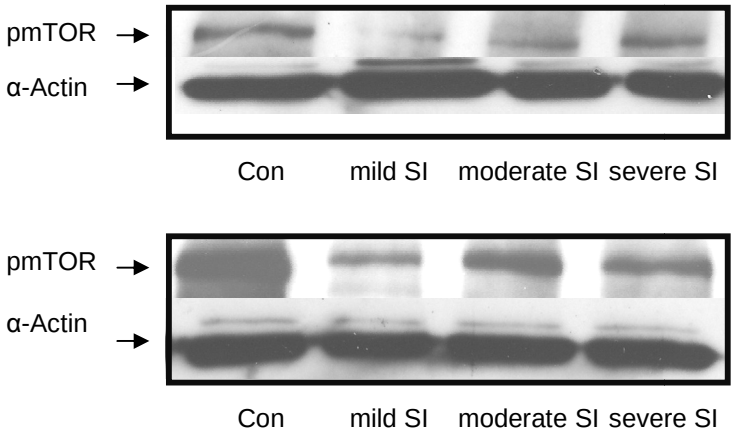

Figure 4.26: pmTOR activation indicated through the 289 kDa band following 4 hrs SI (top) and SI/R (below). A representative blot is shown.

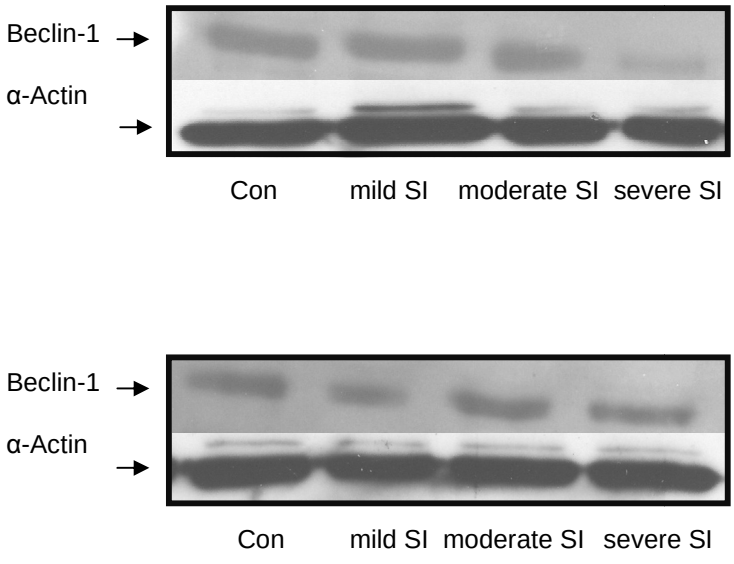

Figure 4.27: Beclin-1 activation indicated through the 57 kDa band following 4 hrs SI (top) and SI/R (below). A representative blot is shown.

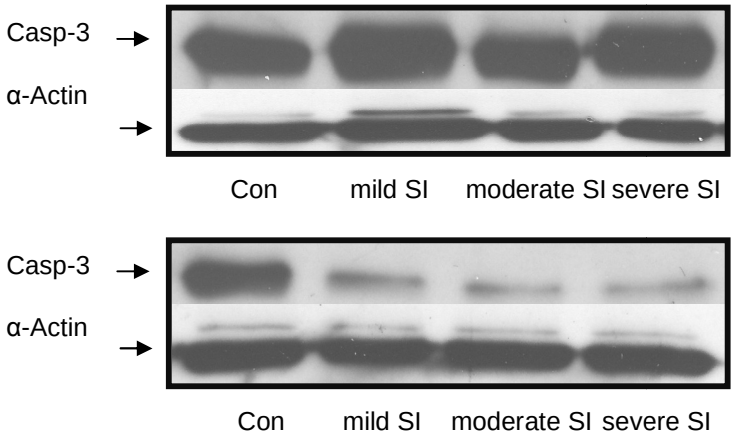

Figure 4.28: Uncleaved caspase-3 indicated through the 35 kDA bands following 4 hrs SI (top) and SI/R (below). A representative blot is shown.

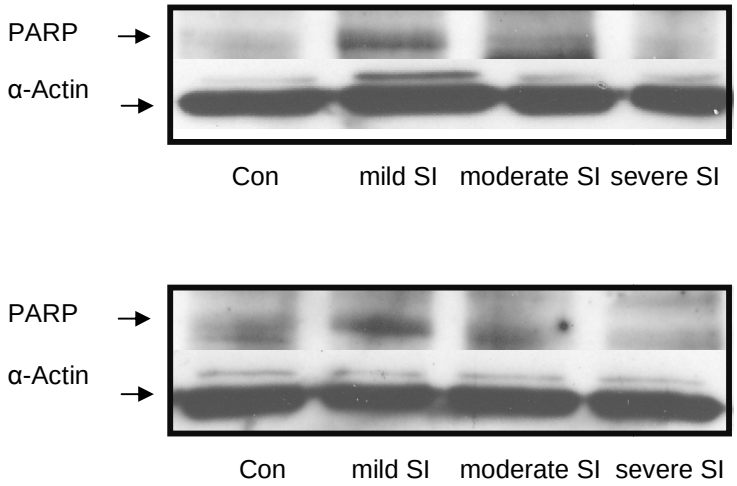

Figure 4.29: PARP cleavage indicated through the 89 kDA band following 4 hrs SI (top) and SI/R (below). A representative blot is shown.

4.3.4. Immunofluorescence and Scanning Electron Microscopy

When quantifying cells with numerous LC3 autophagosomes as an indication for autophagy following 4 hrs ischaemia, our results indicate a significant increase in autophagic activity in mild SI [17.2±2.3% ($p<0.05$)] as well as moderate SI [12.6±1.2% ($p<0.05$)] compared to control cells (0.9±0.4%), with no significant increase in severe SI (7.1±1.3%) (Fig. 4.30). With reperfusion this increase in LC3-positive cells in mild and moderate SI is lost (Fig. 4.31).

The fluorescence LC3 and actin cytoskeleton images indicate a prominent morphology of apoptosis in mild SI as well as a loss of membrane integrity in cells exposed to moderate and severe SI (Fig. 4.32, 4.33). Cells exposed to moderate and severe SI still appear larger and swollen and in most cases with an intact noncondensed nucleus. Immunofluorescence staining for beclin-1 makes this morphology more clear as it also indicates fine cytoskeletal-like cellular morphology (Fig 4.34, 4.35). Cytochrome c signals are present in mild, moderate and severe SI compared to control cells (Fig 4.34, 4.35). Additional to the relocation of HMGB1 from the nucleus to the cytosol, there are also intranuclear speckles of HMGB1 signals visible in all three ischaemic conditions (4.36, 4.37).

The Scanning Electron images taken after 4 hrs SI (Fig. 4.38) support the molecular features described through fluorescence staining. Mild SI resulted in rounded cells with clear membrane blebs indicative of apoptotic cells. Moderate SI and severe SI on the other hand, primarily showed cells which remain flat adherent and swollen in their morphology with less sharp surface features than control cells, indicative of an increased loss of membrane integrity.

4.3.4. $_{4hrs\ SI/R}$ Quantification of cells with numerous LC3 punctae

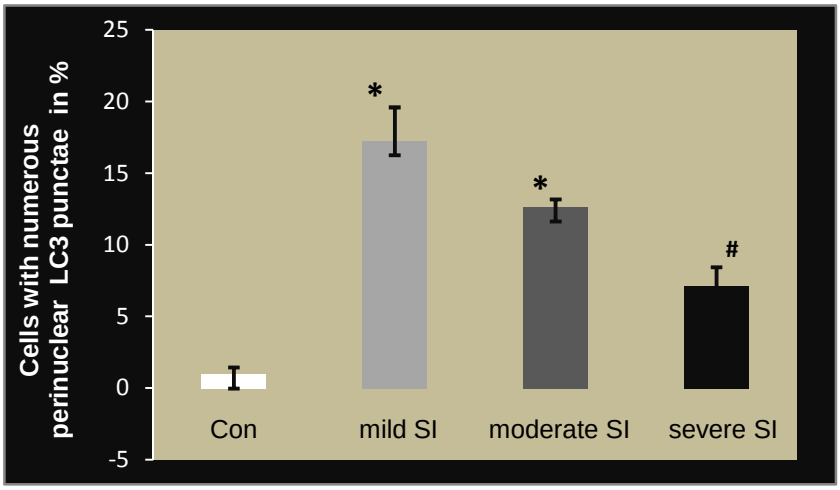

Figure 4.30: 4 hrs SI. Data expressed as mean ± SEM, statistical analysis: ANOVA & Bonferroni correction, * p<0.05 vs Con, # p<0.05 vs mild SI n=9, >150 cells counted.

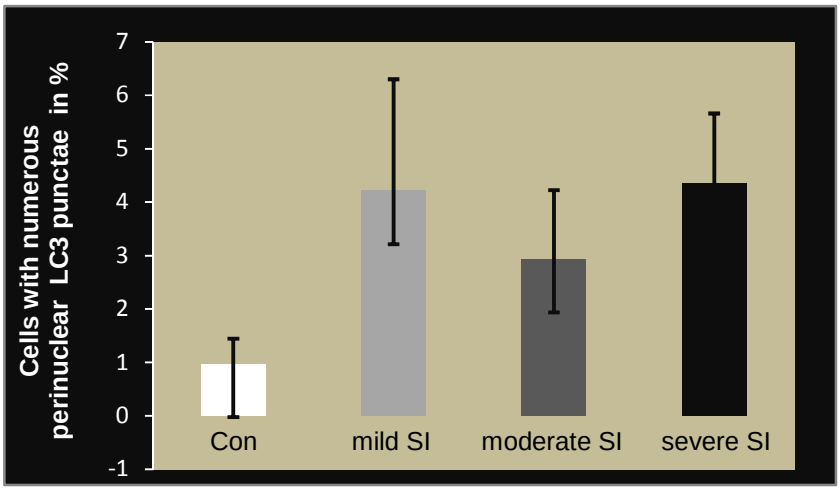

Figure 4.31: 4 hrs SI/R. Data expressed as mean ± SEM, statistical analysis: ANOVA & Bonferroni correction, * p<0.05 vs Con, # p<0.05 vs mild SI n=9, >150 cells counted.

4.3.4. $_{4hrs\ SI/R}$ Fluorescence Microscopy

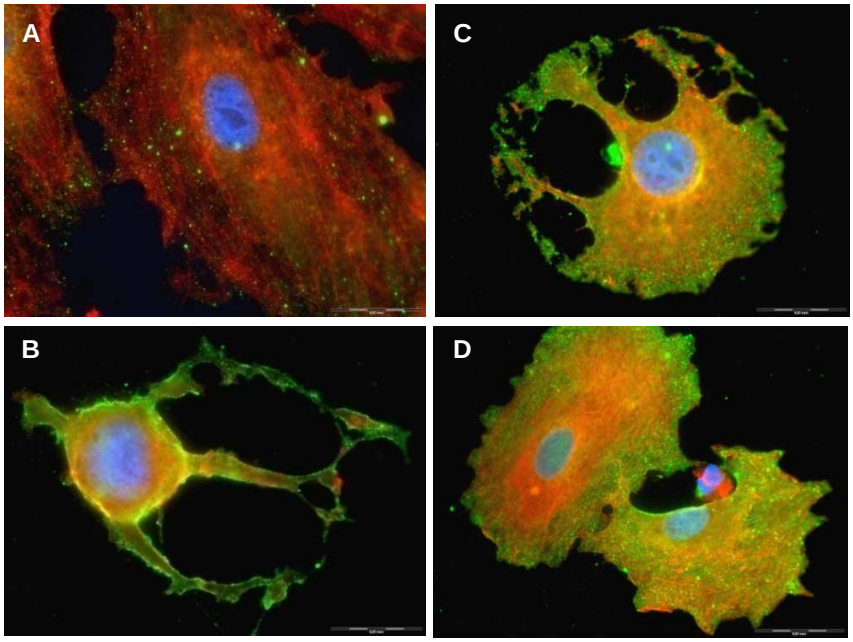

Figure 4.32: 4 hrs SI. H9c-2 myoblasts labelled with LC3/FITC, Actin/TexRed & Hoechst 33342. A: Con, B: mild SI, C: moderate SI, D: severe SI.

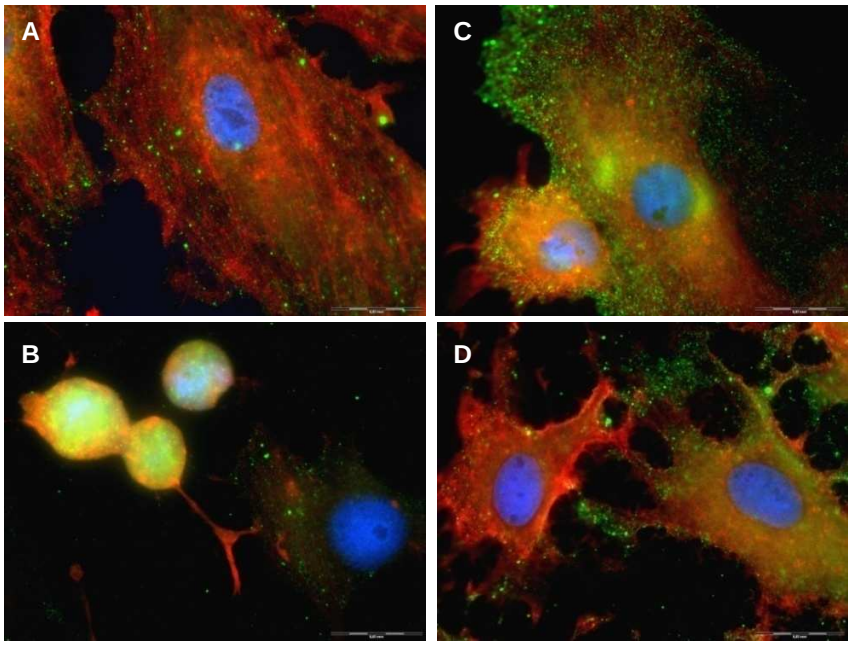

Figure 4.33: 4 hrs SI/R. H9c-2 myoblasts labelled with LC3/FITC, Actin/TexRed & Hoechst 33342. A: Con, B: mild SI, C: moderate SI, D: severe SI.

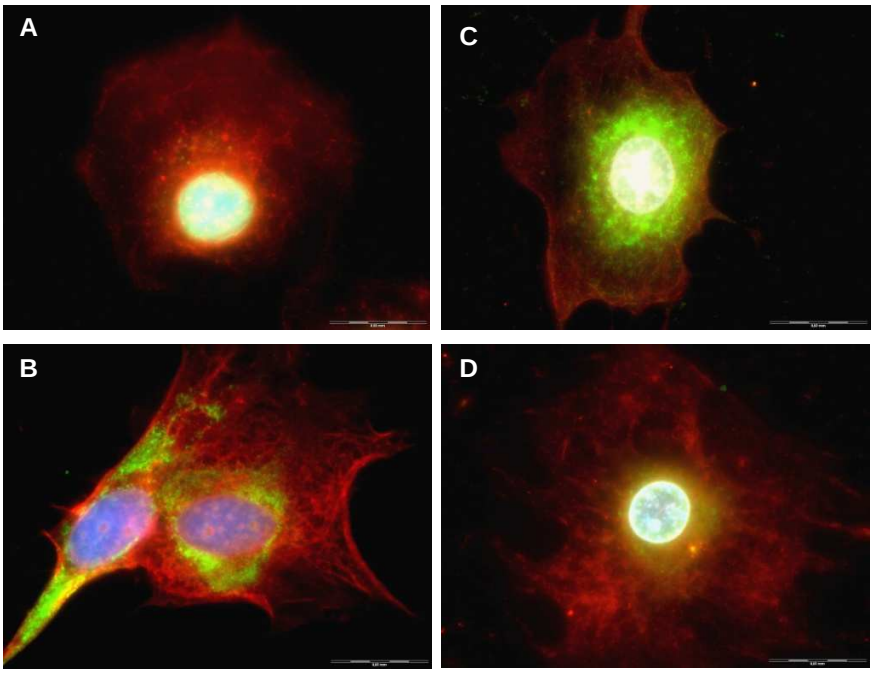

Figure 4.34: 4 hrs SI. H9C2 myoblasts labelled with Cyt-c/FITC, Beclin-1/TexRed & Hoechst 33342. A: Con, B: mild SI, C: moderate SI, D: severe SI.

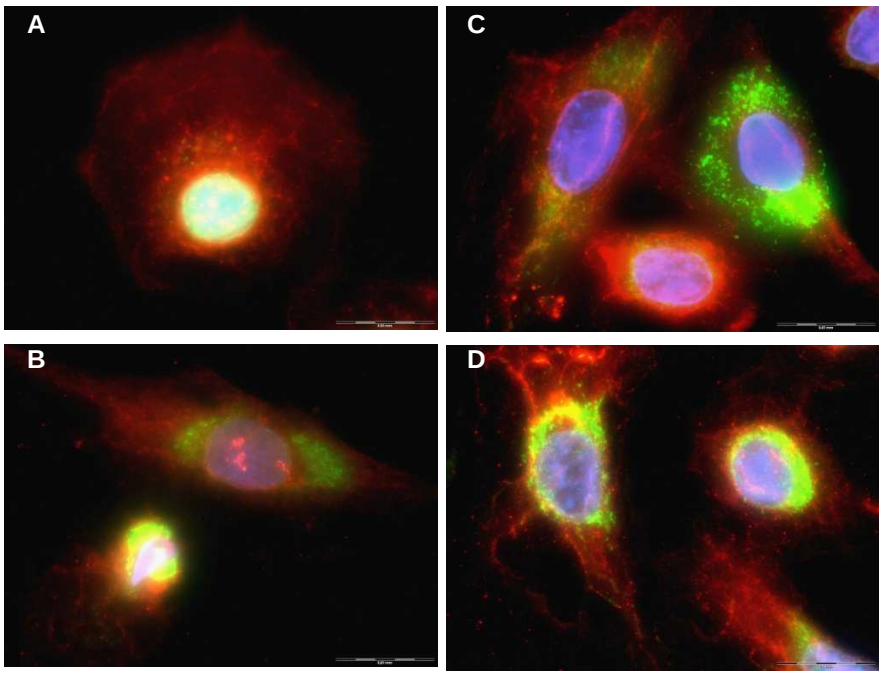

Figure 4.35: 4 hrs SI/R H9C2 myoblasts labelled with Cyt-c/FITC, Beclin-1/TexRed & Hoechst 33342. A: Con, B: mild SI, C: moderate SI, D: severe SI.

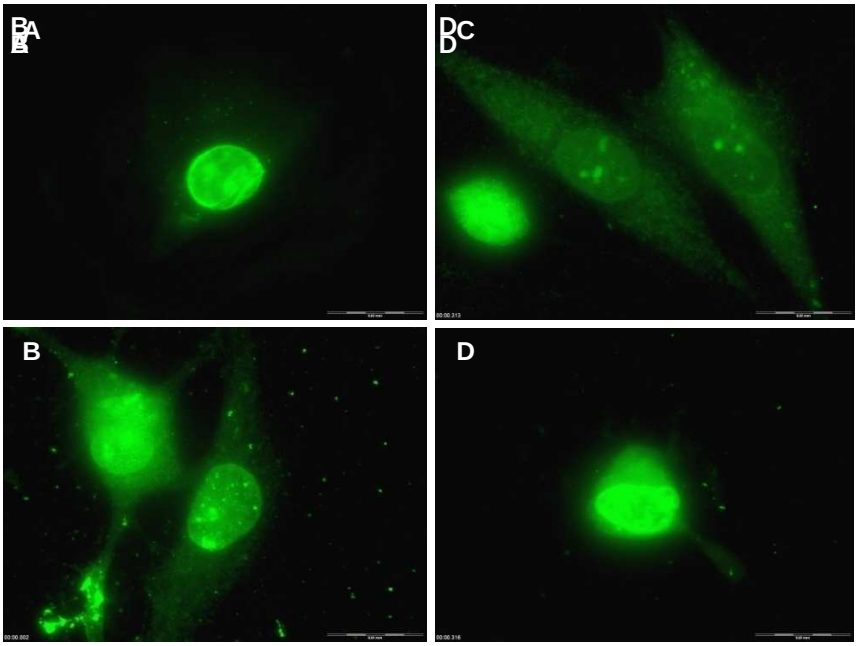

Figure 4.36: 4 hrs SI. H9c-2 myoblasts labelled with HMGB1/FITC A: Con, B: mild SI, C: moderate SI, D: severe SI.

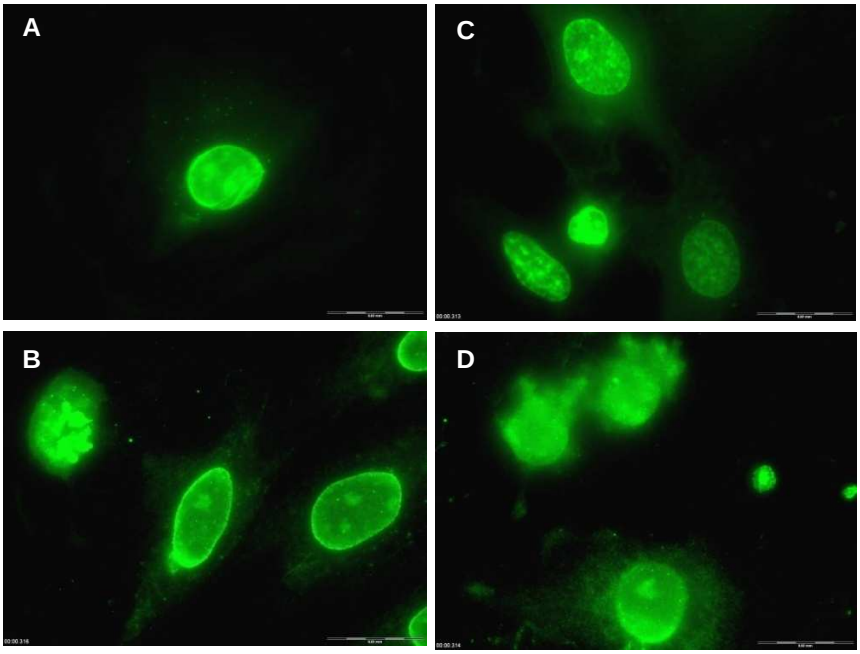

Figure 4.37: 4 hrs SI/R. H9c-2 myoblasts labelled with HMG1/FITC A: Con, B: mild SI, C: moderate SI, D: severe SI.

4.3.4. $_{4hrs\ SI/R}$ Scanning Electron Microscopy (SEM)

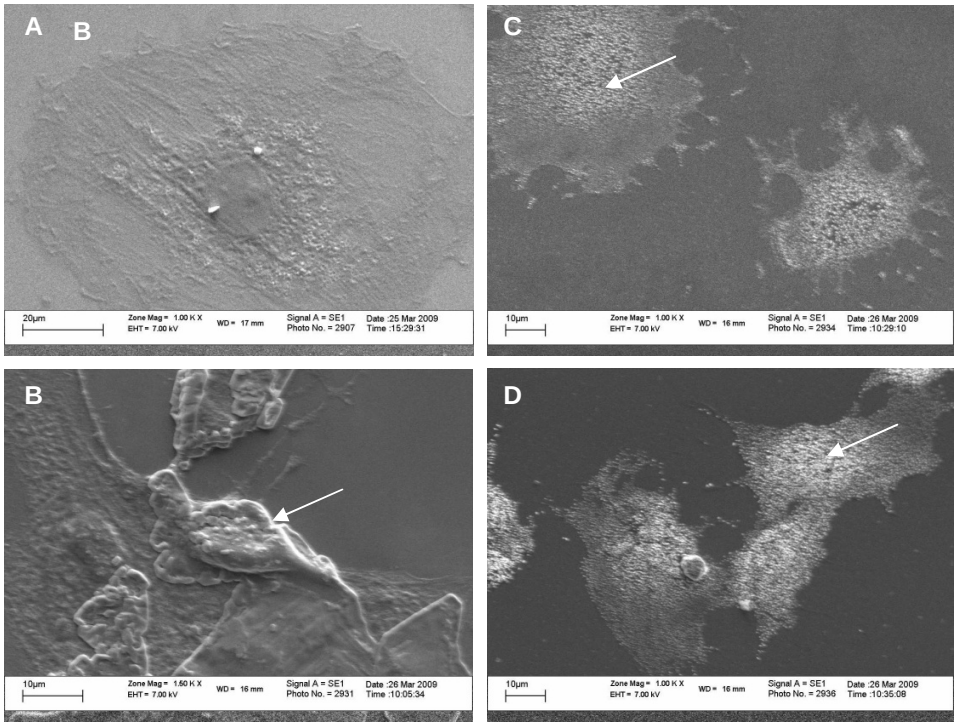

Figure 4.38: 4 hrs SI. SEM micrographs of H9c-2 myoblasts. A: Con, B: mild SI, C: moderate SI, D: severe SI. Cells exposed to mild SI appear rounded off and shrunk, characteristic for apoptosis (B). Cells exposed to moderate and severe SI appear flat and show damaged cell membrane, indicated by its rough structure (C and D).

4.4. Experimental measurements after 8 hrs SI

4.4.1. PI exclusion and nuclear condensation

Following 8 hrs SI, the results for PI positive and pyknotic cells indicate an exacerbation of the results described at 4 hrs SI. In mild SI, a significant increase in PI-positive cells was observed [18.0±2.2% ($p<0.05$)] compared to control cells (0.6±0.4%) (Fig. 4.39). Pyknotic cells in mild SI increased significantly [61.1±2.8% ($p<0.05$)], compared to control cells (4.8±0.8%). In moderate [77.3±5.8% ($p<0.05$)] and severe SI [66.4±4.8% ($p<0.05$)] a significant increase in PI-positive cells was observed. Pyknotic cells increased, reaching significance in moderate SI [31±3.4% ($p<0.05$)] and severe SI [31.2±4.2% ($p<0.05$)] compared to control cells (Fig. 4.39).

With reperfusion no further increase in PI-positive cells was observed in mild SI (19.9±2.9%). However, a significant increase was described in moderate SI [86.9±5.3% ($p<0.05$)] and severe SI [91.5±3.6% ($p<0.05$)] compared to control cells (Fig. 4.40). An increase in pyknotic cells was observed in mild SI [64.3±2.6% ($p<0.05$)], moderate SI [39.5±4.0% ($p<0.05$)] and severe SI [43.5±6.1% ($p<0.05$)] (Fig. 4.40).

4.4.1. $_{8hrs\ SI/R}$ PI exclusion and nuclear condensation

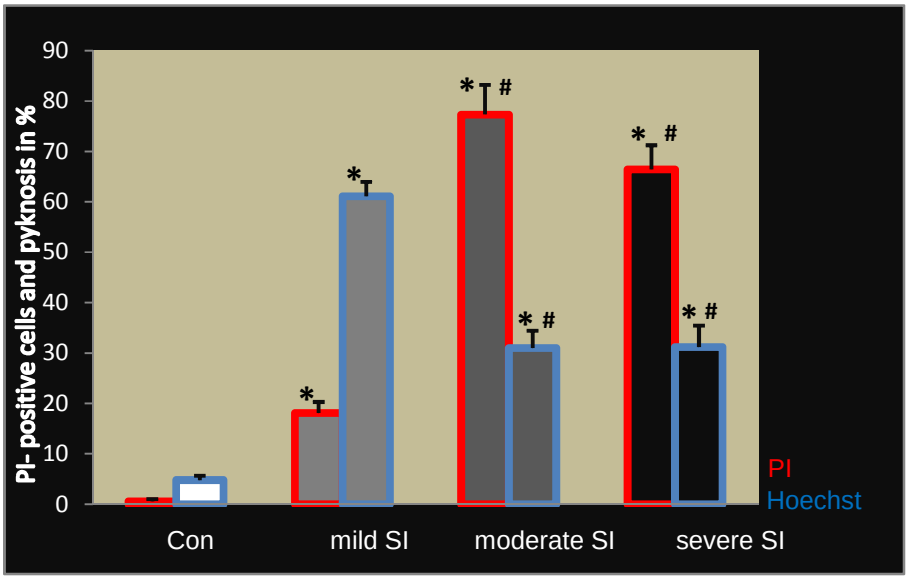

Figure 4.39: 8 hrs SI. Data expressed as mean ± SEM, statistical analysis: ANOVA & Bonferroni correction, * p<0.05 vs Con, # p<0.05 vs mild SI, n=9, >150 cells counted.

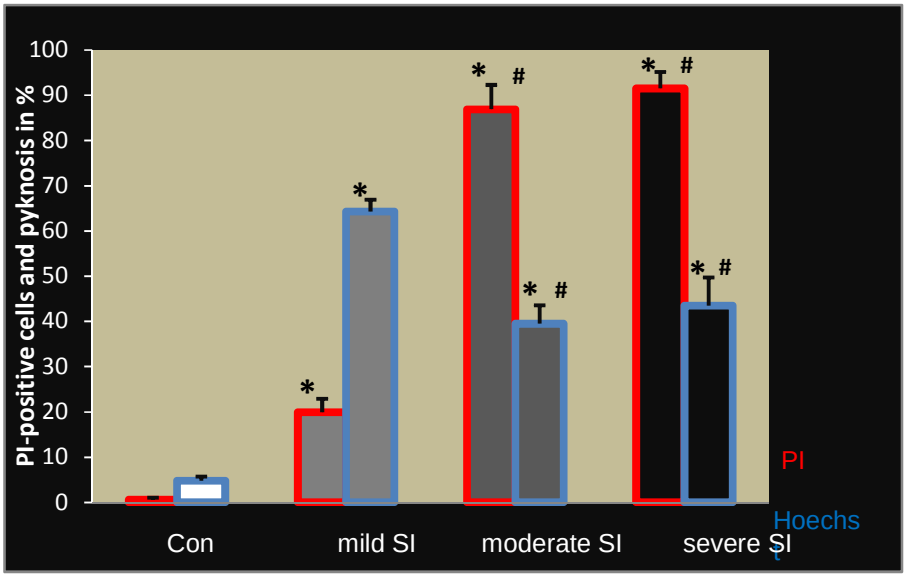

Figure 4.40: 8 hrs SI/R. Data expressed as mean ± SEM, statistical analysis: ANOVA & Bonferroni correction, * p<0.05 vs Con, # p<0.05 vs mild SI, n=9, >150 cells counted.

4.4.2. MTT assay and ATP analysis

As shown in Fig. 4.41, the relative viability based on MTT decreased significantly after 8 hrs mild SI (25±12.6%), moderate SI (16.9±2.5%) and severe SI (8.5±8.9%) compared to control cells. Viability in severe SI was significantly lower [8.5±8.9% ($p<0.05$)] compared to mild SI (25±12.6%). Compared to control ATP levels, ATP remained significantly increased in mild SI (231±27.7%). A significant decrease in ATP was observed in moderate SI [16.9±2.5% ($p<0.05$)] and severe SI [13.4±2.2% ($p<0.05$)], compared to mild SI (Fig. 4.41).

Following 1 hr reperfusion (Fig. 4.42), the relative survival rate of cells increased but remained significantly lower compared to control viability in moderate SI [69.8±13.8% ($p<0.05$)] and severe SI [52.7±5.6.% ($p<0.05$)]. ATP levels returned to control levels in mild SI (107±15.5%) but remained significantly lower in moderate SI [18.9±1.9% ($p<0.05$)] and in severe SI [19±2.5% ($p<0.05$)] compared to control cells (Fig. 4.42).

4.4.2. $_{8hrs\ SI/R}$ MTT assay and ATP analysis

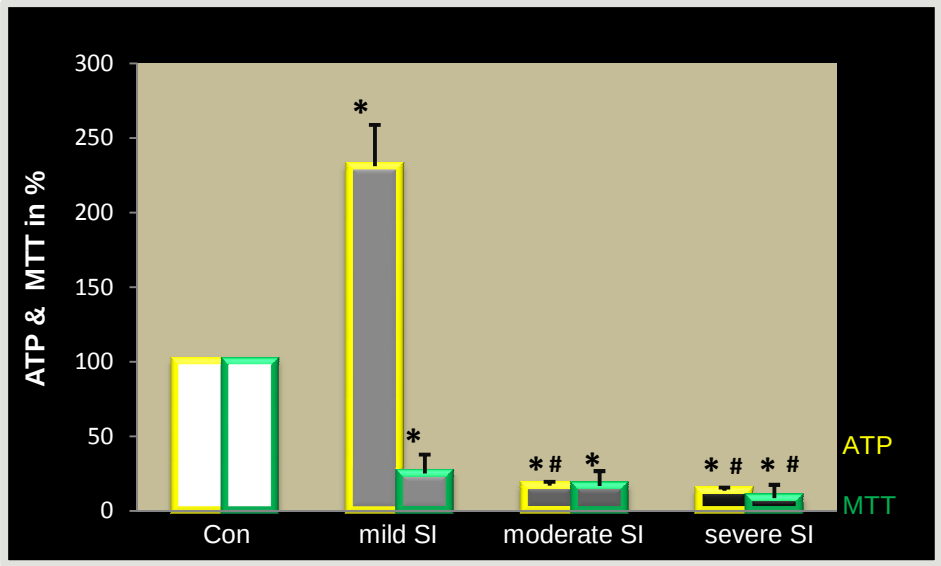

Figure 4.41: 8 hrs SI. Normalised data expressed as mean ± SEM, statistical analysis: ANOVA & Bonferroni correction, * p<0.05 vs Con, # p<0.05 vs mild SI, n=6-9.

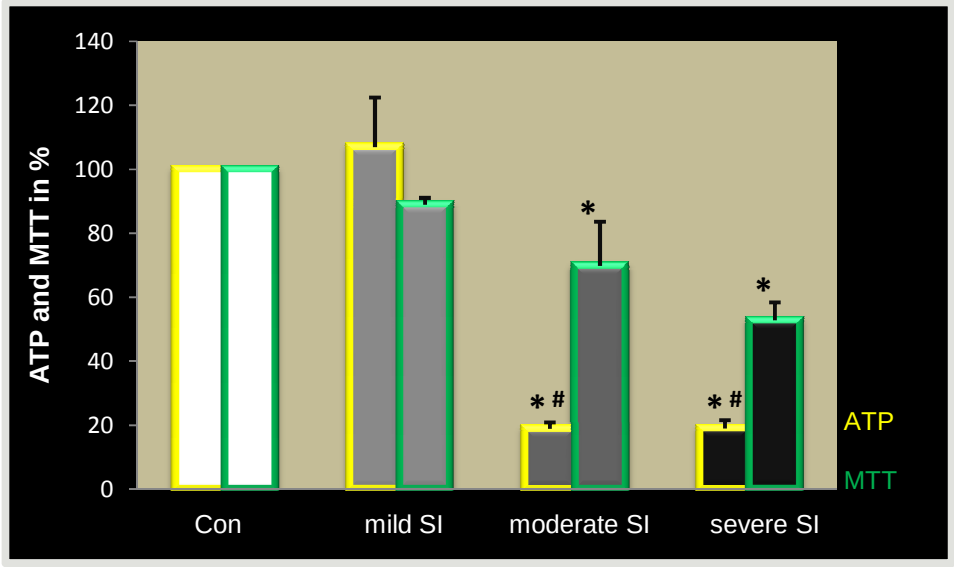

Figure 4.42: 8 hrs SI/R. Normalised data expressed as mean ± SEM, statistical analysis: ANOVA & Bonferroni correction, * p<0.05 vs Con, # p<0.05 vs mild SI, n=6-9.

4.4.3. Western blot analysis

Western blot analysis following 8 hrs ischaemia reveals a gradual increase in signal of phosphorylated AMPK, weakest in mild SI and strongest in severe SI (Fig. 4.43). This phosphorylation pattern is lost with reperfusion. Caspase-3 (Fig. 4.46) and cleaved PARP (Fig. 4.47) analyses reveal strong signals, particlarly in mild SI. No apparent differences in beclin-1 between the groups were observed (Fig. 4.45). The phosphorylation state of mTOR indicates no differences between the groups. However, with reperfusion a decreased mTOR phosphorylation in moderate and severe SI was observed (Fig. 4.44).

4.4.3. $_{8hrs\ SI/R}$ Western blot analysis

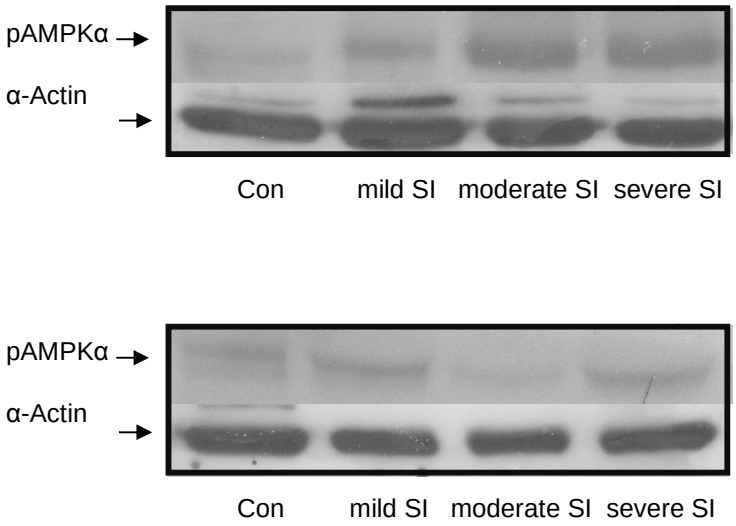

Figure 4.43: pAMPKα activation indicated through the 62 kDa band following 8 hrs SI (top) and SI/R (below). A representative blot is shown.

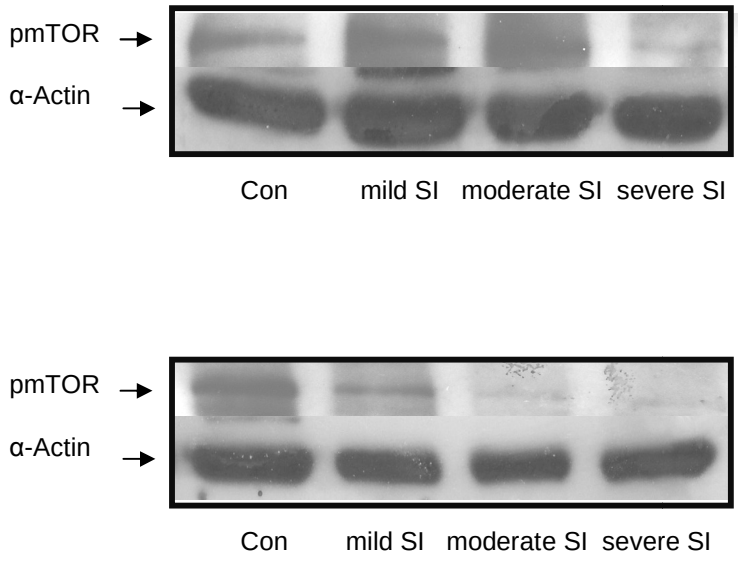

Figure 4.44: pmTOR activation indicated through the 289 kDa band following 8 hrs SI (top) and SI/R (below). A representative blot is shown.

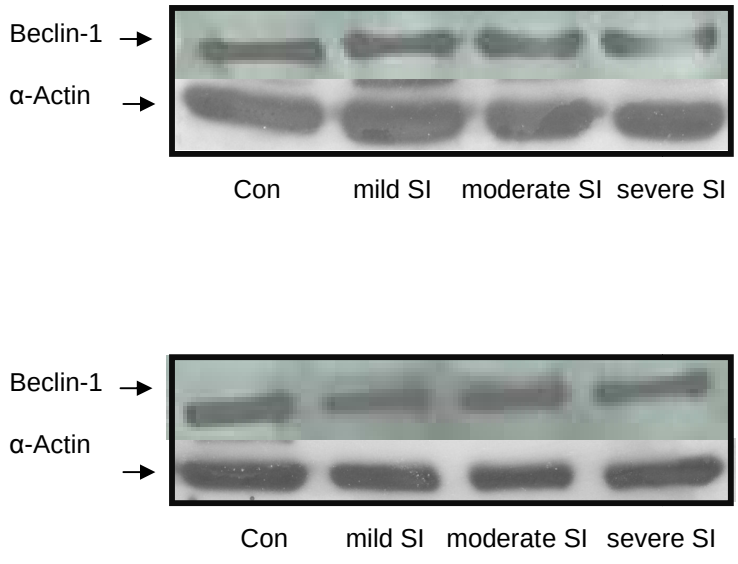

Figure 4.45: Beclin-1 activation indicated through the 57 kDa band following 8 hrs SI (top) and SI/R (below). A representative blot is shown.

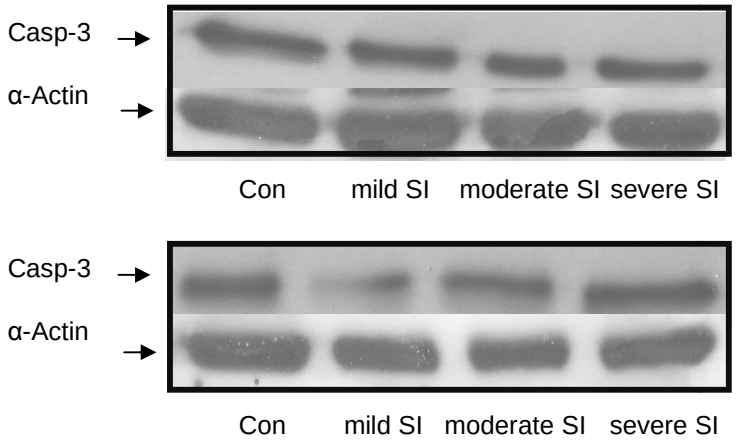

Figure 4.46: Uncleaved caspase-3 indicated through 35 kDA band following 8 hrs SI (top) and SI/R (below). A representative blot is shown.

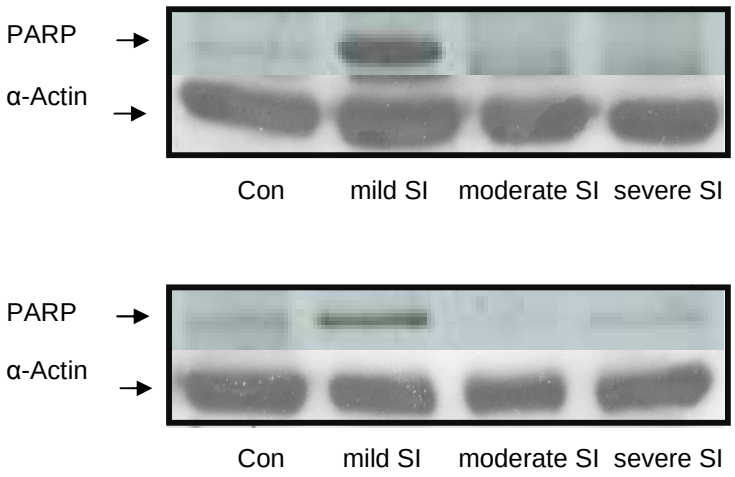

Figure 4.47: PARP cleavage indicated through the 89 kDA band following 8 hrs SI (top) and SI/R (below). A representative blot is shown.

4.4.4. Immunofluorescence and Scanning Electron Microscopy

When quantifying cells with numerous LC3 autophagosomes as an indication of autophagy after 8 hrs ischaemia, the results showed a significant increase in autophagic activity in mild SI [11.7±1.8% ($p<0.05$)] with no significant increase in moderate SI (6.7±1.5%) or severe SI (6.6±2%) respectively (Fig. 4.48) compared to control cells (0.9±0.4%). With reperfusion this increase in LC3-positive cells in mild SI is lost (Fig. 4.49).

The fluorescence images taken after 8 hrs SI indicate the most prominent morphology of apoptosis in mild SI with clear pyknosis but also karyorhexis, resulting in apoptotic bodies indicative of the progression of apoptotic cell death (Fig. 4.50, 4.51). LC3 autophagosomes are still clearly visible in these pyknotic cells (Fig. 4.50, 4.51). The actin signal reveals complete loss of cytoskeletal architecture. Moderate and severe SI indicate complete loss of membrane integrity. However, cells appear still large and swollen with karyorhexis also taking place (Fig. 4.50, 4.51). The fine pattern of beclin-1 signal is completely lost in all three groups, resulting in a more diffuse cytoplasmic beclin-1 signal (Fig. 4.52, 4.53). Also, the cytochrome c signal which is still present in mild, moderate and severe SI shows a particularly diffuse signal in moderate and severe SI, while a more perinuclear granular cytochrome c signal is apparent in cells exposed to mild SI (Fig. 4.52, 4.53). HMGB1 appears to be released from most nuclei in mild, moderate and severe SI, resulting in a fine granular cytoplasmic pattern, often leaving intranuclear speckles of HMGB1 signals (Fig. 4.54, 4.55).

The Scanning Electron images taken after 8 hrs SI (Fig. 4.56) reveal most prominent morphology of apoptosis in mild SI, whilst moderate SI and severe SI show cells which have lost their membrane integrity completely.

4.4.4. $_{8hrs\ SI/R}$ Quantification of cells with numerous LC3 punctae

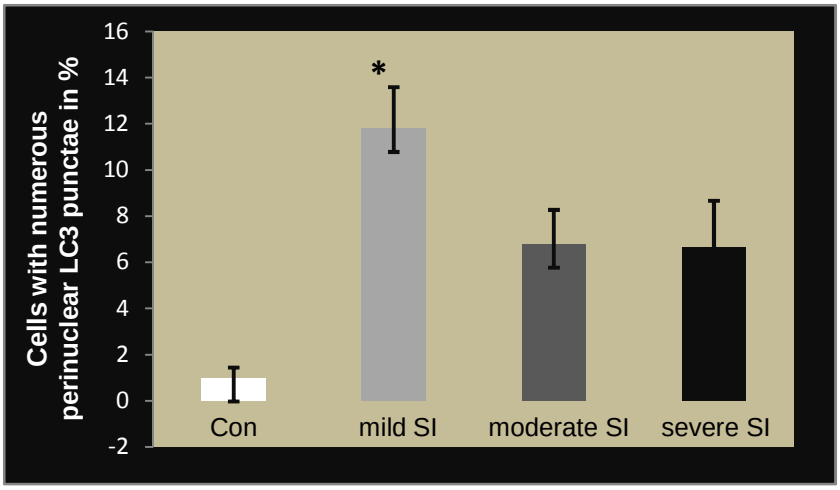

Figure 4.48: 8 hrs SI. Data expressed as mean ± SEM, statistical analysis: ANOVA & Bonferroni correction, * p<0.05 vs Con, # p<0.05 vs mild SI n=9, >150 cells counted.

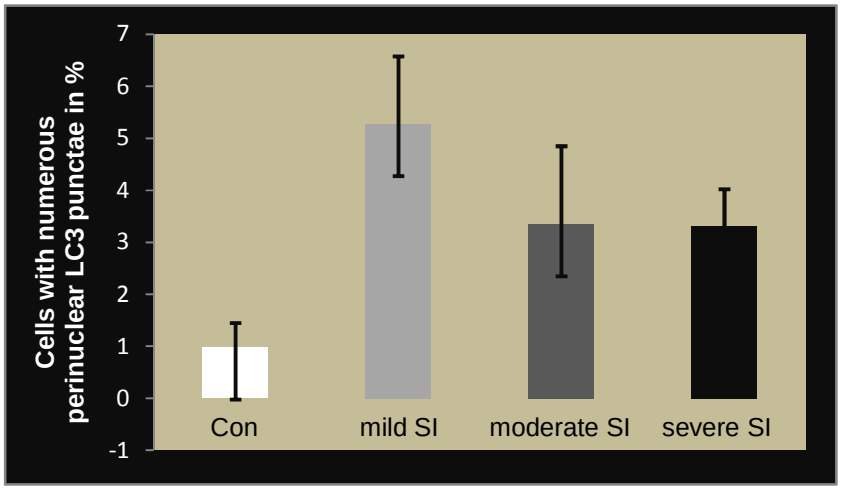

Figure 4.49: 8 hrs SI/R. Data expressed as mean ± SEM, statistical analysis: ANOVA & Bonferroni correction, * p<0.05 vs Con, # p<0.05 vs mild SI n=9, >150 cells counted.

4.4.4. $_{8hrs\ SI/R}$ Fluorescence Microscopy

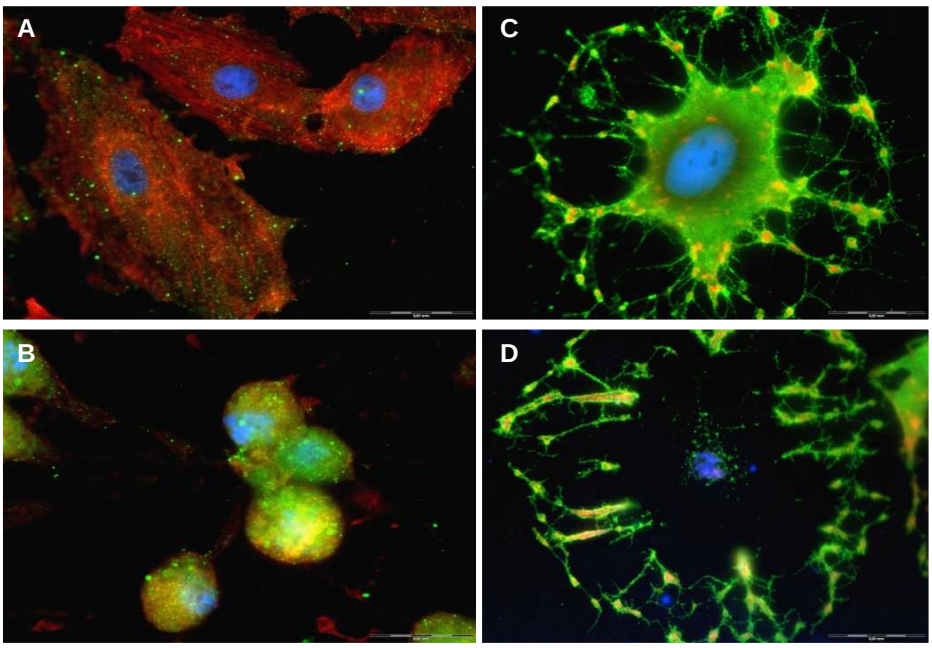

Figure 4.50:8 hrs SI. H9c-2 myoblasts labelled with LC3/FITC, Actin/TexRed & Hoechst 33342. A: Con, B: mild SI, C: moderate SI, D: severe SI.

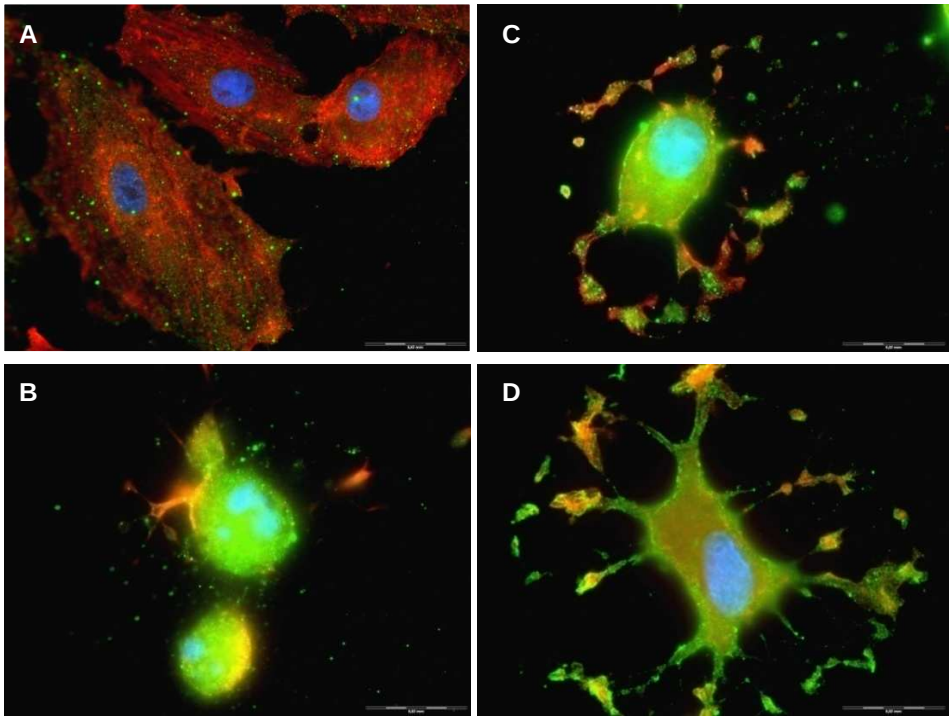

Figure 4.51: 8 hrs SI/R H9c-2 myoblasts labelled with LC3/FITC, Actin/TexRed & Hoechst 33342. A: Con, B: mild SI, C: moderate SI, D: severe SI.

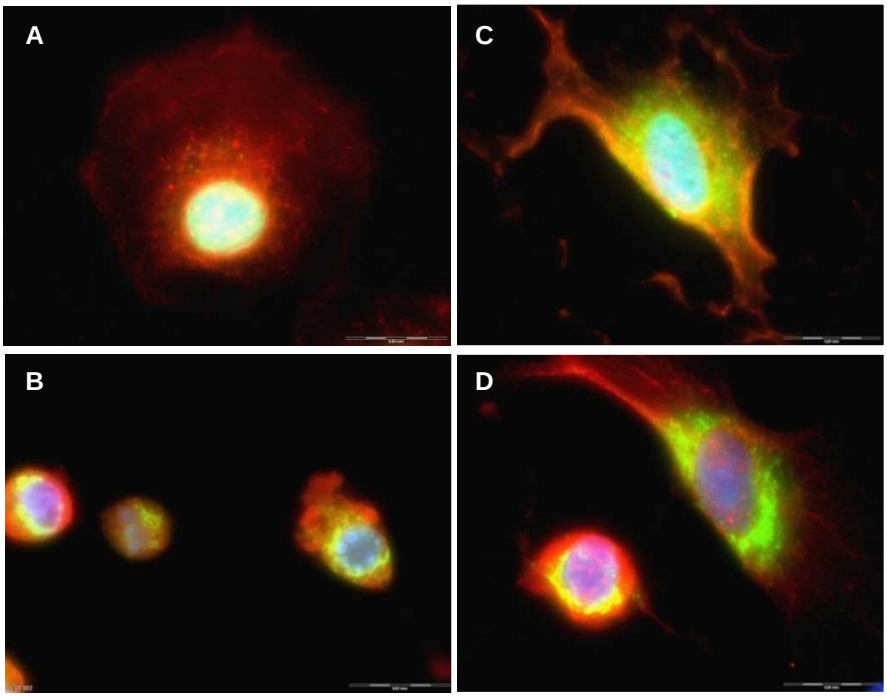

Figure 4.52: 8 hrs SI. H9c-2 myoblasts labelled with Cyt-c/FITC, Beclin-1/TexRed & Hoechst 33342. A: Con, B: mild SI, C: moderate SI, D: severe SI.

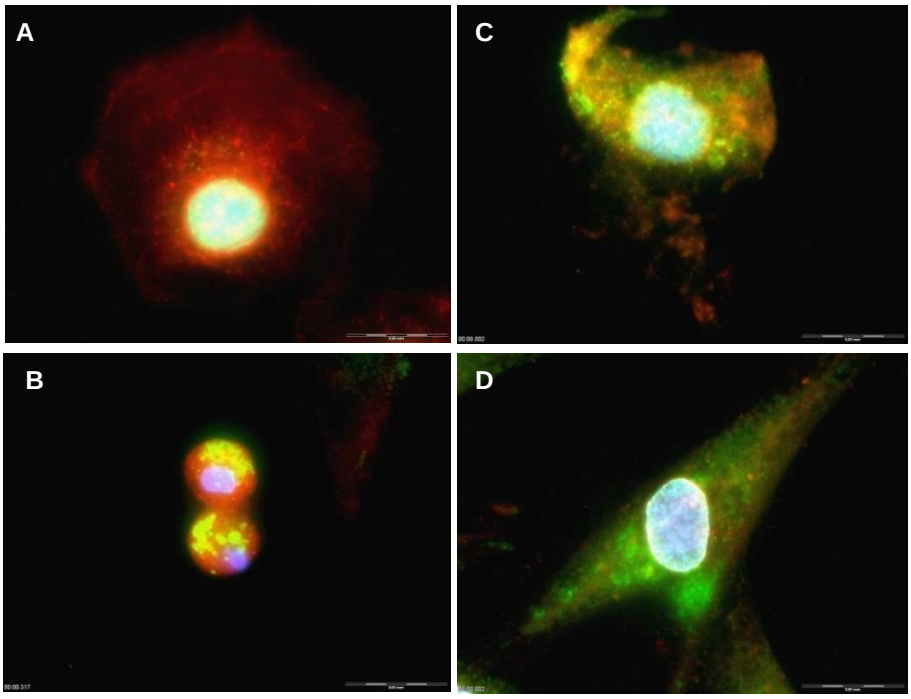

Figure 4.53: 8 hrs SI/R. H9c-2 myoblasts labelled with Cyt-c/FITC, Beclin-1/TexRed & Hoechst 33342. A: Con, B: mild SI, C: moderate SI, D: severe SI.

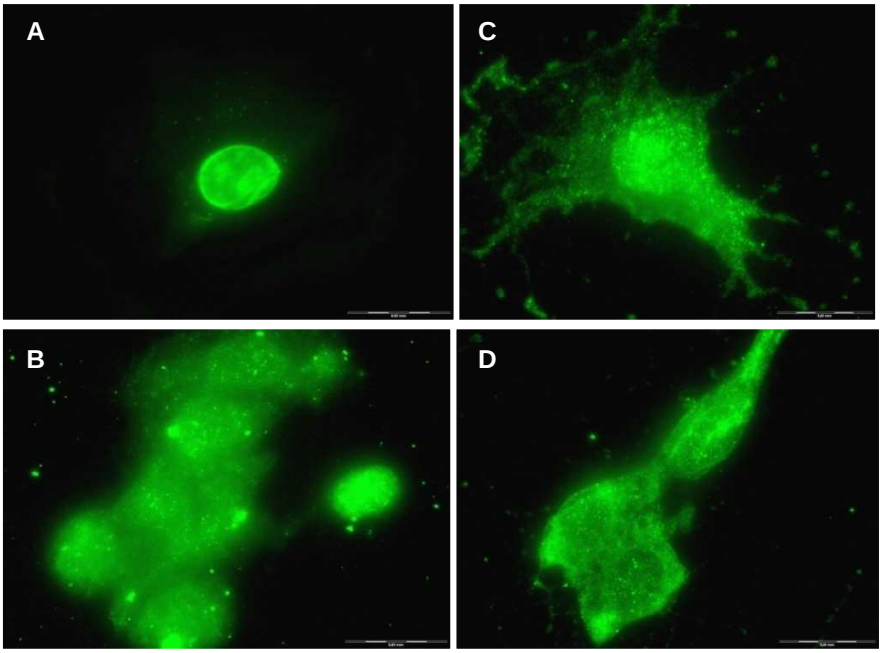

Figure 4.54: 8 hrs SI. H9c-2 myoblasts labelled with HMGB1/FITC. A: Con, B: mild SI, C: moderate SI, D: severe SI.

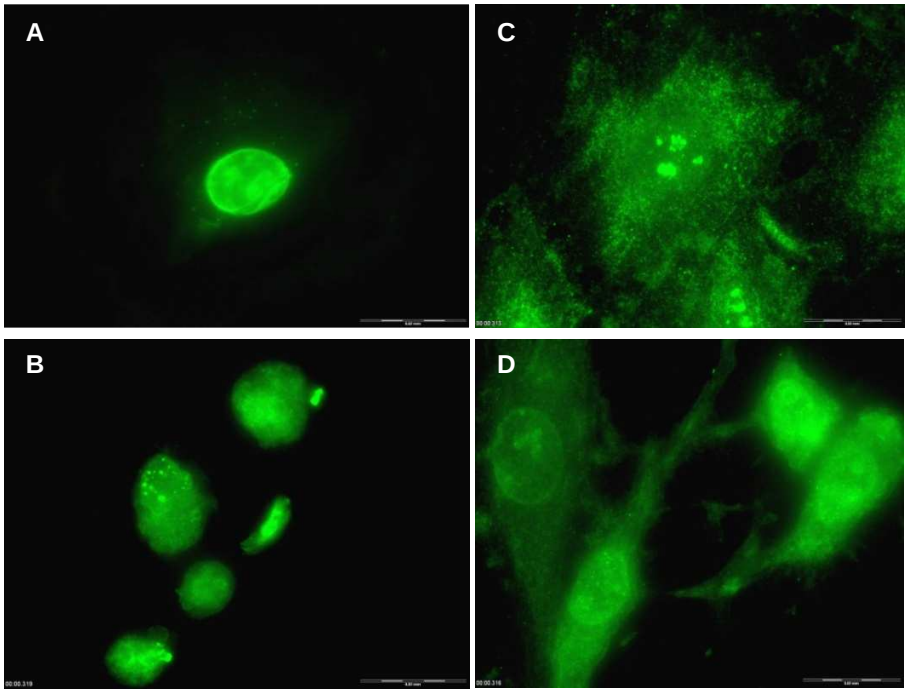

Figure 4.55: 8 hrs SI/R. H9c-2 myoblasts labelled with HMGB1/FITC. A: Con, B: mild SI, C: moderate SI, D: severe SI.

4.4.4.$_{8hrs\ SI/R}$ Scanning Electron Microscopy (SEM)

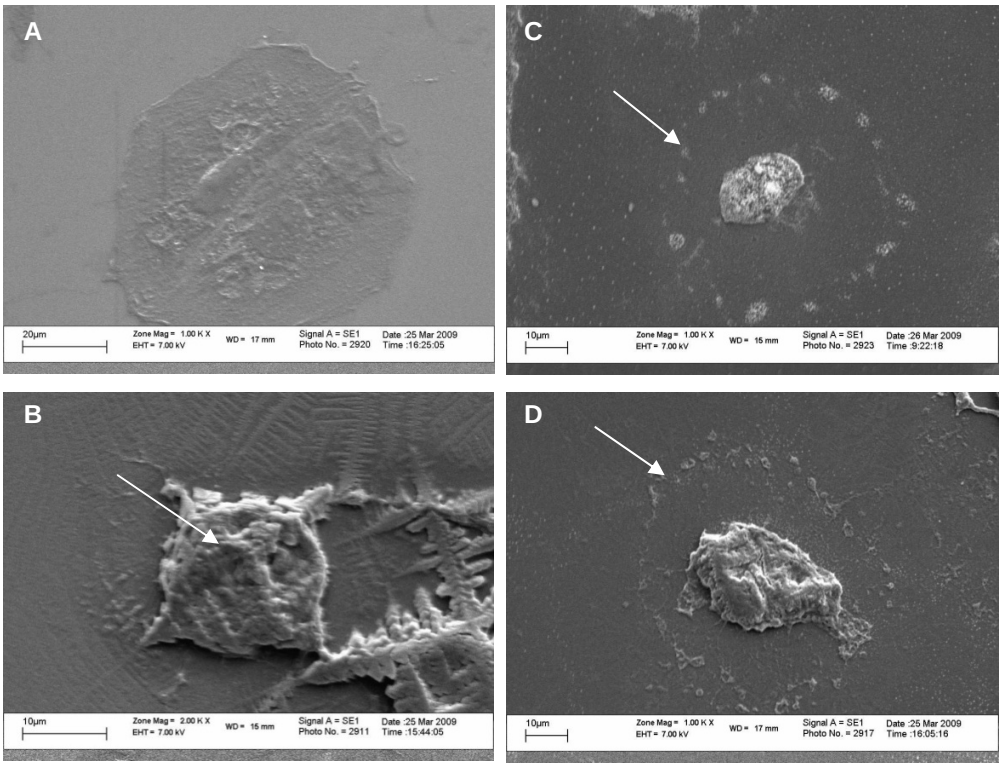

Figure 4.56: 8 hrs SI. SEM micrographs of H9c-2 myoblasts. A: Con, B: mild SI, C: moderate SI, D: severe SI. Cells exposed to mild SI show a shrunk cell soma (B). Cells exposed to moderate and severe SI show a ring of membrane structures and a central soma, indicating cell membrane damage (C and D).

CHAPTER 5 DISCUSSION: TIME POINTS

5.1. Autophagy, apoptosis and necrosis evaluated concomitantly and dynamically

Literature indicates a great need and interest in clarifying the role of apoptosis and necrosis in pathophysiological conditions such as in the ischaemic myocardium. It has been suggested that apoptosis is the major form of myocardial damage during ischaemic injury, with necrotic cell death following apoptosis (Kajustra *et al.*, 1996). Of particular interest is not only the extent and order of myocyte cell death but also the severity and duration of the ischaemic insult, which are important in predicting and ultimately preventing myocyte cell loss. It has also been suggested that apoptosis primarily plays a role in the chronically ischaemic myocardium (Freude *et al*., 1998), while its role in the acute setting remains unclear. The new and growing field of autophagy brings about another dimension of the myocyte response to ischaemic injury (Fig. 5.1). Although autophagy may be activated during cell death, it has been described as the cell's major adaptive strategy in response to metabolic challenges as well as a defence mechanism upon cell injury. In the heart, autophagy has been shown to take a key position in profoundly affecting the process of cell death (Nishida *et al*., 2009, Yu *et al*., 2008, Loos & Engelbrecht, 2009), and in enhancing the heart's tolerance to ischaemia (Hamacher-Brady *et al*., 2006).

The above suggestions and findings imply that autophagy, apoptosis and necrosis are to be evaluated concomitantly and dynamically in context of severity and duration of an ischaemic insult, in order to clarify their respective importance during myocardial injury. A clear understanding of their role during myocardial injury is crucial in order to develop effective therapeutic strategies.

The aims of this study are therefore to (i) characterize the contribution of each cell death type in context of the severity and duration of an ischaemic insult and (ii) to

determine whether manipulation of the autophagic pathway affects this contribution of cell death and translates into protection of the heart. For that purpose, a combination of viability techniques, ATP and MTT measurements, immunofluorescence and electron microscopy, live cell imaging and flow cytometry as well as western blotting, was employed. It was hypothesized that the relative contribution of each mode of cell death is dependent on the duration and severity of the ischaemic insult and is governed by the cells underlying metabolic capacity at a given point in time. It was further hypothesized that the onset of apoptosis and necrosis depends on the cell's autophagic activity prior/during the ischaemic event due to the role of autophagy on the cell's metabolic capacity.

5.2. The effect of mild, moderate and severe simulated ischaemia on apoptosis and necrosis

Our results strongly indicate a differential manifestation of PI positive and pyknotic cells between mild, moderate and severe SI. Mild SI leads to a primarily apoptotic cellular phenotype with more than 60% of cells being pyknotic after 8 hrs SI (Fig. 4.39, 4.40). Importantly, PI-positive cells are only detected after 8 hrs mild SI. However, moderate and severe SI manifest very early in a primarily necrotic cellular phenotype, indicated through early appearance of PI-positive cells. Following 2 hrs SI, a significant increase in PI-positive cells is observed. At this early time point the extent of cell death is, although significant, still rather limited (Fig. 4.2, 4.3). It has been shown that myocytes exposed to short periods of even severe ischaemia may almost completely be restored after reperfusion. However, this restoration is not immediate, indicating the dynamic behaviour of ischaemia/reperfusion injury (Jennings *et al*., 1985). In the own model, after 8 hrs moderate and severe SI, necrotic cells contribute to about two thirds of cell death, worsening upon reperfusion. Only about $^{1}/_{3}$ of cells is pyknotic following 8 hrs moderate and severe SI (Fig. 4.39, 4.40).

Our model of mild SI leads to prominent features of apoptosis already during ischaemia which further increase at reperfusion. It is important to note that reperfusion injury observed in our model likely manifests in a differential manner, with the same morphology primarily present during SI. In mild SI, PI-positive cells made a minor contribution following reperfusion. However, in moderate and severe SI a major contribution has been observed already after 4 hrs SI followed by reperfusion (Fig. 4.21, 4.22). It has been suggested that necrosis (Zhao *et al.,* 2000), but also apoptosis, are ongoing processes during ischaemia and that reperfusion primarily "boosts" apoptosis (Eefting *et al.,* 2003). This is supported by the findings that caspase-3 inhibition during early reperfusion limits apoptotic cell death in myocardial infarction (Mocanu *et al.,* 2000). Our results indicate that this may be dependent on the severity of the ischaemic insult where more severe ischaemic injury primarily leads to necrosis, which is further exacerbated during reperfusion (Fig. 4.22). It is challenging to transfer results from an *in vitro* model into the *ex vivo* scenario. This may, however, be of clinical interest as it may imply a prediction of cell death based on the primary cell death phenotype of the tissue observed during the ischaemic event. A necrotic tissue area may increase with reperfusion. However, apoptotic areas may not necessarily become necrotic but might show a further increase in apoptotic morphology. Due to the implication of inflammation during necrosis this may be of particular importance. It is also of interest that in our model, moderate and severe SI follow a very similar trend in the contribution of apoptosis and necrosis during the progression of the ischaemic injury.

5.3. The effect of mild, moderate and severe simulated ischaemia on cellular ATP and mitochondrial reductive capacity

The results showed a significant increase in ATP during mild SI (Fig 4.4) which reached its maximum at 4 hrs SI with a 10-fold increase compared to control cells (Fig. 4.23) and remained significantly increased even after 8 hrs mild SI (Fig. 4.41). With reperfusion ATP levels matched the ATP levels of control cells. However,

although ATP levels in moderate and severe SI stayed at that of control cells for up to 4 hrs SI, a significant ATP depletion was already observed after 2 hrs SI followed by reperfusion (Fig. 4.5). ATP levels were significantly decreased at 8 hrs moderate and severe SI compared to the ATP levels of control cells (Fig. 4.41, 4.42).

The ATP surge observed in mild SI (Fig. 4.4, 4.23, 4.41) is associated with increased autophagy, manifesting in prominent autophagosome formation (Fig. 4.12, 4.30, 4.48). It may be suggested that the described ATP surge confers a degree of cytoprotection, creating a metabolically more favourable environment compared to the other ischaemic groups, favouring apoptosis over necrosis. Katayama and co-workers described a similar autophagy-associated increase in ATP in glioma cells, which had a cytoprotective effect (Katayama *et al*., 2007). Zamaraeva *et al.* have shown, through real time measurements, an increase in cytosolic ATP during apoptosis. However, autophagy has not been assessed in that model (Zamaraeva *et al.,* 2005). It is of note that these are the only indications in the currently available literature where an ATP increase was observed. The results are therefore highly significant as in most studies conducted the inhibition of glycolysis by 2DG led to a rapid depletion of ATP (Lieberthal *et al.,* 1998, Volbracht *et al.,* 1999, Dagher, 2000, Bogliolo *et al*., 2002, Healy *et al*., 2002, Gonon-Giroud *et al*., 2002). However, in these studies different cell types such as mouse proximal tubular cells, cerebellar granule neurons and bone marrow derived cells have been employed. Also, the ischaemic condition varied in these experiments by maintaining the environment normoxic and by adding 2DG to the growth medium and not employing an ischaemic buffer. The time frame and capacity to upregulate autophagy and to maintain increased autophagy have been shown to be cell type specific (Mizushima *et al*., 2004). Therefore it is likely that in those studies the autophagic machinery was not induced timely, hence no metabolic contribution was made through autophagically-generated ATP. It is also plausible that increased autophagic flux provides substrates to fuel the ATP-consuming processes which may be increased in metabolically stressed cells to counteract the

metabolic perturbations. The ATP surge observed in this study (Fig. 4.4, 4.23, 4.41) may be a manifestation of substrate provision which only becomes visible due to the fact that the demand for ATP consuming processes may abruptly cease as the cell starts to die from apoptosis. This would “unmask” the metabolic effect of increased autophagy on substrate provision and ATP generation which then becomes visible in the measured ATP surge. It has been shown that doxorubicin-induced apoptosis can be reduced by 2-DG treatment (Thakkar & Potten, 1993) possibly indicating a similar scenario where increased autophagy may provide substrates to be utilized, providing a temporary metabolically selective advantage which delays apoptosis. Dietary restriction and 2DG treatment has also shown to reduce ischaemic brain damage (Yu & Mattson, 1999). However, autophagy has not been considered in these studies.

Own MTT results indicate a rapid decrease in mitochondrial reductive capacity in mild, moderate and severe SI already after 2 hrs, indicating the potency of the ischaemic event (Fig. 4.4). After 4 hrs moderate and severe SI the reductive capacity measured by MTT decreased significantly compared to mild SI (Fig. 4.23). It is of note that with reperfusion, although reductive capacity remained significantly lower than control, it increased to an extent (Fig. 4.24). This may be indicative of temporal mitochondrial metabolic down-regulation during SI and partial up-regulation during reperfusion. These results stress that MTT-reductive capacity is only an indication of cellular viability but not a measure of viability per se. Another interesting observation is the finding that after 8 hrs severe SI followed by reperfusion, more than 90% of the cells are PI positive, indicative of non-viable cells which died due to loss of membrane integrity, indicative of necrosis (Fig 4.40). The MTT results, however, revealed still more than 50% of cells with a reductive capacity even if the cell membranes were impaired (Fig. 4.42). These results suggest that mitochondrial enzymes may still be partially functional even when the cell is in the process of losing membrane integrity. These results also support the importance of performing multiple viability tests.

5.4. The effect of mild, moderate and severe simulated ischaemia- metabolic sensing, autophagy and apoptosis

Own western blot results support the abovementioned observation of a differential induction of cell death. The pAMPK results reveal a gradual increase in AMPK phosphorylation in mild, moderate and severe SI, which may indicate the differential metabolic demand prevalent in the three ischaemic conditions (Fig. 4.6, 4.25, 4.43). Mild SI reveals a weak increase in pAMPK, however, in moderate and severe SI a stronger pAMPK pattern is observed. This differential phosphorylation pattern is lost after reperfusion (Fig. 4.6, 4.25, 4.43). Interestingly, only mild SI shows an increase in autophagy (Fig 4.12, 4.30, 4.48), and the loss in pAMPK after reperfusion is also mirrored by a decrease in autophagy (Fig 4.13, 4.31, 4.49). These results are supported by the functional role of AMPK to switch on ATP-producing catabolic pathways and to switch off ATP-consuming processes (Hardie *et al.,* 2003, Luiken *et al.,* 2004). AMPK has been shown to play a direct role in fuel selection in response to the cellular energy status (Houten *et al.*, 2009) by stimulating the protein expression of fatty acid transporters time and dose dependently (Chabowski *et al.*, 2006). AMPK is rapidly inactivated after reperfusion (Takagi *et al*. 2007), which is also observed in our results. It has been shown that autophagy is beneficial during the ischaemic event, whilst having opposing effects in the reperfusion phase. In the mouse heart *ex vivo*, 20 min of ischaemia induces autophagy with a further increase in autophagosome formation during reperfusion (Matsui *et al*., 2007). Furthermore, in glucose-deprived cardiac myocytes, autophagy resulting from ischaemia has been shown to be accompanied by AMPK activation and inhibited by dominant negative AMPK, suggesting an AMPK-dependent mechanism. AMPK is rapidly activated during myocardial ischaemia and leads to an increase in glucose uptake and oxidation as well as fatty acid oxidation (Gottlieb *et al*., 2009). Autophagy is enhanced after reperfusion which is accompanied by an inactivation of AMPK and an increase in beclin-1 (Matsui *et al*., 2007). Most studies also suggest an anti-apoptotic role for AMPK. In another model where autophagy is serially induced in energy-starved and energy-

unstarved conditions, ATP content rapidly recovers after reperfusion. Mice which overexpress AMPK in a dominant negative fashion showed decreased autophagosome formation in response to ischaemia which corresponded with a greater infarct size (Matsui *et al*., 2007). Interestingly, AMPK has shown to be differentially controlled depending on the severity of the ischaemic insult (Matsui *et al*., 2007). However, induction of autophagy during the reperfusion phase was attenuated by beclin-$1^{+/-}$ mice, indicating a beclin-1-dependent but AMPK-independent mode of action. This response was accompanied by a smaller infarct area (Matsui *et al*., 2007).

The pmTOR results in this study indicate, that simulated ischaemia has an effect on mTOR phosphorylation. Our results indicate that pmTOR was not yet affected after 2 hrs SI (Fig. 4.7), however it is decreased after 4 hrs SI (Fig. 4.26), with the greatest decrease visible in mild SI (Fig.4.26). This pattern is also maintained after reperfusion (Fig. 4.26). pmTOR remains decreased in mild, moderate and severe SI after 8 hrs SI/R (Fig. 4.44). These results indicate an association between mTOR induction and autophagy mainly during mild SI, which is mirrored by an increase in cells with numerous LC3 punctae (Fig. 4.12, 4.30, 4.48). mTOR is a key regulator for cell growth and autophagy and it is now generally accepted, that this nutrient sensor kinase negatively regulates autophagy. mTOR is a sensor for amino acids and ATP and can integrate hormonal stimuli via the class I PI3-K/PKB pathway. The class I PI3-K allows membrane binding and activation of Akt/PKB. Activation of this pathway has an inhibitory effect on autophagy (Sarbassov *et al.,* 2005). The phosphatase PTEN which hydrolyzes PIP_3, has a stimulative effect on autophagy by inhibiting the actions of class I PI3-K /PKB (Klionsky, 2005). It is therefore important to note that mTOR controls protein synthesis and autophagic proteolysis through the same pathway although in opposite directions.

The beclin-1 results indicate no significant changes following 2, 4 or 8 hrs SI/R (Fig. 4.8, 4.27, 4.45). It has been demonstrated, that overexpression of beclin-1 protects against SI/R injury (Hamacher Brady *et al*., 2006). In an *ex vivo model*,

beclin-1 expression has been shown to be dramatically enhanced after ischaemia/reperfusion (Takagi *et al*., 2007). The caspase-3 results support a strong induction of apoptosis, particularly in mild SI (Fig. 4.9, 4.28, 4.46). The differential response through apoptosis between mild, moderate and severe SI can be better distinguished when observing the extent of PARP cleavage. Our results indicate cleaved PARP particularly in mild SI (Fig. 4.10, 4.29, 4.47).

Our results indicate a differential induction of apoptosis, which is exacerbated after reperfusion. It has previously been shown that apoptosis may already be induced during ischaemia, but reperfusion may also be required for completion of the apoptotic cascade (Engelbrecht *et al.,* 2004). Our results may be indicative of the progression of apoptosis induction within the apoptotic pathway, which is supported by the observation of nuclear condensation and apoptotic bodies (Fig. 4.2). It has been demonstrated that TUNEL-positive cells are especially increased at the borders of subacute infarcts, indicating areas of mild ischaemic injury (Takemura *et al*., 2006). Our results indicate that apoptosis is the predominant form of cell death in mild SI but not in moderate and severe SI. In experimental models for myocardial infarction it has been shown that particularly in the first 2-4 hours of coronary artery occlusion most cell death manifests with apoptotic morphology (Kajstura *et al*., 1996).

5.5. The effect of mild, moderate and severe simulated ischaemia: fluorescence and scanning electron microscopy

The fluorescence imaging results reveal a distinct differential distribution of autophagy, apoptotic and necrotic cell death. In our model, mild SI resulted in primarily apoptosis with prominent features of autophagy (Fig. 4.14, 4.20, 4.32, 4.38, 4.51, 4.56). Moderate and severe SI resulted primarily in necrosis, with partial apoptosis but no indication of autophagy. In cells exposed to mild SI, the LC3 signal was most prominent in the perinulclear region (Fig. 4.11, 4.14). This may represent the normal location of lysosomes but it may also indicate a particular

area of metabolic need within the cell. Mitochondria, which are highly dynamic and motile, constantly fuse and fragment, and it has also been shown that their intracellular arrangement can manifest around the nucleus due to an intracellular metabolic gradient from the middle of the cell to the periphery (Bereiter-Hahn *et al*., 2009). This may, however, only be restricted to the *in vitro* model, as upregulation of autophagy in the *in vivo* heart does not result in a perinuclear LC3 signal (Mizushima *et al*., 2004). However, the mitochondrial dynamic behaviour is likely to be impaired upon collapse of cytoskeletal architecture, as shown in the actin fluorescence images, which may prevent a functional mitochondrial response upon metabolic stress such as in ischaemic injury. Importantly, only in mild SI, a significant increase in cells with numerous LC3 punctae was observed, which was accompanied by pyknosis, but not necrosis. This may indicate, that a metabolically favorable environment is achieved with autophagy, favoring apoptosis over necrosis, resulting in less detrimental consequences. Yu and Mattson have observed a reduction in ischaemic brain damage, following dietary restriction and 2DG treatment, which may indicate a similar underlying mechanism (Yu & Mattson, 1999). However, autophagy has not been measured in that study. Our findings make clear, that mild SI may serve as an appropriate model to study autophagy.

Our beclin-1 images show, to our knowledge for the first time, a very fine and tubulin-like distribution pattern throughout the cytoplasm (Fig. 4.16). Others (Sun *et al.,* 2008; Pickford *et al.,* 2008) have shown a cytoplasmic but granular signal of beclin-1, in close proximity to tubulin. Based on our fluorescence results, *grey zones* between apoptosis and necrosis become apparent. Our results indicate, for example, cytochrome c release in mild, moderate and severe ischaemia. Moreover, it has been shown that HMGB1 remains bound to chromatin in apoptotic cells due to histone underacetylation (Scaffidi *et al*., 2002). However, in our model also apoptotic cells (SI) seem to cause a relocation of HMGB1. Due to an intact membrane however, triggering of inflammation would be prevented. Flow cytometry analysis may be indicated for future studies to quantify both the release kinetics of cytochrome c and HMGB1.

5.6. Summary

Taken together, these results demonstrate that the duration as well as the severity of the ischaemic insult lead to the induction of a differential cellular response manifesting in distinct cell death morphology. Mild SI induced a primarily apoptotic cell death, whilst moderate SI or severe SI led to both apoptotic and necrotic cell death in our model. Most interestingly and intriguing is the finding that only mild SI shows an almost entirely apoptotic cell death, an accumulation of autophagosomes as well as an ATP surge. These data highlight the role of the severity of an ischaemic insult in context with the cell's metabolic capacity and mode of cell death induced. It is indicated that a mild ischaemic insult leads to an autophagic response and manifestation of apoptosis. It is likely that the autophagic response leads to an intracellular metabolic environment which prevents necrosis but induces apoptosis when a metabolic failure is inevitable.

In contrast, a moderate or severe ischaemic insult leads to necrosis without an autophagic response and with ATP depletion. It is likely that a severe insult does not allow the autophagic machinery to be induced, hence apoptosis may switch rapidly to necrosis (Leist *et al.,* 1997) as the metabolic environment is more rapidly depleted of ATP. Our data highlight the role of the severity of an ischaemic insult in context with the cells metabolic capacity and mode of cell death induced. It is indicated that a mild ischaemic insult leads to an autophagic response and apoptosis, whilst a more severe ischaemic insult leads to necrosis without an autophagic response but ATP depletion.

Importantly, these results suggest that the concomitant study of autophagic activity in the context of apoptosis and necrosis as well as the cellular metabolic performance deserves more attention. These results stress the significance of the severity and duration of the stimulus to induce the autophagic machinery. In the heart, autophagy is induced during both acute and chronic ischaemia as well as during nutrient starvation (Gustafsson *et al*., 2008, Matsui *et al*., 2007). Myocardial

ischaemia is characterized by acidosis which is brought about by the breakdown of ATP, a rise of intracellular phosphates and stimulation of glycogenolysis (Poole-Wilson, 1989). During severe myocardial ischaemia, glycolysis is even more increased due to the dramatic decline in oxidative phosphorylation. However, the uncoupling of glycolysis from glucose oxidation leads to an increase in lactate and protons, which decreases cardiac function. A fall of only 0.2 pH units causes a 50% decline in developed tension (Poole-Wilson, 1989). Reduction in proton production has been shown to counteract this decrease in efficiency (Liu *et al*., 1996). To maintain cardiac metabolism through increased autophagy and hence an increase in generated ATP would counteract the drop in intracellular pH and the accompanied decline in contractility. It may be that only a defined time window for an autophagic response exists, as autophagy is inhibited in severe or prolonged ischaemia (Hamacher-Brady *et al*., 2006, Takagi *et al*., 2007). It is therefore recommended to assess multiple parameters (Mizushima, 2005) to predict the outcome of autophagy either as stress adaptation and survival mechanism, or as a symptom of bioenergetic failure. Only the dissection of these factors may indicate this fine line between survival and death.

In general, our results also highlight the importance of using multiple viability tests to avoid false negative results. For example, a trypan blue-based viability assessment of cells exposed to 8 hrs mild SI would, similar to PI results, show 18% nonviable cells, missing the 61% apoptotic cells, which still have an intact membrane (Fig. 4.39). These data may be of particular interest for the field of cardiovascular research as the results reveal that different *in vitro* models of simulated ischaemia may manifest in a differential mode of cell death, which can only be completely evaluated with a combination of viability tests. Recent guidelines to assess cell death modes suggest the use of multiple and methodologically nonrelated assays (Galuzzi *et al*., 2009), which is in agreement with our results.

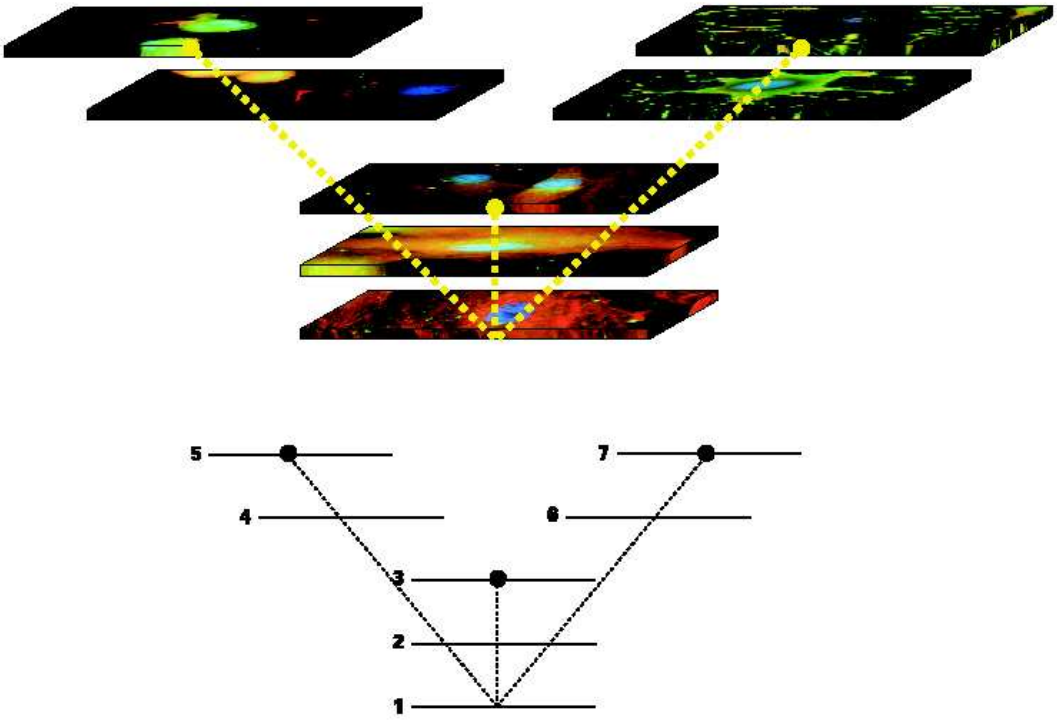

Figure 5.1: Model of the cell's capacity to respond to a defined insult, indicating the typical morphological features of different types of cell death: 'autophagy baseline' 1, 'autophagy induced' 2, 'cell death with autophagy' 3, 'apoptosis induced' 4, 'apoptosis executed' 5, 'necrosis induced' 6 and 'necrosis executed' 7. Cells are counterstained for light chain 3 (LC3) (green), actin (red) and nuclei (blue). The manifestation and overlap of the above morphological features are dependent on the severity of the insult, its duration and the metabolic state of the cell.

CHAPTER 6 RESULTS: ONSET DYNAMICS

6.1. Protocol - onset dynamics in vitro

In order to investigate whether autophagy is contributing to cell death or survival, autophagy was induced by rapamycin treatment and inhibited by 3 MA treatment. It was then investigated whether cell death is accelerated or delayed. Due to the findings of the differential death mode contribution in the first part of this study, we employed mild SI as model for apoptotic and moderate SI as a model for necrotic cell death respectively (Fig. 6.1).

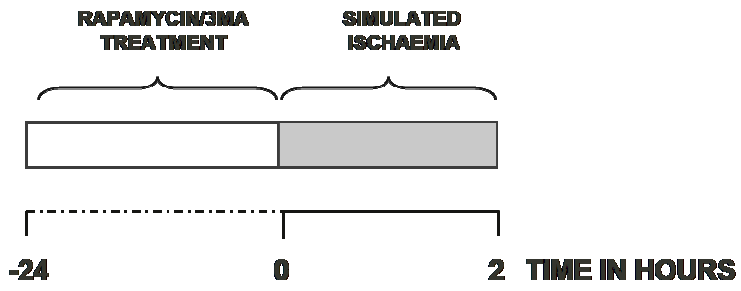

Figure 6.1: ***In vitro*** **experimental protocol for study of onset dynamics with induced or inhibited autophagic activity. Following 24 hrs of treatment with either rapamycin or 3MA, cells were exposed to 2 hrs of mild or moderate SI.**

6.2. Live Cell Imaging

In order to elucidate the relationship between autophagic activity and onset of apoptosis and necrosis, live cell imaging was employed to capture cellular events in real time. Cells seeded on chambered coverglass slides were transfected with a LC3-GFP construct and treated for 24 hrs with either rapamycin or 3-MA. In order to characterize the spatial and functional relationship between autophagosomes, lysosomes and mitochondria, transfected cells were treated with the appropriate organellar dye and images were acquired every 4 seconds.

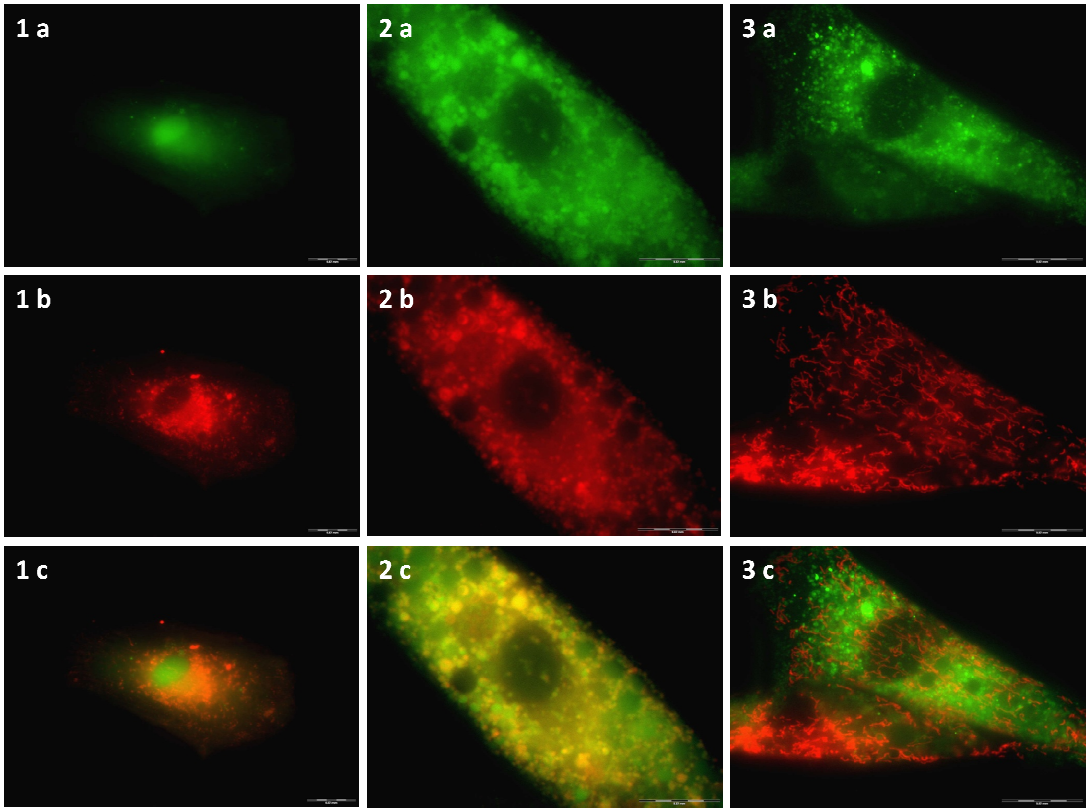

Figure 6.2: Rapamycin treatment results in an rapid increase of autophagosomes (2a) compared to baseline autophagic activity (1a), Following fusion with lysosomes, their degraded content is released and provides additional substrates to be oxidized in respiring mitochondria (3b). H9c-2 myoblasts have been transfected with LC3-GFP (1a-3a), counterstained with Lyostracker Red (1b, 2b) or Tetramethylrhodamine Ethyl Ester (TMRE) (3b) to indicate autophagosomes, lysosmomes and actively respiring mitochondria respectively. An overlay is shown (1c-3c). The data are shown as a movie clip on the CD.

6.2.1. LC-3 imaging

Following a 24 hr treatment period with either rapamycin (micrograph panel$_2$) or 3-MA (micrograph panel$_3$) of cells seeded on chambered coverglass slides were exposed to 2 hrs mild SI (micrographs B_{1-3}) or moderate SI (micrographs C_{1-3}) respectively and then stained for LC3 and nuclear DNA to visualize the autophagic response (Fig. 6.3). A_1-A_3 represent normoxic control cells. Exposure to 2 hrs mild and moderate SI led to a differential autophagic response as seen by the accumulation of LC3 punctae. In control conditions rapamycin treatment led to robust formation of autophagosomes (A_2), whilst 3MA treatment resulted in a diffuse cytoplasmic LC3 signal (A_3) comparable to non-treated cells (A_1). It is therefore highly likely that autophagic flux was upregulated in the cells prior submission to the SI protocol (this is supported by the acridine orange-based flow cytometry and imaging results. See addendum). It can clearly be seen that mild SI induced the generation of autophagosomes (B_1) which was maintained with rapamycin treatment (B_2). This response was less prominent with 3MA treatment (B_3). Cells exposed to moderate SI did not show this prominent autophagosome formation (C_1) only rapamycin treatment (C_2) but not 3MA treatment (C_3) seems to have manifested in autophagosome formation.

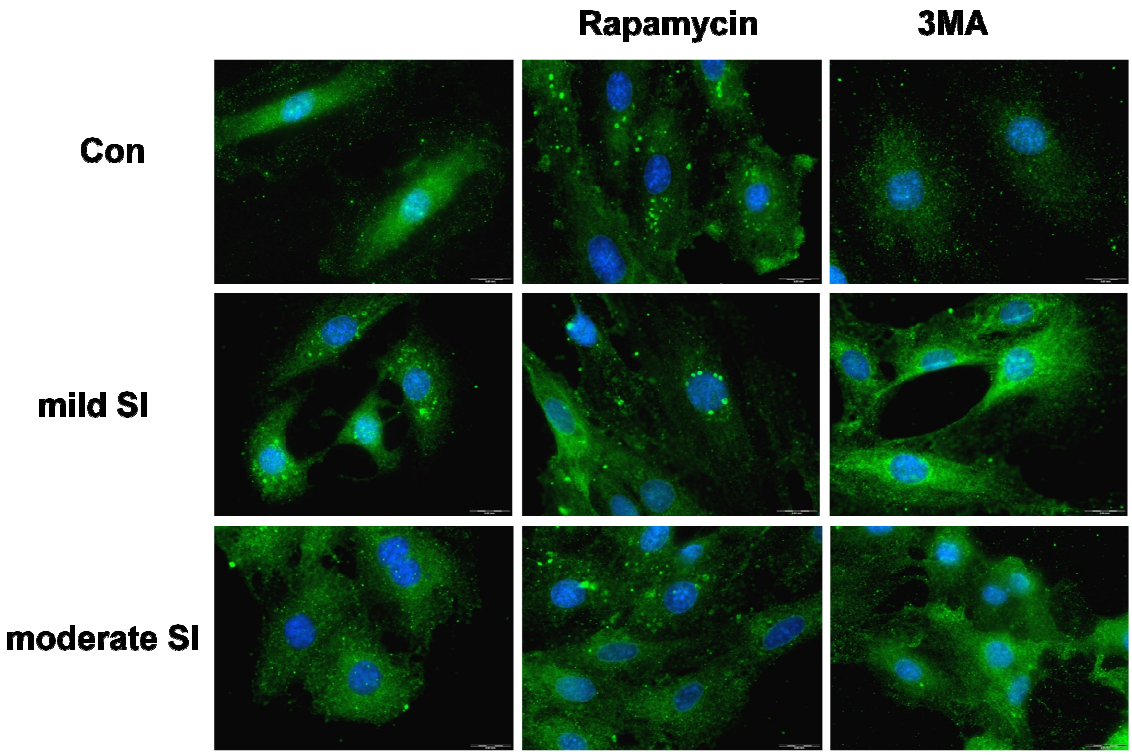

Figure 6.3: Fluorescent micrographs showing LC3 (green) autophagosomes in cells exposed to mild SI (micrographs B_{1-3}) or moderate SI (micrographs C_{1-3}) respectively. Nuclear DNA is indicated in blue by using Hoechst 33342. A_1-A_3 show normoxic control cells.

6.2.2. Propidium Iodide uptake dynamics

In order to assess the dynamic nature of the loss in cellular membrane integrity the dynamic characteristics of PI uptake during simulated ischaemia was investigated by time lapse imaging and multiple regions of interest analysis (ROI) (Fig. 6.4). Loss of membrane integrity is a major morphological feature of necrotic cell death.

Our results (Fig. 6.5, 6.6) indicate a significant delay in the loss of membrane integrity in cells treated with rapamycin (EC 50: 86.4±4.1) compared to moderate

SI (EC 50: 64.7±4.1). 3MA treatment prior to the ischaemic event induced loss of membrane integrity similar to moderate SI (EC 50: 69.4±4.1). Moreover, rapamycin treatment prior to ischaemia manifested in a significantly lower top value of the sigmoid intensity curve (results not shown) compared to simulated ischaemia, indicating not only a delayed loss in membrane integrity but also a weaker influx of the dye propidium iodide manifesting in weaker fluorescence signal at a given time. 3MA treatment prior to the ischaemic event showed a top value similar to moderate SI compared to the control value. These data strongly indicate a delay in necrosis brought about by a rapamycin-induced increase in autophagic activity (Fig. 6.5).

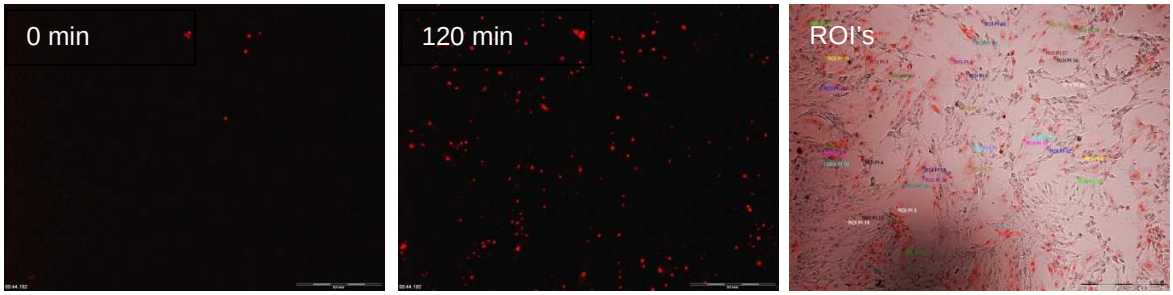

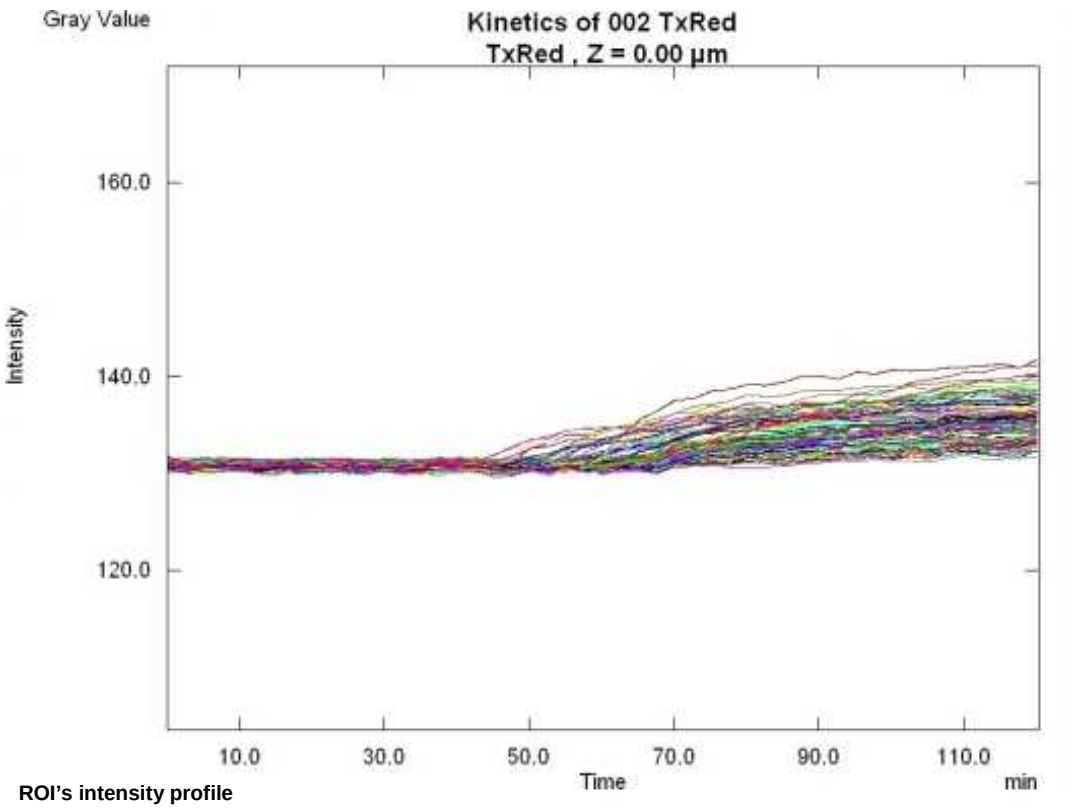

ROI's intensity profile

Figure 6.4: Following 24 hrs treatment with either rapamycin or 3-MA, cells seeded on chambered coverglass slides were exposed to 2 hrs moderate SI, to model a primarily necrotic mode of cell death, whilst images were captured every 180 seconds, to visualize the dynamic characteristics of PI uptake. For each condition >120 ROI's were analyzed. Four independent experiments have been performed.

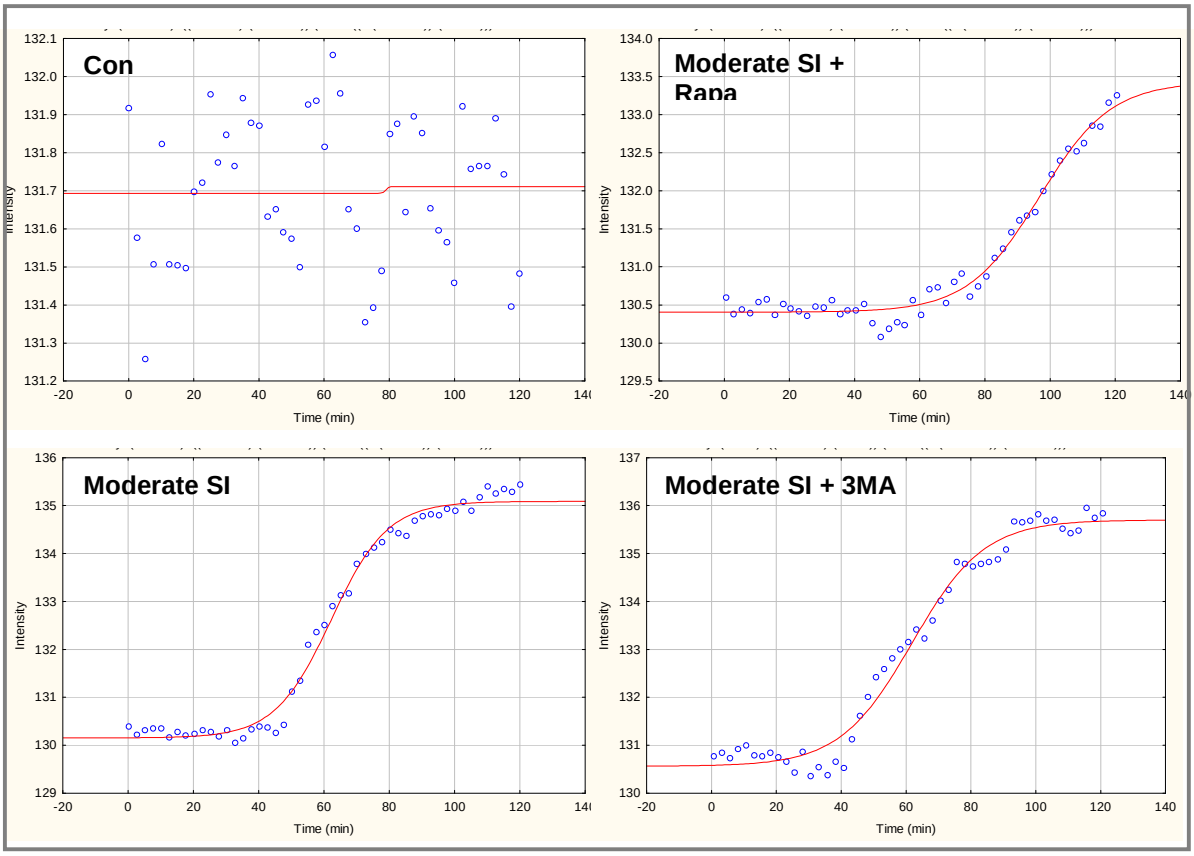

Figure 6.5: Intensity distribution over time, indicating the onset of PI uptake and hence loss in membrane integrity. Fluorescence emission was monitored at 1 frame per 180 seconds for 2 hrs by collection windows for TexRed emission, using a UBG triple bandpass emission filter. For each condition >120 ROI's were analyzed.

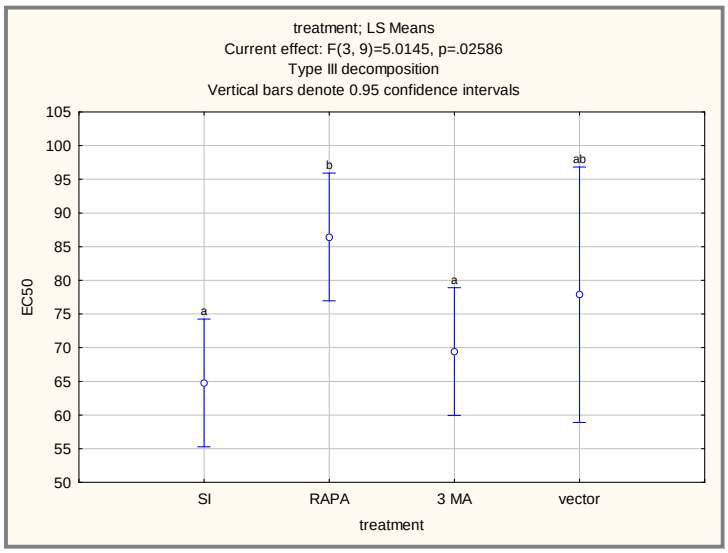

Figure 6.6: EC50 data showing moderate SI (SI), moderate SI + Rapamycin treatment (RAPA), moderate SI + 3MA treatment (3MA). A vector control (DMSO) is also shown. The EC 50 data indicate a significant difference in time, when using rapamycin compared to SI. The vector shows no effect.

6.2.3. Fluorescence Resonance Energy Transfer (FRET) and mitochondrial depolarization dynamics

Caspase-3 activation (Youle & Strasser, 2008) and loss of mitochondrial membrane depolarization (Galluzzi *et al*., 2007) have both been described as a point-of-no-return (PONR) in apoptotic cell death. As previously shown (Tyas *et al*., 2000) and verified in our cell line, the results also show that both depolarization of the mitochondrial inner membrane and the activation of caspase-3 are rapid events and occur in parallel (Fig. 6.8, 6.9). Our real time imaging results indicate a significant delay in the loss of mitochondrial membrane potential in cells treated with rapamycin (EC 50: 1.8 ±0.06) compared to mild SI (EC 50: 0.69±0.01) (Fig. 6.7, 6.10, 6.11). 3MA treatment prior to the ischaemic event induced loss of membrane integrity significantly earlier when compared to mild SI (EC 50: 0.36 ±0.38.) and hence had a more detrimental effect (Fig. 6.10, 6.11). These findings are in agreement with a recent study, which has demonstrated that the inhibition of autophagy increases loss of mitochondrial depolarization (Qadir *et al.,* 2008).

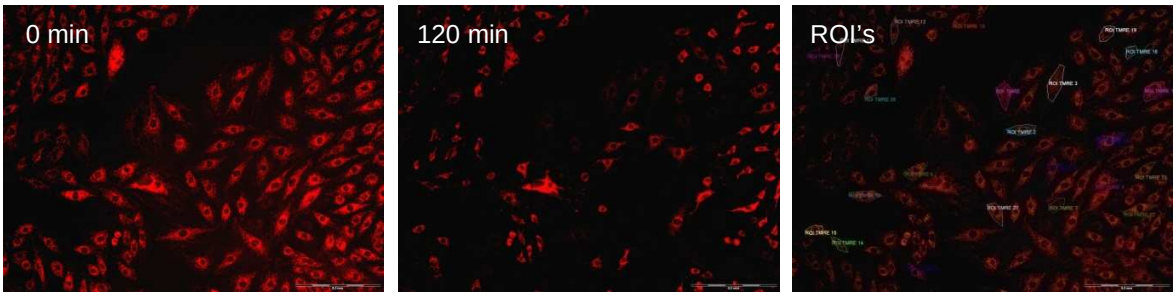

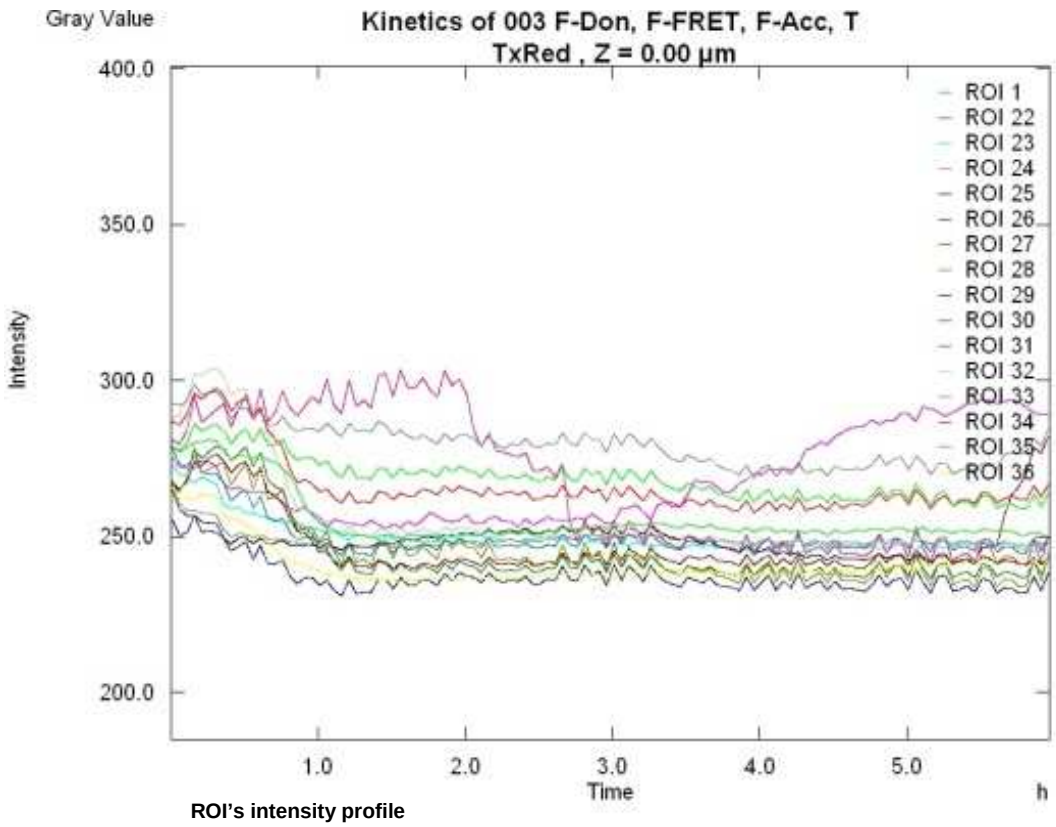

Figure 6.7: Following 24 hrs treatment with either rapamycin or 3-MA, cells seeded on chambered coverglass slides were exposed to 2 hrs mild SI, to model a primarily apoptotic mode of cell death, whilst images were captured every 180 seconds to visualize the dynamic characteristics of caspase-3 activity and loss of mitochondrial membrane potential. For each condition >120 ROI's were analyzed. Four independent experiments have been performed.

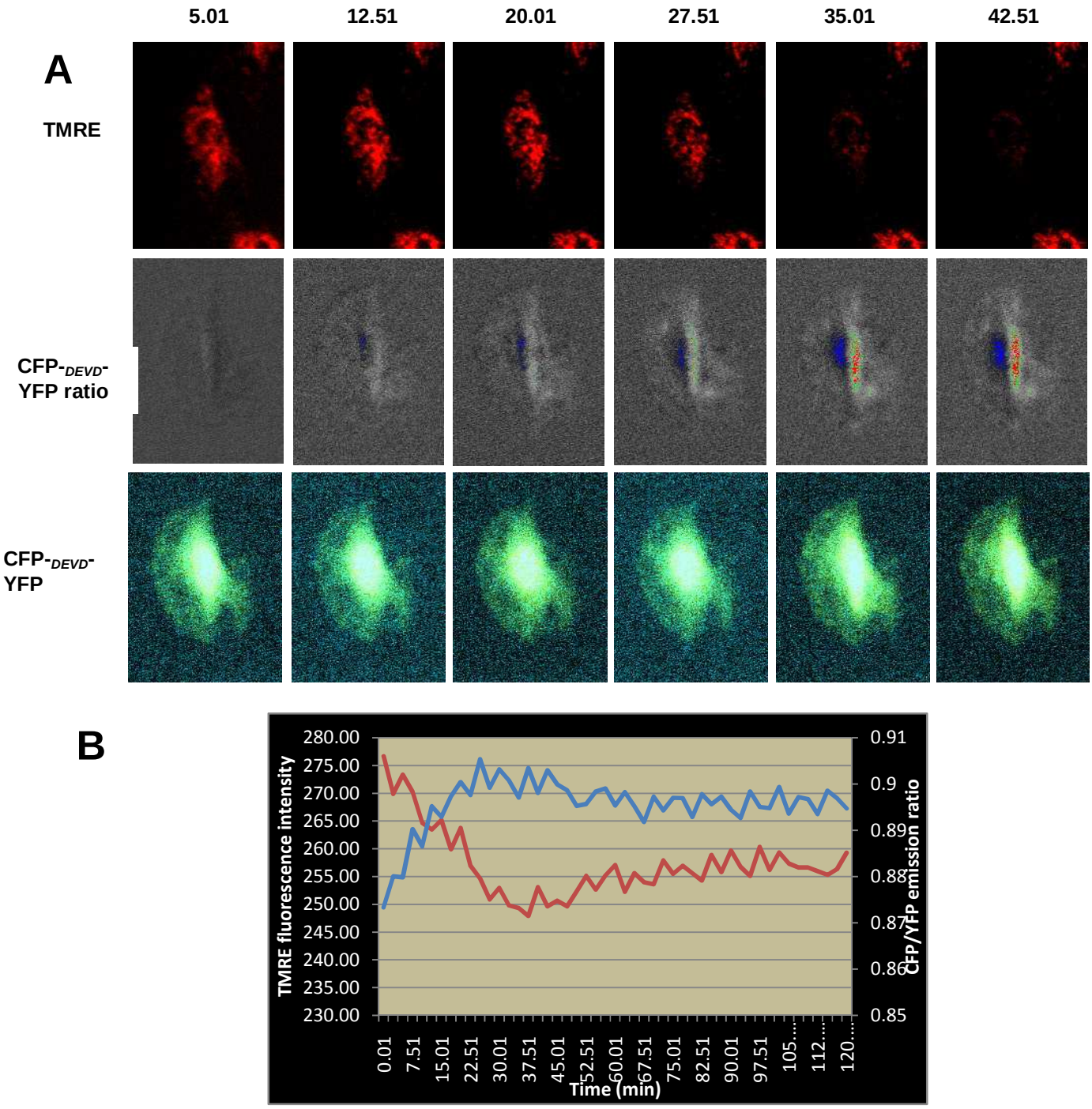

Figure 6.8: Depolarization of the mitochondrial inner membrane and the activation of caspase-3 are rapid events and occur in parallel. H9c-2 cells were exposed to mild SI whilst the CFP/YFP emission ratio and the TMRE fluorescence intensity were measured simultaneously. As TMRE intensity decreases (red lines), the CFP/YFP ratio increases (blue lines) (B). The CFP/YFP ratio of a representative cell was plotted alongside the TMRE fluorescence intensity over 120 min duration of imaging (A).

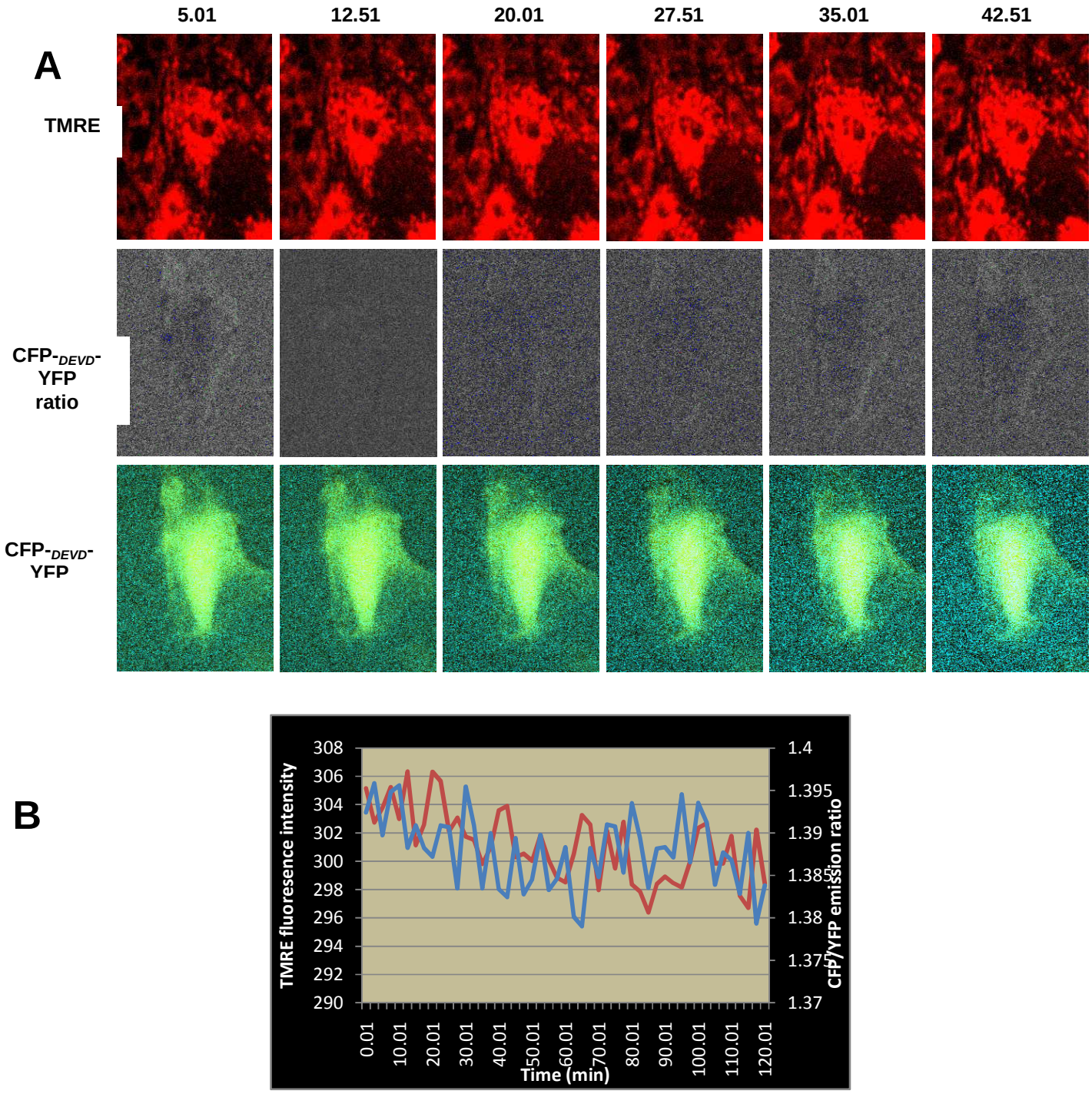

Figure 6.9: H9c-2 cells were maintained under normoxic conditions whilst the CFP/YFP emission ratio and the TMRE fluorescence intensity were measured simultaneously. TMRE intensity (red lines) and CFP/YFP ratio (blue lines) remain unchanged (B). The CFP/YFP ratio of a representative cell was plotted alongside the TMRE fluorescence intensity over 120 min duration of imaging (A).

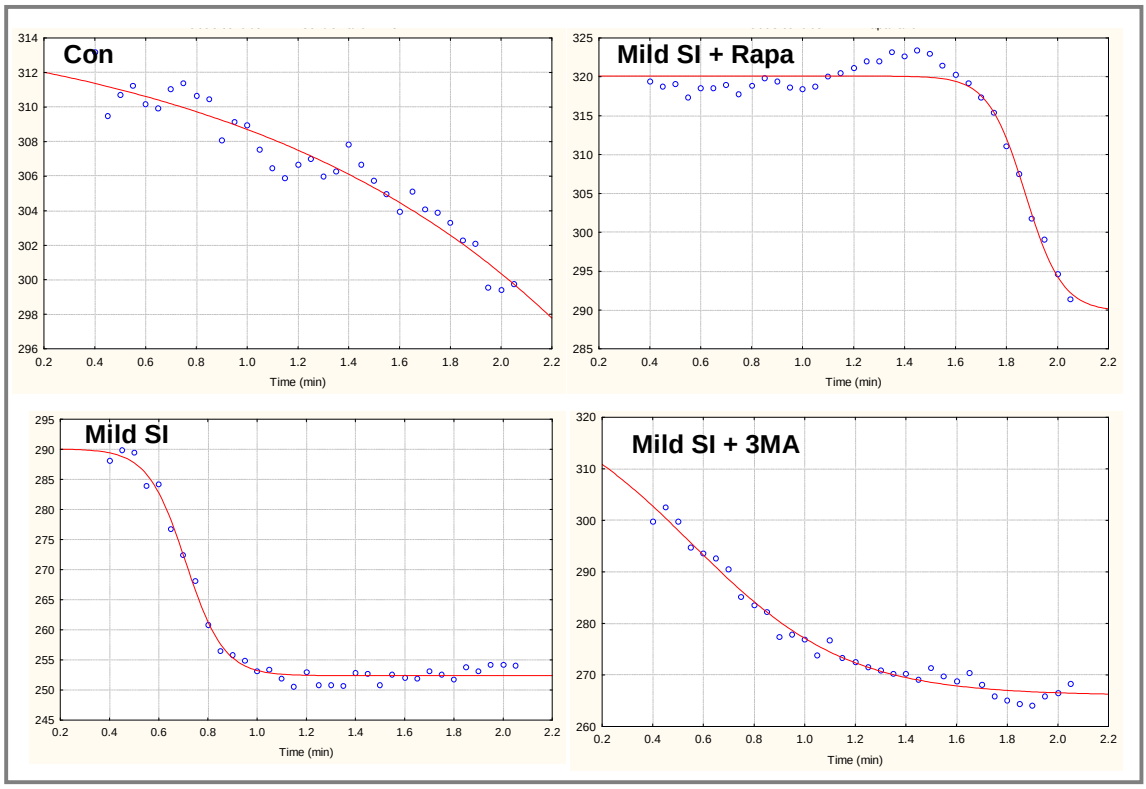

Figure 6.10: Intensity distribution over time, indicating the loss in mitochondrial membrane depolarization. Fluorescence emission was monitored at 1 frame per 180 seconds for 2 hrs by collection windows for TexRed emission, using a UBG triple bandpass emission filter. For each condition >120 ROI's were analyzed.

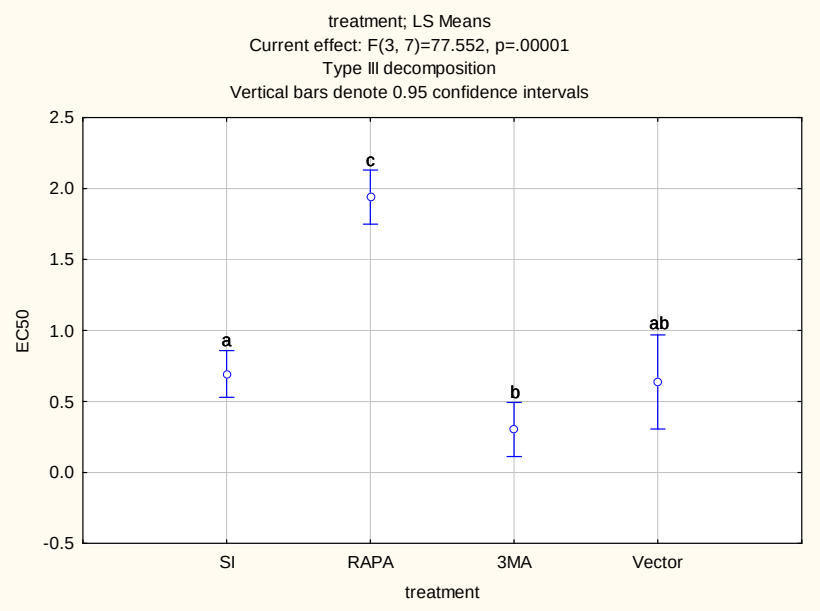

Figure 6.11: EC50 data showing mild SI (SI), mild SI + Rapamycin treatment (RAPA), mild SI + 3MA treatment (3MA). A vector control (DMSO) is also shown. The EC 50 data indicate a significant difference in time, when using rapamycin or 3MA, compared to SI. The vector shows no effect.

6.3. Flow Cytometry

In order to quantify the propidium iodide and Tetramethylrhodamine Ethyl Ester intensity dynamics described through real time imaging, flow cytometry was performed. Following a 24 hr treatment period with either rapamycin or 3-MA, cells were seeded in tissue culture flasks, exposed to 2 hrs mild or moderate SI and collected for analysis on the flow cytometer. At least 5000 events of the gated population were recorded. Based on a 3-dimensional representation of the forward and side scatter, the differential morphology of cells exposed to mild or moderate SI is revealed (Fig. 6.12).

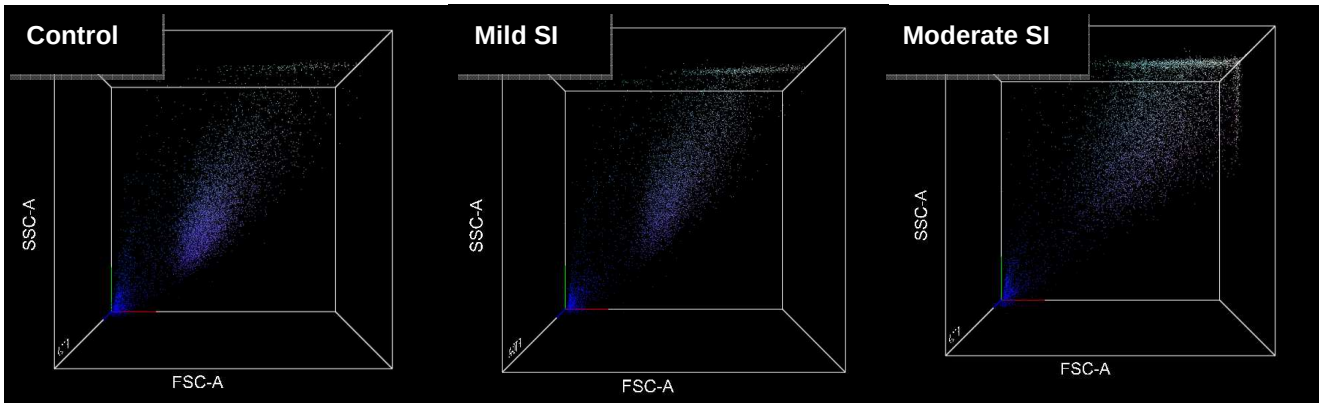

Figure 6.12: Based on a 3-dimensional representation of the forward and side scatter, the earlier described differential morphology is revealed. Mild SI shows a tight and slightly upshifted population compared to control condition, indicating apoptosis-associated cell shrinkage and increase in granularity. Moderate SI on the other hand shows a broadened and slightly right-shifted population, indicating necrosis-associated cell swelling.

6.3.1. PI exclusion

In order to quantify the abovementioned dynamics of PI uptake, flow cytometry was performed following 2 hrs moderate SI (Fig. 6.12). Our results show a significant decrease in PI-positive cells in moderate SI + Rapa [8.4±0.1% ($p<0.05$)] compared to cells exposed to moderate SI (16±2.5%). 3MA treatment (17.7±1.5%) did not result in further increase in PI-positive events compared to moderate SI (16±2.5%) (Fig. 6.13).

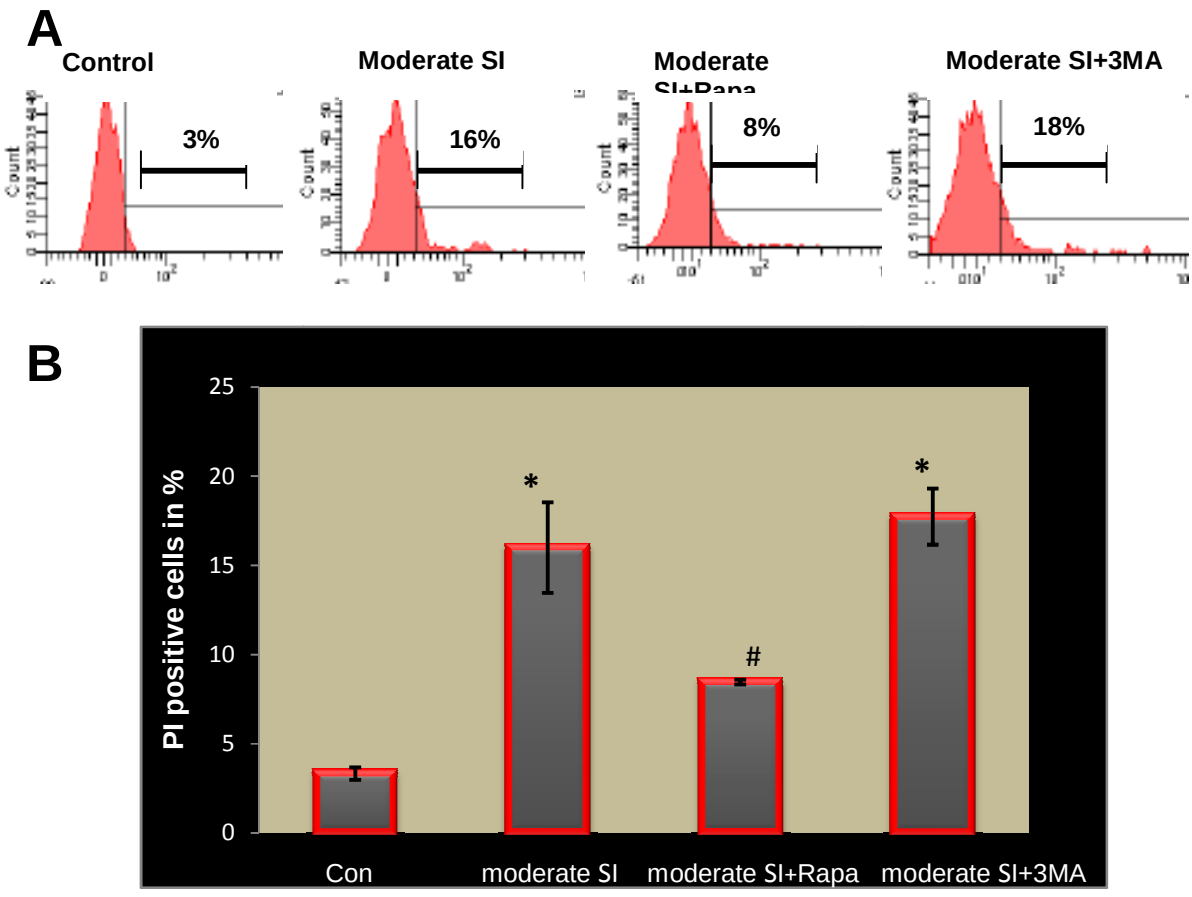

Figure 6.13: PI positive cells in % (B) assessed by flow cytometry following 24 hrs rapamycin and 3MA treatment and 2 hrs moderate SI. Data expressed as mean ± SEM, statistical analysis: ANOVA & Bonferroni correction, * $p<0.05$ vs Con, # $p<0.05$ vs moderate SI, n=3. A representative intensity histogram is shown (A).

6.3.2. Tetramethylrhodamine Ethyl Ester (TMRE) intensity analysis

In order to quantify the above described dynamics of mitochondrial depolarization (Fig. 6.7, 6.10) flow cytometry was performed following 2 hrs mild SI. Our results show a significant increase in TMRE mean intensity signal in mild SI + Rapa [91.9±8% ($p<0.05$)] compared to cells exposed to mild SI (72.4±0.7%). 3MA treatment (71.1±0.9%) did not result in further decrease in TMRE mean intensity compared to mild SI (72.4±0.7%) (Fig. 6.14, 6.15).

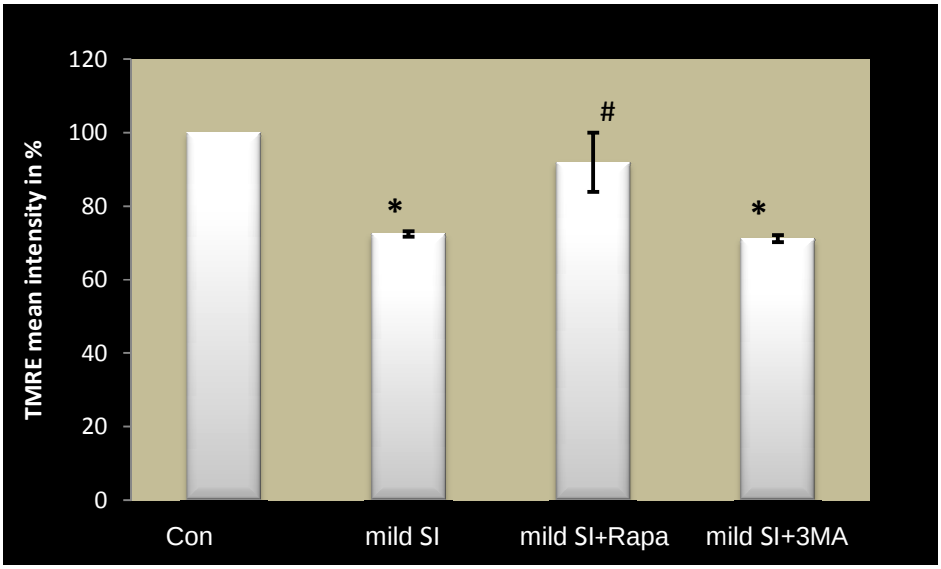

Figure 6.14: TMRE mean intensity in % assessed by flow cytometry following 24 hrs rapamycin and 3MA treatment and 2 hrs mild SI. Data expressed as mean ± SEM, statistical analysis: ANOVA & Bonferroni correction, * p<0.05 vs Con, # p<0.05 vs mild SI, n=3.

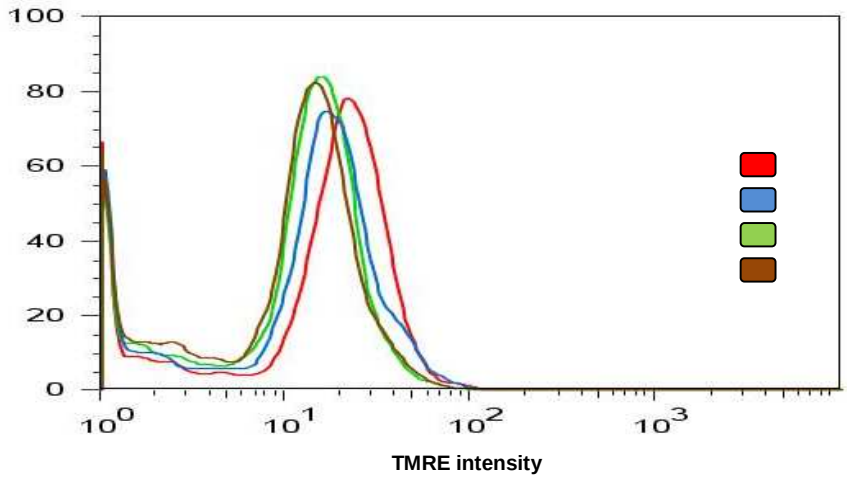

Figure 6.15: TMRE intensity histogram showing the intensity profile of Con (red); mild SI (green); mild SI + Rapa (blue) and mild SI+3MA (brown).

6.3.3. Reactive oxygen species (ROS) assessment

In order to investigate the role of oxidative damage in H9c-2 cells during mild and moderate SI when pretreated with rapamycin or 3MA, cells were loaded with DCF (Fig. 6.16) and analyzed by flow cytometry. A 24 hr treatment period of cells with rapamycin without any ischaemic insult decreased DCF mean intensity significantly [91.5±0.9% ($p<0.05$)] compared to control cells (Fig. 6.17). In contrast, 3MA treatment increased DCF mean intensity significantly [105.8±1.7% ($p<0.05$)] compared to control cells. Cells exposed to 2 hrs mild SI showed no changes in DCF mean intensity compared to control cells. However, mild SI + Rapa showed significant increase in DCF mean intensity [158.8±7.4% ($p<0.05$)] compared to cells exposed to mild SI (114.2±1.6%) (Fig. 6.18, 6.19). The mean DCF signal increased significantly in mild SI+3MA [214.3±20.6% ($p<0.05$)] compared to mild SI (114.2±1.6%). These results indicate that mild SI per se does not increase ROS production significantly. However, increased autophagy prior to the ischaemic event does (Fig. 6.18, 6.19). The inhibition of autophagy by 3MA leads to an even more robust increase in ROS. The same DCF intensity pattern can be observed in cells exposed to 2 hrs moderate SI (Fig. 6.20, 6.21). Cells exposed to 2 hrs moderate SI showed no changes in DCF mean intensity compared to control cells. However, moderate SI + Rapa showed a significant increase in DCF mean intensity [225.2±27.8% ($p<0.05$)] compared to cells exposed to moderate SI (142.6±8.5%). The mean DCF signal increased significantly in moderate SI+3MA [265.1±18% ($p<0.05$)] compared to moderate SI + Rapa (225.2±27.8%) (Fig. 6.20, 6.21).

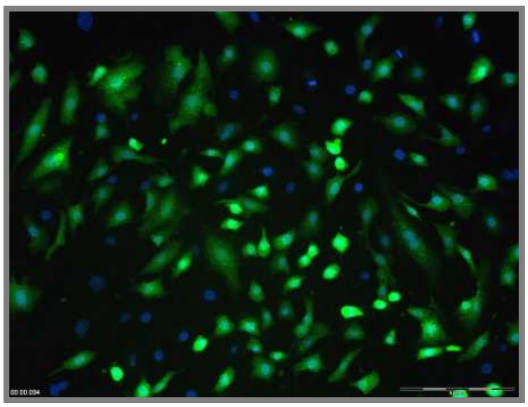

Figure 6.16: H9c-2 myoblasts following incubation with DCF and Hoechst 33342.

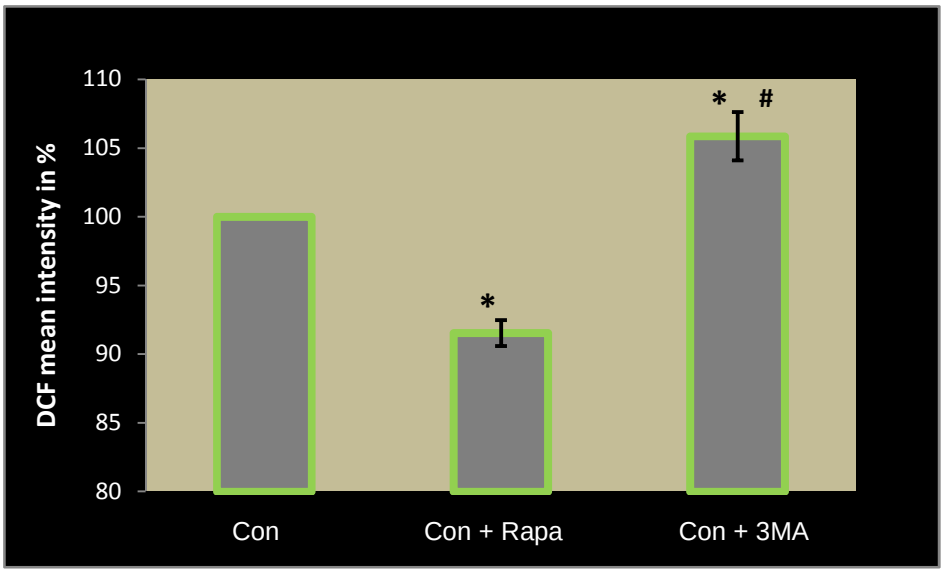

Figure 6.17: DCF mean intensity in % assessed by flow cytometry following 24 hrs rapamycin and 3MA treatment, kept under control conditions. Data expressed as mean ± SEM, statistical analysis: ANOVA & Bonferroni correction, * p<0.05 vs Con, # p<0.05 vs Con+Rapa, n=3.

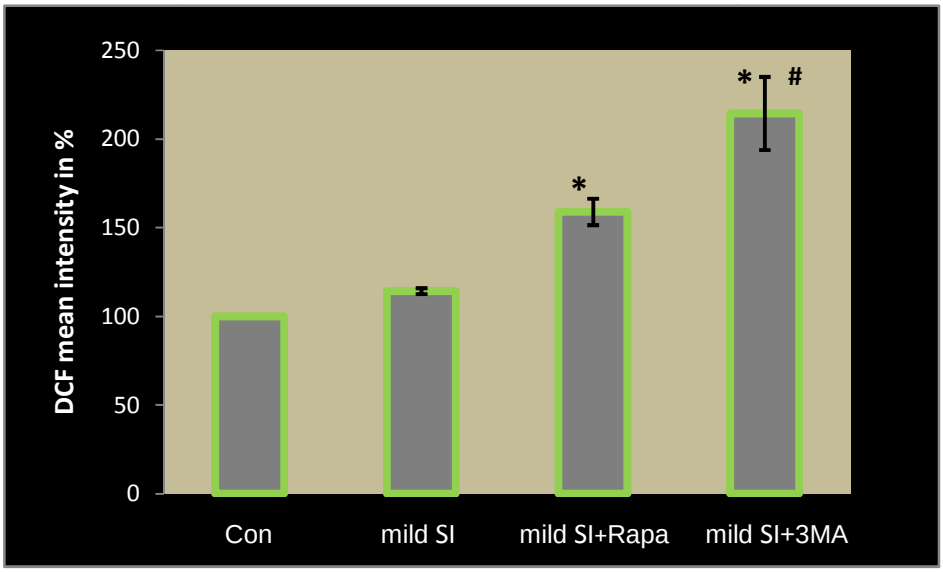

Figure 6.18: DCF mean intensity in % assessed by flow cytometry following 24 hrs rapamycin and 3MA treatment and 2 hrs mild SI. Data expressed as mean ± SEM, statistical analysis: ANOVA & Bonferroni correction, * p<0.05 vs Con, # p<0.05 vs mild SI, n=3.

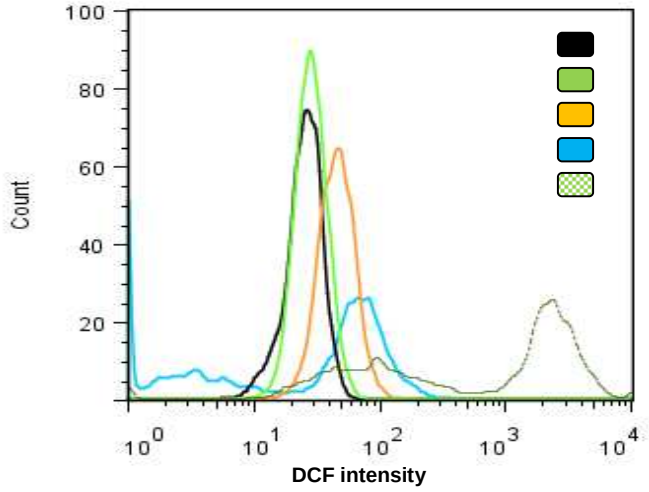

Figure 6.19: DCF intensity histogram showing the intensity profile of Con (black); mild SI (green); mild SI + Rapa (orange) and mild SI+3MA (blue). H_2O_2 has been employed as positive control and is shown as green dotted line.

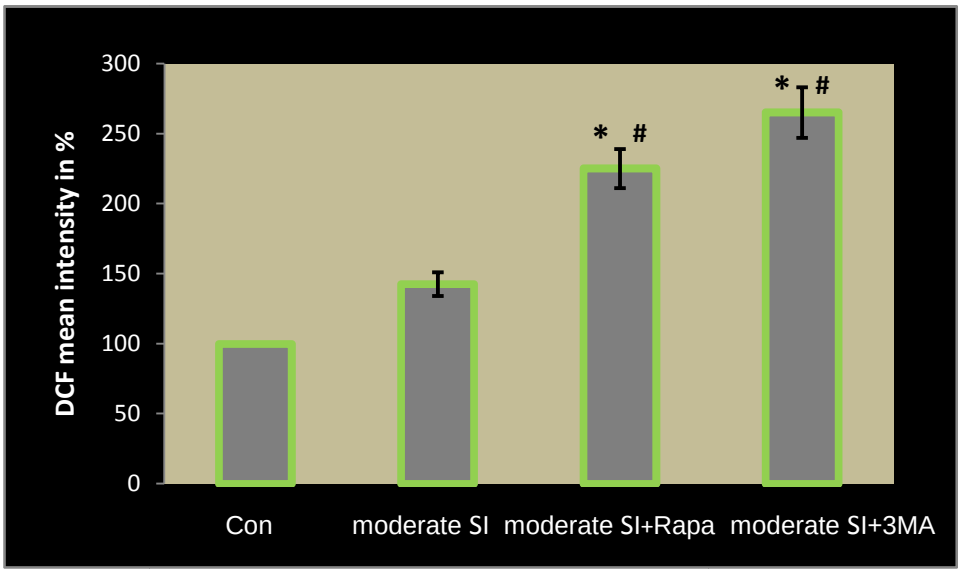

Figure 6.20: DCF mean intensity in % assessed by flow cytometry following 24 hrs rapamycin and 3MA treatment and 2 hrs moderate SI. Data expressed as mean ± SEM, statistical analysis: ANOVA & Bonferroni correction, * p<0.05 vs Con, # p<0.05 vs mild SI, n=3.

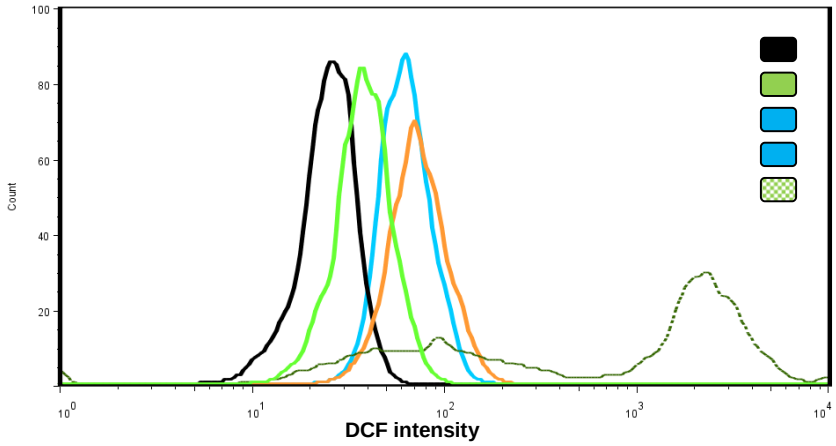

Figure 6.21: DCF intensity histogram showing the intensity profile of Con (black); moderate SI (green); moderate SI + Rapa (blue) and moderate SI+3MA (orange). H_2O_2 has been employed as positive control and is shown as green dotted line.

6.4. ATP

Following a 24 hr treatment period with either rapamycin or 3-MA, cells were exposed to 2 hrs mild or moderate SI, followed by 1 hr reperfusion and collected for ATP analysis. A 24 hr treatment period of cells with rapamycin without any ischaemic insult significantly decreased ATP [81.6±4.8% ($p<0.05$) vs 100%] compared to control cells (Fig. 6.22). In addition, 3MA treatment also decreased ATP significantly [74.5±3.9% ($p<0.05$)] compared to control cells. As shown in the first part of the study, cells exposed to 2 hrs mild SI showed significant increase in ATP [264.7±70.4% ($p<0.05$)] compared to control cells. However, this ATP surge is completely lost in mild SI+Rapa (118.2±30.5%) as well as in mild SI+3MA (123.2±32.7%) (Fig. 6.23). In addition, as described earlier, cells exposed to 2 hrs moderate SI showed no significant change in ATP (99.5±39.5%) compared to control cells. These ATP levels are maintained in moderate SI+Rapa (60.6±13.6%) as well as in moderate SI+3MA (54.8±13.2%), with no significant changes (Fig. 6.24).

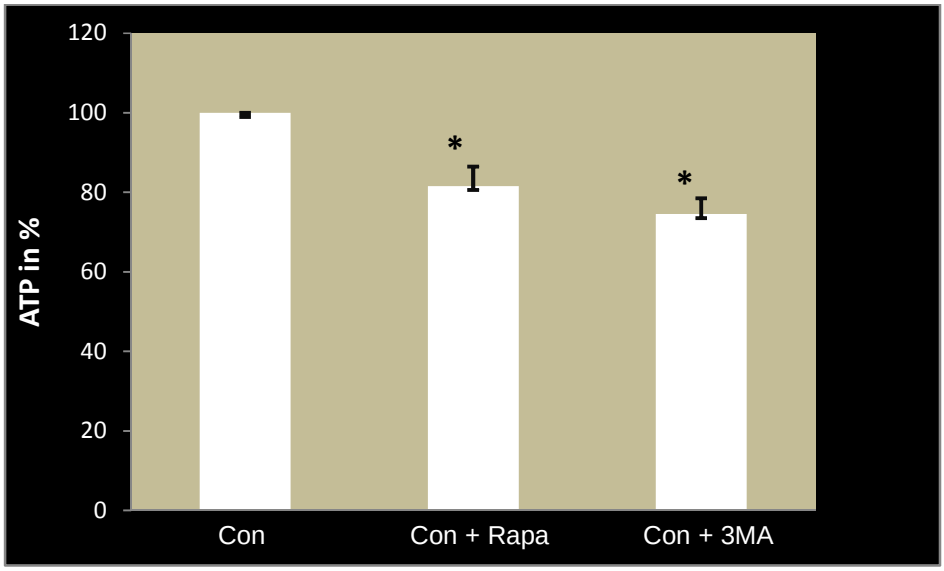

Figure 6.22: ATP levels of control cells following 24 hrs rapamycin and 3MA treatment. Data expressed as mean ± SEM, statistical analysis: ANOVA & Bonferroni correction, * p<0.05 vs Con, n=16.

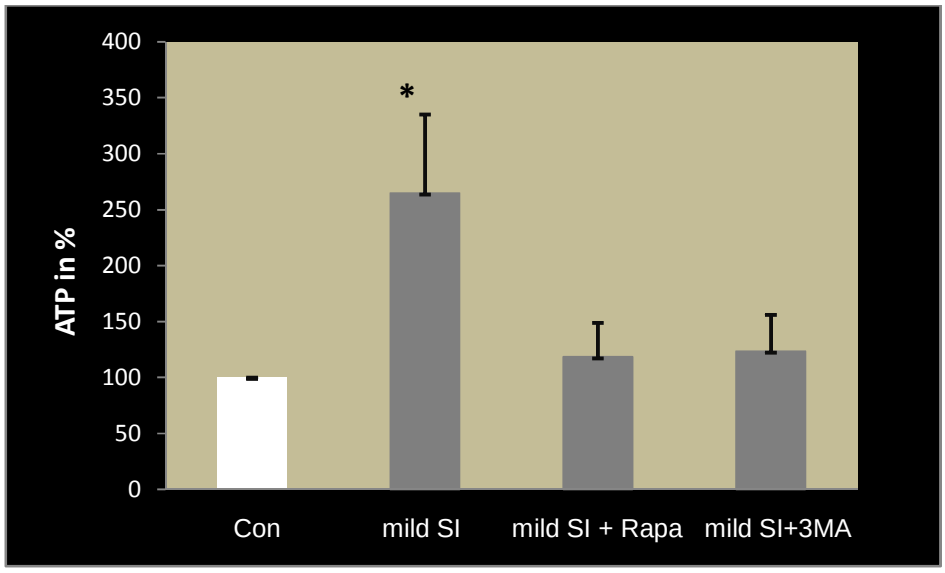

Figure 6.23: ATP levels following 24 hrs rapamycin and 3MA treatment and 2 hrs mild SI. Data expressed as mean ± SEM, statistical analysis: ANOVA & Bonferroni correction, * p<0.05 vs Con, n=10.

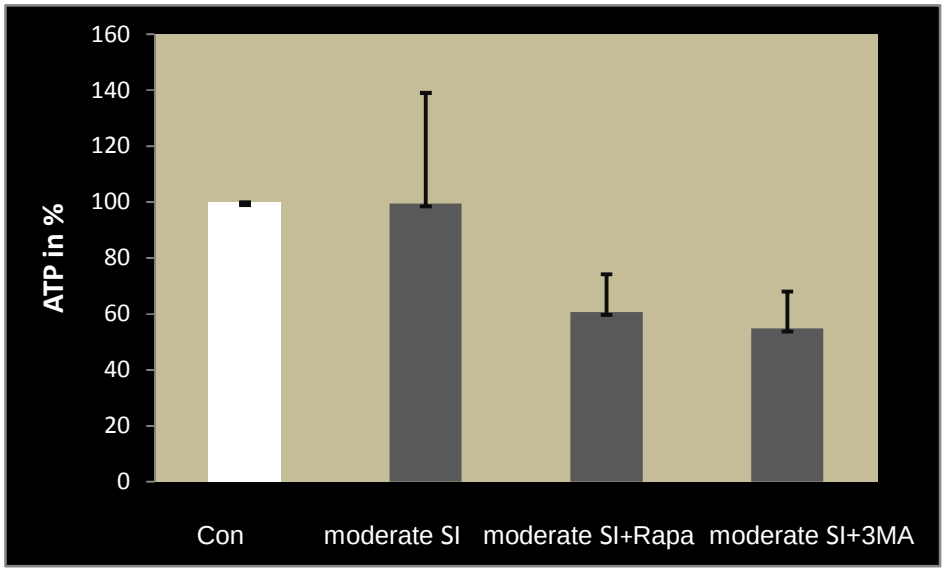

Figure 6.24: ATP levels following 24 hrs rapamycin and 3MA treatment and 2 hrs moderate SI. Data expressed as mean ± SEM, statistical analysis: ANOVA & Bonferroni correction, * p<0.05 vs Con, # p<0.05 vs moderate SI, n=10.

CHAPTER 7 DISCUSSION: ONSET DYNAMICS

7.1. *In vitro* onset dynamics of apoptosis and necrosis

Cellular processes are of highly dynamic nature and there is a growing attempt to capture such processes and cellular responses in real time. Due to the development of novel techniques and innovative strategies, both the *in vitro* (Gong *et al*., 2007) and *in vivo* environment (De Saint-Hubert *et al*., 2009, Schoenberger *et al*., 2008) can be studied and cellular responses or cell death captured through, for example, molecular imaging techniques. A major advantage of a real-time approach lies in the fact that it allows the study of a cellular response in its dynamic nature. Literature suggests that autophagy plays a fundamental role in the cell's survival mechanism (Lockshin & Zakeri, 2004, Degterev *et al*., 2005). Although it may be activated in cell death, evidence suggests that in most cases it is not a contributing factor (Han *et al*., 2007). When cell death is viewed as a dynamic response, interchanging the terminology for apoptosis or necrosis "inhibition" with "onset delay" is needed. This view suggests that autophagy promotes cell survival primarily by delaying the onset of apoptosis and necrosis. It also proposes that autophagic response time, capacity and net flux determine the time of death onset by creating a metabolically favourable intracellular environment.

Our findings of a protective role of autophagy are in agreement with a number of studies. An inhibition of autophagy in isolated cardiomyocytes, exposed to anoxia-reoxygenation, has been shown to increase necrotic cell death which was further increased by additional inhibition of apoptosis (Dosenko *et al*., 2006). On the other hand, enhancing autophagic flux in cardiac myocytes protects them against ischaemic injury by reducing apoptosis (Hamacher-Brady *et al.*, 2006). When autophagy is enhanced through overexpressing bcl-2 in cardiac HL-1 cells, proapoptotic molecules such as Bax are reduced (Hamacher-Brady *et al.*, 2006). Moreover, autophagy has been described in the ischaemic myocardium following

six episodes of ischaemia with an increase in cathepsin D, beclin-1 and other autophagic indicators.

7.2. *In vitro* onset dynamics – ROS assessed by flow cytometry

In the myocardium all cell types generate ROS specifically through the mitochondrial electron transport chain, xanthine oxidases, 'uncoupled' nitric oxide synthases, cytochrome P450 and NADPH oxidases (Akki *et al.,* 2009). An important parameter for maintaining a metabolically favorable environment is the role of autophagy in degenerating damaged and oxidized proteins, thus indicating its role in the homeostasis of cellular oxidative stress. Reactive oxygen species (ROS) is a side product of mitochondrial respiration which initiates cell damaging peroxidation chain reactions. Amino acid starvation-induced H_2O_2 generation in mitochondria has been shown to lead to Atg4 oxidization which enables autophagosome formation to proceed (Scherz-Shouval *et al*., 2007). An apoptotic-like response has been described when oxidative damage is left unrepaired (Arcangioli & Hassine, 2009), hence, sensing ROS and reacting to it through increased degradation of oxidatively damaged proteins (Moore, 2008, Zheng *et al*., 2006) would decrease the load of oxidatively damaged structures, thus preserving mitochondria function for longer.

Our results indicate a profound effect of autophagy on ROS generation. Under normoxic conditions, increased autophagy through rapamycin treatment induces a significant decrease in ROS (Fig. 6.17). In contrast, the inhibition of autophagy through 3MA treatment induces a significant increase in ROS (Fig. 6.17). These results are important, as they indicate the effect of autophagic activity on ROS generation in cells under normoxic conditions and normal metabolic performance. The cells have not been metabolically challenged through ischaemic injury, which in itself may result in a change in mitochondrial activity and ROS generation. However, when increasing or decreasing autophagy prior to the ischaemic insult, ROS increases significantly in both scenarios (Fig. 6.18-6.21).

How can these findings be explained? It is likely that mitochondria as crucial nexus in the generation of ROS and ATP in response to changing autophagic activity are responsible for the observed results. Firstly, as damaged or depolarized mitochondria are selectively eliminated through autophagy (Lemasters, 2005), a decrease in mitochondrial load is rapidly achieved, creating a role for autophagy in sequestering death-promoting molecules, protein aggregates and pro-apoptotic signals. Secondly, and possibly more important, autophagy may through substrate supply increase mitochondrial activity with a resultant increase in ROS.

We hypothesize that rapamycin treatment induces increased autophagic activity which, through substrate provision, results in increased mitochondrial activity. This effect combined with the ischaemic insult, translates into the increased ROS generation observed in both mild and moderate SI (Fig. 6.18, 6.20). However, although ROS increases even further with 3MA treatment followed by SI, the underlying mechanism is likely to be different. 3MA treatment results in decreased autophagic activity as seen in the control cells (Fig. 6.17). However, the ischaemic insult combined with the lost autophagic "ROS defense system" now translates into a robust increase in ROS generation (Fig. 6.18, 6.20).

Rapamycin renders cells more susceptible to the cytotoxic effect of tumour necrosis factor-α (TNF-α) (Djavaheri-Mergny *et al*., 2007), indicating autophagy as a primary response scheme to decrease ROS. Furthermore, both TNF-α and ROS cause an increase in beclin-1 expression (Djavaheri-Mergny *et al*., 2007). This is consistent with the observation that the protective effect of rapamycin is lost when inhibiting cytochrome c release (Menzies *et al.,* 2006). This mechanism of delaying apoptosis onset would provide a protective time-window in which the primary inducing stimulus could cease and the cell could more likely recover. Recently it has been shown that activation of autophagy by rapamycin suppresses LPS-mediated ROS production and protects myocytes against LPS toxicity, indicating that autophagy limits damaging ROS production (Yuan *et al.,* 2008).

In contrast, when using the inhibitor of autophagy, 3MA, ROS increases even more in SI (Fig. 6.18, 6.20), indicating the role of basal autophagy in sequestering oxidized and death-promoting molecules and protein aggregates. Moreover, the generation of ROS itself has been proposed to regulate autophagy (Huang & Brumell, 2009) and is in fact needed for the autophagic process to take place (Kaushik & Cuervo, 2006). An investigation of mitochondrial load/weight, their activity and oxygen consumption as well as the use of a mitochondria-specific ROS dye is proposed for future work.

7.3. *In vitro* onset dynamics – ATP availability

These results (Fig 6.22-6.24) indicate that the extent of autophagic activity influences cellular ATP availability. The exact mechanisms, however, remain to be elucidated. How can the difference in ATP between mild and severe ischaemia be explained? In mild SI, increased autophagosomes are present. We hypothesize that the increased autophagic flux results in an increased supply of metabolites. As the cells are dying apoptotically the demand for ATP drops, while the supply is increased. However, as ATP-consuming processes cease to function, less ATP is actually utilized. When increasing autophagy with rapamycin, prior to mild SI, the observed ATP surge disappears. This is associated with increased survival indicated by the TMRE results. The increased autophagic flux results in an increased supply of metabolites. However, as cells stay alive and ATP- consuming processes remain functional, ATP is now utilized, resulting in the loss of the ATP surge.

This hypothesis may also explain the results observed in moderate SI. Here, no ATP surge is observed after 2 hrs SI. Cells are dying primarily necrotically, however, with baseline levels of autophagy as there is no indication for increased autophagosomes. Hence, the supply in metabolites remains at baseline levels. As the cells are starting to die the demand for ATP drops, ATP-consuming processes cease to function, while the supply remains at basal levels. When increasing

autophagy with rapamycin prior to moderate SI, ATP levels remain constant. Similar to the scenario in mild SI the increased autophagic flux results in an increased supply of metabolites. However, as cells stay alive, indicated by the decrease in PI positive cells, ATP consuming processes remain functional. ATP is now utilized with the result that ATP levels remain constant.

Mutations in autophagy genes manifest with defects in mitochondrial maintenance, resulting in mitochondria with lower oxygen consumption rates, lower membrane potential and higher reactive oxygen species (ROS) levels (Zhang *et al*., 2007), indicating a vital relationship between autophagy and the cell's ATP-generating system. The intracellular ATP availability may be modulated by the autophagic flux, therefore favouring and promoting a cellular response other than necrosis and delaying apoptosis (Loos & Engelbrecht, 2009). It has been shown that the accumulation of autophagic vacuoles in the myocardium precedes apoptotic cell death (González-Polo *et al.*, 2005), and that the incidence of apoptotic cardiomyocytes is significantly increased at the borders of infarcted tissue (Takemura *et al*., 2006), indicating the metabolic gradient in that area. Both glucose deprivation and amino acid deprivation but not serum starvation, induce autophagy in cardiac myocytes (Matsui *et al*., 2007). Furthermore, ischaemia-induced autophagy may be mediated through the eukaryotic elongation factor-2 (eEF2) rather than via mTOR inhibition, leading to an inhibition of protein synthesis (Horman *et al*., 2003) which is most sensitive to energy supply.

In addition, to assess an autophagic response it may be necessary to consider the cell's own energetic profile and energy demand under control conditions to define its response to starvation. The cell's metabolic turnover may be a crucial factor in determining the context-dependent behaviour of autophagy (Cuervo *et al*., 2005, Bergmann, 2007) and may explain tissue-specific autophagic response kinetics. Autophagy is active at a basal level in most of the cells in the organism, although individual autophagic capacity may vary (Codongo & Meijer, 2005). An indirect indication of a causal link between the cell's metabolism and basal autophagy may be given through metabolically different - yet histologically identical - tissue types

which rely differentially on glycolysis and oxidative phosphorylation (Mizushima *et al*., 2004). A transgenic mouse model expressing green fluorescent protein-light chain 3 (GFP-LC3) revealed differential autophagic response kinetics which might indicate tissue-specific metabolic demands. Organs with a high degree of energy requirement such as the myocardium often show the highest rates of autophagy, which possibly reflects a continuous ATP demand (Mizushima *et al*., 2004). Mice lacking Atg5 which is part of the autophagy conjugation system, die during the neonatal period. $Atg5^{-/-}$ mice also show myocardial damage, have decreased amino acid levels and decreased cardiac ATP production (Levine & Yuan, 2005). As ATP production indicates the energy contribution of basal autophagy turn-over, this is of importance when describing autophagy kinetically. The baseline level of autophagy, the threshold which triggers additional autophagy, the time needed in doing so, as well as the flux through the autophagic pathway are likely to determine the degree of resistance to a given stress stimulus (Moore, 2008, Hamacher-Brady *et al*., 2006).

The above results indicate that mitochondria are a crucial nexus in the generation of ROS and ATP and deserve a closer investigation regarding differential cellular autophagic flux, particularly under conditions of increased metabolic stress.

7.4. Summary

In summary, our data provide as far as known a unprecedented direct evidence that increased autophagy delays the loss of cellular membrane integrity and delays caspase-3 activation as well as mitochondrial depolarization in ischaemic cardiomyocytes. Our results show a profound effect of increased autophagy on the onset of apoptosis as well as necrosis under simulated ischaemic conditions by providing cellular protection. The above results acquired through real-time imaging suggest that an increase in autophagic responsiveness and flux as induced through rapamycin treatment, provides a selective advantage for tissue against injury, possibly by maintaining intracellular ATP levels and nutrients and shifting

the PONR for apoptosis and necrosis to a later point (Fig. 7.1, 7.2). Our results also show that decreased autophagy may induce apoptosis earlier (Fig. 7.1, 7.2). Therefore a fast response to a decreasing intracellular ATP concentration with the induction of additional autophagy is crucial. In our model, intracellular ATP levels decrease with rapamycin treatment as well as with 3MA treatment. This leaves cells exposed to SI with seemingly less ATP. However, it is likely that increased autophagy provides metabolic substrates and a more favourable metabolic environment, which may be responsible for maintaining ATP-consuming processes for longer, hence maintaining membrane integrity and mitochondrial function. Our data therefore indicate that autophagic flux impacts the metabolic balance sheet of the heart.

7.5. *In vitro* model: shortcomings

A shortcoming of this model may lie in the fact that the inhibition of glycolysis with 2-deoxy-D-glucose which traps phosphate as 2-deoxy-D-glucose-phosphate, is an irreversible process. It functions as a phosphate binding agent therefore leads to the depletion of inorganic phosphate from the cells, creating a phosphate shortage, with the result that ATP and creatine phosphate levels decrease. The reperfusion phase in that particular case truly represents only a re-oxygenation phase, allowing mitochondrial respiration to proceed. Other models make use of iodoacetic acid (IAA) as an inhibitor of the glycolytic enzyme 3-phosphoglyceraldehyde dehydrogenase to achieve relatively specific but also irreversible inhibition of glycolysis (Corbett & Lees, 1997). Although this *in vitro* model is suitable to study the molecular mechanisms involved in the cell death process, the non-contracting nature of the cells demands careful interpretation of results compared to contracting isolated cardiomyocytes in terms of ATP demand and work performance. In the ischaemic myocardium, necrosis has been observed when ATP is depleted (Neely et al., 1973). However, our *in vitro* model indicated an increase in PI positive cells in moderate ischaemia, even when ATP levels are still high, indicating differences in metabolic conditions between the models. Moreover,

it appears that multiple viability tests may be of particular importance in the *in vitro* setting. TTC staining after 2 or more hours of reperfusion agrees very closely with infarct size measured 3-4 days later, indicating a short period of dynamic behavior only during the actual time of injury development. For future experiments, it is advised to employ a range of autophagy inhibitors in order to increase specificity of autophagy inhibition. Bafilomycin A1 as well as 3MA, although commonly used to inhibit autophagy (Maruyama *et al.,* 2008), are not very specific. 3MA may in fact also be used as a substrate by the cell. Better inhibitors of autophagy are siRNAs against genes required for autophagy, such as beclin-1, Atg5, and Atg7 (Quadir *et al*., 2008).

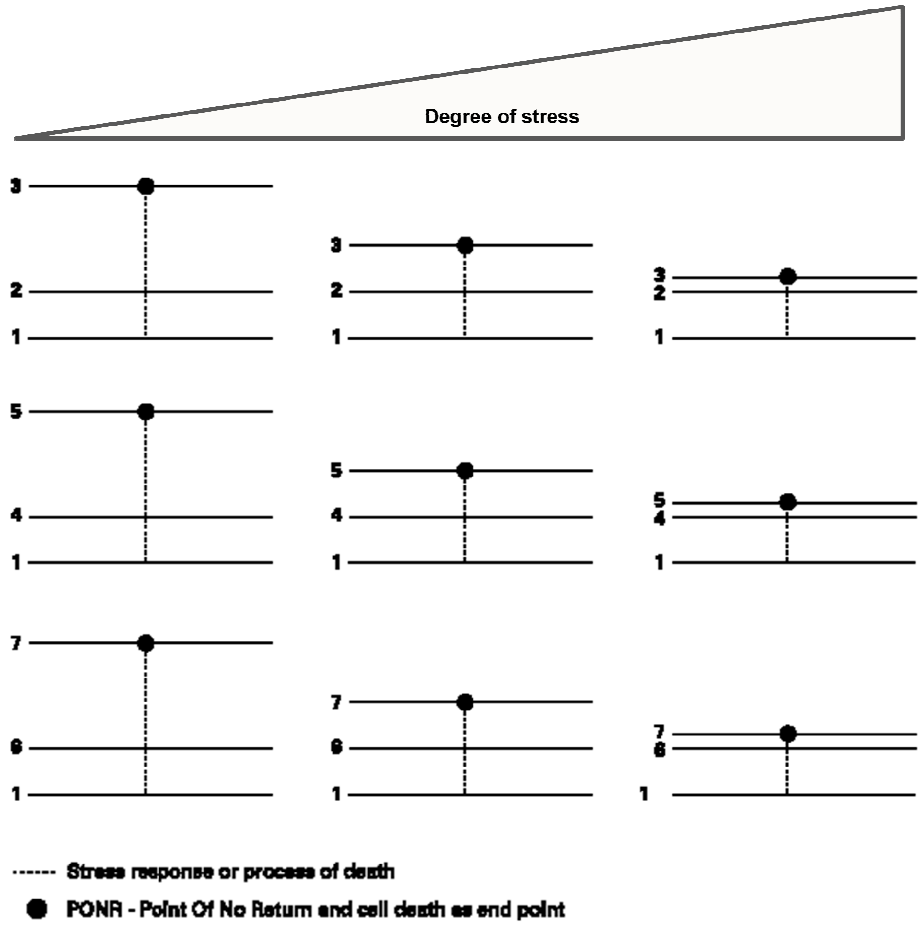

Figure 7.1: Relationship between the severity of the insult and the induction, execution of cell death: With increasing degree of a stressful insult, but a steady autophagic flux, cell death is reached earlier, the z-distance between 2 and 3, 4 and 5 as well as 6 and 7 decreases. 'autophagy baseline' 1, 'autophagy induced' 2, 'cell death with autophagy' 3, 'apoptosis induced' 4, 'apoptosis executed' 5, 'necrosis induced' 6 and 'necrosis executed' 7. The z-distance between the micrographs may indicate the process (induction) and endpoint (execution) of dying, separated by the point-of-no-return, PONR. The degree of stress may determine the position of the PONR.

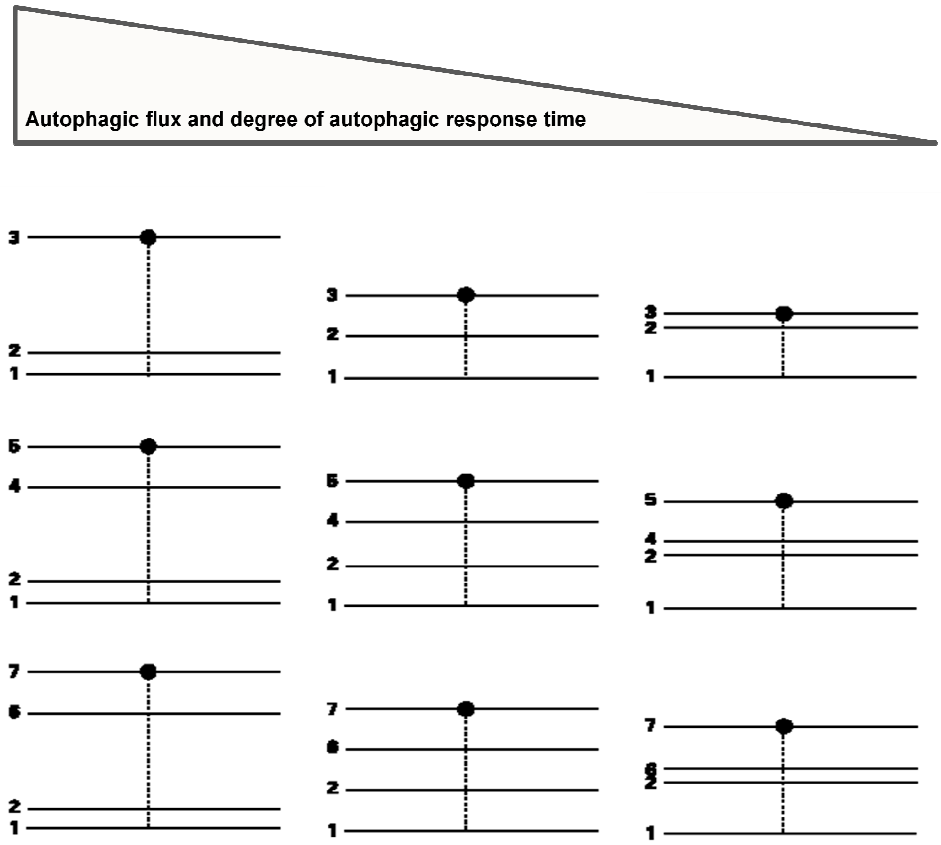

Figure 7.2: Relationship between autophagic flux, autophagic response time (time required to induce additional autophagy) and the induction/execution of cell death: With decreasing autophagic flux and more time needed to induce additional autophagy, cell death is reached earlier, the z-distance between 2 and 3, 2 and 5 as well as 2 and 7 decreases. Vice versa, with increasing autophagic flux and less time needed to induce additional autophagy, cell death is reached later, the z-distance between 2 and 3, 2 and 5 as well as 2 and 7 increases. 'autophagy baseline' 1, 'autophagy induced' 2, 'cell death with autophagy' 3, 'apoptosis induced' 4, 'apoptosis executed' 5, 'necrosis induced' 6 and 'necrosis executed' 7. The z-distance between the micrographs may indicate the process (induction) and endpoint (execution) of dying, separated by the point-of-no-return, PONR. The degree of stress and autophagic flux may determine the position of the PONR.

CHAPTER 8 RESULTS: FUNCTIONAL RECOVERY

8.1. Functional recovery: three durations of ischaemia

In order to assess the effect of the severity of an ischaemic insult on myocardial function, hearts were subjected to 10, 20 or 30 min of sustained ischaemia (normothermic total global ischaemia) followed by reperfusion (Fig. 8.1).

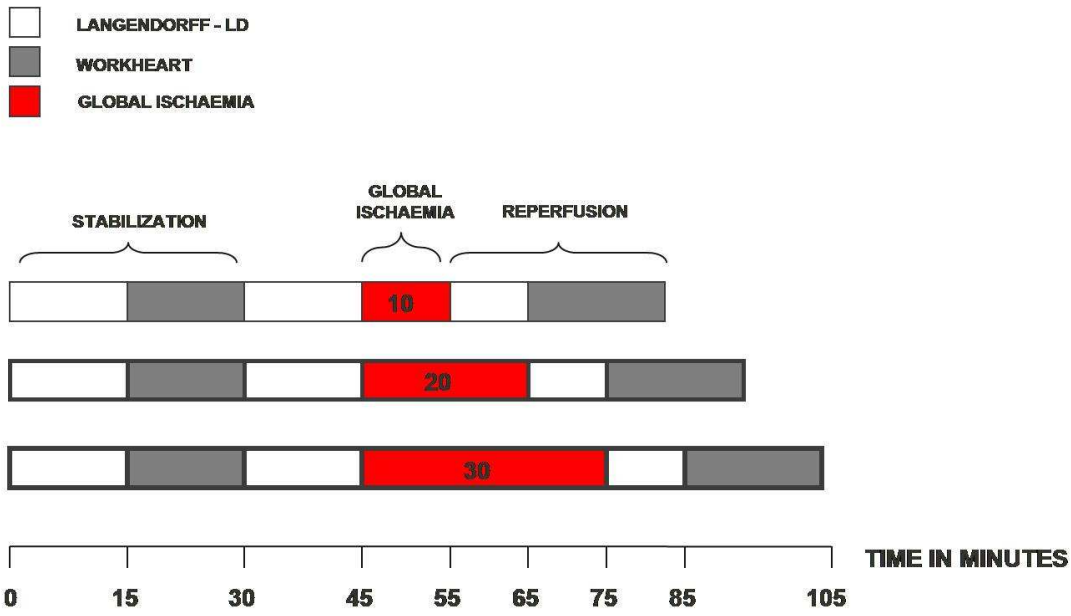

Figure 8.1: ***In vivo*** **experimental protocol. Hearts were submitted to a protocol of 10, 20 or 30 min global ischaemia, followed by 30 min of reperfusion respectively.**

A significant decrease in myocardial function compared to control values assessed by cardiac output, stroke volume and mean external power is described. Ten min of global ischaemia induced a significant decrease in cardiac output [42.4 ml/min±4.5 ($p<0.05$)] compared to control values (62.1 ml/min±4.3), which further decreased significantly after 20 min of global ischaemia (10.6 ml/min±1.4) (Fig. 8.2). These results were mirrored when measuring stroke volume (Fig. 8.3) and mean external power produced by the left ventricle (Fig. 8.4). Hearts subjected to 30 min of sustained ischaemia were unable to recover (Fig. 8.2, 8.3, 8.4).

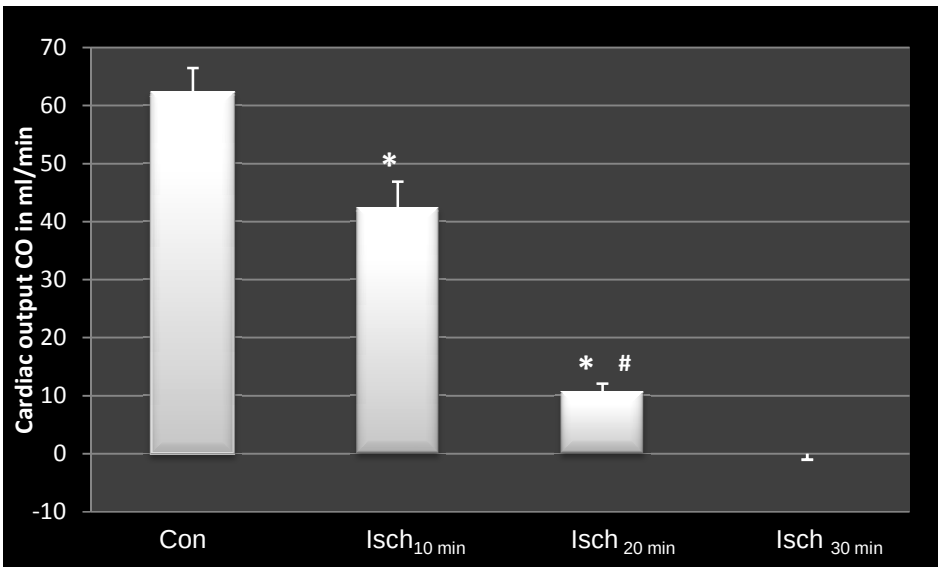

Figure 8.2: Cardiac output CO in ml/min (CO=Coronary (Qe) + aortic (Qa) flow rates). Data expressed as mean ± SEM, statistical analysis: ANOVA & Bonferroni correction, * $p<0.05$ vs Con, $^{\#}$ $p<0.05$ vs SI $_{10\ min}$, n=6.

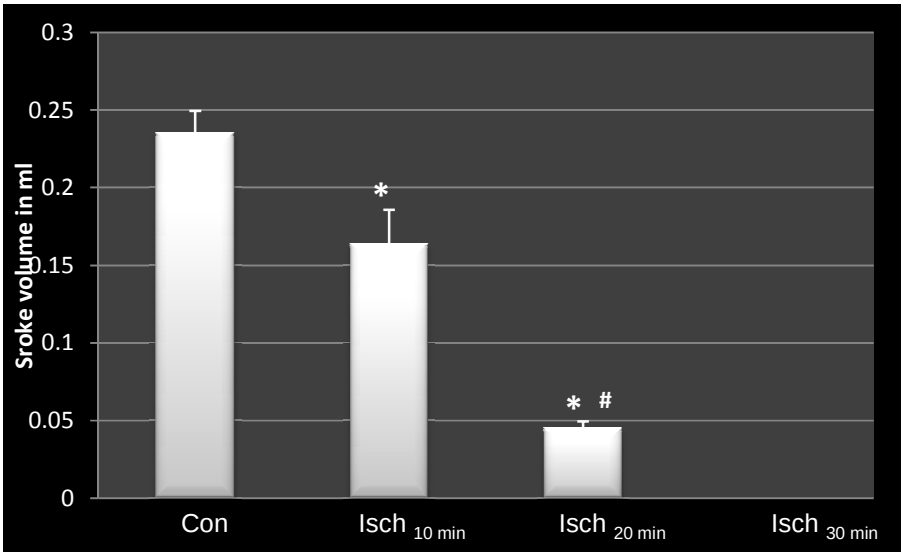

Figure 8.3: Stroke volume in ml (SV=CO/heart rate). Data expressed as mean ± SEM, statistical analysis: ANOVA & Bonferroni correction, * p<0.05 vs Con, # p<0.05 vs SI $_{10\ min}$, n=6.

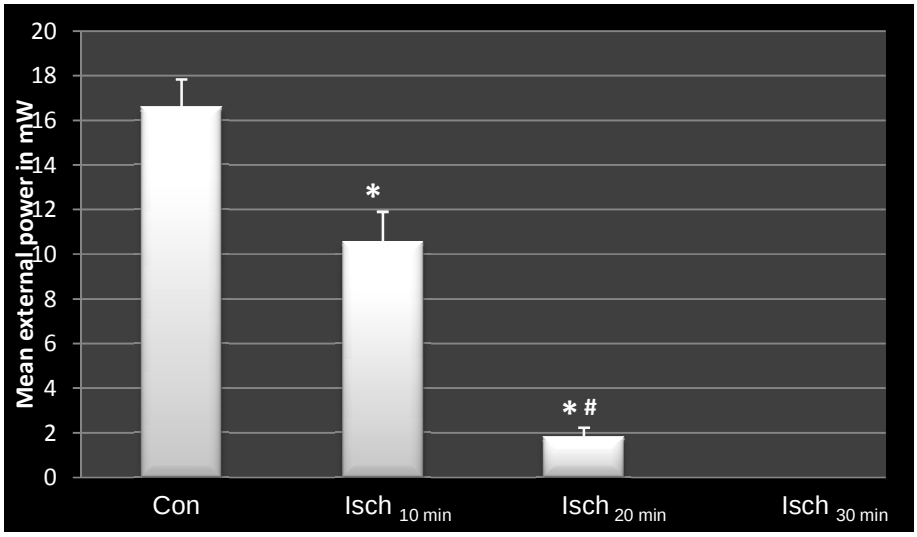

Figure 8.4: Mean external power produced by the left ventricle TW [Tw = 0.002222 (Aortic pressure PAO-11.25)(Cardiac output CO)]. Data expressed as mean ± SEM, statistical analysis: ANOVA & Bonferroni correction, * p<0.05 vs Con, # p<0.05 vs SI $_{10\ min}$, n=6.

8.2. Functional recovery: Rapamycin and 3MA treatment

However, when hearts were stabilized and then perfused with 1 nM rapamycin for 10 min in working heart mode, followed by 40 min retrograde perfusion in the Langendorff mode followed by their subjection to 20 min sustained ischaemia (Fig. 8.5), cardiac output significantly improved [12.5 ml/min±2.3 ($p<0.05$)] compared to 20 min global ischaemia (0.6 ml/min±0.5). In contrast, 3MA treatment did not improve functional recovery (6.1 ml/min±2.5) (Fig. 8.6). These results were mirrored when measuring mean external power produced by the left ventricle (Fig. 8.7).

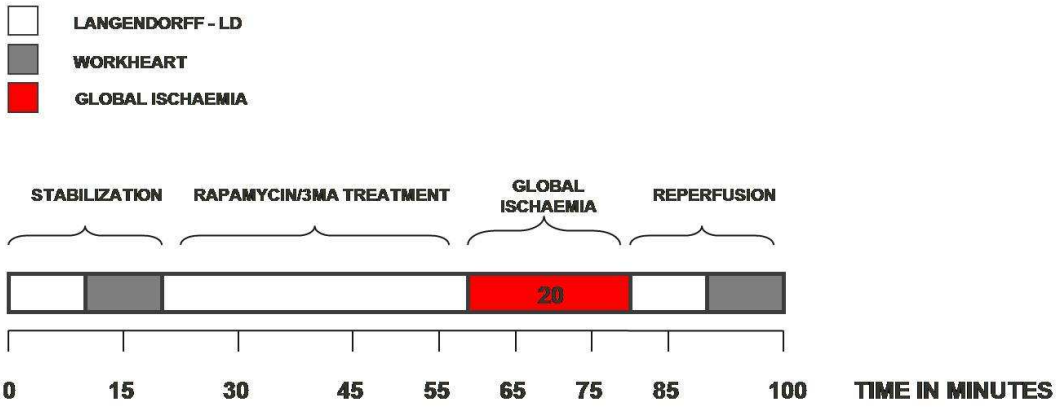

Figure 8.5: *In vivo* experimental protocol of global ischaemia with induced and inhibited autophagic activity. Following perfusion with rapamycin or 3MA, hearts were submitted to a protocol of 20 min global ischaemia, followed by 30 min reperfusion.

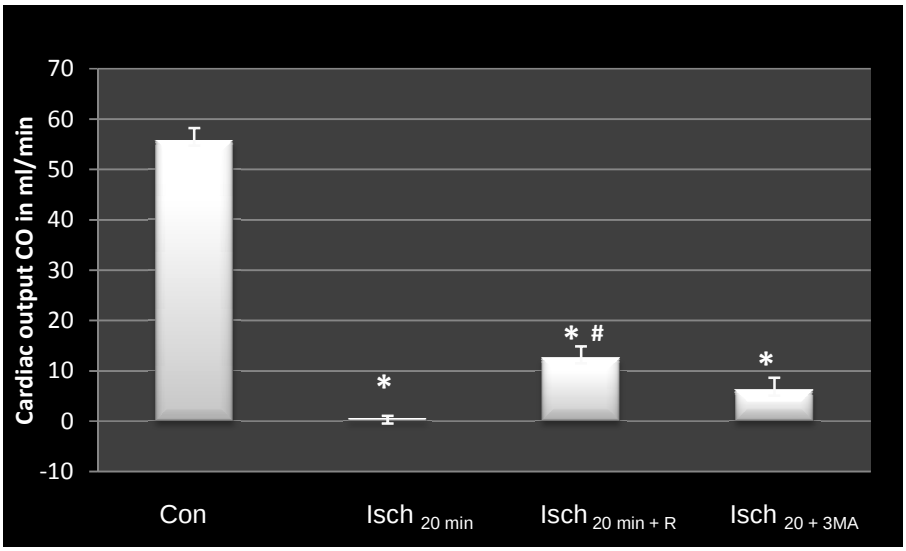

Figure 8.6: Cardiac output CO in ml/min (CO=Coronary (Qe) + aortic (Qa) flow rates). Data expressed as mean ± SEM, statistical analysis: ANOVA & Bonferroni correction, * p<0.05 vs Con, # p<0.05 vs SI $_{20\ min}$, n=8.

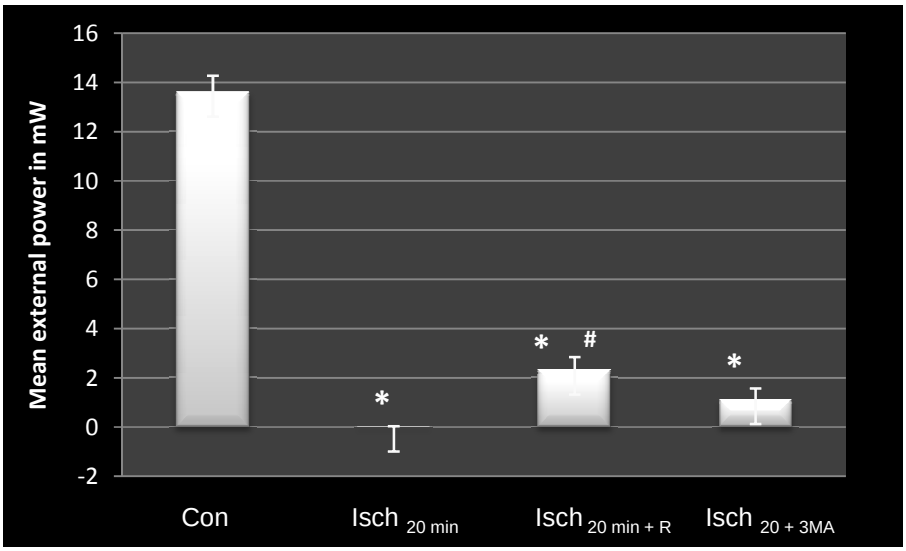

Figure 8.7: Mean external power produced by the left ventricle TW [Tw = 0.002222 (Aortic pressure PAO-11.25)(Cardiac output CO)]. Data expressed as mean ± SEM, statistical analysis: ANOVA & Bonferroni correction, * p<0.05 vs Con, # p<0.05 vs SI $_{20\ min}$, n=8.

CHAPTER 9 DISCUSSION FUNCTIONAL RECOVERY

9.1. *Ex vivo* model: functional recovery

The aim of this part of the study is to determine whether the protective effects observed in the *in vitro* model of simulated ischaemia are also evident in the perfused heart model. A standard laboratory model of severe total ischaemia (Opie, 1991) has been chosen, where the effect of three different time points on the dynamic character of ischaemic injury development and functional performance was assessed. Hearts were subjected to sustained ischaemia (normothermic total global ischaemia) by simultaneous clamping of both aorta and left atrial supply tubes. This perfusion model of global ischaemia has been shown to result in total anoxia within 20 seconds (Opie, 1991).

Our results are in agreement with the current literature; it is to the best of our knowledge, however novel, that functional recovery improves upon rapamycin treatment specifically in a rat heart model of global ischaemia, using rapamycin in the perfusate. Rapamycin, an antibiotic derived from *Streptomyces hygrosopius,* binds to mTOR and attenuates protein synthesis whilst inducing autophagy. It has been used for many years as an immunosuppressant in the treatment of organ rejection (Khan *et al*., 2006). The inhibition of mTOR in the cardiovascular arena has been shown to be effective as it reduces coronary artery re-stenosis when impregnating stents with rapamycin (Khan *et al*., 2006). In the mouse heart, rapamycin has also shown to confer to preconditioning-like protection against ischaemic injury, when injected intraperitoneal prior to heart excision, with a decrease in TUNEL and trypan blue positive cells (Khan *et al*., 2006), indicating a beneficial effect when autophagy is pharmacologically upregulated. Moreover, mTOR inhibition has recently been shown to substantially regress left ventricular hypertrophy (McMullen *et al*., 2004). It also preserved left ventricular fractional shortening and decreased collagen deposition significantly (Gao *et al*., 2006). The importance of mTOR in governing cardiac growth and controlling the homeostasis

of protein synthesis and autophagy has been shown in a transgenic mouse model, where mTOR kinase activity was knocked out. In these mice myocardial function was impaired through reduced ejection fraction and shortening (Shen *et al*., 2008). This may indicate a role for autophagy in the onset and progression of heart failure, particularly in the phase of cardiac hypertrophy, preventing or delaying its commencement and slowing down its progression.

9.2. Summary

The *ex vivo* results indicate that myocardial function rapidly declines during global ischaemia and that rapamycin treatment improves functional recovery significantly. It remains to be elucidated whether increased autophagy in the heart improves myocardial energetics, which translates into improved functional recovery. Current literature seems to indicate that this may likely be the case. Under normal conditions glucose, lactate and fatty acids are the main energy substrates maintaining cardiac function (Kantor *et al*., 2000, Ashrafian *et al*., 2007). The adult heart derives 60-90% of its energy from fatty acid metabolism and 10-40% through glycolysis (Kodde *et al*., 2007). Oxygen availability is fundamental, as >90% of cardiac ATP production is generated through oxidative phosphorylation (Kodde *et al*., 2007) via the reducing equivalents NADH and $FADH_2$ produced in the tricarboxylic acid (TCA) cycle. In addition, however, a growing body of evidence strongly suggests another fundamental level of substrate interregulation. Proteomics of the oxygenated myocardium reveals that 11% of the identified proteins are involved in electron transport, 11% in carbohydrate metabolism and 10% in protein metabolism (Lam *et al*., 2007), indicating an almost equal distribution between the metabolic control of carbohydrate and protein breakdown. Proteins make up about one sixth of the wet mass of the heart (Gevers, 1984). As cardiac proteolysis is a fast responding and complete degradation mechanism, amino acids for utilization can be generated rapidly (Gevers, 1984), suggesting a profound role in cardiac protein turnover. These findings support the view that autophagy contributes to the metabolic balance sheet of the heart and highlight the

relevance of autophagic processes when ATP becomes limited. We propose that autophagically-generated amino acids and substrate intermediates form an integral and possibly underestimated part of substrate interregulation to control the efficiency of ATP production in the heart (Fig. 9.1).

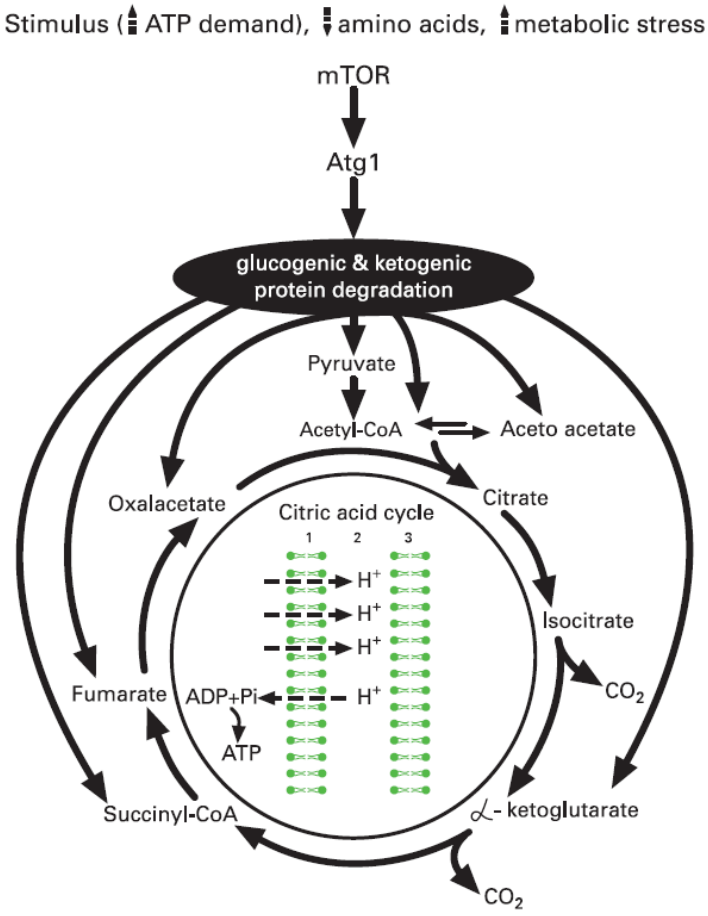

Figure 9.1: Relationship between increased autophagy and amino acid generation. An increase in autophagic flux, mediated through decreased nutrients, increased metabolic stress and increased ATP demand could rapidly generate amino acids as alternative fuels. They may be converted into pyruvate or TCA cycle intermediates (glucogenic amino acids) or acetyl and acetoacetyl-CoA (ketogenic amino acids) and have multiple entrypoints into the TCA cycle.

Chronic or less severe conditions of the heart such as mild ischaemia, hypoxia, hypobaric stress or dietary restriction may have a differential effect on autophagy and metabolic substrate availability, as they provide a larger timewindow for the autophagic machinery to be induced. Such conditions in turn, may provide insights into the dynamics of autophagy regulation. Most interestingly, in the chronically ischaemic myocardium a proteomics approach revealed an increased expression of beclin-1, LC3 (microtubule-associated protein 1 light chain 3) and cathepsin D (Yan *et al*., 2005), indicating an increased flux through the autophagic pathway. In that way deleterious effects of chronic ischaemia may be limited, as the metabolic environment becomes more beneficial. It has been suggested that an upregulation of autophagy may be part of a “smart heart” response where myocardial function and metabolism adjust in response to ischaemia (Yan *et al*., 2005). Also, myocardial amino acid metabolism is markedly influenced by exposure to hypoxia, indicating an adaptation with alterations in substrate utilization (Rumsey *et al*., 1999). For example, hypoxia has shown to decrease the total amount of cytosolic free amino acids in the heart, particularly arginine and glutamine (Gabrys *et al*., 2003) and to enhance the capacity for glucose phosphorylation (Rumsey *et al*., 1999). Interestingly, the immature heart, which relies more on glucose as substrate compared to the adult myocardium, also showed much higher resting concentrations of amino acids, which are depleted during acute hypoxia (Caputo, 2006). During mild myocardial ischaemia, glycolysis is accelerated due to the decreased capacity of mitochondrial ATP supply. In this period, where glycolysis and glucose oxidation are not uncoupled yet, autophagy might function as an ally supporting glucose oxidation via TCA cycle intermediates. The multiple substrate entrypoints of the TCA cycle intermediates might provide a fast metabolic response (Fig. 9.1).

In summary, autophagy may counteract the detrimental effects of fatty acid oxidation, as it “partners” with glucose oxidation, keeping the TCA cycle flux high. Treatment with partial fatty acid oxidation inhibitors (pFOXi) (e.g. Trimetazidine) combined with AMPK-mediated and mTOR-mediated autophagy using rapamycin,

might maximize glucose oxidation and delay the deleterious uncoupling of glycolysis from glucose oxidation (Lam & Lopaschuk, 2007). Rapamycin induces a rapid increase in autophagosomes which, after fusion with lysosomes may release their degraded content and thus provide additional fuel to be oxidized in the mitochondria. These data indicate that autophagy may be metabolically more potent in a setting which is less severe. We suggest future work to indicate the role of autophagy in myocardial energy homeostasis. This may include the use of a GFP-LC3 transgenic mouse model (Mizushima *et al*., 2004), which would allow to visualize whether areas of increased autophagic activity may exist in the metabolically-challenged myocardium in a similar manner as microzones of discrete heterogeneous areas of anoxic tissue, which have been visualized through NADH fluorescence (Steenbergen *et al*., 1979).

CHAPTER 10 SUMMARY AND CONCLUSIONS

10.1. Is autophagy beneficial or detrimental? A model is proposed

It has been suggested that autophagy plays a dual role in the heart where it can protect against or contribute to cell death, depending on the stimulus (Gustafsson *et al*., 2008). However, the cell's metabolic demands and substrate profile may be crucial in determining this context-dependent behaviour of autophagy. Therefore, we propose a conceptual model which considers the role of autophagy in energy homeostasis (Loos & Engelbrecht, 2009). According to this model, the extracellular (A) and intracellular (B) environment will determine whether autophagy leads to an adaptive and protective response (C_P) or whether bioenergetic failure and autophagic cell death (C_F) is the manifestation of a response unable to meet the metabolic demands of the cardiac myocyte (Fig. 10.1). This model indicates autophagy as a highly dynamic stress response where A (the severity and duration of an ischaemic insult) and B (the autophagic baseline flux, autophagic response time, the substrate utilization profile and the metabolic capacity at the insult onset) determine its outcome. A and B may then define the timewindow for and the efficiency and outcome of a given autophagic response according to $\downarrow A+\uparrow B\rightarrow C_P$ and $\uparrow A+\downarrow B\rightarrow C_F$. This dynamic approach may predict the likelihood of cell death with autophagy or cell survival, based on the cell's metabolic demands and substrate profile, and may explain the context-dependent behaviour of autophagy. It also indicates that a metabolic perspective on the position of autophagy in the heart is crucial to further reveal its significance in the context of the onset of myocardial apoptosis and necrosis. If this model is valid, then A and B show a differential profile during detrimental energetic perturbations such as myocardial ischaemia and heart failure and hence define the functional role of autophagy in these conditions.

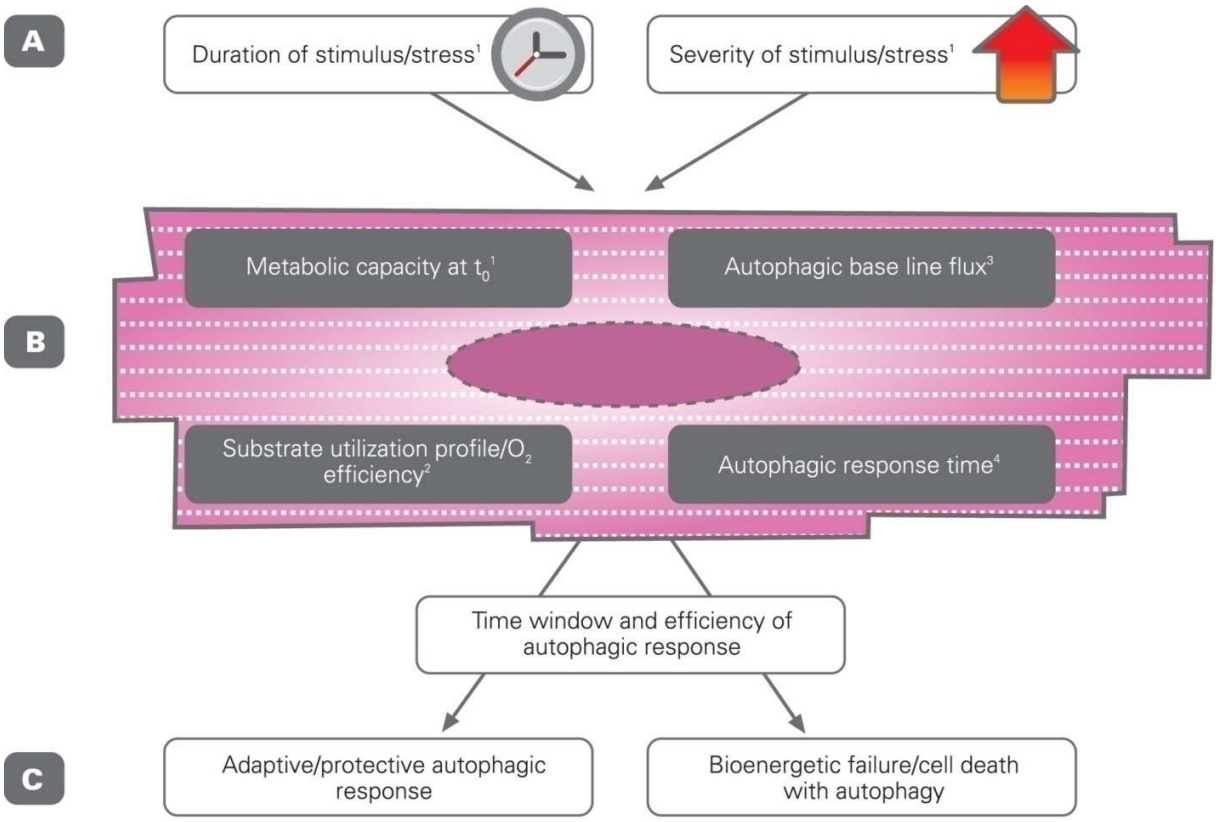

Figure 10.1: Proposed conceptual model defining the functional role of autophagy in cardiomyocytes. The extracellular (A) and intracellular (B) environment may determine whether autophagy leads to an adaptive and protective response (C_P) or whether bioenergetic failure and autophagic cell death (C_F) will manifest. A (severity and duration of an ischaemic insult) and B (autophagic baseline flux, autophagic response time, substrate utilization profile and metabolic capacity at the insult onset) determine its outcome according to: ↓A+↑B→ C_P and ↑A+↓B→ C_F.

10.2. Final Conclusions

This study of myocardial injury highlights a number of important aspects.

Firstly, it becomes clear that the metabolic microenvironment of the cell has an influence on the distribution of the manifestations of cell death. It was hypothesized that the relative contribution of cell death with autophagy, apoptosis and necrosis is dependent on the duration and severity of the ischaemic insult and is governed by the cell's underlying metabolic capacity at a given point in time. Since our results indicate that this is the case, the hypothesis is verified. In our model a mild ischaemic insult leads to the induction of autophagy and apoptosis, whilst a moderate and severe insult primarily induces necrosis without aspects of autophagy.

Secondly, it was hypothesized that the onset of apoptosis and necrosis depends on the cell's autophagic activity prior to the ischaemic event due to an impact of autophagy on the cell's metabolic capacity. Our results strongly indicate that this is the case, thus verifying the hypothesis and further substantiating the concomitant analysis of autophagy, apoptosis and necrosis. Upregulation of autophagy prior to an ischaemic insult delays cleavage of caspase-3, loss of mitochondrial depolarization and loss of membrane integrity, hence the onset of apoptosis and necrosis. Our results indeed clarify that autophagic activity plays a fundamental role in influencing the onset of apoptosis and necrosis and delaying their onset significantly when upregulated (Fig. 7.1). The obtained results show that rapamycin treatment is protective in the cellular model and improves functional recovery after global ischaemia in the perfused rat heart model.

Lastly, these results indicate the significance of monitoring autophagy, apoptosis and necrosis concomitantly, in order to assess the viability of the myocardium. The use of multiple techniques is essential to place the metabolic performance into context with cell death morphological features. It remains to be elucidated which

exact mechanisms are underlying the observed impact of autophagy on apoptosis and necrosis. Our results indicate that the mitochondria as nexus between ROS and ATP generation play a pivotal part in the mechanism by which increased autophagy confers cytoprotection.

In summary, our results strongly indicate that autophagy may rather be seen as a stress response of the cell, aimed at maintaining energy homeostasis in order to fuel ATP- consuming processes, which are vital for maintaining cellular function. Based on the obtained results it appears unlikely that autophagy is a mode of cell death *per se* in the myocardium. It becomes clear that it may be highly beneficial if the onset of apoptosis and necrosis as well as a change in autophagic activity be studied dynamically. This will allow the study of the exact time of the onset of apoptosis and necrosis in context with the exact intra and extracellular metabolic parameters present. Such an approach may prove beneficial in order to assess the potential reversibility of cell death.

A dynamic approach may allow opportunities for new treatment strategies, focussed on delaying the onset of each death mode rather than inhibiting it, by controlling the cell's inherent autophagic machinery. Such strategies may be based on combined therapy, targeting autophagic as well as apoptotic pathways (McMullen *et al*., 2004). This may have particular implications for the treatment of terminal differentiated cells during brain (Amaravadi *et al*., 2007) or myocardial injury (Ravikumar *et al*., 2006, Camarata *et al*., 1994) which ranks among the primary causes of morbidity and mortality (Artal-Sanz & Tavernarakis, 2005).

10.3. Future Prospects

Despite the therapeutic advances in reducing cardiovascular-derived morbidity and mortality through optimizing myocardial metabolic disturbances, little attention has been paid to the role of autophagy and autophagically-derived amino acids in the diseased myocardium. However, literature indicates that autophagy affects

myocardial repair function in response to injury and influences cell death dynamics (Loos & Engelbrecht, 2009). A severe decrease in substrate availability and an increase in ATP demand translate into AMPK activation and mTOR inhibition which induces the autophagic machinery to respond rapidly (Meijer *et al*., 2004) and reducing protein synthesis concomitantly. Due to the dynamic nature of autophagy, it is suggested to not only re-consider the concepts of temporal and spatial border zones in the diseased myocardium (Hearse *et al*., 1981) but also to extend the dynamic role of autophagy in the gradual progression of metabolism and injury, into the setting of myocardial hypertrophy and heart failure. This approach may concentrate on the temporal correlation of ATP depletion and autophagic activity in myocardial regions of "tolerable", "critical" and "lethal" ischaemia (Hearse *et al*., 1983) as well as the association of autophagic flux, metabolic parameters (Loos & Engelbrecht, 2009) and myocardial hypertrophy. The wavefront phenomenon and concept of irreversible injury (Reimer & Jennings, 1979) may be related to the PONR and onset dynamics described in this study. A modernized tissue sampling device which enables the collection of multiple tissue samples across the area of injury [and which has been employed for a short period in the past (Hearse *et al*., 1981)], may be useful to answer those urgent questions and to co-localize the degree of myocardial energy deficiency or hypertrophy with autophagic activity and cell death kinetic parameters (Loos & Engelbrecht, 2009). More studies are urgently needed to unravel the ATP changes observed in mild and moderate SI with rapamycin and 3MA treatment and to understand the underlying mechanism thereof. It becomes very clear that the study and control of autophagic flux is of the utmost importance for understanding its exact role in steering cellular energy homeostasis and in influencing cell death onset. The appearance of autophagic vacuolization, as indicated by the LC3 pattern, is not in itself evidence that autophagic flux is elevated. We believe that those studies have to focus on autophagic flux control and the ATP charge ratio within a supply/demand system (Wieser & Krumschnabel, 2001, Buttgereit & Brand, 1995) in order to unmask the changes observed in ATP as well as ROS generation.

The outcome of differential amino acid oxidation rates at increasing levels of autophagy as well as the substrate turnover time for each amino acid (turnover time a = [intermediate a]/TCA cycle flux) may indicate flux and duration of autophagy. Such differential investigation may reveal the ATP yield per amino acid molecule and carbon atom and expose the effect of increased autophagy on pyruvate/acetate oxidation. Current treatment regimens may be complemented with the aid of caloric restriction diet (Hannigan *et al*., 2009, Bursch *et al*., 2008) or rapamycin treatment (Ravikumar *et al*., 2006, Menzies *et al*., 2006, Halapas *et al*., 2008) to delineate whether the control of myocardial autophagy can become part of therapeutic strategies to manage cardiac energetics. In managing cellular energy homeostasis for the benefit of survival, autophagy may serve as key regulator to unlock interventions through metabolic-based therapy. Most crucially, this present study indicates that the role of autophagic flux in delaying the onset of cell death through the modification of cellular metabolic performance and possibly substrate availability and preference, deserves more study.

Acknowledgements

We would like to thank Dr Tamotsu Yoshimori and Dr Tavaré for providing the GFP-LC3 and CFP-DEVD-YFP constructs.

ADDENDUM

Dose response trials before start of study

Characterization of H9c-2 cell viability-time points using ischaemic buffer without 2DG, pH 6.2.

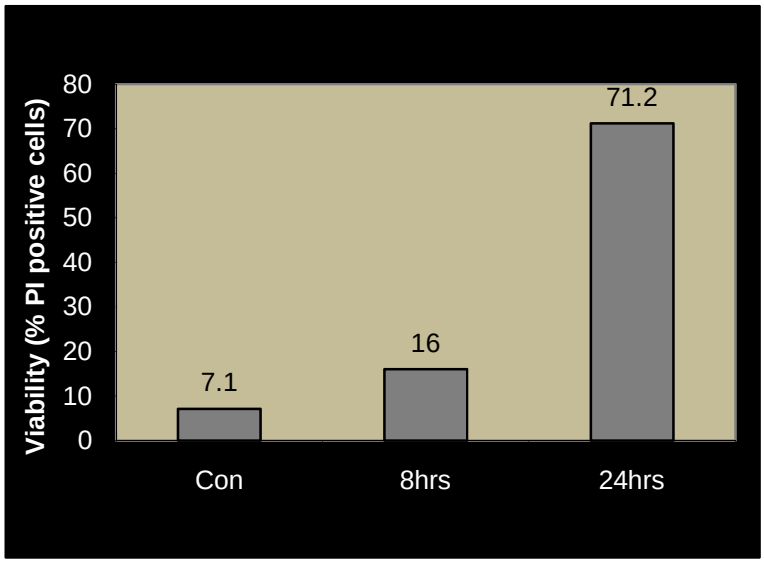

Figure A.1: Minor response after 8 hrs. The use of ischaemic buffer with 2DG, pH 6.4 is suggested.

Using ischaemic buffer with 2DG, pH 6.4 as well as 0.5 or 1.0 mM (Lin, 2004, Seyedi 2002) sodium dithionate.

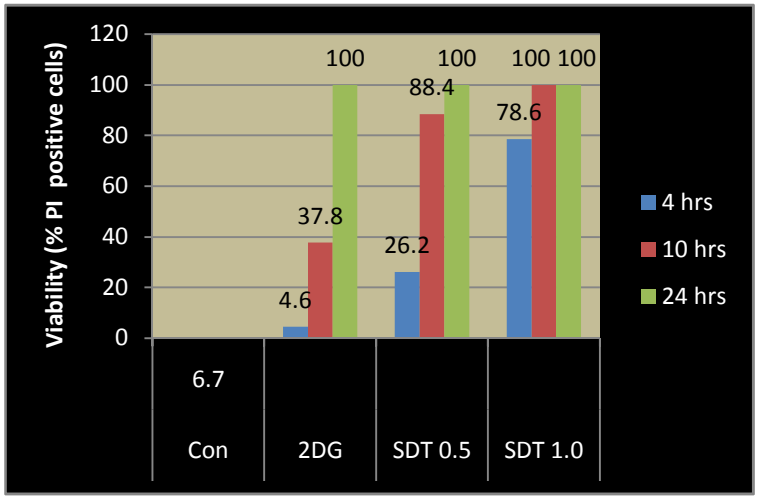

Figure A.2: Ischaemic buffer+2DG is suitable as it results in 37.8 % non viable cells after 10 hrs SI. 0.5 mM SDT more suitable than 1 mM SDT as it results in 88.4 % non viable cells after 10 hrs SI. But less than 10 hrs as longest time point SI is required. The time points 2, 4 and 8 hrs are suggested.

Although literature suggests a frame of reference regarding the concentration of rapamycin to be used in H9c-2 cells, we verified this in our system. To evaluate the induction of autophagy, a dose response with 25 nM, 50 nM and 100 nM rapamycin for 1 hr and 24 hrs was conducted, and assessed by fluorescence microscopy and flow cytometry.

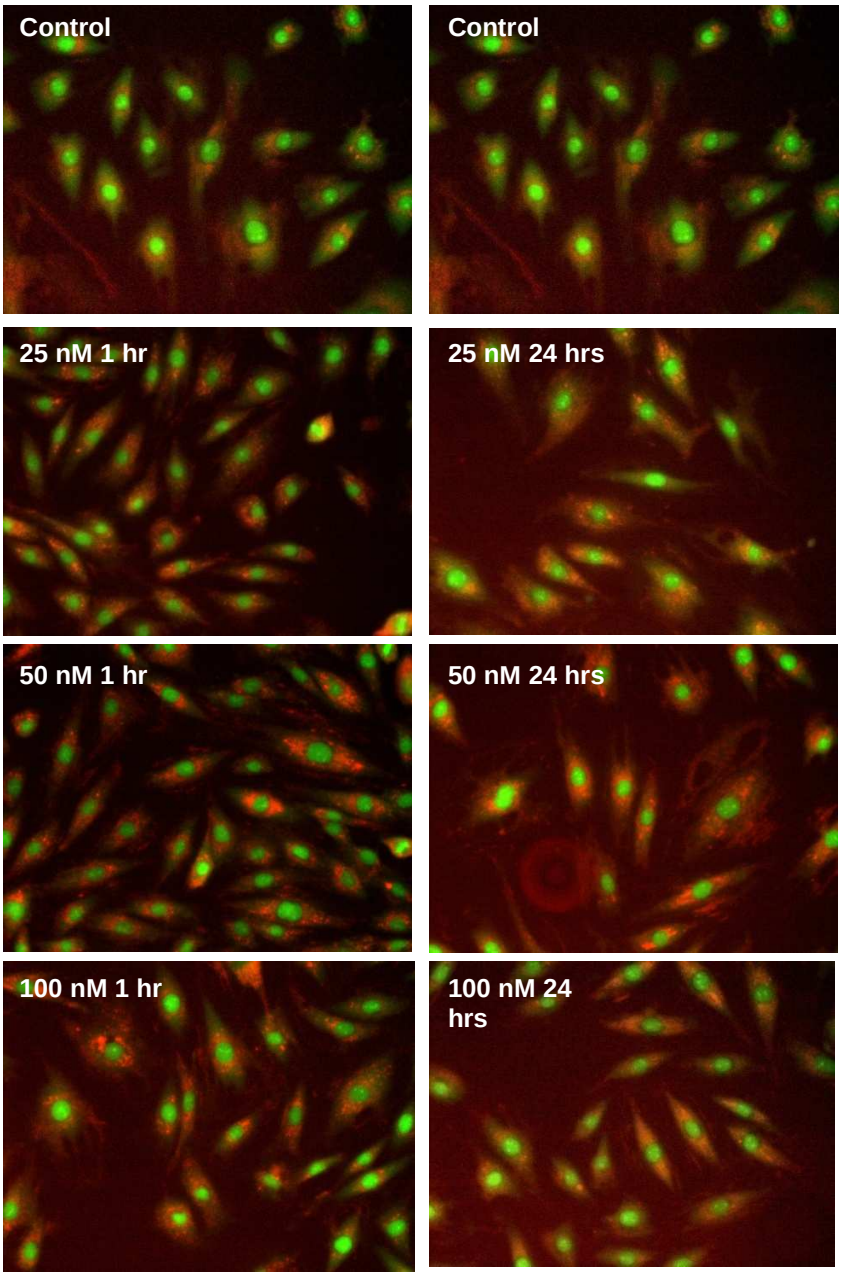

Figure A.3: Images showing acridine orange (AO) signal. AO signal appears stronger already following 1 hr treatment.

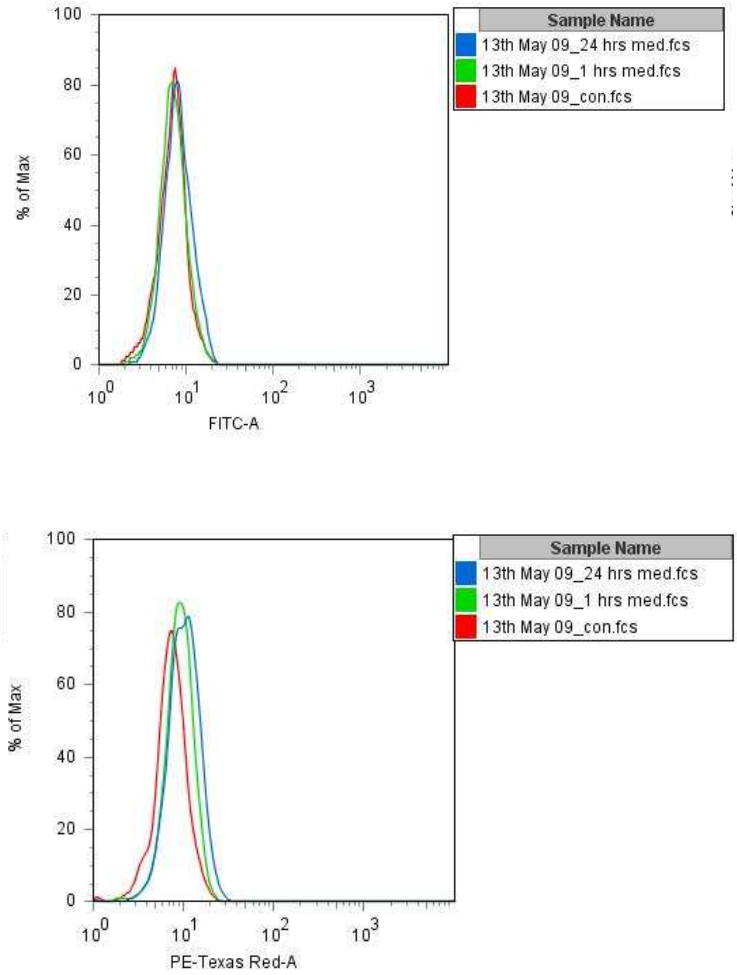

Figure A.4: A clear response can be seen based on the right-shift of the intensity histogram in the red channel (PE-Texas Red), indicating an increase in acidic vesicular organelles (AVO's) suggesting an increase in autophagic activity. Red: Control, Green: 1 hr rapamycin treatment, Blue: 24 hrs rapamycin treatment. The 24 hr time point with 50nM rapamycin were therefore chosen to be employed in the second part of the study.

Ischaemic buffer without 2DG or SDT

The effect of the ischemic buffer without 2DG or SDT was investigated at the 2 hr SI time point.

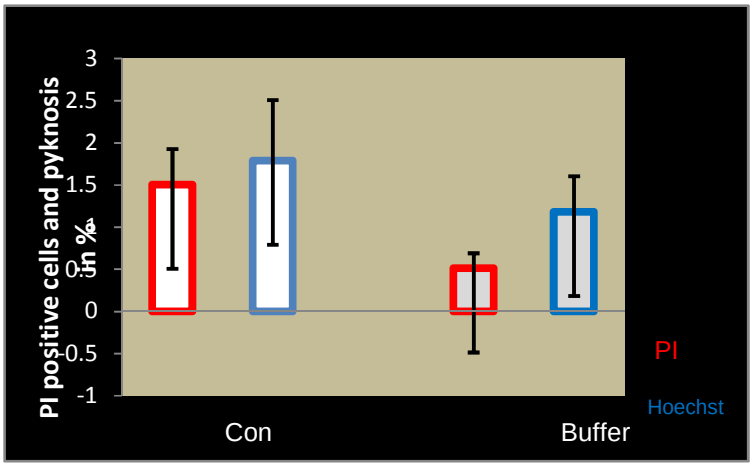

Figure A.5: 2 hrs SI Data expressed as mean ± SEM, statistical analysis: ANOVA & Bonferroni correction,* p<0.05 vs Con, n=9, >150 cells counted.

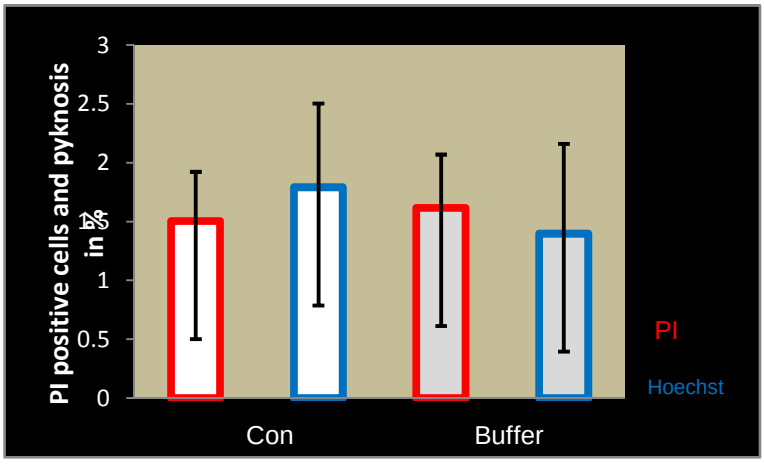

Figure A.6: 2 hrs SI/R Data expressed as mean ± SEM, statistical analysis: ANOVA & Bonferroni correction,* p<0.05 vs Con, n=9, >150 cells counted.

The above results indicate no significant effect of the buffer without 2DG or SDT on % PI positive cells or % pyknotic cells following 2 hrs SI (Hoechst: Con: 1.7%±0.7%; Buffer: 1.1%±0.4%, PI: Con: 1.5%±0.4%; Buffer: 0.5%±0.1%) followed by 1 hrs reperfusion (Hoechst: Con: 1.7%±0.7%; Buffer: 1.3%±0.7%, PI: Con: 1.5%±0.4%; Buffer: 1.6%±0.4%).

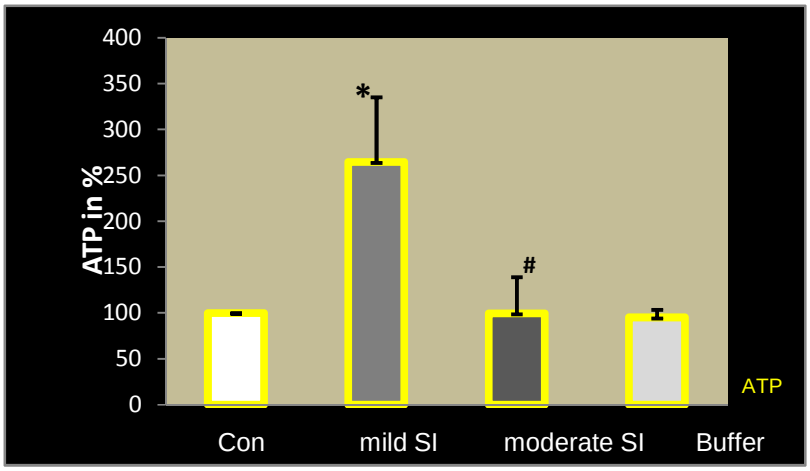

Figure A.7: 2 hrs Data expressed as mean ± SEM, statistical analysis: ANOVA & Bonferroni correction, * p<0.05 vs Con, # p<0.05 vs mild SI, n=8.

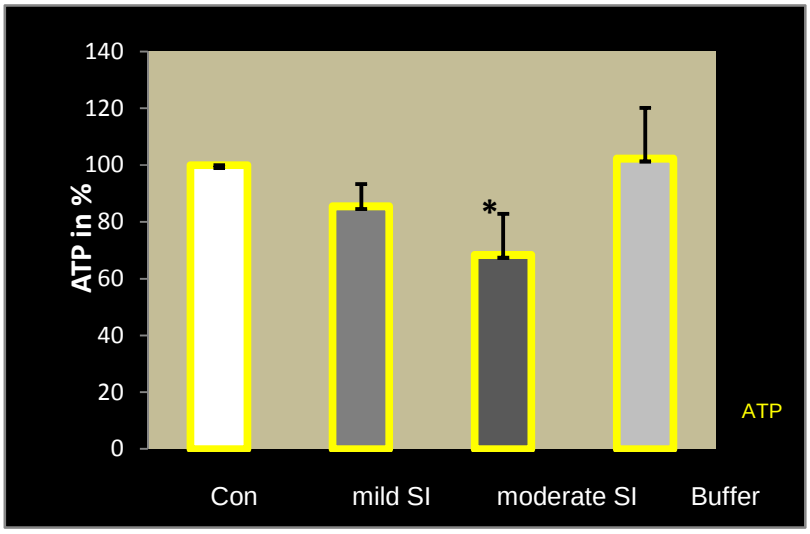

Figure A.8: 2 hrs R Data expressed as mean ± SEM, statistical analysis: ANOVA & Bonferroni correction, * p<0.05 vs Con, # p<0.05 vs mild SI, n=8.

The above results indicate no significant effect of the buffer without 2DG or SDT on % ATP in cells following 2 hrs SI (ATP: Con: 100±0; mild SI: 264 ±62.1; moderate SI: 99.5 ±39.5; Buffer: 95.01±8.4) followed by 1 hrs reperfusion (ATP: Con: 100±0; mild SI: 85.5±; moderate SI: 68.3±14.4; Buffer: 102.3±17.9).

Trial for fluorescence imaging in the whole heart

In order to investigate, whether global ischaemia would lead to defined areas with increased autophagic activity, according to the heterogeneous areas of anoxic tissue, which have been visualized before (Steenbergen, 1979), we aimed to perform a whole tissue immunofluorescence staining. LC-3 (green) and PI (red) were used to identify the extent and localization of an autophagic response and necrotic tissue damage respectively. Images were acquired using the Xenogen *In Vivo* Imaging System (IVISO of Caliper/Xenogen).

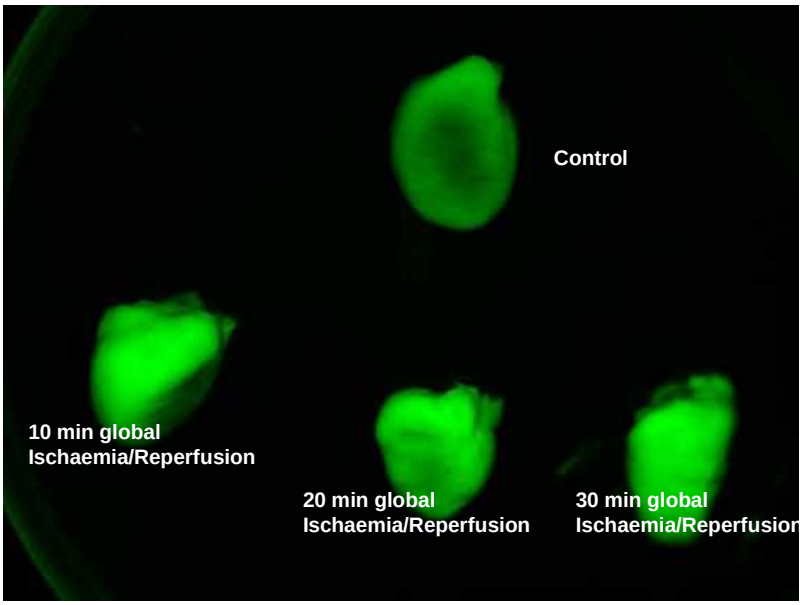

Figure A.9: Hearts were exposed to 10, 20 or 30 min global ischaemia or ischaemia/reperfusion.

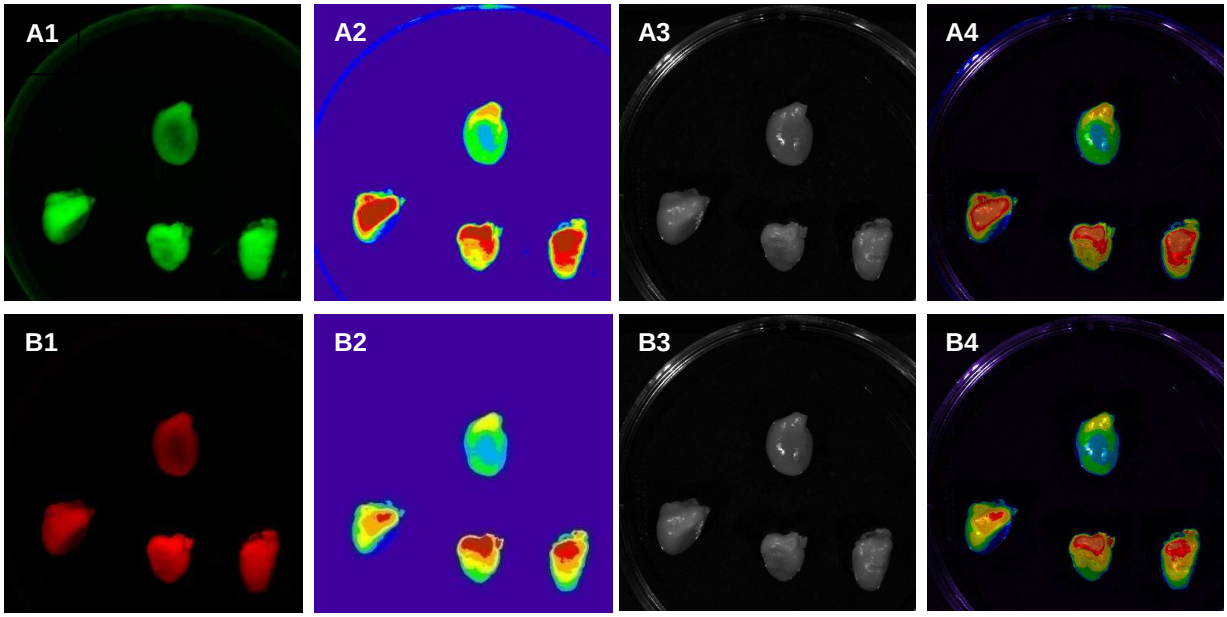

Figure A.10: Whole organ fluorescence micrographs of hearts submitted to 10, 20 and 30 min global ischaemia. Hearts were stained for LC-3 (green, A-panel) and PI (red, B-panel) to indicate autophagic- and necrotic areas respectively. Images show the fluorescence emission (A/B1), an intensity based cold/warm/hot LUT (A/B2), a normal light photograph (A/B3) and an overlay of the latter two.

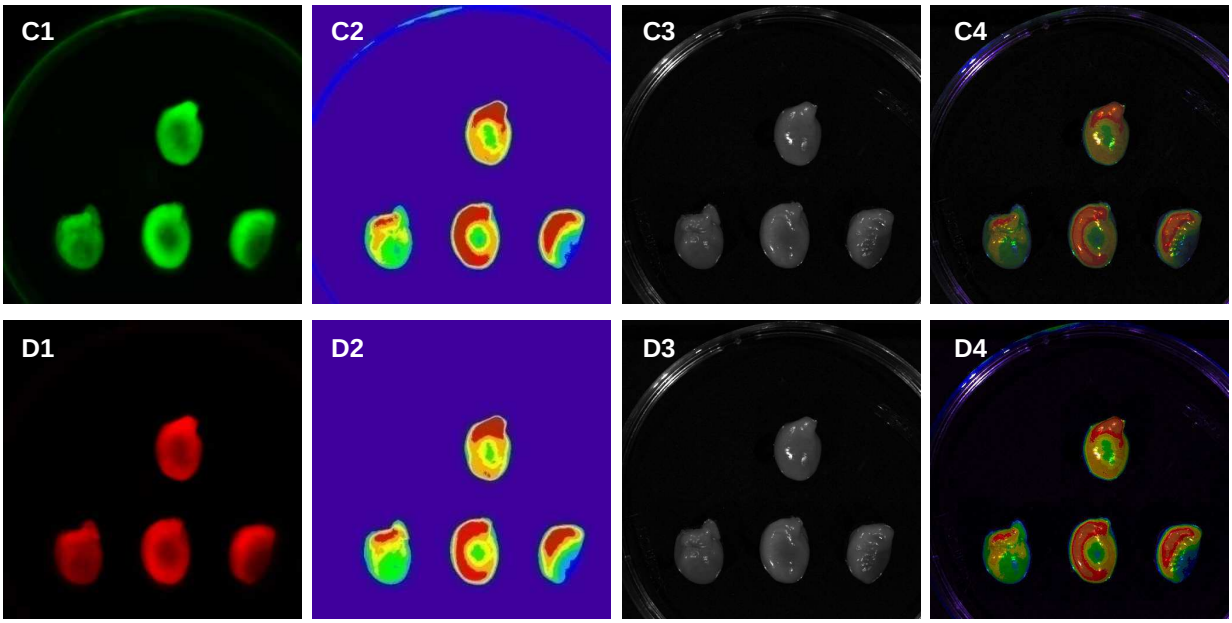

Figure A.11: Whole organ fluorescence micrographs of hearts submitted to 10, 20 and 30 min global ischaemia followed by reperfusion. Hearts were stained for LC-3 (green, A-panel) and PI (red, B-panel) to indicate autophagic- and necrotic areas respectively. Images show the fluorescence emission (C/D1), an intensity based cold/warm/hot LUT (C/D2), a normal light photograph (C/D3) and an overlay of the latter two.

The images indicate differences in the intensity between control hearts and hearts exposed to global ischaemia/reperfusion. Both, LC-3- and PI emission intensity appear to be increased in hearts exposed to global ischaemia. We feel however, that the staining methodology deserves optimization, before being able to draw any conclusions.

Histology of the myocardium

Histology

Haematoxylin Eosin (H&E)

In order to assess myocardial morphology, hearts were stained with haematoxylin/eosin.

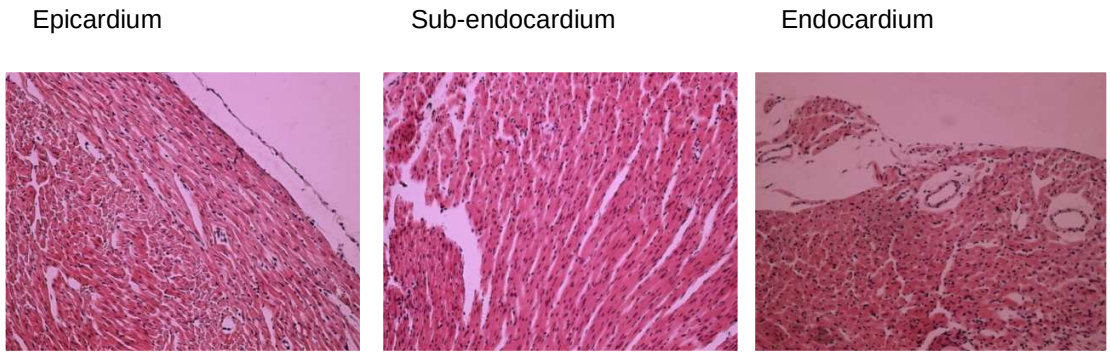

Figure A.12: Control hearts showing the morphology of a normal myocardium.

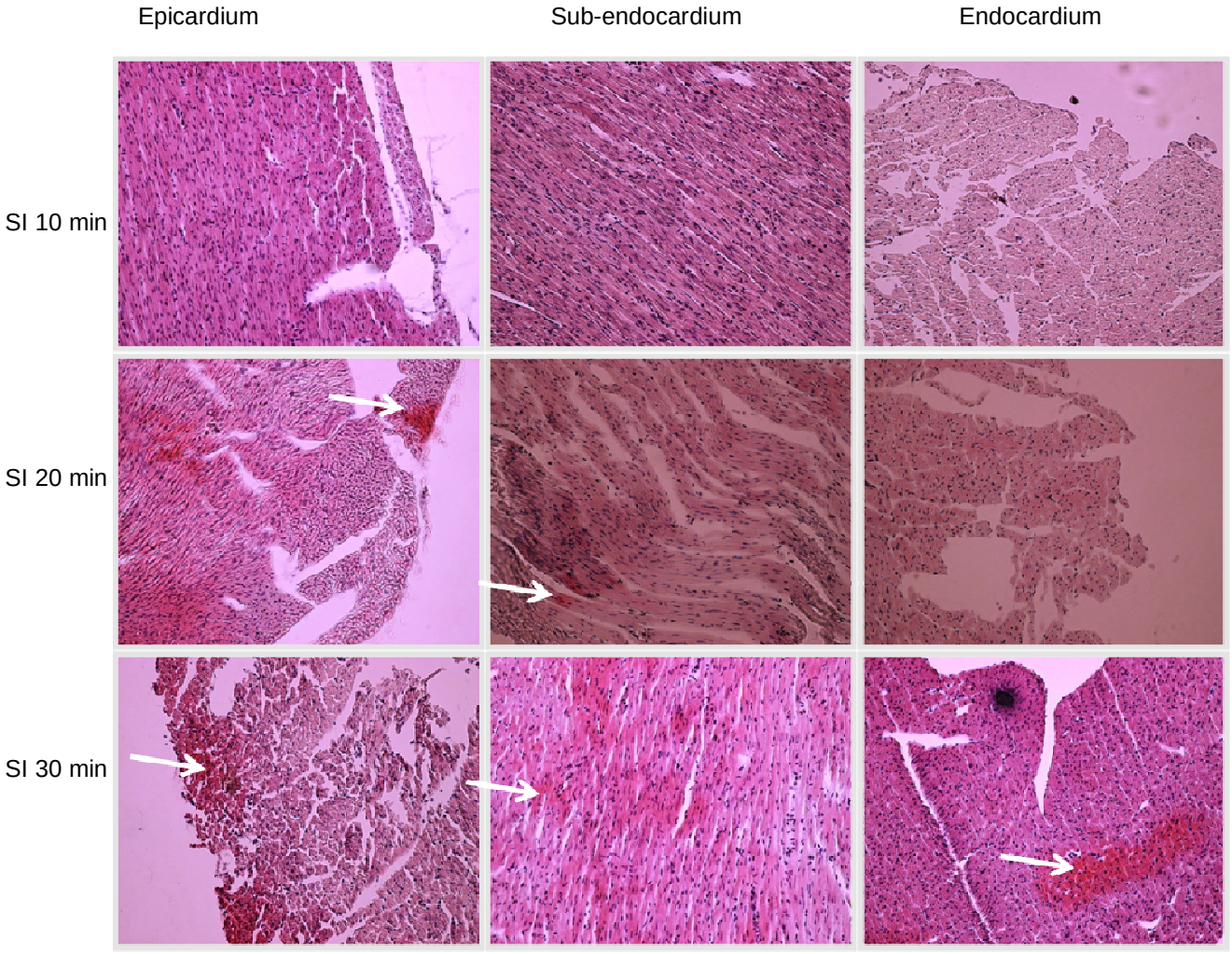

Figure A.13: Micrographs showing hearts submitted to 10, 20 and 30 min global ischaemia. The epicardium, sub-endocardium and epicardium is shown.

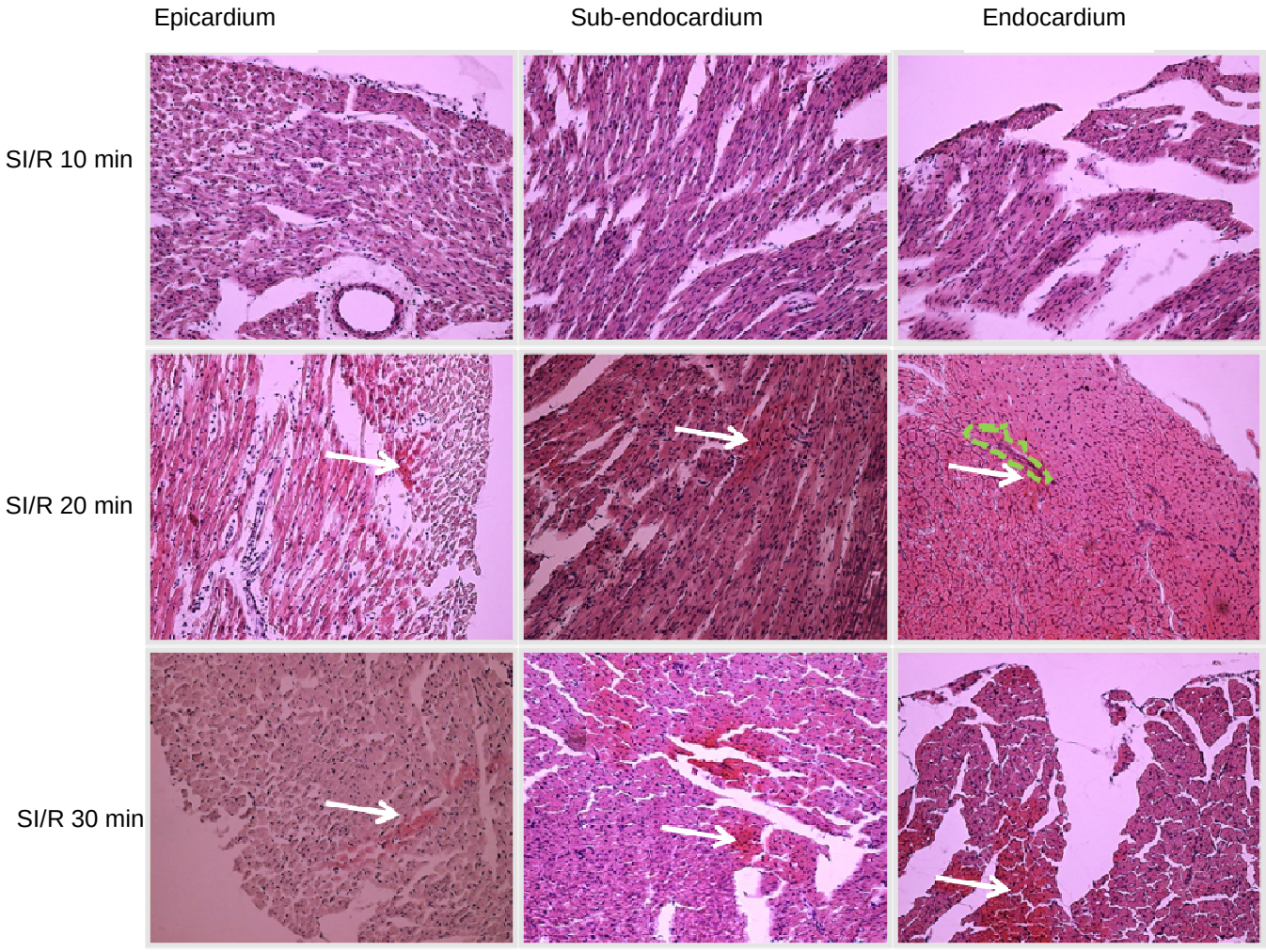

Figure A.14: Micrographs showing hearts submitted to 10, 20 and 30 min global ischaemia followed by reperfusion. The epicardium, sub-endocardium and epicardium is shown. Arrows indicate patches of non-homogeneous hematoxyln/eosin distribution at 20 and 30 min SI and SI/R, possibly indicative for acidophilic regions. These regions were also found in close proximity to blood vessels.

Immunofluorescence

To evaluate the induction of autophagy, apoptosis or necrosis, hearts were subjected to immune-fluorescence staining for LC-3, cleaved PARP and HMGB1 respectively. Nuclei were counterstained with Hoechst 33342.

Epicardium Sub-endocardium Endocardium

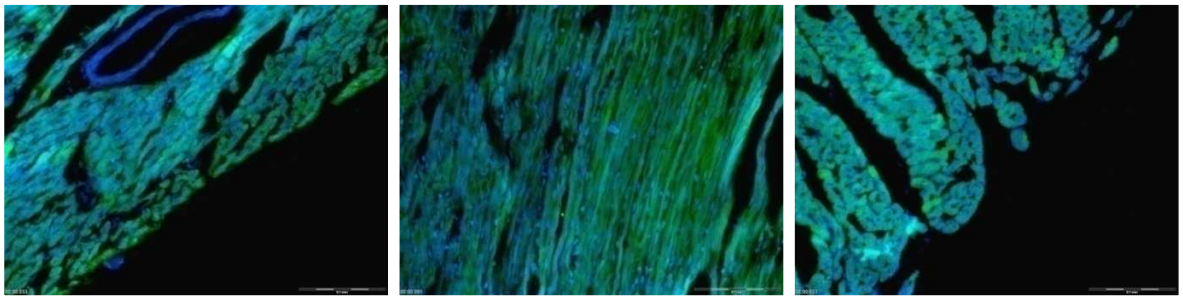

Figure A.15: Control hearts showing a weak and homogeneously distributed LC-3 FITC signal (green), indicative for myocardial baseline autophagic activity.

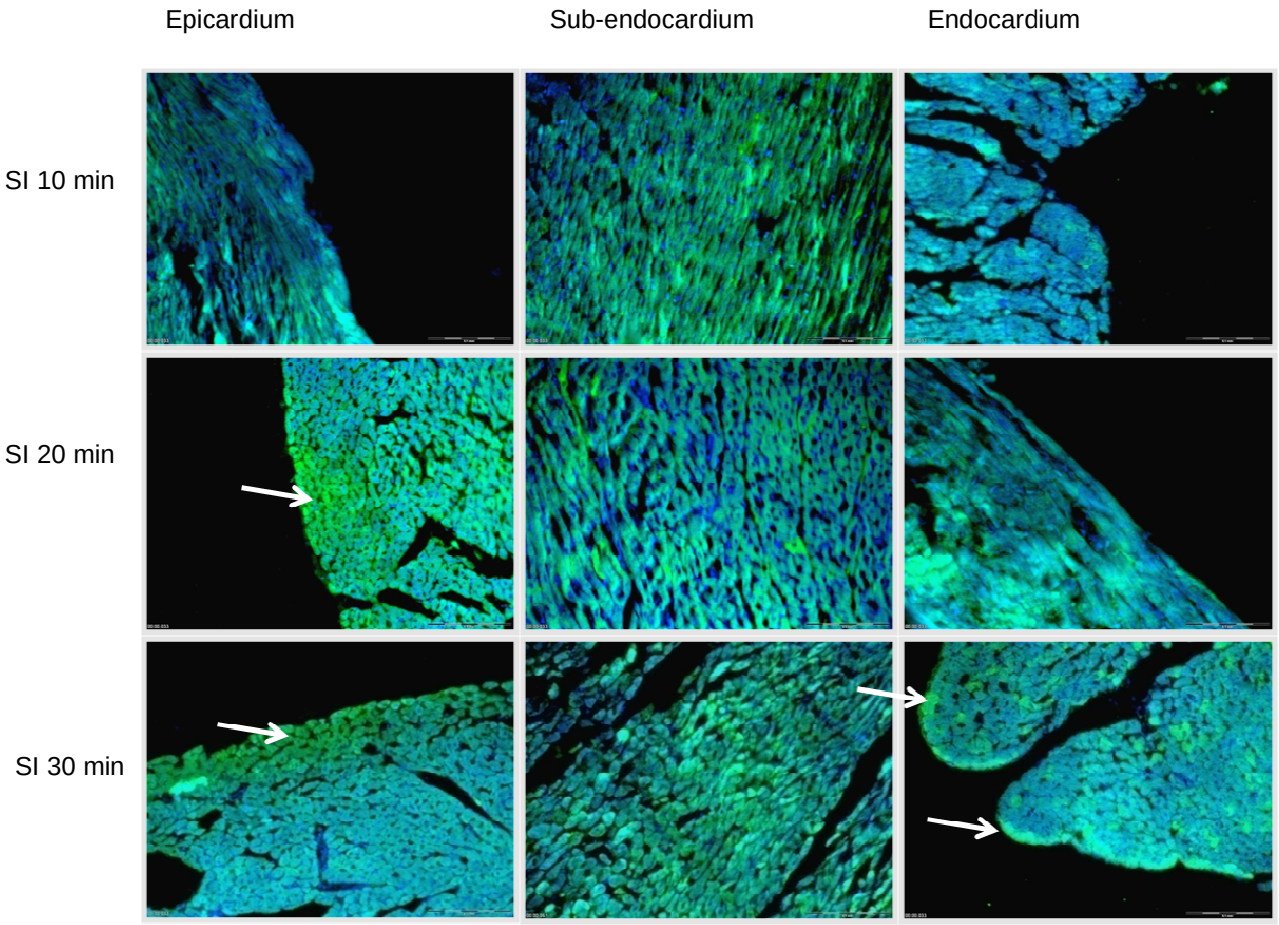

Figure A.16: Fluorescence micrographs showing LC-3 FITC signal (green) of hearts submitted to 10, 20 and 30 min global ischaemia.

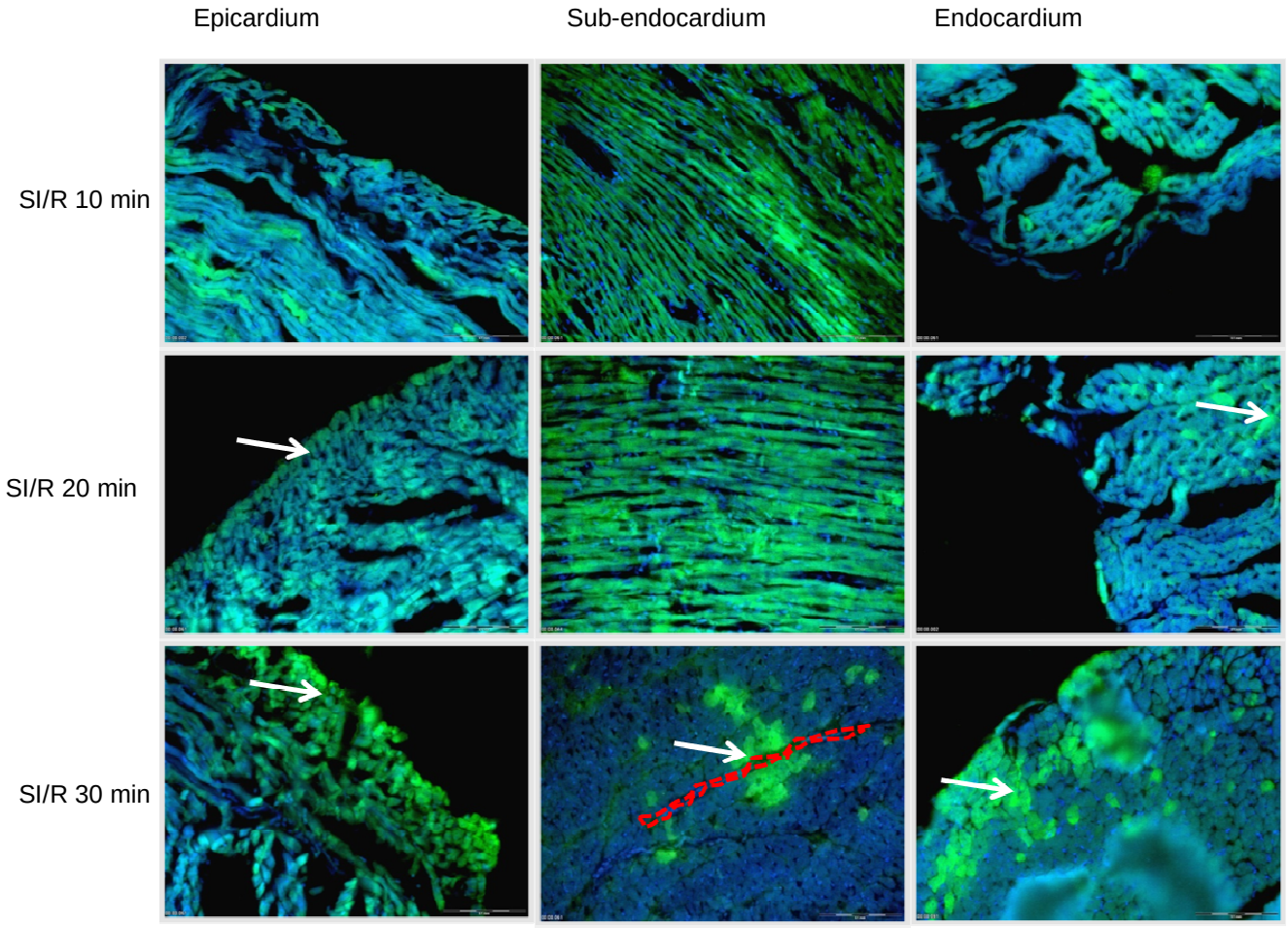

Figure A.17: Micrographs showing hearts submitted to 10, 20 and 30 min global ischaemia followed by reperfusion. Arrows indicate areas with strong signal for LC-3 FITC (green) at 20 and more prominent at 30 min SI and SI/R, indicative for regions where autophagic activity has been increased. Note the patch-like pattern in proximity to blood vessels as well as the lining of endo- and epicardium.

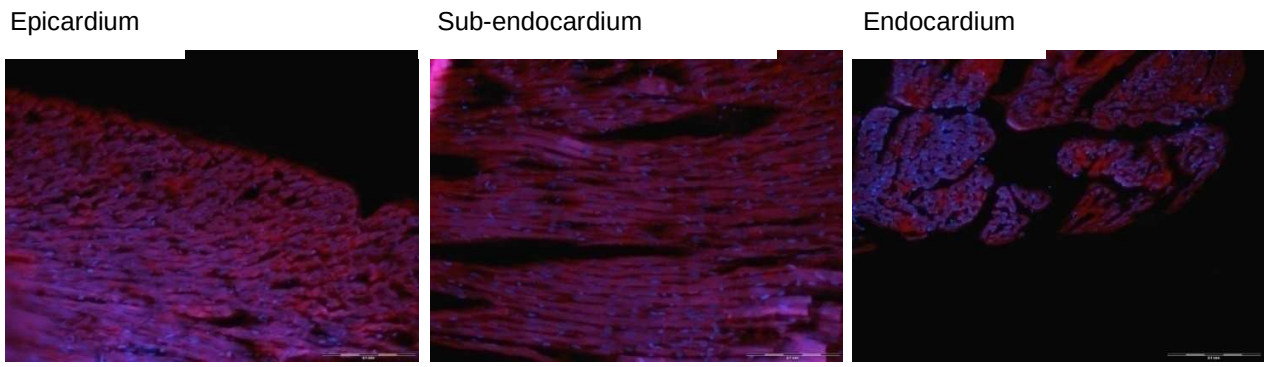

Figure A.18: Control hearts showing a weak and evenly distributed cleaved PARP TexRed signal (red).

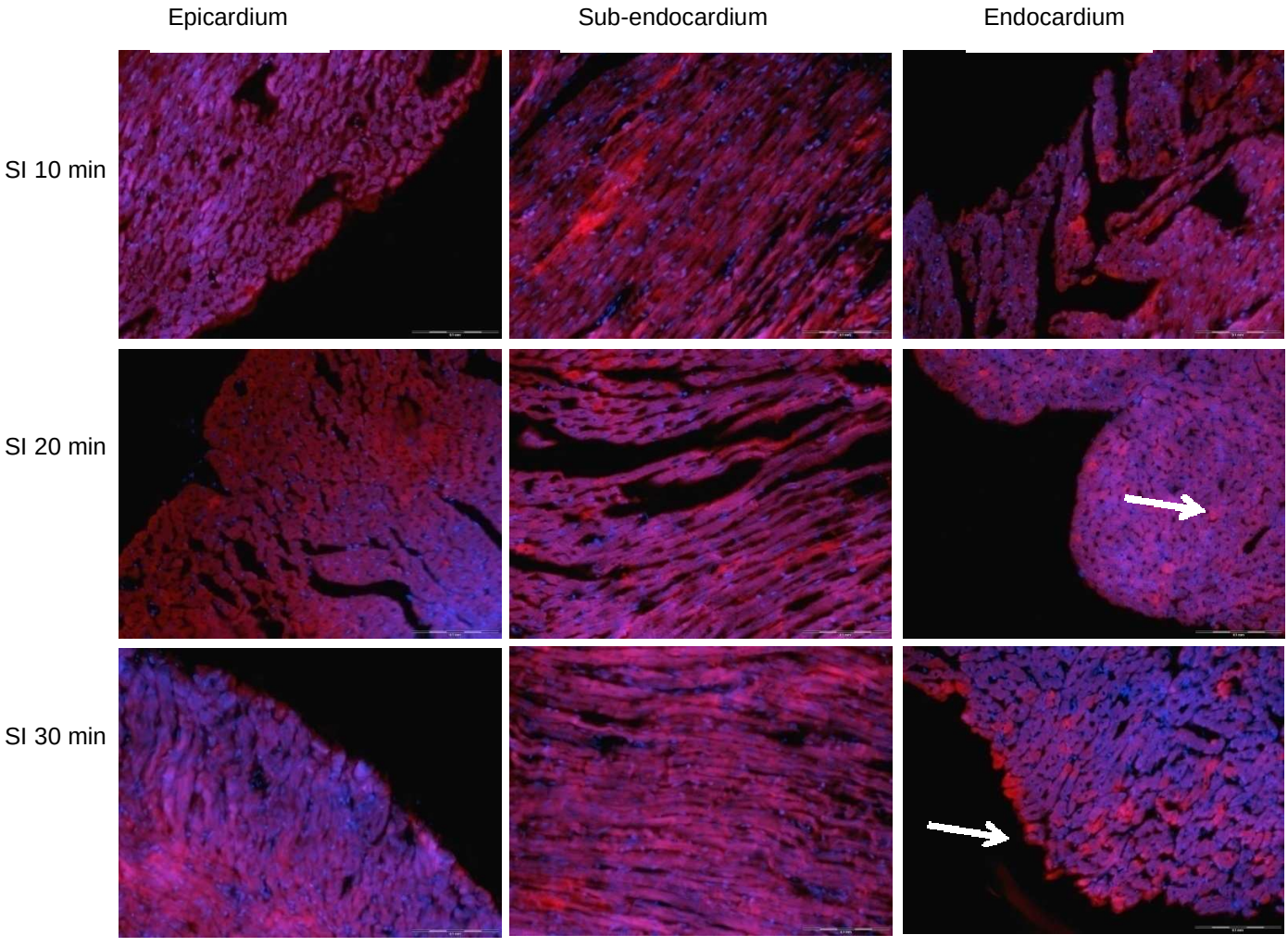

Figure A.19: Fluorescence micrographs showing cleaved PARP TexRed signal (red) of hearts submitted to 10, 20 and 30 min global ischaemia.

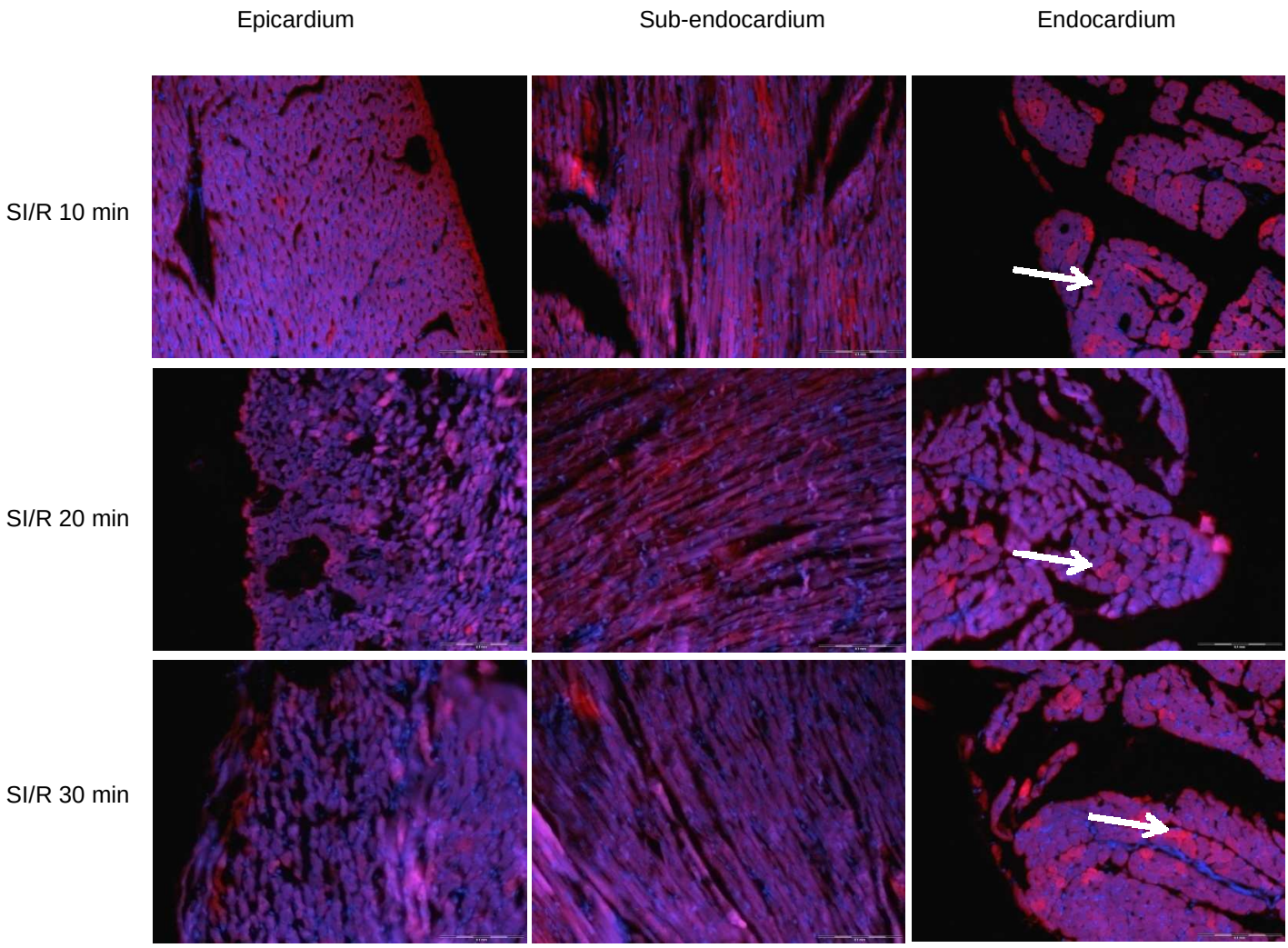

Figure A.20: Fluorescence micrographs showing hearts submitted to 10, 20 and 30 min global ischaemia followed by reperfusion. Arrows indicate areas with strong signal for cleaved PARP TexRed (red) primarily at 30 min SI and SI/R, indicative for regions where apoptosis has been executed.

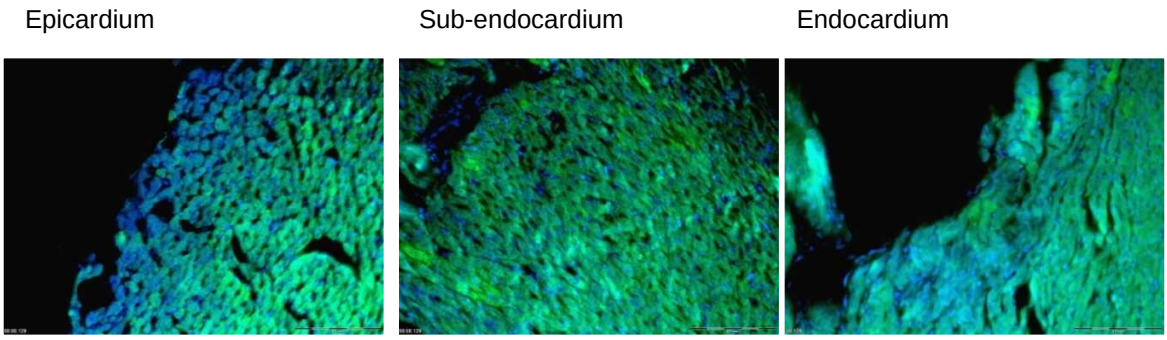

Figure A.21: Control hearts showing a weak and evenly distributed HMGB1 FITC signal (green).

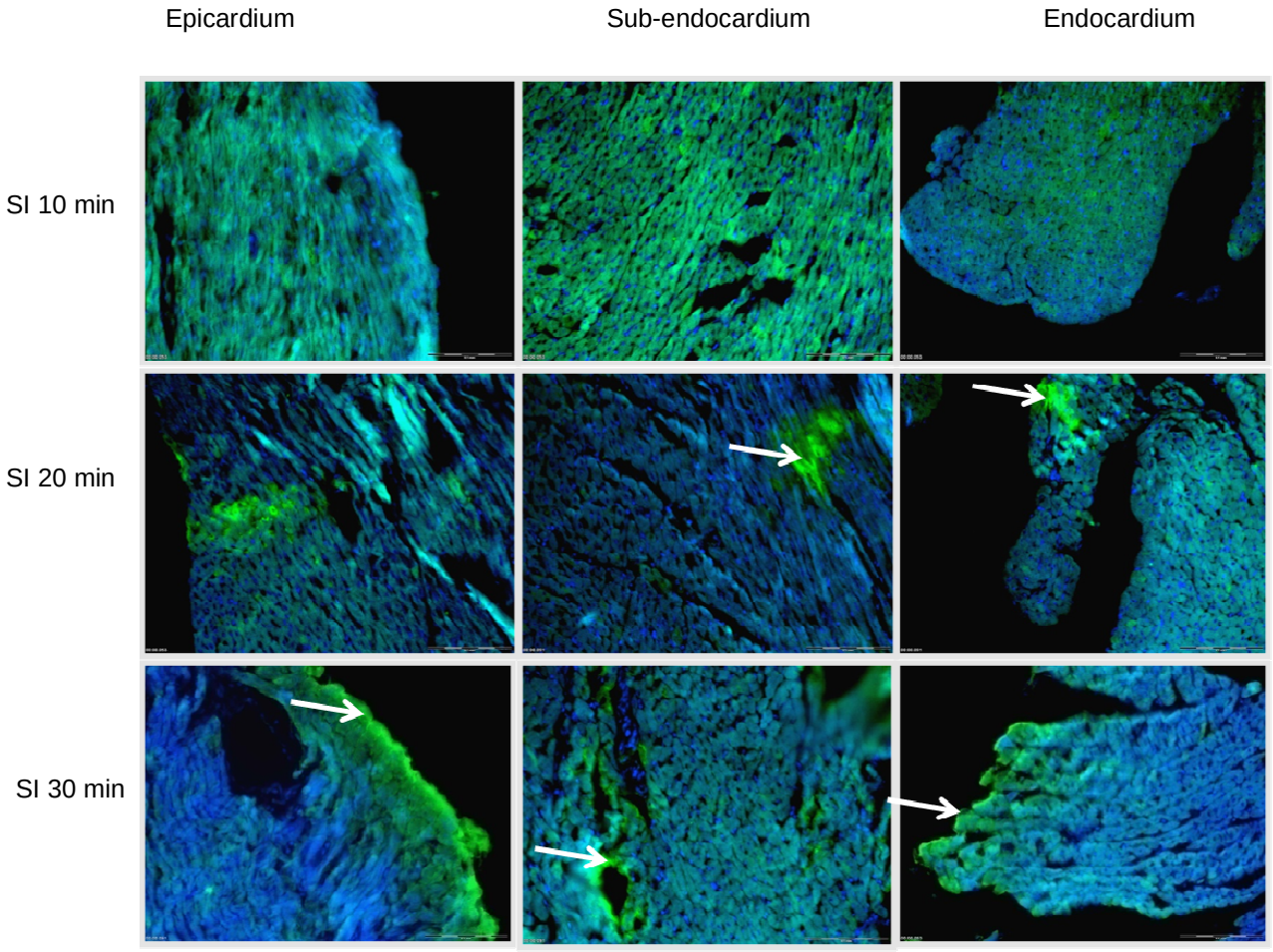

Figure A.22: Fluorescence micrographs showing HMGB1 FITC signal (green) of hearts submitted to 10, 20 and 30 min global ischaemia.

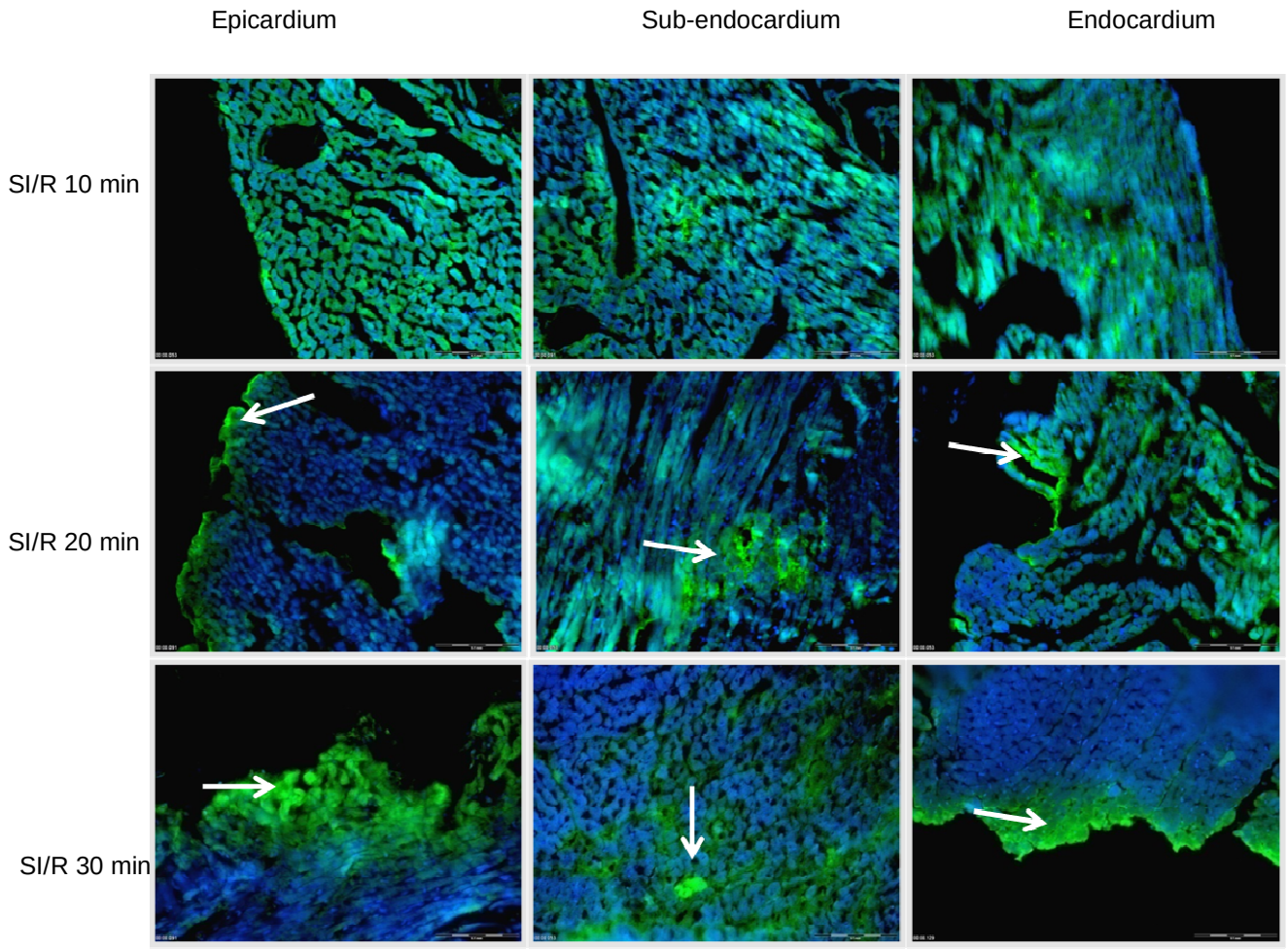

Figure A.23: Fluorescence micrographs showing hearts submitted to 10, 20 and 30 min global ischaemia followed by reperfusion. Arrows indicate areas with strong signal for HMGB1 FITC (green) at 20 and 30 min SI and SI/R, indicative for regions where HMGB1 has been released. Note the lining of endo- and epicardium.

The above preliminary results indicate that autophagy (LC-3 positive areas), apoptosis (PARP-positive areas) and necrosis (HMGB1positive areas) appear to be concomitantly induced in the heart exposed to global ischaemia. More work is needed to correlate such areas to metabolic- and autophagic flux parameters in these regions.

REFERENCES

Agnetti G, Maraldi T, Fiorentini D, Giordano E, Prata C, Hakim G, Muscari C, Guarnieri C and Caldarera CM. Activation of glucose transport during simulated ischemia in H9c2 cardiac myoblasts is mediated by protein kinase C isoforms. Life Sciences. 2005; 78: 264 – 270.

Aki T, Mizukami Y, OkaY, Yamaguchi K, Uemura K, Fujimiya T *et al*. Phosphoinositide 3-kinase accelerates necrotic cell death during hypoxia. Biochem J. 2001; 358:481-487.

Aki T, Yamaguchi K, Fujimiya T and Mizukami Y. Phosphoinositide 3-kinase accelerates autophagic cell death during glucose deprivation in the rat cardiomyocyte-derived cell line H9c2. Oncogene. 2003;22:8529-8535.

Akki A, Zhang M, Murdoch C, Brewer A, and Shah A M. NADPH oxidase signaling and cardiac myocyte function. J Mol Cell Cardiol. 2009; 47:15-22.

Albeck JG, Burke JM, Aldridge BB, Zhang M, Lauffenburger DA and Sorger P. Quantitative analysis of pathways controlling extrinsic apoptosis in single cells. Molecular Cell. 2008; 30:11-25.

Al-Dadah AS, Voeller K, Schuessler RB, Damiano RJ, and. Lawton JS. Maintenance of Myocyte Volume Homeostasis During Stress by Diazoxide is Cardioprotective. Ann Thorac Surg. 2007; 84:857– 63.

Amaravadi RK, Yu D, Lum JJ, Bui T, Christophorou MA, Evan GI *et al*. Autophagy inhibition enhances therapy-induced apoptosis in a Myc-induced model of lymphoma. J Clin Invest. 2007; 117:326–336.

Apetoh L, Ghiringhelli F, Tesniere A, Criollo A, Ortiz C, Liderau R *et al*. The interaction between HMGB1 and TLR4 dictates the outcome of anticancer chemotherapy and radiotherapy. Immunol Rev. 2007; 220:47-59.

Arcangioli B and Hassine SB. Unrepaired oxidative DNA damage induces an ATR/ATM apoptotic-like response in quiescent fission yeast. Cell Cycle. 2009; 8:15.

Artal-Sanz M and Tavernarakis N. Proteolytic mechanisms in necrotic cell death and neurodegeneration. FEBS Lett. 2005; 579:3287-3296.

Ashrafian H, Frenneaux MP, Opie LH. Metabolic mechanisms in heart failure. Circulation. 2007;116:434-448.

Asoh S, Mori T, Nagai S, Yamagata K, Nishimaki K, Miyato Y, Shidara Y and Ohta S. Zonal necrosis prevented by transduction of the artificial anti-death FNK protein. Cell Death Differ. 2005; 12:384–394.

Azad MB, Chen Y, Henson ES, Cizeau J, McMillan-Ward E, Israels SJ and Gibson SB. Hypoxia induces autophagic cell death in apoptosis-competent cells through a mechanism involving BNIP3. Autophagy. 2008; 4:2:195-204.

Baba M, Takeshige G, Baba N and Ohsumi Y. Ultrastrucmral Analysis of the Autophagic Process in Yeast: Detection of Autophagosomes and Their Characterization. J Cell Biol. 1994; 124, 6:903-913.

Bampton ETW, Goemans CG, Niranjan D, Mizushima N and Tolkovsky A. The dynamics of autophagy visualized in live cells. Autophagy. 2005;1:1:23-36.

Baroldi G. Myocardial necrosis: the need for definition. J Mol Cell Cardiol. 1974; 6:401-402.

Bereiter-Hahn, J, Jendrach M. Mitochondrien-Dynamik bei Stress und Altern. Biospektrum. 2009; 15:392-395.

Bergmann A. Autophagy and Cell Death: No Longer at Odds. Cell. 2007; 131:1032-1034.

Bogliolo M, Borghini S, Abbondandolo A and Degan P. Alternative metabolic pathways for energy supply and resistance to apoptosis in Fanconi anaemia. Mutagenesis. 2002; 17:25-30.

Bonaldi T, Talamo F, ScafÆdi P, Ferrera D, Porto A, Bachi A, Rubartelli A, Agresti A and Bianchi ME. Monocytic cells hyperacetylate chromatin protein HMGB1 to redirect it towards secretion. EMBO J. 2003; 22, 20:5551- 5560.

Bonavitaa F, Stefanellia C, Giordanoa E, Columbarob M, Facchinia A, Bonafe'a F, Caldareraa CM and Guarnieria C. H9c2 cardiac myoblasts undergo apoptosis in a model of ischemia consisting of serum deprivation and hypoxia: inhibition by PMA. FEBS Lett. 2003; 536:85-91.

Bonfoco E, Krainc D, Ankarcrona M, Nicotera P and Lipton SA. Apoptosis and necrosis: Two distinct events induced, respectively, by mild and intense insults with N-methyl-D-aspartate or nitric oxide/superoxide in cortical cell cultures. Neurobiology. 1995; 92:7162-7166.

Boya P, Gonzalez-Polo RA, Casares N, Perfettini JL, Dessen P, Larochette N, Metivier D, Meley D, Souquere S, Yoshimori T, Pierron G, Codogno P and Kroemer G. Inhibition of Macroautophagy Triggers Apoptosis. Mol Cell Biol. 2005; 25:1025-1040.

Bradford MM. A rapid and sensitive method for the quantitation of microgram quantities of protein utilizing the principle of protein-dye binding. Anal Biochem. 1976. 72: 248-54.

Braunwald E. Editorial: Reduction of myocardial-infarct size. N Engl J Med. 1974; 291:525-526.

Bursch W, Karwan A, Mayer M, Dornetshuber J, Fröhwein U, Schulte-Hermann R, *et al*. Cell death and autophagy: cytokines, drugs, and nutritional factors. Toxicology 2008; 254:147-157.

Buttgereit F and Brand MD. A hierarchy of ATP-consuming processes in mammalian cells. Biochem J. 1995; 312:163-167.

Camarata PJ, Heros RC and Latchaw RE. "Brain Attack": The Rationale for Treating Stroke as a Medical Emergency. Neurosurgery. 1994; 34:144-158.

Caputo M. Metabolites in congenital heart disease. The effects of cyanosis, age, and pathology. Ann Thorac Surg 2006; 81:943-949.

Carloni S, Carnevali A, Cimino M and Balduini W. Extended role of necrotic cell death after hypoxia-ischemia-induced neurodegeneration in the neonatal rat. Neurobiol Dis. 2007; 27:354-361.

Chabowski A, Momken I, Coort SLM, Calles-Escandon J, Tandon NN, Glatz JFC, Luiken JJFP and Bonen A. Prolonged AMPK activation increases the expression of fatty acid transporters in cardiac myocytes and perfused hearts. Mol Cell Biochem. 2006; 288: 201-212.

Chan FKM, Shisler J, Bixby JG, Felices M, Zheng L, Appel M *et al*. A role for Tumor Necrosis Factor receptor-2 and Receptor-interactng Protein in Programmed Necrosis and antiviral responses. JBC. 2003; 278:51613-51621.

Chiechomska IA and Tolkovsky AM. Non-autophagic GFP-LC3 puncta induces by saponin and other detergents. Autophagy. 2007; 3:6:586-590.

Clausen T and Gissel H. Role of Na^+,K^+ pumps in restoring contractility following loss of cell membrane integrity in rat skeletal muscle. Acta Physiol Scand. 2005; 183:263-271.

Codogno P and Meijer AJ. Autophagy and signaling: their role in cell survival and cell death. Cell Death Differ. 2005; 12:1509-1518.

Coetzee WA and Opie LH. Effects of components of ischemia and metabolic inhibition on delayed afterdepolarizations in guinea pig papillary muscle. Circ Res. 1987; 6:157-165.

Cohen MV, Baines CP and Downey J M. Ischemic preconditioning: from adenosine receptor to KATP channel. Annu Rev Physiol. 2000; 62:79-109.

Corbett AD and Lees GM. Depressant effects of hypoxia and hypoglycaemia on neuro-effector transmission of guinea-pig intestine studied in vitro with a pharmacological model. Br J Pharmacol. 1997; 120:107-115.

Corcelle E, Djerbi N, Mari M, Nebout M, Fiorini C, Fénichel P *et al*. Control of the autophagy maturation step by the MAPK ERK and p38. Autophagy. 2007; 3:1:57-59.

Cuervo AM, Bergamini E, Brunk UT, Dröge W, Ffrench M and Terman A. Autophagy and Aging. The Importance of Maintaining “Clean” Cells. Autophagy. 2005; 1:3:131-140.

Cuervo AM. Autophagy: Many paths to the same end. Mol Cell Biochem. 2004; 263:55-72.

Cumming DV, Heads RJ, Brand NJ, Yellon DM, Latchman DS. The ability of heat stress and metabolic preconditioning to protect primary rat cardiac myocytes. Basic Res Cardiol. 1996; 91:79-85.

Cumming RC, Simonsen A and Finley KD. Quantitative Analysis of Autophagic Activity in Drosophila Neural Tissues By Measuring The Turnover Rates Of Pathway Substrates. Methods Enzymol. 2008; 451:639-651.

Dagher PC. Modeling ischemia in vitro: selective depletion of adenine and guanine nucleotide pools. Am J Physiol Cell Physiol. 2000; 279:1270-1277.

De Duve C and Wattiaux R. Functions Of Lysosomes. Ann Rev Physiol. 1966; 28:435-92.

De Saint-Hubert M, Prinsen K, Mortelmans L, Verbruggen A and Mottaghy FM. Molecular imaging of cell death. Methods. 2009; 48:178–187.

Debnath J, Baehrecke EH and Kroemer G. Does Autophagy Contribute to Cell Death? Autophagy. 2005; 1:2:66-74.

Debnath J, Mills KR, Collins NL, Reginato MJ, Muthuswami SK and Brugge JS. The role of apoptosis in creating and maintaining luminal space within normal and oncogene-expressing mammary acini. Cell. 2002; 111:29-40.

Decker RS, Wildenthal K. Lysosomal alterations in hypoxic and reoxygenated hearts. Am J Pathol. 1980; 98:425-444.

Degterev A, Huang Z, Boyce M, Li Y, Jagtap P, Mizushima N *et al*. Chemical inhibitor of nonapoptotic cell death with therapeutic potential for ischemic brain injury. Nat Chem Biol. 2005; 1:112-119.

Deminoff SJ and Herman PK. Identifying Atg1 substrates. Autophagy. 2007; 3:6:667-673.

Denecker G, Vercammen D, Declereq W ad Vandenabeele P. Apoptotic and necrotic cell death induced by death domain receptors. CMLS. 2001; 58:356-370.

Denecker G, Vercammen D, Steemans M, Vanden Berghe T, Brouckaert G, Van Loo G *et al*. Death receptor-induced apoptotic and necrotic cell death: differential role of caspases and mitochondria. Cell Death Differ. 2001; 8:829-840.

Dice FJ. Chaperone-Mediated Autophagy. Autophagy. 2007; 3:4:295-299.

Doran JP, Howie AJ, Townend JN and Bonser RS. Detection of myocardial infarction by immunohistological staining for C9 on formalin fixed, paraffin wax embedded sections. J Clin Pathol. 1996; 49:34-37.

Dosenko VE, Nagibin VS, Tumanovska LV and Moibenko AA. Protective effect of autophagy in anoxia-reoxygenation of isolated cardiomyocytes? Autophagy. 2006; 2:4:305-306.

Dougherty C, Kubasiak LA, Prentice H, Andreka P, Bishopric NH and Webster KA. Activation of c-Jun N-terminal kinase promotes survival of cardiac myocytes after oxidative stress. Biochem J. 2002; 362:561-571.

Dyck JRB and Lopaschuk GD. AMPK alterations in cardiac physiology and pathology: enemy or ally? J Physiol. 2006; 574:95-112.

Edinger LE, Thompson CB. Death by design: apoptosis, necrosis and autophagy. Curr Opin Cell Biol. 2004; 16:663-669.

Eefting F, Rensing B, Wigman J, Pannekoek WJ, Liu WM, Cramer MJ, Lips DJ and Doevendans PA. Role of apoptosis in reperfusion injury. Cardiovasc Res. 2004; 61: 414– 426.

Engelbrecht A-M, Niesler C, Page C and Lochner A. p38 and JNK have distinct regulatory functions on the development of apoptosis during simulated ischaemia and reperfusion in neonatal cardiomyocytes. Basic Res Cardiol. 2004; 99: 338 – 350.

Erlich E, Mizrachy L, Segev O, Lindenboim L, Zmira O, Adi-Harel S *et al*. Differential interactions between beclin 1 and bcl-2 family members. Autophagy. 2007; 3:6:561-568.

Erlich S, Shohami E and Pinkas-Kramarski RP. Neurodegeneration induces upregulation of beclin 1. Autophagy. 2006; 2:1:49-51.

Essmann F, Bantel H, Totzke G, Engels IH, Sinha B, Schulze-Osthoff K and Janicke RU. Staphylococcus aureus alpha-toxin-induced cell death: predominant necrosis despite apoptotic caspase activation. Cell Death Differ. 2003; 10:1260-1272.

Esumi K, Nishida M, Shaw D, Smith TW and Marsh JD. NADH measurements in adult rat myocytes during simulated ischemia. Am J Physiol. 1991; 260:1743–1752.

Fass E, Amar N and Elazar Z. Identification of essential residues for the c-terminal cleavage of mammalian LC3. Autophagy. 2007; 3:1:48-50.

Ferraro E and Cecconi F. Autophagic and apoptotic response to stress signals in mammalian cells. Arch Biochem Biophys. 2007; doi 10.1016.

Ferraro E, Pulicati A, Cencioni MT, Cozzolino M, Navoni F, di Martino S *et al*. Apoptosome-deficient Cells Lose Cytochrome c through Proteasomal Degradation but Survive by Autophagy-dependent Glycolysis. Mol Biol Cell. 2008; 19: 3576-3588.

Festjens N, Vanden Berghe T and Vandenabeele P. Necrosis, a well-orchestrated form of cell demise: Signalling cascades, important mediators and concominant immune response. Biochim Biophys Acta. 2006; 1757:1371-1387.

Freude B, Masters TN, Kostin S, Robicsek F, Schaper J. Cardiomyocyte apoptosis in acute and chronic conditions. Basic Res Cardiol. 1998; 93:85-89.

Fuertes G, Martin de Llano JJ, Villarroya A, Rivett AJ and Knecht E. Changes in the proteolytic activities of proteasomes and lysosomes in human fibroblasts produced by serum withdrawal, amino-acid deprivation and confluent conditions. Biochem J. 2003; 375:75-86.

Fuglesteg BN, Suleman N, Tiron C, Kanhema T, Lacerda L, Andreasen TV, Sack MN, Jonassen AK, Mjøs OD, Opie LH and Lecour S. Signal transducer and activator of transcription 3 is involved in the cardioprotective signalling pathway activated by insulin therapy at reperfusion. Basic Res Cardiol. 2008; 103: 444–453.

Furuya N, Yu J, Byfield M, Pattingre S and Levine B. The evolutionary conserved domain of beclin 1 is required for vps34 binding, autophagy and tumor suppressor function. Autophagy. 2005; 1:1:46-52.

Gabrys J, Konecki J, Shani J, Durczok A, Bielaczyc G, Kosteczko A, *et al*. Proteinous amino acids in muscle cytosol of rats heart after exercise and hypoxia. Receptors Channels. 2003; 9:301-307.

Galluzzi L *et al*. Targeting post-mitochondrial effectors of apoptosis for neuroprotection. Biochim Biophys Acta. 2008; doi:10.1016/j.bbabio.2008.09.006.

Galluzzi L, Aaronson SA, Abrams J, Alnemri ES, Andrews DW, Baehrecke EH *et al*. Guidelines for the use and interpretation of assays for monitoring cell death in higher eukaryotes. Cell Death Differ. 2009; 16: 1093-1107.

Galluzzi L, Zamzami N, de La Motte Rouge CL, Brenner C and Kroemer G. Methods for the assessment of mitochondrial membrane permeabilization in apoptosis. Apoptosis. 2007; 12: 803–813.

Gao XM, Wong G, Wang B, Kiriazis H, Moore XL, Su YD, *et al*. Inhibition of mTOR reduces chronic pressure-overload cardiac hypertrophy and fibrosis. J Hyperten. 2006; 24:1663-1670.

Gardella S, Andrei C, Ferrera D, Lotti LV, Torrisi MR, Bianchi ME *et al*. The nuclear protein HMGB1 is secreted by monocytes via a non-classical, vesicle-mediated secretory pathway. EMBO rep. 2002; 3:995-1001.

Gevers W. Protein metabolism of the heart. J Mol Cell Cardiol. 1984; 16:3-32.

Golbs A, Heck N and Luhmann HJ. A new technique for real-time analysis of caspase-3 dependent neuronal cell death. J Neurosci Methods. 2007; 161:234-243.

Golstein JC, Muňoz-Pinedo C, Ricci J-E, Adams SR, Kelekar A, Schuler M *et al*. Cytochrome c is released in a single step during apoptosis. Cell Death Differ. 2005; 12:453-462.

Golstein P and Kroemer G. Cell death by necrosis: towards a molecular definition. TiBS. 2006; 32: 37-42.

Gomez LA, Alekseev AE, Aleksandrova LA, Brady PA and Terzic A. Use of the MTT assay in adult ventricular cardiomyocytes to assess viability: effects of adenosine and potassium on cellular survival. J Mol Cell Cardiol. 1997; 29: 1255-1266.

Gong B, Lim MCY, Wanderer J, Wyttenbach A and Morton AJ. Time-lapse analysis of aggregate formation in an inducible PC12 cell model of Huntington's disease reveals time-dependent aggregate formation that transiently delays cell death. Brain Res Bull. 2008; 75: 146–157.

Gonin-Giraud S, Mathieu A-L, Diocou S, Tomkowiak M, Delorme G and Marvel J. Decreased glycolytic metabolism contributes to but is not the inducer of apoptosis following IL-3-starvation. Cell Death Differ. 2002; 9: 1147-1157.

González-Polo RA, Boya P, Pauleau AL, Jalil A, Larochette N, Souquère S, *et al*. The apoptosis/autophagy paradox: autophagic vacuolization before apoptotic death. J Cell Sci 2005; 118:3091-3102.

Goodwin CJ, Holt SJ, Downes S and Marshall NJ. Microculture tetrazolium assays: a comparison between two new tetrazolium salts, XTT and MTS. J Immunol Methods. 1995; 179:95-103.

Gottlieb RA, Finley KD, Mentzer RM. Cardioprotection requires taking out the trash. Basic Res Cardiol 2009; 104:169-180.

Grandgirard D, Studer E, Monney L, Belser T, Fellay I, Borner C *et al*. Alphaviruses induce apoptosis in bcl-2-overexpressing cells: evidence for a caspase-mediated, proteolytic inactivation of bcl-2. EMBO J 1998; 17:1268-1278.

Grover G, Atwal K, Sleph P, Wang FL, Monshizadegan H, Monticello T *et al*. Excessive ATP hydrolysis in ischemic myocardium by mitochondrial F_1F_0-ATPase: effect of selective pharmacological inhibition of mitochondrial ATPase hydrolase activity. Am J Physiol Heart Circ Physiol. 2004; 287:H1747-H1755.

Grover G, Atwal K, Sleph P, Wang FL, Monshizadegan H, Monticello T *et al*. Excessive ATP hydrolysis in ischemic myocardium by mitochondrial F_1F_0-ATPase: effect of selective pharmacological inhibition of mitochondrial ATPase hydrolase activity. Am J Physiol Heart Circ Physiol. 2004; 287:H1747-H1755.

Gustafsson ÅB and Gottlieb RA. Recycle or die: the role of autophagy in cardioprotection. J Mol Cell Cardiol. 2008; 44:654-661.

Halapas A, Armakolas A, Koutsilieris M. Autophagy: a target for therapeutic interventions in myocardial pathophysiology. Expert Opin Ther Targets. 2008; 12:1509-1522.

Hamacher-Brady A, Brady NR and Gottlieb RA. The interplay between pro-death and pro-survival signaling pathways in myocardial ischemia/reperfusion injury: apoptosis meets autophagy. Cardiovasc Drugs Ther. 2006; 20:445-462.

Hamacher-Brady A, Brady NR, Gottlieb RA. Enhancing macroautophagy protects against ischemia/reperfusion injury in cardiac myocytes. J Biol Chem 2006; 281:29776-29787.

Han SI, Kim YS, Kim TH. Role of apoptotic and necrotic cell death under physiologic conditions. BMB. 2008; 41:1-10.

Han W, Li L, Qui S, Lu Q, Pan Q Gu Y *et al*. Shikonin circumvents cancer drug resistance by induction of a necroptotic death. Mol Cancer Ther. 2007; 6:1641-9.

Hanley PJ, Mickel M, Löffler M, Brandt U and Daut J. K_{ATP} channel-independent targets of diazoxide and 5-hydroxydecanoate in the heart. J Physiol. 2002; 542:735-741.

Hannigan AM, Gorski SM. Macroautophagy. The key to a healthy diet? Autophagy 2009; 5:2:140-151.

Hardie D G, Scott JW, Pan DA and Hudson ER. Management of cellular energy by the AMP-activated protein kinase system. FEBS Lett. 2003; 546: 113-120.

Harhaji-Trajkovic L, Vilimanovich U, Kravic-Stevovic T, Bumbasirevic V and Trajkovic V. AMPK-mediated autophagy inhibits apoptosis in cisplatin-treated tumor cells. JCMM. 2008.

Healy DA, Watson RWG and Newsholme P. Glucose, but not glutamine, protects against spontaneous and anti-Fas antibody-induced apoptosis in human neutrophils. Clin Sci. 2002; 103:179-189.

Hearse DJ, Crome R, Yellon DM, Wyse R. Metabolic and flow correlates of myocardial ischaemia. Cardiovasc Res. 1983; 17:452-458.

Hearse DJ, Yellon DM, Chappel DA, Wyse RKH, Ball GR. A high velocity device for obtaining multiple, contiguous, myocardial biopsies. J Mol Cell Cardiol. 1981; 13:197-206.

Hearse DJ, Yellon DM. The “border zone” in evolving myocardial infarction: controversy or confusion? Am J Cardiol. 1981; 47:1321-1334.

Hengartner MO. The biochemistry of apoptosis. Nature. 2000; 407:770-776.

Hofmeyr J-HS, Cornish-Bowden A. Regulating the cellular economy of supply demand. FEBS Lett. 2000; 476: 47-51.

Holler N, Zaru R, Micheau O, Thome M, Attinger A, Valitutti S *et al*. Fas triggers an alternative, caspase-8-independent cell death pathway using the kinase RIP as effector molecule. Nat Immunol. 2000; 1:489-495.

Horman S, Beauloyes C, Vertommen D, Vanoverschelde JL, Hue L, Rider MH. Myocardial ischemia and increased heart work modulate the phosphorylation state of eukaryotic elongation factor-2. J Biol Chem. 2003; 43:41970-41976.

Houten S M, Chegary M, te Brinke H, Wijnen W J, Glatz JFC, Luiken JJFP *et al*. Pyruvate dehydrogenase kinase 4 expression is synergistically induced by AMP-activated protein kinase and fatty acids. Cell Mol Life Sci. 2009; 66: 1283-1294.

Høyer-Hansen M and Jäättelä M. AMP-activated protein kinase. A universal regulator of autophagy? Autophagy. 2007; 3:4:381-383.

Hreniuk D, Garay M, Gaarde W, Monia BP, Mckay RA and Cioffi CL. Inhibition of C-Jun N-Terminal Kinase 1, but not c-Jun N-Terminal Kinase 2, suppresses apoptosis induced by ischemia/reoxygenation in rat cardiac myocytes. Mol Pharmacol. 2001; 59:867-874.

Huang J and Brumell JH. NADPH oxidases contribute to autophagy regulation. Autophagy. 2009; 5: 6: 1-3.

Huber H, Rehm M, Plchut M, Dussmann H and Prehn J. APOPTO-Cell-a simulation tool and interactive database for analyzing cellular susceptibility to apoptosis. Bioinformatics. 2007; 23:648-650.

Izyumov DS, Avetisyan AV, Pletjushkina OY, Sakharov DV, Wirtz KW, Chernyak BV *et al.* ‘‘Wages of Fear’’: transient threefold decrease in intracellular ATP level imposes apoptosis. Biochim Biophys Acta. 2004; 1658: 141-147.

Jafri MS, Dudycha SJ, O’Rourke B. Cellular energy metabolism: models of cellular respiration. Annu Rev Biomed Eng. 2001; 3:57-81.

Reimer KA and Jennings RB. The "wavefront phenomenon" of myocardial ischemic cell death. II. Transmural progression of necrosis within the framework of ischemic bed size (myocardium at risk) and collateral flow. Lab Invest. 1979 Jun;40(6):633-44.

Jennings RB, Schaper J, Hill ML, Steenbergen C, Reimer JR and Reimer KA. Effect of reperfusion late in the phase of reversible ischemic injury. Changes in cell volume, electrolytes, metabolites, and ultrastructure. Circ Res. 1985; 56: 262-278.

Kabeya Y, Mizushima N, Ueno T, Yamamoto A, Kirisako T, Noda T *et al*. LC3, a mammalian homologue of Atg8p, is localized in autophagosome membranes after processing. EMBO J. 2000; 19:5720-5728.

Kadowaki M, Karim MR, Carpi A and Miotto G. Nutrient control of macroautophagy in mammalian cells. Mol Aspects Med. 2006;27:426-443.

Kagan VE, Bayir A, Bayir H, Stoyanovsky D, Wipf P, Atkinson J *et al.* Mitochondria-targeted disruptors and inhibitors of cytochrome c/cardiolipin peroxidase complexes: A new strategy in anti-apoptotic drug discovery. Mol Nutr Food Res. 2009; 53: 104-114.

Kajustra JW, Cheng W, Reiss K, Clark WA, Sonneblick EH, Krajewski S, Reed JC, Olivetti G, Anversa P. Apoptotic and necrotic myocyte cell deaths are independent contributing variables of infarct size in rats. Lab Invest. 1996; 79:949-956.

Kantor PF, Lucien A, Kozak R, Lopaschuk GD. The antianginal drug trimetazidine shifts cardiac energy metabolism from fatty acid oxidation to glucose oxidation by inhibiting mitochondrial long-chain 3-ketoacyl coenzyme A thiolase. Circ Res 2000; 86:580-588.

Karantza-Wadsworth V, Shyam P, Kravchuk O, Chen G, Mathew R, Jin S *et al*. Autophagy mitigates metabolic stress and genome damage in mammary tumorigenesis. Genes Dev. 2007; 21: 1621-1635.

Katayama M, Kawaguchi T, Berger MS and Pieper RO. DNA damaging agent-induced autophagy produces a cytoprotective adenosine triphosphate surge in malignant glioma cells. Cell Death Differ. 2007; 14: 548-558.

Kaushik S and Cuervo AM. Autophagy as a cell-repair mechanism: activation of chaperone-mediated autophagy during oxidative stress. Mol Aspects Med. 2006; 27: 444-454.

Kerr JFR, Wyllie AH, Currie AR. Apoptosis: a basic biological phenomenon with wide-ranging implications in tissue kinetics. Br J Cancer. 1972; 26:239-257.

Kerr JFR. Shrinking necrosis: a distinct mode of cell death. J Pathol.1971; 105:13-20.

Khan SA, Salloum F, Das A, Xi L, Vetrovec GW, Kukreja RC. Rapamycin confers preconditioning-like protection against ischemia-reperfusion injury in isolated mouse heart and cardiomyocytes. J Mol Cell Cardiol. 2006; 41:256-264.

Kihara A, Kabeya Y, Ohsumi Y and Yoshimori T. Beclin-phosphatidylinositol 3-kinase complex functions at the trans-Golgi network. EMBO rep. 2001; 2:330-335.

Kimchi A. Programmed cell death: from novel gene discovery to studies on network connectivity and emerging biomedical implications. Cytokine Growth Factor Rev. 2007; 18:435-440.

Kimes BW and Brandt BL. Properties of a clonal muscle cell line from rat heart. Exp Cell Res.1976; 98:367-381.

Kimura S, Noda T and Yoshimori T. Dissection of the autophagosome maturation process by a novel reporter protein, tandem fluorescent-tagged LC3. Autophagy. 2007; 3:5:452-460.

Kiselyov K, Jennings Jr JJ, Rbaibi Y and Chu CT. Autophagy, mitochondria and cell death in lysosomal storage diseases. Autophagy. 2007; 3:3: 259-262.

Klionsky DJ, Abeliovich H, Agostinis P, Agrawal DK, Aliev G, Askew DS *et al.* Guidelines for the use and interpretation of assays for monitoring autophagy in higher eukaryotes.Autophagy. 2008; 4, 2: 151-175.

Klionsky DJ, Cuervo AM and Seglen PO. Methods for monitoring autophagy from yeast to human. Autophagy. 2007; 3:3:181-206.

Klionsky DJ, Meijer AJ, Codogno P, Neufeld TP and Scott RC. Autophagy and p70S6 kinase. Autophagy. 2005; 1:1:59-61.

Klionsky DJ. Getting into the flow. Autophagy. 2008; 4:2: 139-140.

Klionsky DJ. Monitoring autophagy in yeast: the Pho8Delta60 assay. Methods Mol Biol. 2007; 390:363-71.

Klionsky DJ. The correct way to monitor autophagy in higher eukaryotes. Autophagy. 2005;1:2:65-65.

Klionsky DJ. The molecular machinery of autophagy:unanswered questions. J Cell Sci. 2005;118:7-18.

Kloner RA, Rezkalla SH. Cardiac protection during acute myocardial infarction: where do we stand in 2004? J Am Coll Cardiol. 2004; 44:276-286.

Kodde IF, van der Stok J, Smolenski RT, de Jong JW. Metabolic and genetic regulation of cardiac energy substrate preference. Comp Biochem Physiol. 2007; 146:26-39.

Kostin S, Pool L, Elsässer A, Hein S, Drexler HCA, Arnon E *et al*. Myocytes die by multiple mechanisms in failing human hearts. Circ Res. 2003; 92:715-724.

Krijnen PAJ, Cillessen SAGM, Manoe R, Muller A, Visser C A, Meijer CJLM, Musters RJP, Hack CE, Aarden LA and Niessen HWM. Clusterin: a protective mediator for ischemic cardiomyocytes? Am J Physiol Heart Circ Physiol. 2005; 289:2193-2202.

Kroemer G, El-Deiry WS, Golstein P, Peter ME, Vaux D, Vandenabeele P, Zhivotovsky B, Blagosklonny MV, Malorni W, Knight RA, Piacentini M, Nagata S and Melino G. Classification of cell death: recommendations of the Nomenclature Committee on Cell Death. Cell Death Differ. 2005; 12:1463-1467.

Kroemer G, Galluzzi L, Vandenabeele P, Abrams J, Baehrecke EH, Blagosklonny MV *et al.* Classification of cell death: recommendations of the Nomenclature Committee on Cell Death 2009. Cell Death Differ. 2009; 16:3-11.

Krysko DV, D'Herde K and Vandenabeele P. Clearance of apoptotic and necrotic cells and its immunological consequences. Apoptosis. 2006; 11:1709-1726.

Krysko DV, Vanden Berghe T, D'Herde K, Vandenabeele P. Apoptosis and necrosis: detection, discrimination and phagocytosis. Methods. 2008; 44:205-221.

Kuma A, Matsui M and Mizushima N. LC3, an autophagosome marker, can be incorporated into protein aggregates independent of autophagy. Autophagy. 2007; 3:4:323-328.

Kunapuli S, Rosanio S and Schwarz E. "How do cardiomyocytes die?" Apoptosis and autophagic cell death in cardiac myocytes. J Card Fail. 2006; 12:381-391.

Kunchithapautham K and Rohrer B. Apoptosis and autophagy in photoreceptors exposed to oxidative stress. Autophagy. 2007; 3:5:433-441.

Lam L, Arthur J, Semsarian C. Proteome map of the normal murine ventricular myocardium. Proteomics. 2007; 7:3629-3633.

Latta M, Künstle G, Leist M and Wendel A. Metabolic depletion of ATP by fructose inversely controls CD95- and tumor necrosis factor receptor 1-mediated hepatic apoptosis. J Exp Med. 2000; 191:1975-1985.

Lazda EJ, Batchelor WH and Cox PM. Immunohistochemical detection of myocardial necrosis in stillbirth and neonatal death. Pediatr Dev Pathol. 2000; 3:40-47.

Leber B, Lin J, Andrews DW. Embedded together: The life and death consequences of interaction of the Bcl-2 family with membranes. Apoptosis. 2007; 12:897–911.

Leist M and Jäättelä M. Triggering of apoptosis by cathepsins. Cell Death Differ. 2001; 8:324-326.

Leist M and Nicotera P. The shape of cell death. Biochem Biophys Res Commun. 1997; 236:1-9.

Leist M, Single B, Castoldi AF Kuhnle S and Nicotera P. Intracellular adenosine triphosphase (ATP) concentration: A switch in the decision between apoptosis and necrosis. J Exp Med.1997; 185:1481-1486.

Leist M, Single B, Naumann H, Fava E, Simon B, Kuhnle S *et al*. Inhibition of mitochondrial ATP generation by nitric oxide switches apoptosis to necrosis. Exp Cell Res.1999; 249:396-403.

Lemasters JJ, Nieminen AL, Qian T, Trost LC, Elmore SP, Nishimura Y *et al.*
The mitochondrial permeability transition in cell death: a common mechanism in necrosis, apoptosis and autophagy. Biochim Biophys Acta. 1998; 1366:177-96.

Lemasters JJ. Mechanism of Hepatic Toxicity V. Necrapoptosis and the mitochondrial permeability transition: shared pathways to necrosis and apoptosis. Am J Physiol. 1999; 276:G1-G6.

Lemasters JJ. Selective mitochondrial autophagy, or mitophagy, as a targeted defense against oxidative stress, mitochondrial dysfunction, and aging. Rejuvenation Res. 2005; 8:3-5.

Levine B and Yuan J. Autophagy in cell death: an innocent convict? J Clin Invest. 2005; 115:2679-2688.

Levine B, Sinha S and Kroemer G. Autophagy in higher eukaryotes—a matter of survival or death. Autophagy. 2008; 4:5:600-606.

Levrand S, Vannay-Bouchiche C, Pesse B, Pacher P, Feihl F, Waeber B *et al.* Peroxynitrite is a major trigger of cardiomyocyte apoptosis in vitro and in vivo. Free Rad Biol Med. 2006; 41:886-895.

Li Y, Xing D and Chen Q. Dynamic monitoring of apoptosis in chemotherapies with multiple fluorescence reporters. Mol Imaging Biol. 2009; DOI: 10.1007/s11307-008-0195-7.

Liang XH, Jackson S, Seaman M, Brown K, Kempkes B, Hibshoosh H *et al*., Induction of autophagy and inhibition of tumorigenesis by beclin 1. Nature. 1999; 42:672-676.

Liang XH, Kleeman LK, Jiang HH, Gordon G, Goldman JE, Berry G *et al*. Protection against fatal sindbis virus encephalitis by beclin, a novel Bcl-2-interacting protein. J Virol. 1998; 72:11:8586-8596.

Lieberthal W, Menza SA and Levine JS. Graded ATP depletion can cause necrosis or apoptosis of cultured mouse proximal tubular cells. Am J Physiol Renal Physiol. 1998; 274: 315-327.

Lin Y, Devin A, Rodriguez Y, Liu Z. Cleavage of the death domain kinase RIP by caspase-8 prompts TNF-induced apoptosis. Genes Dev. 1999. 13:2514-2526.

Liu B, Clanachan AS, Schulz R, Lopaschuk GD. Cardiac efficiency is improved after ischemia by altering both source and fate of protons. Circ Res. 1996; 79:940-948.

Lockshin RA and Zakeri Z. Apoptosis, autophagy, and more. IJBCB. 2004; 36:2405-2419.

Loos B, Engelbrecht AM. Cell death: a dynamic response concept. Autophagy. 2009; 5:5:1-14.

Loos B, Smith R and Engelbrecht A-M. Ischaemic preconditioning and TNF-α-mediated preconditioning is associated with a differential $cPLA_2$ translocation pattern in early ischaemia. Prostaglandins Leukot Essent Fatty Acids. 2008; 78:403-413.

Luiken JJFP, Coort SLM, Koonen DPY, Bonen Arend and Glatz JFC. Signalling components involved in contraction-inducible substrate uptake into cardiac myocytes. Proc Nutr Soc. 2004; 63: 251-258.

Maiuri MC, Criollo A, Tasdemir E, Vicencio JM, Tajeddine N, Hickman JA, Geneste O and Kroemer G. BH3-Only proteins and BH3 mimetics induce autophagy by competetively disrupting the interaction between Beclin-1 and Bcl-2/Bcl-X_L. Autophagy. 2007; 3:4:374-376.

Maiuri MC, Zalckvar E, Kimchi A and Kroemer G. Self-eating and self-killing: crosstalk between autophagy and apoptosis. Mol Cell Biol. 2007; 8:741-752.

Manfredi G, Yang L, Gajewski CD and Mattiazzi M. Measurement of ATP in mammalian cells. Methods. 2002; 26:317-326.

Marin S, Lee WNP, Bassilian S, Lim S, Boros LG, Centelles JJ *et al*. Dynamic profiling of the glucose metabolic network in fasted rat hepatocytes using [1,2-13C2]glucose. Biochem J. 2004; 381:287-294.

Martinet W, De Meyer GRY, Andries L, Herman AG and Kockx MM. Detection of autophagy in tissue by standard immunohistochemistry. Autophagy. 2006; 2:1:55-57.

Martinet W, Schrijvers DM, Herman AG and De Meyer GRY. Z-VAD-fmk-induced non-apoptotic cell death of macrophages. Autophagy. 2006; 2:4:312-314.

Maruyama R, Goto K, Takemura G, Ono K, Nagao K, Horie T *et al.* Morphological and biochemical characterization of basal and starvation-induced autophagy in isolated adult rat cardiomyocytes. Am J Physiol Heart Circ Physiol. 2008; 295: H1599–H1607.

Matsui Y, Takagi H, Qu X, Abdellatif M, Sakoda H, Asano T, *et al*. Distinct roles of autophagy in the heart during ischemia and reperfusion. Roles of AMP-activated protein kinase and Beclin 1 in mediating autophagy. Circ Res. 2007; 100:914-922.

Mavrakis M, Lippincott-Schwartz J, Stratakis CA and Bossis I. mTOR kinase and the regulatory subunit of protein kinase A (PRKAR1A) spatially and functionally interact during autophagosome maturation. Autophagy. 2007; 3:2:151-153.

McIlroy J, Chen D, Wjasow C, Michaeli T and Backer JM. Specific activation of p85-p110 phosphatidylinositol 3'kinase stimulates DNA synthesis by ras-and p70S6 kinase-dependent pathways. Mol Cell Biol. 1997.17:248-255.

McMullen JR, Sherwood MC, Tarnavsaki O, Zhang L, Dorfman AL, Shioi T *et al*. Inhibition of mTOR signaling with rapamycin regresses established cardiac hypertrophy induced by pressure overload. Circulation. 2004; 109:3050-3055.

Medeiros D. Assessing mitochondria biogenesis. Methods. 2008; 46:288-294.

Meijer AJ and Codogno P. AMP-activated protein kinase and autophagy. Autophagy. 2007; 3:3:238-240.

Meijer AJ, Dubbelhuis PF. Amino acid signaling and the integration of metabolism. Biochem Biophys Res Commun. 2004; 313:397-403.

Meldrum KK, Meldrum DR, Hile KL, Burnett AL and Harken AH. A novel method of ischemia in renal tubular cells which closely parallels *in vivo* injury. J Surg Res. 2001;99:288-293.

Menzies FM, Ravikumar B, Rubinsztein DC. Protective roles for induction of autophagy in multiple proteinopathies. Autophagy. 2006; 2:3:224-225.

Mistiaen WP, Somers P, Knaapen M and Kockx M. Autophagy as mechanism for cell death in degenerative aortic valve disease. Autophagy. 2006; 2:3:221-223.

Miyata S, Takemura G, Kawase Y, Li Y, Okada H, Maruyama R *et al.* Autophagic cardiomyocyte death in cardiomyopathic hamsters and its prevention by granulocyte colony-stimulating factor. Am J Pathol. 2006; 168: 386-397.

Mizukami Y, Iwamatsu A, Aki T, Kimura M, Nakamura K, Nao T *et al*. ERK1/2 regulates intracellular ATP levels through α-enolase expression in cardiomyocytes exposed to ischemic hypoxia and reoxygenation. JBC. 2004; 279:50120-50131.

Mizushima N and Yoshimori T. How to interpret LC3 immunoblotting. Autophagy. 2007; 3:6:542-545.

Mizushima N, Yamamoto A, Matsui M, Yoshimori T and Ohsumi Y. In vivo analysis of autophagy in response to nutient starvation using transgenic mice expressing a fluorescent autophagosome marker. Mol Biol Cell. 2004; 15: 1101-1111.

Mizushima N. The pleiotropic role of autophagy: from protein metabolism to bactericide. Cell Death Differ. 2005; 12:1535-1541.

Mizushima N. Collaboration of proteolytic systems. Autophagy. 2007; 3:3:179-180.

Mizushima N. Methods for monitoring autophagy. IJBCB. 2004; 36:2491-2502.

Mocanu MM, Baxter GF and Yellon DM. Caspase inhibition and limitation of myocardial infarct size: protection against lethal reperfusion injury. Br J Pharmacol. 2000; 130, 197- 200.

Moore MN. Autophagy as a second level protective process in conferring resistance to environmentally-induced oxidative stress. Autophagy. 2008; 4:2:254-256.

Morgan MJ, Kim YS and Liu ZG. TNFalpha and reactive oxygen species in necrotic cell death. Cell Res. 2008; 18:343-9.

Murray C J and Lopez A D. Alternative projections of mortality and disability by cause 1990-2020: Global Burden of Disease Study. Lancet.1997; 349: 1498-504.

Neely JR, Rovetto MJ, Whitmer JT, Morgan HE. Effects of ischemia on function and metabolism of the isolated working rat heart. Am J Physiol. 1973 Sep;225(3):651-8.

Neufeld TP. Contribution of Atg-1dependent autophagy to TOR-mediated cell growth and survival. Autophagy. 2007; 3:5: 477-479.

Nicotera P, Leist M, Single B and Volbracht C. Execution of Apoptosis: Converging or Diverging Pathways? Biol Chem. 1999; 380:1035-1040.

Nishida K, Kyoi S, Yamaguchi O, Sadoshima J, Otsu K. The role of autophagy in the heart. Cell Death Differ. 2009; 16:31-38.

Nixon RA. Autophagy in neurodegenerative disease: friend, foe or turncoat? Trends Neurosci. 2006; 29:528-535.

O'Connell AR and Stenson-Cox C. A more serine way to die: Defining the characteristics of serine protease-mediated cell death cascades. Biochim Biophys Acta. 2007;1773:1491-1499.

Opie LH. The Heart. Physiology and Metabolism. Second edition. Raven Press. New York, 1991.

Pacher P and Hajnóczky G. Propagation of the apoptotic signal by mitochondrial waves. EMBO J. 2001; 20: 4107-4121.

Patel HH, Head BP, Petersen HN , Niesman IR, Huang D, Gross GJ, Insel PA and Roth DM. Protection of adult rat cardiac myocytes from ischemic cell death: role of caveolar microdomains and δ-opioid receptors. Am J Physiol Heart Circ Physiol. 2006; 291: H344–H350.

Petiot A, Ogier-Denis E, Blommaart EFC, Meijer AJ and Codogno P. Distinct classes of phosphatidyl 3'-kinases are involved in signaling pathways that control macroautophagy in HT-29 cells. JBC. 2000; 275:992-998.

Pickford F, Masliah E, Britschgi M, Lucin K, Narasimhan R, Jaeger P A, Small S, Spencer B, Rockenstein E, Levine B and Wyss-Coray T. The autophagy-related protein beclin-1 shows reduced expression in early Alzheimer disease and regulates amyloid β accumulation in mice. J Clin Invest. 2008; 118: 2190-2199.

Poole-Wilson PA. Regulation of intracellular pH in the myocardium; relevance to pathology. Mol Cell Biochem.1989; 89:151-155.

Qadir M A, Kwok B, Dragowska W H, To K H, Le D, Bally MB, and Gorski SM. Macroautophagy inhibition sensitizes tamoxifen-resistant breast cancer cells and enhances mitochondrial depolarization. Breast Cancer Res Treat. 2008; 112:389–403.

Qu X, Yu J, Bhagat G, Furuya N, Hibshoosh H, Troxel a *et al*. Promotion of tumorigenesis by heterozygous disruption of the beclin 1 autophagy gene. J Clin Invest. 2003; 112: 1809-1820.

Ramadass R and Bereiter-Hahn J. How DASPMI reveals mitochondrial membrane potential: fluorescence decay kinetics and steady-state anisotropy in living cells. Biophys J. 2008; 95: 4068–4076.

Rami A, Bechmann I and Stehle JH. Exploiting endogenous anti-apoptotic proteins for novel therapeutic strategies in cerebral ischemia. Prog Neurobiol. 2008; 85: 273-296.

Ravikumar B, Berger Z, Vacher C, O'Cane CJ and Rubinsztein DC. Rapamycin pre-treatment protects against apoptosis. Hum Mol Genet. 2006; 15:7:1209-16.

Ravikumar B, Stewart A, Kita H, Kato K, Duden R and Rubinsztein DC. Raised intracellular glucose concentrations reduce aggregation and cell death caused by mutant Huntington exon 1 by decreasing mTOR phosphorylation and inducing autophagy. Hum Mol Genet. 2003; 12:9:985-994.

Rothermel BA and Hill JA. Myocyte autophagy in heart disease. Autophagy. 2007; 3:6:632-634.

Rumsey WL, Abbott B, Bertelsen D, Mallamaci M, Hagan K, Nelson D, *et al*. Adaptation to hypoxia alters energy metabolism in rat heart. Am J Physiol 1999; 276:71-80.

Saelens X, Festjens N, Parthoens E, Vanoverberghe I, Kalai M, Kuppeveld F *et al*. Protein synthesis persists during necrotic cell death. JCB. 2005; 14:545-551.

Samara C, Syntichaki P and Tavernarakis N. Autophagy is required for necrotic cell death in Caenorhabditis elegans. Cell Death Differ. 2008; 15: 105-112.

Sapirstein, A. and Bonventre, J. V. Specific physiological roles of cytosolic phospholipase A(2) as defined by gene knockouts. Biochim Biophys Acta. 2000; 1488: 139-48.

Sarbassov DD, Ali SM, Sabatini DM. Growing roles for the mTOR pathway. Curr Opin Cell Biol 2005; 17:596-603.

Scaffidi P, Misteli T and Bianchi ME. Release of chromatin protein HMGB1 by necrotic cells triggers inflammation. Nature. 2002; 418: 191-195.

Schilling WP, Snyder D, Sinkins WG and Estacion M. Palytoxin-induced cell death cascade in bovine aortic endothelial cells. Am J Physiol Cell Physiol. 2006; 291:C657-C667.

Schlueter C, Weber H, Meyer B, Rogalla P, Röser K, Hauke S and Bullerdiek J. Angiogenetic signaling through hypoxia HMGB1: an angiogenetic switch molecule. Am J Pathol. 2005; 166: 1259-1263.

Schoenberger J, Bauer J, Moosbauer J, Eilles C and Grimm D. Innovative strategies in in vivo apoptosis imaging. Curr Med Chem. 2008; 15:187-194.

Seglen PO and Gordon PB. 3-Methyladenine: Specific inhibitor of autophagic/lysosomal protein degradation in isolated rat hepatocytes. Proc Natl Acad Sci USA.1982; 79:1889-1892.

Seyedi N, Koyama M, Mackins CJ. Ischemia promotes renin activation and angiotensin formation in sympathetic nerve terminals isolated from the human heart: contribution to carrier-mediated norepinephrine release. J Pharmacol Exp Ther. 2002; 302:539-44.

Shen WH, Chen Z, Shi S, Chen H, Zhu W, Penner A, *et al*. Cardiac restricted overexpression of kinase-dead mammalian target of rapamycin (mTOR) mutant impairs the mTOR-mediated signaling and cardiac function. J Biol Chem 2008; 283:13842-13849.

Shiraishi J, Tatsumi T, Keira N, Akashi K, Mano A, Yamanaka S *et al*. Important role of energy-dependent mitochondrial pathways in cultured rat cardiac myocyte apoptosis. Am J Physiol Heart Circ Physiol. 2001; 281:H1637-H1647.

Shroff EH, Snyder C and Chandel N. Bcl-2 family members regulate anoxia-induced cell death. Antioxid Redox Signal. 2007; 9:1405-1409.

Shvets E, Fass E and Elazar Z. Utilizing flow cytometry to monitor autophagy in living mammalian cells. Autophagy. 2008; 4:5:621-628.

Siddhanta U, McIlroy J, Sha A, Zhang Y and Bcker JM. Distinct roles for the p110α and hVPS34 phosphatidyl 3'-kinases in vesicular trafficking, regulation of the actin cytoskeleton and mitogenesis. J Cell Biol. 1998. 146:1647-1659.

Simone C. Signal-dependent control of autophagy and cell death in colorectal cancer cells. Autophagy. 2007; 3:5:468-471.

Single B, Leist M and Nicotera P. Differential effects of Bcl-2 on cell death triggered under ATP-depleting conditions. Exp Cell Res. 2001; 262:8-16.

Sloviter RS. Apoptosis: a guide for the perplexed. Trends Pharmacol Sci. 2002; 23:19-24.

Srinivas V, Bohensky J, Zahm AM and Shapiro IM. Autophagy in mineralizing tissues: Microenvironmental perspectives. Cell Cycle. 2009; 4:8.

Steenbergen C, Deleeuw G, Barlow C, Chance B and Williamson JR. Heterogeneity of the hypoxic state in perfused rat heart. Circ Res. 1977; 41:606-615.

Stephens L, Williams R and Hawkins P. Phosphoinositide 3-kinases as drug targets in cancer. Curr Opin Pharmacol. 2005; 5:357-365.

Stridh H, Fava E, Single B, Nicotera P, Orrenius S and Leist M. Tributyltin-induced apoptosis requires glycolytic adenosine triphosphate production. Chem Res Toxicol.1999; 12:874-882.

Sun Q, Fan W, Chen K, Ding X, Chen S and Zhong Q. Identification of Barkor as a mammalian autophagy-specific factor for Beclin 1 and class III phosphatidylinositol 3-kinase. PNAS. 2008; 105: 19211-19216.

Sybers HD, Ingwall J, DeLuca M. Autophagy in cardiac myocytes. Recent Adv Stud Cardiac Struct Metab. 1978; 12:453-463.

Takagi H, Matsui Y, Hirotani S, Sakoda H, Asano T and Sadoshima J. AMPK mediates autophagy during myocardial ischemia in vivo. Autophagy. 2007; 3:3:405-407.

Takagi H, Matsui Y, Sadoshima J. The role of autophagy in mediating cell survival and death during ischemia and reperfusion in the heart. Antioxid Redox Signal. 2007; 9:1373-1381.

Takemura G, Fujiwara H. Morphological aspects of apoptosis in heart diseases. J Cell Mol Med. 2006; 10:56-75.

Tatsumi T, Shiraishi J, Keira N, Akashi K, Mano A, Yamanaka S *et al.* Intracellular ATP is required for mitochondrial apoptotic pathways in isolated hypoxic rat cardiac myocytes. Cardiovas Res. 2003; 59:428-440.

Tavernarakis N. Cardiomyocyte necrosis: Alternative mechanisms, effective interventions. Biochim Biophys Acta. 2007.1773:480-482.

Thakkar NS and Potten CS. Inhibition of doxorubicin-induced apoptosis in vivo by 2-Deoxy-o-glucose. Cancer Res. 1993; 53: 2057-2060.

Tyas L, Brophy VA, Pope A, Rivett AJ and Tavaré M. Rapid caspase-3 activation during apoptosis revealed using fluorescence-resonance energy transfer. EMBO rep. 2000; 1:266-270.

Vieira OV, Bothello RJ, Rameh L, Brachmann SM, Matsuo T, Davidson HW *et al*. Distinct roles of class I and class III phosphatidylinositol 3-kinases in phagosome formation and maturation. JCB. 2001; 155:19-25.

Volbracht C, Leist M and Nicotera P. ATP controls neuronal apoptosis triggered by microtubule breakdown or potassium deprivation. Mol Med. 1999; 5: 477-489.

Walls KC, Klocke BJ, Saftig P, Shibata M, Uchiyama Y, Roth KA *et al*. Altered regulation of Phosphatidylinositol 3-kinase signaling in cathepsin D-deficient brain. Autophagy. 2007; 3:3:222-229.

Wang X, Martindale JL, Liu Y and Holbrook NJ. The cellular response to oxidative stress: influences of mitogen-activated protein kinase signaling pathways on cell survival. Biochem J. 1998; 333:291-300.

Wattiaux R and Wattiaux-De Coninck S. Effects of ischemia on lysosomes. Int Rev Exp Pathol. 1984; 26: 85-106.

Wieser W and Krumschnabel G. Hierarchies of ATP-consuming processes: direct compared with indirect measurements, and comparative aspects. Biochem J. 2001; 355: 389-395.

Will Y, Hynes J, Ogurtsov VI and Papkovsky DB. Analysis of mitochondrial function using phosphorescent oxygen-sensitive probes. Nat Protoc. 2006; 1:6:2563-72.

Yamashima T. Ca^{2+}- dependent proteases in ischemic neuronal death. A conserved 'calpain-cathepsin cascade' from nematodes to primates. Cell Calcium. 2004; 36:285-293.

Yamashima T. Implication of cysteine proteases calpain, cathepsin and caspase in ischemic neuronal death of primates. Prog Neurobiol. 2000; 62:273-295.

Yan L, Vatner DE, Kim SJ, Ge H, Masurekar M, Massover WH, *et al*. Autophagy in chronically ischemic myocardium. Proc Natl Acad Sci. 2005; 102:13807-13812.

Yang AJ, Chandswangbhuvana D, Margol L and Glabe CG. Loss of endosomal/lysosomal membrane impermeability is an early event in amyloid Aβ1-42 pathogenesis. J Neurosci Res. 1998; 52:691-698.

Yorimitsu T and Klionsky DJ. Autophagy: molecular machinery for self-eating. Cell Death Differ. 2005; 12:1542-1552.

Yoshimori T, Kamimoto T, Shoji S, Hidvegi T, Mizushima N, Umebayashi K and Perlmutter DH. Intracellular inclusions containing mutant α1-Antitrypsin Z are propagated in the absence of autophagic activity. J Biol Chem. 2006; 281: 4467-4476.

Youle RJ and Strasser A. The BCL-2 protein family: opposing activities that mediate cell death. Nature Rev Mol Cel Biol. 2008; 9: 47-59.

Yu FY and Mattson MP. Dietary restriction and 2-deoxyglucose administration reduce focal ischemic brain damage and improve behavioral outcome: evidence for a preconditioning mechanism. J Neurosci Res.1999; 57:830-839.

Yu L, Alva A, Su H, Dutt P, Freundt E, Welsh S *et al*. Regulation of ATG7-beclin 1 program of autophagic cell death by caspase-8. Science. 2004; 304:1500-1502.

Yu L, Wan F, Dutta S, Welsh S, Liu Z, Frendt E *et al*. Autophagic programmed cell death by selective catalase degradation. PNAS. 2006; 103:4952-4957.

Yu L, Lenardo MJ and Baehrecke EH. Autophagy and Caspases. Autophagy. 2004; 3:9:1124-1126.

Yu L, Strandberg L, Lenardo MJ. The selectivity of autophagy and its role in cell death and survival. Autophagy. 2008; 4:5:567-573.

Yuan H, Perry CN, Huang C, Iwai-Kanai E,1 Carreira RS, Glembotski CC and Gottlieb RA. LPS-induced autophagy is mediated by oxidative signaling in cardiomyocytes. Am J Physiol Heart Circ Physiol. 2009; 296: H470-H479.

Yue TL, Wang C, Gu JL, Ma XL, Kumar S, Lee JC *et al*. Inhibition of extracellular signal-regulated kinase enhances ischemia/reoxygenation-induced apoptosis in cultured cardiac myocytes and exaggerates reperfusion injury in isolated perfused heart. Circ Res. 2000; 86:692-699.

Zamaraeva MV, Sabirov RZ, Maeno E, Ando-Akatsuka Y, Bessonova SV and Okada Y. Cells die with increased cytosolic ATP during apoptosis: a bioluminescence study with intracellular luciferase. Cell Death Differ. 2005; 12: 1390-1397.

Zhang Y, Qi H, Taylor R, Xu W, Liu LF, Jin S. The role of autophagy in mitochondria maintenance. Autophagy. 2007; 3:4:337-346.

Zhao Z-Q, Nakamura M, Wang N-P, Wilcox JN, Shearer S, Ronson RS, Guyton RA and Vinten-Johansen J. Reperfusion induces myocardial apoptotic cell death. Cardiovas Res. 2000; 45: 651–660.

Zhdanov AV, Ward MW, Prehn JHM and Papkovsky DB. Dynamics of intracellular oxygen in PC12 cells upon stimulation of neurotransmission. JBC. 2008; 283:9:5650-5661.

Zhu C, Xu F, Wang X, Shibata M, Uchiyama T, Blomgren K *et al*. Different apoptotic mechanisms are activated in male and female brains after neonatal hypoxia-ischaemia. J Neurochem. 2006; 96:1016-1027.

Ziporen L, Donin N, Shmushkovich T, Gross A and Fishelson Z. Programmed necrotic cell death induced by complement involves a bid-dependent pathway. J Immunol. 2009; 182: 515–521.